OPTIMIZATION OF ARSENIC(III) AND MERCURY(II) REMOVAL FROM NON-COMPETITIVE AND COMPETITIVE SORPTION SYSTEMS ONTO ACTIVATED CARBON

Jonas Bayuo

A Thesis Submitted in Fulfilment of the Requirements for the Degree of Doctor of Philosophy in Materials Science and Engineering of the Nelson Mandela African Institution of Science and Technology

Arusha, Tanzania

July, 2024

ABSTRACT

Heavy metals exist in the ecosystem both naturally and due to anthropogenic activities and as recalcitrant pollutants; they are non-biodegradable and cause acute and chronic diseases to human beings and many lifeforms. As a result, the removal of heavy metals from aqueous systems using sorbent materials produced from agricultural wastes is one of the new innovative treatment techniques. In this study, the biosorption and desorption characteristics of heavy metal ions from non-competitive and competitive aqueous solutions onto hybrid granular activated carbon produced from maize residues were investigated. The efficient sequestration of As(III) and Hg(II) ions from both monocomponent and bicomponent synthetic wastewater was found to show dependence on the physicochemical properties of the biosorbent and the studied independent biosorption process factors. The regenerated biosorbent could be reused up to the eighth cycle for the sequestration of As(III) and Hg(II) ions from the synthetic wastewater without significantly losing its adsorptive properties. The applicability of the biosorbent synthesized from the maize residues for the simultaneous decontamination of heavy metals found in real industrial wastewater as a function of several biosorption factors showed that the biosorbent could competitively decontaminate over 96% of As, Hg, Pb, Cd, and Cr in 100 mL textile wastewater in batch mode. The regeneration of the spent biosorbent using 0.10 M HCl showed that the biosorbent is capable of being recycled and reused severally for the sequestration of As, Hg, Pb, Cd, and Cr from the textile wastewater and even up to the ten cycles for a duration of 4 h. The optimization of the competitive removal of As and Hg ions in the co-existence of other heavy metals in the textile wastewater by the CCD-RSM resulted in maximum removal efficiencies of 97.72 and 99.99%, respectively. The characterization of the hybrid granular activated carbon using SEM, TEM, XRD, BET, and FTIR showed that the biosorbent surface characteristics could facilitate the removal of heavy metals from the non-competitive and competitive biosorption media. The main biosorption mechanism of the heavy metal ions on the biosorbent was mainly chemisorption involving surface complexation. Therefore, this novel biosorbent is found to be promising and could effectively be employed for heavy metals remediation in aquatic environments. The outcomes of this study are expected to make a significant contribution to the design of low-cost and efficient industrial wastewater treatment systems such as a dynamic batch rector for heavy metal removal using locally available bio-adsorbents.

DECLARATION

I, Jonas Bayuo, do hereby declare to the Senate of the Nelson Mandela African Institution of Science and Technology (NM-AIST) that this thesis is my original work and that it has neither been submitted nor being concurrently submitted for a degree award in any other institution.

Jonas Bayuo 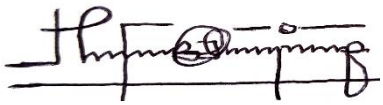

Name of Candidate **Signature** **Date**

The above declaration is confirmed by:

Dr. Mwemezi J. Rwiza 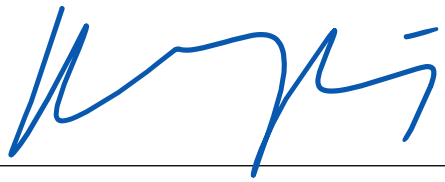

Name of Supervisor 1 **Signature** **Date**

Prof. Kelvin Mark Mtei 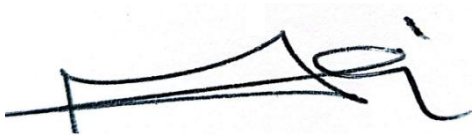

Name of Supervisor 2 **Signature** **Date**

Prof. Joon Weon Choi 

Name of Supervisor 3 **Signature** **Date**

COPYRIGHT

This thesis is copyright material protected under the Berne Convention, the Copyright Act of 1999 and other international and national enactments, on behalf, of intellectual property. It must not be reproduced by any means, in full or in part, except for short extracts in fair dealing; for researcher private study, critical scholarly review, or discourse with an acknowledgment, without the written permission of the office of Deputy Vice Chancellor for Academic, Research and Innovation on behalf of both the author and the Nelson Mandela African Institution of Science and Technology (NM-AIST).

CERTIFICATION

The undersigned certify that they have read and hereby recommend for acceptance by the Nelson Mandela African Institution of Science and Technology a thesis titled ***"Optimization of arsenic(III) and mercury(II) removal from non-competitive and competitive sorption systems onto activated carbon"*** in partial fulfillment of the requirements for the degree of Doctor of Philosophy in Materials Science and Engineering of the Nelson Mandela African Institution of Science and Technology.

ACKNOWLEGEMENTS

The completion of this PhD thesis was made possible by the guidance, mentorship, and technical and material support of my supervisors, Dr. Mwemezi J. Rwiza and Prof. Kelvin Mark Mtei of the Nelson Mandela African Institution of Science and Technology (NM-AIST), Tanzania, and Prof. Joon Weon Choi of the Institute of Green Bio Sciences and Technology (GBST), Seoul National University, South Korea. Not forgetting their encouragement, inspiration, and the time, they spent on this work during the conception, data collection, and publication of the findings of this research.

I sincerely appreciate the effort of the Partnership for Applied Sciences, Engineering, and Technology-Regional Scholarship and Innovation Fund (PASET-Rsif) under whose sponsorship this study was successful. I am also thankful to my International Partner Institution (IPI); the Institute of Green Bio Sciences and Technology (GBST), Seoul National University, South Korea from where I underwent advanced training and research. Additionally, I thanked the Carnegie Corporation of New York (CCNY) as one of the DOCTAS Grant recipients to support my research activities at the Seoul National University, South Korea.

My profound gratitude also goes to all professors and lecturers in the Department of Materials Science and Engineering (MaSE), School of Materials, Energy, Water, and Environmental Sciences (MEWES) under whose personal support, assistance, and motivation this research work has been a reality.

Finally, I am thankful to the management of the Arusha Technical College (ATC) for granting me access to the Water Quality Laboratory where some of the experiments of this research were conducted.

DEDICATION

To my wife, Miss Gifty Abisiba, and our two girls, Angela Ngmentero Bayuo and Florine Favor Ngmenkpieo Bayuo, for bearing with me in my long and frequent stays abroad during the period of my study. The joy is ours!

TABLE OF CONTENTS

LIST OF TABLES

LIST OF FIGURES

LIST OF APPENDICES

LIST OF ABBREVIATIONS

AAS	Atomic Absorption Spectrophotometer
AC	Ash Content
AHH	Arachis Hypogea Husk
AMOS	Alumina Modified Onion Skin
ANOVA	Analysis of Variance
ASTM	American Society for Testing and Materials
BD	Bulk Density
BET	Brunauer-Emmett-Teller
CCD	Central Composite Design
ChPHMBNPs	Chitosan Modified-Polyhexamethylene Biguanide
CY	Carbon Yield
CVAAS	Cold Vapour Atomic Absorption Spectrophotometer
DOE	Design of Experiment
EDS	Energy Dispersive Spectrometer
EDTA	Ethylenediaminetetraacetic acid
FCC	Fixed Carbon Content
FT-IR	Fourier Transform Infrared Spectrometer
GGBFS	Ground Granulated Blast-Furnace Slag
GGN	Green-Graphene Nanosheets
HGAC	Hybrid Granular Activated Carbon

IN	Iodine Number
MAL	Maximum Acceptable Level
MC	Moisture Content
MCh	Magnetic Chitosan
PH-g-MMA	Peanut Hull-g-Methyl Methacrylate Biopolymer
pH_{pzc}	pH of Point of Zero Charge
PG	Phosphogypsum
PS	Phosphorus slag
rpm	Resolutions per Minute
RSM	Response Surface Methodology
SEM	Scanning Electron Microscope
TEM	Transmission Electron Microscope
TGA	Thermogravimetric Analyzer
USEPA	United States Environmental Protection Agency
VM	Volatile Matter
WHO	World Health Organization
XRD	X-Ray Diffractometer
XRF	X-Ray Fluorescence
ZIF	Zeolitic Imidazolate Framework

LIST OF SYMBOLS

As	Arsenic
Ca^{2+}	Calcium ions
CaCl	Calcium chloride
Cd	Cadmium
Cl^{-}	Chloride ions
Co	Cobalt
Cr	Chromium
Cu	Copper
g	Grams
g/L	Grams per liter
g/mol	Grams per mol
h	Hour
H^{+}	Hydrogen ions
HCl	Hydrochloric acid
HCO_3^{-}	Bicarbonate ions
Hg	Mercury
$HgCl_2$	Mercuric chloride
HNO_3	Nitric acid
H_3PO_4	Phosphoric acid
H_2SO_4	Sulphuric acid

K	Kelvin
K^+	Potassium ions
M	Molar
Mg^{2+}	Magnesium ions
$MgCl_2$	Magnesium chloride
mg/g	Miligram per gram
mg/L	Milligram per litre
min	Minutes
mL	Milililtre
Mn	Manganese
N	Normality
Na^+	Sodium ions
$NaAsO_2$	Sodium arsenite
$NaBH_4$	Sodium borohydride
NaCl	Sodium chloride
$NaNO_3$	Sodium nitrate
NaOH	Sodium hydroxide
$NaSO_4$	Sodium thiosulphate
Ni	Nickel
OH^-	Hydroxide ions
Pb	Lead

$\mathbf{SO_4^{2-}}$	Sulphate ions
$\mathbf{TiO_2}$	Titanium oxide
Zn	Zinc
ZnO	Zinc oxide
°C	Degree Celcius
$\mathbf{\Delta H^0}$	Enthalpy
$\mathbf{\Delta S^0}$	Entropy
$\Delta \boldsymbol{G^0}$	Gibbs Free Energy
µm	Micrometre
%	Percentage

CHAPTER ONE

INTRODUCTION

1.1 Background of the Problem

Heavy metals are harmful contaminants that exist in aquatic environments due to human activities such as industrialization, urbanization, technological advancement, and agriculture. Heavy metals like arsenic (As), zinc (Zn), manganese (Mn), cadmium (Cd), lead (Pb), chromium (Cr), mercury (Hg), and copper (Cu), which are harmful to plants, animals, and humans, are present in domestic, municipal, and industrial wastewater that originates from several anthropogenic activities (Manjuladevi *et al.,* 2018; Boulaiche *et al.,* 2019; Khorshidi *et al.,* 2020; Egirani *et al.,* 2021). Metal plating, mining, metal smelters, alloying, storage batteries, plastics, wood preservatives, and textiles manufacturing as well as agricultural sources where fertilizers, pesticides, and fungicidal spray are heavily utilized contribute to heavy metals pollution in the aqueous systems (El-Bouhy *et al.,* 2021). Different from organic contaminants, heavy metals are unable to break down chemically or biologically into less harmful forms. However, they could only transform to become less harmful species. For instance, highly toxic Hg(II) is usually converted to a less toxic Hg(0) species (Priyadarshanee & Das, 2021), As(III) to As(V) (Biswas & Sarkar, 2019), and Cr(VI) to Cr(III) (Mohamed *et al.,* 2020). Due to their inability to degrade, these hazardous heavy metals persist in the ecosystem and cause serious health problems to all living things. These toxic heavy metal ions constantly bioaccumulate in the bodies of all lifeforms through the food web (Dawodu *et al.,* 2020). When excessive heavy metal ions accumulate in biological cells, they can result in cancer, and cause harm to the brain, kidney, liver, reproductive, and neurological systems, which can lead to death (Ali *et al.,* 2019).

As emphasized by the Agency for Toxic Substances and Disease Registry, As and Hg are among the ‘‘First Top Hazardous Substances’’ and are required to be reduced to an acceptable level when present in aqueous solutions due to their detrimental consequences on the ecosystem, which comprises humans, animals and all other living species (Wang *et al.,* 2021). Long-term exposure to As and Hg ions, even at lower concentration levels, can result in acute and chronic conditions including cancer, cardiovascular ailments, and death. The excessive presence of As in aquatic systems has been known globally to be a life-threatening concern (Razzak *et al.,* 2021). On the other hand, Hg is very poisonous, specifically in aquatic

environments, and can build up through food chains after being consumed by living organisms (Raj & Maiti, 2019). Environmental imbalances are caused by the excessive release of Hg into the ecosystem, which also affects human health (Tang *et al.,* 2022).

Considering the toxicity of As and Hg, various purification technologies including chemical coagulation, membrane processes, ion exchange, nano-filtration, and adsorption, have been used to decontaminate As and Hg from wastewater (Sharma *et al.,* 2019). However, apart from the adsorption technology, most of these remediation processes have several significant flaws that restrict their use, such as high operating expenses, the need for professional manpower, the production of concentrated sludges, high power consumption, and chemical requirements (Shahedi *et al.*, 2020; Nyangi, 2021; Siriwardena *et al.,* 2021). Therefore, the abatement of As and Hg species using natural sorbent materials is highly recommended because they are cheap and have been found to possess several surface functional groups capable of binding various heavy metals (Alalwan *et al.,* 2020). As a result, several possible sources of inexpensive agro-based biosorbents are presently being explored to see how well they perform in removing As(III) and Hg(II) ions from single-component sorption systems (Wu *et al.,* 2018; Jagirani *et al.,* 2020; Türkmen *et al.,* 2022; Abou-Taleb *et al.,* 2021; Egirani *et al.,* 2021; El-Bouhy *et al.,* 2021). However, very few studies are dedicated to binary and multi-metal adsorption, which is holistic and practical to study since the existence of one metal species in wastewater is unfeasible.

Even though the influence of independent factors on As(III) and Hg(II) adsorption has indeed been extensively substantiated in the literary works, there are many setbacks due to the over-reliance on several samples, lengthy time for experimental runs, and elevated input costs as well as no interactive effects between the various independent adsorption variables studied (Choudhary & Bhattacharyya, 2020; Khan *et al.,* 2021; Yan *et al.,* 2021; Türkmen *et al.,* 2022). Multivariate experimental designs, for instance, the response surface methodology (RSM) of Design Expert (Stat-Ease, version 13), can reduce experimental uncertainty and time requirements while ensuring the sequestration of As(III) and Hg(II) species from water systems at the lowest possible cost (Iqbal *et al.,* 2016; Moradi *et al.,* 2016; Karami *et al.,* 2017).

The RSM is a quick and efficient statistical technique that uses the interactive effects of two or more process-independent factors and optimizes the process with the least number of experimental runs. The main interactive effect of the most significant independent factors, interactions with other factors, and quadratic effects that affect the response variable(s) are all

elucidated by the RSM. The RSM has been employed successfully for factorial designs-based chemical process optimization, predictions, and interpretations (Afolabi *et al.,* 2021). As a result, the use of multivariate experimental design is growing in recognition and use within the scientific community. In comparison to conventional methods, multivariate experimental designs provide several key advantages, including speedy implementation, inexpensive costs, and concurrent exploration of multiple effects of independent factors on a response variable (Hinkelmann, 2012). All though the conventional approach to the optimization of process-independent factors involves a multi-factorial design, it only treats one parameter at a time while maintaining the numerical values of the other process factors. As a result, the traditional one-parameter-at-a-time design of optimization necessitates a lot of time and resources (Jain *et al.,* 2021).

Maize is utilized as a raw material in a wide range of industries, including alcoholic beverages, medicines, oil, flour, food sweeteners, cosmetics, gum, and paper (Sharma *et al.,* 2019). However, the stalks, cobs, and tassels, which are abundant agriculture residues find very little or no use. Mostly, animals do not feed on these residues, and they are usually burnt without utilization, thereby constituting an environmental nuisance. Besides, maize plant biomass is carbon-rich in nature and possesses lignocellulose constituents containing several functional groups with good abilities to adsorb heavy metals from aqueous systems. No study has ever reported on the modeling and optimization of As(III) and Hg(II) ions removal from wastewater by a novel hybrid granular activated carbon derived from maize plant biomass using a multivariate experimental design approach.

To the best of our knowledge, limited research has been conducted utilizing central composite design (CCD) of the response surface methodology (RSM) to design, model, and remove As(III) and Hg(II) ions from wastewater, hence, every parameter is always optimized manually. Due to the high cost, time commitment, need for several trials, and failure to highlight the interacting behavior of the process factors, the manual optimization of As(III) and Hg(II) ions removal from non-competitive and competitive sorption systems is neither economical nor viable in real-world industrial applications. The present study utilizes a novel hybrid granular activated carbon prepared from maize plant biomass for As(III) and Hg(II) removal from non-competitive and competitive sorption systems using a design of experiment (DOE). The effects of independent factors on As(III) and Hg(II) optimization removal from non-competitive and competitive sorption systems were also investigated in a batch mode using CCD-RSM. The

present study of maize-derived activated carbon for the removal of arsenic and mercury from wastewater offers a sustainable, cost-effective solution for mitigating heavy metal contamination and promoting environmental and health protection.

1.2 Statement of the Problem

In recent times, the underutilization of agricultural waste materials has resulted in environmental problems due to inadequate disposal. Similarly, non-biodegradable toxicants including noxious heavy metals are commonly spotted in industrial effluents and wastewater discharged from mining, metallurgical, tannery, chemical, and pharmaceutical industries (Zeng *et al.*, 2020). As(III) and Hg(II) are of environmental worry because they are part of the top five main poisonous heavy metals, which are the subject of many studies (Hashemi *et al.*, 2019; Vega-Páez *et al.*, 2019).

Several studies have dealt with the applicability of many adsorbents in decontaminating heavy metals from monocomponent adsorption systems (Gaur *et al.*, 2018; Jayasri & Suthindhiran, 2017; Rodríguez-Romero *et al.*, 2020; Egirani *et al.*, 2021). However, a few studies are dedicated to binary and multi-component adsorption systems. In binary and multi-component systems, the heavy metals removal could show dependence on the biosorbent properties, solution, and the interaction among the different adsorbates present in the system. Also, the interactive behavior of diverse heavy metal ions on the adsorbent surface may be capable of altering each heavy metal ion uptake capacity.

Undoubtedly, studies have reported on maize plants and their various parts have been utilized in removing contaminants from wastewater through biosorption (Chen *et al.*, 2020; Liu *et al.*, 2020; Mahdi & Jaafar, 2020). However, most biosorption studies adopt single, or many biosorbents obtained from several parts of the maize plant residues. However, no study considered hybrid adsorbents derived from different parts of this agricultural by-product. Widespread studies are essential to explore the possibilities of biosorbents derived from diverse parts of an agricultural by-product that can effectively enhance the biosorption process of heavy metals.

1.3 Rationale of the Study

The main problem of the conventional adsorption method is the expensiveness of commercial adsorbents, which upsurges the price of water and wastewater purification. Therefore, there is

an urgent call for easy and environmentally-friendly treatment approaches by employing novel, inexpensive, and naturally existing materials as biosorbents. Presently, greater attention has been focused on the practicality of applying low-cost biosorbents derived from natural materials in removing heavy metals from wastewater (Mustapha *et al.,* 2019; Belachew & Hinsene, 2020). The biosorption of heavy metals onto biomass surfaces has been acknowledged as a proficient procedure in wastewater treatment (Dawodu *et al.*, 2020). The biosorbents prepared from agricultural by-products have proven to be dependable in the depollution of toxic ions from wastewater and they are accessible all the time, priceless, simple to process, more efficient, and recyclable (Alatabe & Kariem, 2019; Kumar *et al.,* 2020; Samaraweera *et al.,* 2020).

Many studies have explored the adsorption of toxicants found in single solute systems using single or several adsorbents (Mahdi *et al.,* 2018; Daneshvar *et al.,* 2019; Manzoor *et al.,* 2019; Mitra & Kumar, 2019). Therefore, the quantity of studies reporting on monocomponent biosorption systems is increasing every day whilst the elimination of heavy metals in binary and multi-solute systems is seldom reported in the literature. It is crucial to examine the simultaneous binding effects of two or more metal ions on an adsorbent from a mixture of different heavy metals in aqueous media.

1.4 Research Objectives

1.4.1 General Objective

The general objective of the study is to optimize the biosorption behavior of arsenic and mercury ions from non-competitive and competitive sorption systems onto hybrid activated carbon derived from maize plant residues.

1.4.2 Specific Objectives

The study seeks to accomplish the following specific objectives:

(i) To investigate the biosorption and desorption characteristics of As(III) and Hg(II) ions from single and bicomponent synthetic wastewater onto activated carbon.

(ii) To optimize the equilibrium biosorption parameters influencing non-competitive removal of As(III) and Hg(II) ions from synthetic wastewater onto activated carbon.

(iii) To test the applicability of the activated carbon in the concurrent removal of As and Hg co-existing with other heavy metals in textile wastewater as a function of independent influencing factors.

(iv) To optimize the independent factors influencing the competitive adsorptive removal of As and Hg ions from the multicomponent textile wastewater onto activated carbon.

1.5 Research Questions

The study intended to answer the following questions:

(i) What are the biosorption and desorption characteristics of As(III) and Hg(II) ions from single and bicomponent synthetic wastewater onto activated carbon?

(ii) What are the optimal conditions for the non-competitive removal of As(III) and Hg(II) ions from synthetic wastewater using activated carbon?

(iii) How effective is the activated carbon in the concurrent removal of As and Hg in the presence of other heavy metals from textile wastewater under varying influencing factors?

(iv) What are the optimal conditions for the competitive adsorptive removal of As and Hg ions from multicomponent textile wastewater using activated carbon?

1.6 Significance of the Study

The current study sought to add knowledge to the search for promising agricultural waste materials that could be utilized as low-cost biosorbents for the adsorptive removal of diverse toxic heavy metals from aquatic environments. Therefore, this study will proffer solutions in areas of treatment of agricultural, mining, and industrial wastewater being released into the environment, especially in developing countries using locally available sorbent materials. Besides, it will provide environmentally friendly disposal methods for metal ions–impregnated sorbent materials. This will help in curbing environmental pollution and also promote the practicability and application of the biosorption technology at the industrial scale level. Furthermore, biosorption using agricultural waste materials as non-conventional biosorbents will lead to waste reduction and minimize the cost of waste disposal.

1.7 Delineation of the Study

Heavy metal contamination in water and wastewater poses significant environmental and health risks. The main aim of this study was to optimize the biosorption behavior of arsenic (As) and mercury (Hg) ions from non-competitive and competitive sorption systems onto activated carbon derived from maize biomass. The biosorption and desorption characteristics of As(III) and Hg(II) ions as well as the optimization of the equilibrium biosorption parameters affecting the removal of these heavy metals from synthetic wastewater using the activated carbon was investigated. More so, the potential of the activated carbon for the concurrent removal of As and Hg in the presence of other heavy metals in textile wastewater was tested. Additionally, the optimization of the independent factors influencing the competitive adsorptive removal of As and Hg from the multicomponent textile wastewater was investigated. All the biosorption experiments were conducted in batch mode and the central composite design of the response surface methodology was used in the optimization of As and Hg removal from the synthetic and real wastewater using the as-prepared activated carbon from maize biomass.

All in all, this study presents an economical and sustainable approach to wastewater treatment for the purpose of safeguarding both human health and the natural environment by decontaminating arsenic and mercury as well as other heavy metals from wastewater using activated carbon produced from maize biomass.

CHAPTER TWO

LITERATURE REVIEW

2.1 Heavy Metal Pollution in the Environment

In recent years, there has been a growing public awareness about environmental protection, which can be seen both globally and locally. Global worries have suddenly increased over pollution due to heavy metals discharged from various sources into the environment (Zhang *et al.,* 2018; Zhang *et al.,* 2019; Calderón *et al.,* 2020; Yuanling Li *et al.,* 2021; Rafique *et al.,* 2022; Amita Sharma *et al.,* 2022; Wang *et al.,* 2023). These heavy metals continue to remain in the ecosystem because they are non-degradable nor destroyable. The availability of heavy metals in the ecosystem is attributable to numerous environmental parameters, notably among them are natural phenomena and several anthropogenic activities (Samaniego & Tanchuling, 2019).

Heavy metals negatively influence the ecosystem, including the land, water, and living things. Due to its soluble nature, it interferes with human physiological processes and causes several health problems (Dewi *et al.,* 2023). Heavy metals pose a serious hazard to public health because of their non-biodegradable nature, which makes it easy for them to accumulate in cells and tissues of all lifeforms in significant amounts. Impaired development and growth, organs and neurological system damage, cancer, as well as death are some of its consequences (Rai *et al.,* 2023).

Due to the risks associated with ingesting heavy metal ions, the World Health Organization (WHO) has established guidelines for the maximum acceptable level of intake by humans (Nezami *et al.,* 2023). Additionally, the United States Environmental Protection Agency (USEPA) established the possible allowable contamination levels and toxicity due to the discharge of heavy metals as summarized in Table 1 (Bakshe & Jugade, 2023; Fiyadh *et al.,* 2023; Kumar *et al.,* 2023).

According to Abidli *et al.* (2021), the discharge of heavy metal ions into the ecosystem occurs over wide-ranging processes and pathways including natural processes (1), and anthropogenic activities (2), leading to detrimental effects in the environment including direct pollution of the aquatic environment (3), plants (4), as well as triggering toxic effects on humans (5) through different intake paths such as food chain (drinking water and food), inhalation, and skin contact

(6) as shown in Fig. 1.

Table 1: Maximum allowable contamination levels for various heavy metals

Heavy metal	MAL (mg/L)	Sources of heavy metal pollution
As	0.05	Mining and smelting, steel factories, pesticides, pigments, and paints industry.
Hg	0.001	Mining, ceramics, battery, pigments, and paints industries.
Cr	0.05	Metallurgical, chemical, cement, steel, pesticide, printing and graphics, pigments, and paints industries.
Cd	0.01	Fertilizer, pesticide, battery, printing and graphics, pigments and paints, and metal smelting industries.
Ni	0.2	Metallurgical, electroplating, steel, battery, mining, and paper mills industries.
Zn	0.8	Galvanizing, brass, metal plating, ceramic, electrical, steel, pesticide, battery, printing and graphics, pigments, and paints industries.
Pb	0.06	Pesticide, battery, electrical, lead smelters, mining and plumbing, ceramics, steel, printing and graphics, pigments, and paints industries.
Cu	0.25	Mining, metal smelting, machinery, iron and steel, fertilizer, fly ash, ceramics, electrical, and pesticide industries.

The pollution of surface and groundwater water, as well as soils, sediments, and air with perilous heavy metals, cause health problems for living organisms (Sarma *et al.*, 2019; Khan *et al.*, 2020; Sonone *et al.*, 2020; Zhang *et al.*, 2021). There could be a high tendency for heavy metal ions concentration to build up in living tissues once they become part of the food chain and cause severe health disorders when ingestion exceeds the permitted concentration (Kumar *et al.*, 2019; Pasricha *et al.*, 2021; Steingräber *et al.*, 2022). Besides, it has been established that

highly toxic heavy metal ions can damage red blood cells and cause hypertension, anemia, and neurological malfunction in humans even at small concentration levels (Samuel *et al.*, 2021; (Xiao *et al.*, 2023).

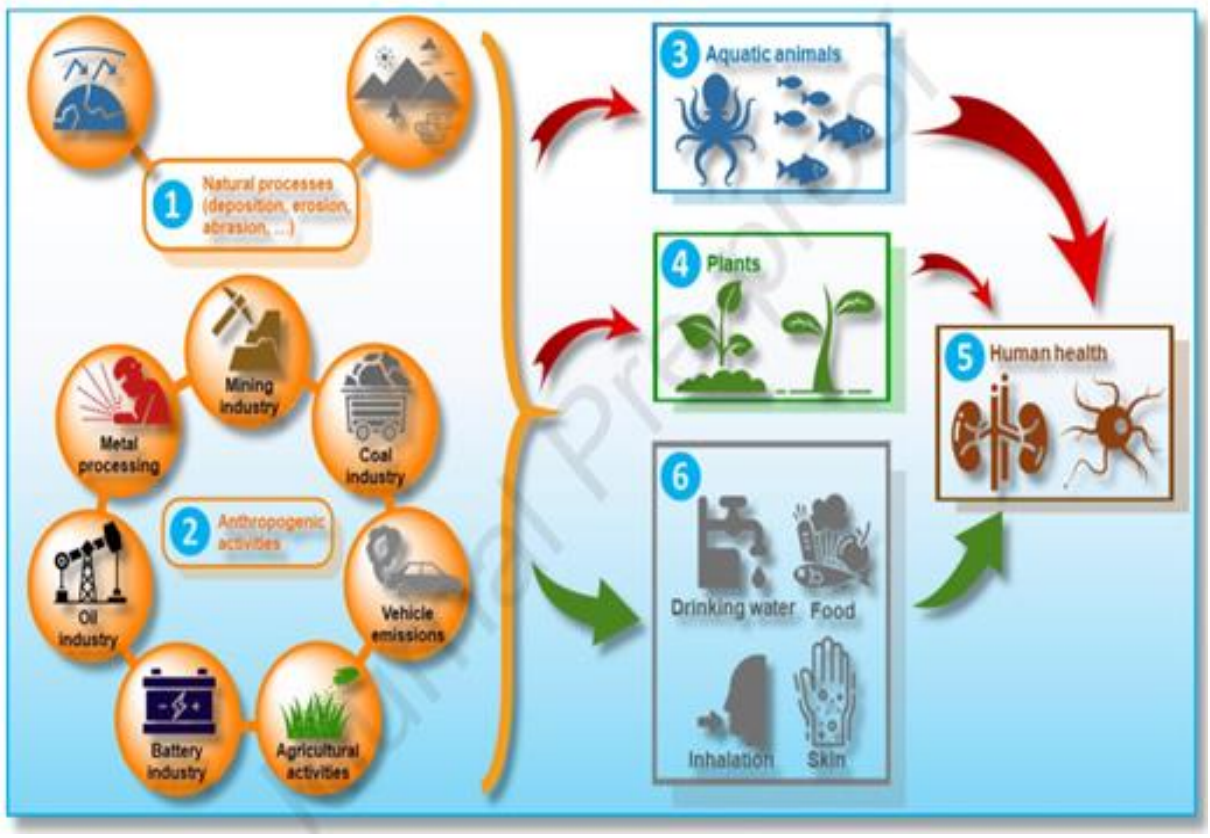

Figure 1: Schematic illustration of the pathway of heavy metals and metalloids pollutants in the ecosystem (Abidli *et al.*, 2021)

Several heavy metals are recognized to be noxious to human beings and other living species when consumed beyond the concentration required for healthy growth. Some of these heavy metals such as (arsenic (As), chromium (Cr), cadmium (Cd), lead (Pb), nickel (Ni), mercury (Hg), and zinc (Zn), and their harmful effects in living organisms when bio-accumulated in higher concentration than their acceptable levels are presented in Fig. 2.

Heavy metals are known to be dangerous pollutants and their presence in aquatic environments due to many industrial developments has led environmentalists and researchers to be much more concerned attributable to their harmfulness. In order to remove heavy metals from the environment, effective wastewater treatment is needed (Fiyadh *et al.*, 2023).

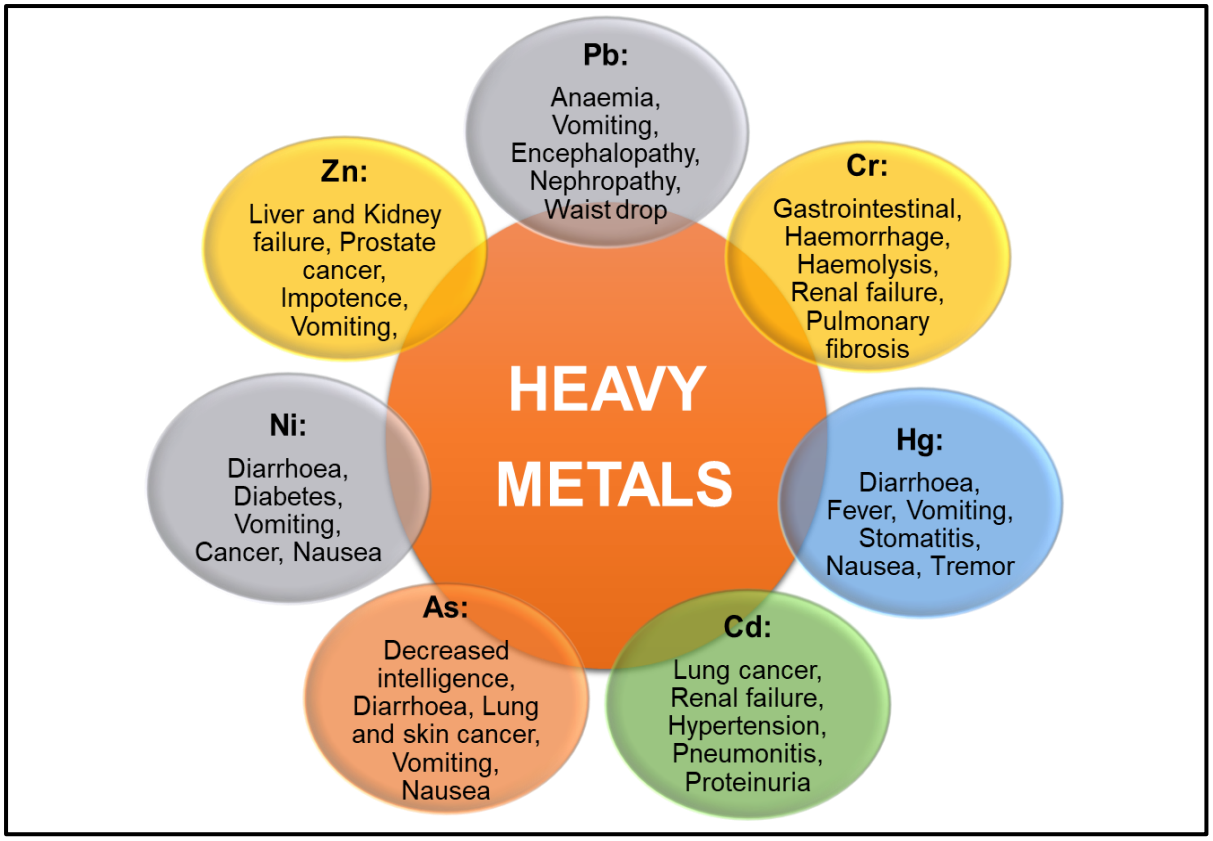

Figure 2: The effects of various heavy metals on human health (Mohd *et al.*, 2021)

2.2 Technologies for Heavy Metals Removal

The main conventional and non-conventional methods used in heavy metals decontamination from water and wastewater as shown in Fig. 3 include the following electrodialysis, reverse osmosis, ion exchange, chemical precipitation, adsorption, and biosorption (Zenebe, 2014; Mohd *et al.*, 2021; Bayuo *et al.*, 2023). However, the technique preferred in heavy metals removal is dependent on several factors namely technique efficiency, environmental influence, and cost of operation. In this study, some of the conventional and non-conventional treatment technologies for the sequestration of heavy metals from water systems are discussed.

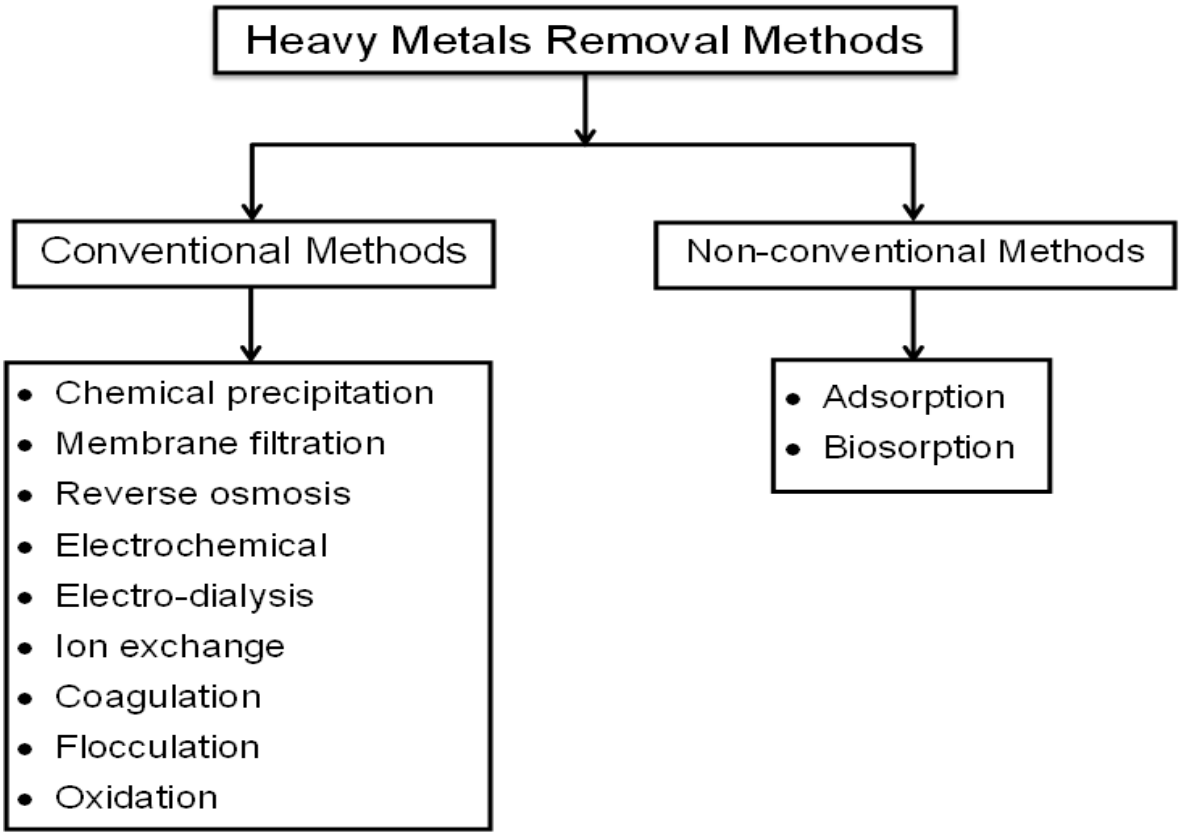

Figure 3: Different conventional and non-conventional methods for heavy metals removal from aquatic environments

2.2.1 Electro-dialysis Method

This approach removes ionic species from aqueous solutions when ion-exchange membranes are used together with electrical potential differences (Waghmare, 2015). In between the anode and the cathode are a succession of cation and anion exchange membranes. The anions travel to the anode, while cations migrate to the cathode. These ions pass through the membrane and are captured by the electrodes with opposite charges (Choi, 2016). The cost and low efficacy of this approach for removing trace concentrations of contaminants from aqueous systems are its drawbacks (Zhang *et al.*, 2012).

2.2.2 Ion Exchange

An ion exchanger is a solid that can exchange cations or anions from the environment (Baysal *et al.*, 2013). Ion exchange is the process of replacing an ion that has been removed from a liquid phase with another ionic species. The ion exchange process continues until the resin exchange capacity of the resin is depleted. Other chemicals must be used to regenerate the exhausted resin, replacing the ions acquired during the ion exchange process, restoring the resin

to its original composition, and allowing it to be reused in the next cycle (Xu & Dong, 2008).

Generally, water is often routed through an ion-exchange polymer, which is a water-insoluble material capable of exchanging a portion of its ions in an aqueous solution for other ions with identical charges (Kumar & Jain, 2013). For the exchange to take place, the electrical charge of the toxic substance and the ions inside the polymer have to be similar (Mbugua *et al.*, 2014). According to Kumar and Jain (2013), ion-exchange properties can be found in a variety of natural organic materials, or they can be added to them through chemical modification. By employing nitric acid as an oxidant or introducing the sulphonic acid group with strong sulphuric acid, ion exchangers are produced from natural materials such as wood, fibers, peat, and coal. Although the resins are quite pricey, ion exchange may effectively and selectively remove heavy metal ions to parts per million levels (Pakzadeh & Batista, 2011). Furthermore, the ion-exchange method of water treatment is environmentally favorable. However, ion exchange has several drawbacks when it comes to removing heavy metals, including poor wettability, small surface area, poor selectivity, sluggish adsorption rates, and regeneration concerns. The efficacy of the ion-exchange process may be impaired by the presence of suspended particles. In practice, ion exchange is unable to meet the treatment goal, and pre-filtration is required to remove suspended materials that could clog the resin bed mechanically. It also leads to fouling of suspended solids in water and has low efficacy in removing trace levels of contaminants (Zhang *et al.*, 2012).

2.2.3 Chemical Precipitation

This approach entails converting dissolved elements into insoluble solids and then removing them using sedimentation or filtration (Barakat, 2011; Gautam *et al.*, 2016). The most popular method for detoxifying dissolved metal ions from contaminated water sources is chemical precipitation. Metal ions are converted to suspended particles using precipitating chemicals such as calcium hydroxide, ferric chloride, sodium hydroxide, or ferrous sulphate. By settling and/or filtration, the particles that have been formed are removed from the solution (Li *et al.*, 2019).

The precipitation process is straightforward and cost-effective. However, because the method is not adaptable, it is not a feasible choice for wastewater treatment. To decrease heavy metal concentration to a level suitable for disposal, chemical precipitation requires the utilization of many chemicals. Furthermore, the fundamental weakness of chemical precipitation is that it

produces sludge with harmful substances, which must be disposed of in a landfill and this is the European Union's last priority when it comes to waste management policies. Moreover, the generated sludge needs to be disposed of safely. An additional problem with the precipitation treatment approach is that the concentration of the metal ions in the treated wastewater cannot be decreased below the precipitate's solubility. It also changes the pH of water, necessitating pH correction. As a result, alternative approaches like adsorption should be used to safeguard the environment.

2.2.4 Reverse Osmosis

Semi-permeable membranes are used in reverse osmosis to extract heavy metal ions from diluted effluent (Abdi & Kazemi, 2015). In this technique, water molecules are forced through a semi-permeable membrane at increased pressure (Malik *et al.*, 2010). This pressure should be sufficient to counteract osmotic pressure. The pressure needed is determined by the pollutant concentration in the water supplied and to be treated (Rani *et al.*, 2014). The water molecules are allowed to pass through the membrane, however, other pollutants and salts are prohibited and are dumped into the concentrate stream (Dula & Duke, 2019). The reverse osmosis membrane rejects toxins based on sizes and charges. The impurities in the feed water could include ions, particles, colloids, or microorganisms (Wimalawansa, 2013). This process is extremely efficient, produces no waste, and does not necessitate pH balancing or regeneration. However, it comes at a high capital and operating expense, poses a disposal challenge for wastewater containing heavy metal ions, and results in the loss of water. More specifically, membrane treatment of industrial wastewater is confined to a few applications where the membrane's characteristics and environmental resistance are appropriate for the application (Mulopo, 2015).

2.2.5 Membrane Separation Techniques

Pressure, concentration, electrodialysis, electrically driven membrane processes, and temperature-driven membrane processes are all examples of water treatment processes. Reverse osmosis, ultrafiltration, and nanofiltration, as well as high-pressure and low-pressure filtration, are among the processes used. Contaminants including heavy metals, color, and dissolved solids can be removed from wastewater via membrane filtering. This technique's ability to produce solid-free effluents is particularly a unique characteristic. Membrane separation methods also have many advantages, including a small system, low chemical

consumption, and easy operation and maintenance. The membrane separation technology has the disadvantage of inadequate removal of small molecular weight molecules and consumes a lot of energy, notwithstanding the benefits. Membrane fouling, which can develop from the clogging of inorganic and organic elements in the membrane pores, is another constraint of membrane processes. Membrane fouling reduces the rate of treated water production and shortens the membrane life, lowering the economic efficiency of membrane operations.

2.2.6 Coagulation and Flocculation Technologies

Coagulation refers to the process of destabilizing colloids by removing the forces that hold them apart. Cationic coagulants decrease colloids' negative charge (zeta potential) by supplying positive electric charges. Particles collide, as a result, forming huge particles (flocs). Coagulation is always used in conjunction with flocculation to remove particles that sedimentation or filtration alone cannot remove (Mohd *et al.,* 2021). Colloids are small particles with a size of less than one meter. They are accountable for the color and water turbidity due to their poor settling qualities. Clays, metal oxides, proteins, and microorganisms, as well as some organic molecules, are among them. The fact that they all have a negative charge keeps them from aggregating and settling in still water and so this, combined with the colloidal particles' interactions with the water, prevents them from aggregating and settling. Colloids and trivalent ions such as Al(III) and Fe(III), which are present in aluminum and ferric salts can be used as chemical coagulants to aggregate the particles (Dula & Duke, 2019).

These technologies, coagulation, and flocculation are utilized in municipal wastewater purification plants to handle both industrial and treated sewage effluent. The most widespread application, however, is found in the field of potable water purification (Bratby, 2016). However, coagulation and flocculation technologies for water purification have been found to be highly costly when chemicals and sludge disposal are taken into account. As a result, it is vital to develop and employ low-cost alternatives for wastewater treatment (Fabre *et al.,* 2020).

2.2.7 Electrochemical Method

Wastewater is treated electrochemically via electro-deposition, electrooxidation, electro-flotation, and electrocoagulation (Reza & Singh, 2010). The electrochemical procedure for wastewater treatment was developed by mixing sewage and saltwater in a ratio of 3:1 and electrolyzing it to purify the sewage produced onboard ships. The electrochemical method was widely used to treat industrial wastewater such as tannery effluent, distillery effluent, cattle

effluent, olive mills, and textiles effluents. Electrolytic procedures are costly, and they necessitate specialized equipment and upkeep. As a result, the creation of an alternate treatment approach is critical.

Treatment techniques including solvent extraction, complexation, electrodeposition, foam flotation, and cementation can also remove heavy metals, but they have drawbacks such as slow kinetics and insufficient selectivity. However, among these, adsorption technology has emerged as the first line of defense, particularly for contaminants that are resistant to other methods of removal (Sharma *et al.,* 2019; Mohd *et al.,* 2021).

2.2.8 Adsorption Technique

The adsorption technique is the most reliable and appropriate in several purifications, separations, waste treatment processes, and chemical compound recovery, especially in industrial systems. Adsorption is widely replacing almost all the other purification and separation methods attributable to its high efficiency in removing most pollutants from aqueous media (Abd El-Ghany *et al.,* 2023). The other methods have been recognized to be expensive and require high consumption of time, chemicals, and energy, as well as the creation of secondary pollutants (Bayuo *et al.,* 2019). Adsorption is the mass transfer of the contaminant (adsorbate) to be removed from the liquid or gas phases onto a solid (adsorbent) interface where it gets accumulated due to physical and/or chemical interactions as represented in Fig. 4 Hence, adsorption may occur as a result of neither physical nor chemical interactions and it can also involve both interactions. While in physical adsorption the adsorbate molecules form a multilayer on the adsorbent surface, chemical adsorption leads to the formation of a monolayer by the adsorbate molecules as displayed in Fig. 4 (Soliman & Moustafa, 2020).

In adsorption, the high price of commercial adsorbents is recognized as the main hindrance to industrial applications. For instance, considering the economic factors and industrial applications, it is not advisable to employ commercial adsorbents in water and wastewater purification. As a result, the emphasis on heavy metals adsorption is directed toward using natural materials in addition to certain waste products resulting from agricultural and industrial operations, which are abundantly present. Generally, agricultural waste materials have little economic value, are inexpensive, and are available everywhere in large quantities (Hu *et al.,* 2020). Therefore, adsorption using natural and agro-based materials as bio-adsorbents is highly recommended and the main relevance of this technique against conventional water and

wastewater treatment techniques are cost-effectiveness, high efficacy, fewer chemicals consumption, and bio-adsorbent recycling and heavy metal ions retrieval capabilities (Milani *et al.*, 2018; Pan *et al.*, 2020; Tokay & Akpınar, 2021). For instance, studies have shown the effective use of agricultural waste materials including sugarcane bagasse, rice husk, sawdust, coconut husk, oil palm shell, neem bark, jack fruit peel and orange peels, papaya seeds, rice husks, and spent tea in decontaminating heavy metals (Rahdar *et al.*, 2019; Rahman *et al.*, 2023).

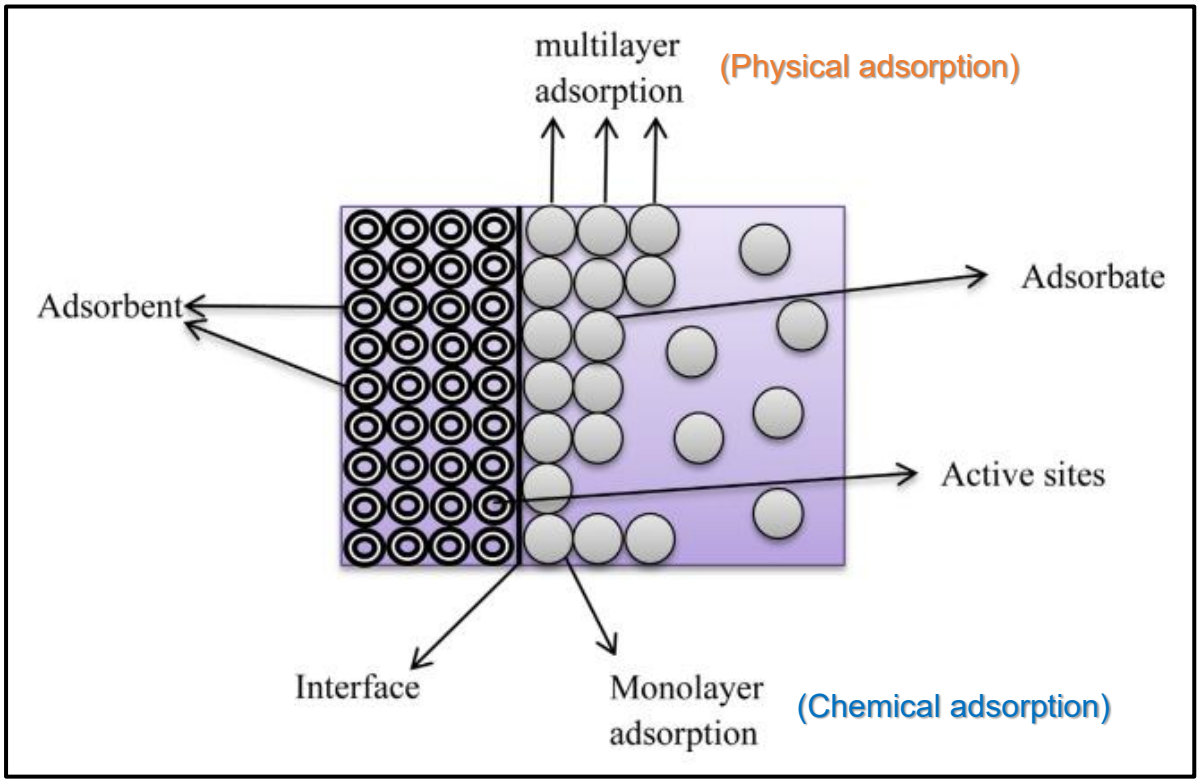

Figure 4: A schematic diagram showing the adsorption of adsorbate molecules on the surface of the adsorbent

Adsorption of heavy metals from aquatic environments by various adsorbents is usually influenced by several independent variables as a function of two dependent variables, which include removal efficiency (%) and uptake capacity (mg/g). Some of these independent influencing variables include contact time, pH of the solution, adsorbent particle size, adsorbent dose, initial metal ion concentration, and temperature.

2.3 Independent Biosorption Affecting Parameters

During the sorption process, many independent factors affect the removal efficiencies and sorption capacities of the prospective adsorbents or biosorbents. Previous studies have affirmed

that the physicochemical characteristics of the solutions, such as contact/shaking time, pH, adsorbent dose, particle size, initial metal ion concentration, agitation/shaking speed, temperature, and interfering ions, have a significant impact on the efficiency of any adsorbent. The adsorbent ability, selectivity, adsorption rate, and the number of heavy metals to be removed are all affected by these process variables. To study the interaction between these independent factors/parameters, a significant number of adsorption studies have been compiled.

2.3.1 Contact/Shaking Time

Heavy metals removal is influenced by the contact/shaking time between the adsorbing material and the aqueous solution. The longer the contact period, the more likely equilibrium has been achieved, and hence adsorption has achieved its optimum (Azadegan *et al.,* 2019). The adsorption process will not be completed successfully if no enough contact time is allowed (Salah, 2015). According to studies, the degree of contaminants removal from wastewater utilizing biomaterials is greater at the start of the remediation phase. This is due to the fact that as the interaction process progresses, the reaction sites become saturated, resulting in a reduced contaminant uptake rate (Rahdar *et al.,* 2019). Adsorbent dosage, contaminant concentration, temperature, and adsorbent surface groups all influence the optimum contact time.

2.3.2 Agitation/Shaking Speed

The adsorption process is also affected by agitation/shaking speed, and heavy metal reduction can be found to be best at a specific speed that must be determined by testing. The adsorption process can be sped up or slowed down by agitation. A faster agitation speed, on the other hand, does not always imply a faster rate of adsorption (Kaakani, 2012). However, according to Dhoble *et al.* (2018), the removal efficacy increases with increasing agitation speed, which could be attributed to more collisions within the adsorbent particles, allowing more active sites on the adsorbent surface to be accessible for the number of metal ions.

2.3.3 pH of the Solution

Adsorption operations are influenced by the pH of the aqueous phase because H^+ and OH^- ions are released into the solution. A higher pH emits more H^+ ions, which may interact with the adsorbent or adsorbate, slowing down the adsorption rate. An alkaline pH solution, on the other hand, produces OH^-, which might react with the adsorbent or adsorbate. The detoxification of heavy metal ions from the aquatic media is mostly influenced by pH. It affects the surface

charge of the adsorbent, ionization degree, and the adsorbate speciation in general (Lenka *et al.,* 2021). As a result, the pH of an aqueous solution being evaluated for its sorption ability has an indisputable effect on the metal ions uptake since, within a particular pH range, the majority of adsorption processes increase with an increase in pH until at a point where an increment leads to a reduction in the adsorption rate. The functional groups on the surface of the adsorbents and the adsorbate aqueous solutions can be linked to the pH dependency on heavy metals uptake (Kumar *et al.,* 2016).

The influence of pH on the elimination of toxic heavy metals in the aqueous systems is critical and the pH effect occurs when heavy metals combine with protons to create hydrogen heavy metals at low pH. Furthermore, at high pH, there is an oversupply of hydroxide ions, which prevents heavy metal ions from diffusing (Bayuo *et al.,* 2019). As a result of the pH of the aqueous solution controlling the adsorbent's surface charge, it shows greater dependence on the decontamination of heavy metals from wastewater.

2.3.4 Adsorbent Particle Size

The adsorbent particle size is one of the critical characteristics that have a significant impact on the adsorbent's adsorptive capacity. The adsorbent removal efficiency and adsorption capacity of the adsorbent vary with particle size; the adsorption capability rate reduces as particle size increases, while it enhances as particle size lowers. The surface area of the adsorbent increases as its size decreases, and a larger surface area indicates a larger active site for adsorption (Memon *et al.,* 2021). At various sizes, the impact of the particle size on the adsorption should be assessed since this type of information aids in the design of a full-scale adsorption system for commercial use.

Apart from adsorption at the adsorbent surface, intra-particle diffusion from the surface of the pores of the adsorbent is a possibility. As a result, bigger particle sizes are more resistant to mass transfer (Ahmaruzzaman, 2011). Due to several inhibitory variables including resistance to mass transfer actions, contact time, and blockage of the diffusional route, the interior adsorbent particle surface area may not be fully exploited, resulting in a lower adsorption capacity. Regardless, the adsorption efficiency is mostly determined by the availability of the surface area for the adsorbate interactions (Emenike *et al.,* 2016).

2.3.5 Adsorbent Dosage

The adsorbent weight determines the adsorbent's ability for a particular adsorbate concentration. As more active adsorption sites are provided by increasing the dosage of the adsorbent, more contaminants are removed from the aqueous phases. This could be due to enhanced surface and pore volume accessibility at higher dosages, as well as a larger surface area (Pyrzynska, 2019). Increasing the surface area of the adsorbent is one technique to reduce the amount of adsorbent to be used in removing the adsorbate. This can be accomplished by utilizing adsorbents with very small dimensions. As larger surface areas are more effective at adsorption, the same adsorbent may need fewer dosages once processed than its bigger counterpart (Baby *et al.,* 2018). However, with the unsaturation of the available sorption sites generated by large adsorbent dosages and the adsorbate interactions, the adsorption density usually drops (Mbugua *et al.,* 2014).

2.3.6 Heavy Metal Ion Concentration

The initial concentration of heavy metal ions can change the removal efficiency and adsorption capacity due to a range of factors such as the availability of specific surface functional groups and the ability of these surface functional groups to entangle heavy metal ions from aquatic environments. The solution of the initial metal ion concentration can act as an influential driving force in overcoming the resistivity of mass transfer between the liquid and solid phases (Jjagwe *et al.,* 2021). By increasing the initial metal ion concentration in the aqueous environment, the adsorbent capacity is quickly depleted. This is because the number of accessible adsorption sites for a given dose of the adsorbent is restricted, and at high concentrations, they become saturated (Zhao *et al.,* 2020). The better the adsorption rate, the lower the metal ion concentration, as there is less adsorbate for the adsorbent to extract (Afroze & Sen, 2018). Some adsorbents, on the other hand, behave exceptionally well at high initial adsorbate concentrations, and so have a higher adsorption capacity. Due to their adsorption capacity, these adsorbents are advantageous (Kaakani, 2012).

More so, the initial concentration is one of the ways through which heavy metal ion mobility to the adsorbent's surface might be aided (Sahmoune *et al.,* 2011; Taha *et al.,* 2011). To examine the impact of baseline concentration on heavy metal adsorption utilizing agricultural adsorbents, a large number of experiments have been undertaken and reported. The interaction between optimum adsorption capacity and baseline concentration of heavy metal ions has been

established as a general trend. With rising initial concentration, the trends suggested increasing heavy metal ions uptake capacity (Liu *et al.*, 2018; Khan *et al.*, 2019; Xia *et al.*, 2020).

2.3.7 Temperature

Adsorption is temperature-dependent, and it can alter the adsorption system making it endothermic or exothermic in nature (Iftekhar *et al.*, 2018). A large number of biosorption studies on the influence of temperature on heavy metals removal have been conducted. Not only does temperature affect the solubility of metals, but it also affects the rate of diffusion (Mohubedu *et al.*, 2019). As a result of the diverse functional groups on the surfaces of agricultural adsorbents, temperature is recognized as an essential factor in heavy metals adsorption (Emenike *et al.*, 2016; Soliman & Moustafa, 2020).

Due to the generation of new adsorption sites on the surface of the adsorbent, raising the temperature of the solution improves the uptake capacity of heavy metal ions and increases the kinetic energy of the adsorption system (Lenka *et al.*, 2021). Nonetheless, according to Park *et al.* (2014), the increase in temperature can cause physical deformation of the adsorbent. As a result, in many adsorption experiments, ambient temperature is commonly used.

2.3.8 Interfering Ions

Anions such as carbonates, chlorides, nitrates, phosphates, and bicarbonates, as well as heavy metals, may be present in aqueous systems. The concentration of these ions varies by geographical region and can influence contaminant sorption on the adsorbent (Foroutan *et al.*, 2019). The order of heavy metals removal interference is given as $HCO_3^- > SO_4^{2-} > Cl^-$ for the various biosorbents. In most studies, heavy metals uptake was not reduced by chloride, sulphate, or nitrate ions, but bicarbonate significantly reduced heavy metals take-up. This is attributed to the ability of the bicarbonate to compete with heavy metal ions for active sites on the adsorbents (Kanaujia *et al.*, 2015). In general, the adsorption rate is inversely related to the aqueous system ionic potential. As the ionic strength increased, the adsorbents' ability to absorb metal ions declined. This could be due to an upsurge in the concentration of the competitive cations in the aqueous solution, which affects metal ion activity (He *et al.*, 2018). Real wastewater comprises diverse metal ions, not just only heavy metals. For instance, the common metal ions found in real wastewater include Na^+, K^+, $Mg^{2+,}$ and Ca^{2+} but chemical compounds such as KCl, $CaCl_2$, $MgCl_2$, and $NaNO_3$ are usually introduced into synthetic wastewater to investigate the effect of ionic potential in competitive heavy metals sequestration.

2.4 Application of Conventional Adsorbents in Heavy Metals Decontamination

Earlier adsorbents used for heavy metal ions removal were commercial adsorbents and have been used globally and extensively for controlling water contamination. In literature, the commonly utilized conventional adsorbents are activated carbons, ion-exchange resins (polymeric organic resins), and inorganic materials such as activated alumina, silica gel, zeolites, and molecular sieves. However, only four types of generic adsorbents have enormous surface areas and have dominated the commercial use of adsorption: activated carbons > zeolites > silica gel > activated aluminas (Crini *et al.*, 2019).

Silica gel is worldwide recognized as an inorganic polymer that is used in chromatographic columns. Its high porous surface topology and enormous specific surface area are key for effective metal ions interaction. In furtherance, silica gel is easily available as a substrate for immobilizing various chemical functional groups (Li *et al.*, 2019). Several silicate-derived gels have been explored to extract, stabilize, and/or decontaminate arsenic and other heavy metal ions from water and wastewater (Li *et al.*, 2020). Due to its strong physical strength, endurance, and high chemical stability, silica gel has been utilized in the sequestration of certain contaminants including solid wastes (El-Moselhy *et al.*, 2017; Li *et al.*, 2020). El-Moselhy *et al.* (2017) were successful in developing hydrated iron oxide nanoparticles using a silicate matrix, resulting in high arsenic detoxification. Mesoporous silica materials of MCM-41 type were efficiently utilized by Zhu *et al.* (2017) in the removal of Cu(II), Pb(II), and Cd(II) from aqueous solutions. More so, a silica gel material modified with nitrilotriacetic acid (NTA-silica gel) was applied for the elimination of Cu(II), Cd(II), and Pb(II) from the aqueous system, which indicates high removal efficiency of the three heavy metal ions (Li *et al.*, 2019). Furthermore, silica gel polymer was proven to be effective in Ni(II) removal from aqueous solution (He *et al.*, 2017).

Zeolites are micro-porous crystal-like solids with definite structures and are naturally-occurring materials comprising hydrated aluminosilicate with maximum cation exchangeability with metal ions (Chmielewská, 2019). Zeolite has a highly porous structure in three-dimensional crystal lattices that display strong cation interaction and ion exchange ability with heavy metal ions (Flores *et al.*, 2017). Due to their high porosity and sieving characteristics, zeolites are a good choice for removing heavy metal ions from untreated wastewater. They also have a high ion exchange ability, and the exchangeable ions (Na^+, Ca^{2+}, and K^+ ions) are largely harmless (Obaid *et al.*, 2018). Based on their quick advancements in

properties, zeolites are gaining in popularity and are being used in a variety of innovative applications. Biomedical, radioprotection, wastewater purification, biosensor, pure, and applied chemical applications are all driving interest in them.

When using zeolites in sorption, the surface area is not a matter of concern because it is a selective process and it is reversible (Singh & Kaushal, 2013). Zeolites are used practically in the fuel industries as water softeners, the manufacture of detergents, catalysts, and molecular sieves. Quite a lot of zeolites have been employed as adsorbents for the treatment of contaminants in water and wastewater. A zeolite produced from fly ash was capable of decontaminating Hg(II) and Pb(II) ions from aqueous media (Kobayashi *et al.*, 2020). Chen *et al.* (2020) designed and prepared zeolite cotton as a form of filter for household water treatment. More so, zeolite composite adsorbents were applied to simultaneously detoxify heavy metals and total coliforms from wastewater (Fanta *et al.,* 2019). A high-quality zeolite type A was produced and utilized successfully in removing heavy metals from water systems (Meng *et al.,* 2017). Besides, zeolite-alginate composites were found to be promising in the Pb(II) removal from contaminated water solutions (Kragović *et al.,* 2018). Makki (2014) employed zeolite A4 for Cd(II) and Pb(II) decontamination in water. Also, Cu(II), Ni(II), and Pb(II) ions in an acid mine drainage were removed using Philippine natural zeolite (Olegario-Sanchez & Pelicano, 2017).

Activated alumina is one of the most extensively utilized adsorbents for heavy metal sequestration due to its high affinity for metal ions (Deravanesiyan *et al.,* 2015). It consists of porous aluminum oxide with a wide surface area that is resilient to thermal stress and abrasion. It does not swell, shrink, soften, or disintegrate throughout the adsorption process *(Mondal et al.,* 2016). Furthermore, activated alumina has outstanding adsorption capabilities and a high ion uptake capacity, as well as being cost-effective, safe, and ecologically friendly, making it suitable for use in wastewater treatment (Wang *et al.,* 2019). Activated alumina has a good surface area and is frequently applied to get rid of oxygenates and mercaptans of hydrocarbons and especially, fluorides in water (Ahamad *et al.,* 2018).

A nano-alumina was produced and used effectively in As(V) decontamination from an aqueous solution (Prabhakar & Samadder, 2020). Also, novel γ-alumina nanoparticles were developed for Ni(II) decontamination from the solvent phase and found proficient (Agarwal *et al.,* 2016). In a study, a mesoporous carbon stabilized alumina was employed in removing Cd(II) and Pb(II) ions from aqueous media (Yang *et al.,* 2016). Besides, an alumina composite was shown to be

effective in the removal of both Cr(VI) and methylene blue from aqueous solutions (Kunde *et al.*, 2019).

Globally, the elimination of noxious pollutants in water has been attributed to activated carbons. The well-known and lasting adsorbent in water and wastewater treatment is charcoal. The preparation of activated charcoal involves three stages; dehydration, carbonization, and activation. Due to the high surface area of activated carbons, they are highly recognized and recommended as proficient adsorbents for water contaminants treatment and gas purification (Zaimee *et al.*, 2021). Activated carbons are black and made up of solid carbonaceous materials with high porosity, internal surface area, and mechanical strength. Granular activated carbon, powdered activated carbon, and activated carbon cloth are among the different forms of activated carbon used to remove contaminants from water and wastewater (Chai *et al.*, 2021). The constant utilization of activated carbons has produced fruitful outcomes in contaminant management processes (Crini *et al.*, 2019). Hu *et al.* (2013) report the applicability of humic acid-impregnated activated carbon in removing Cu(II). Meanwhile, Jjagwe *et al.* (2021b) previously reviewed the synthesis and application of granular activated carbon from biomass waste materials for water treatment. Besides, Manjuladevi *et al.* (2018) investigated Cr(VI), Ni(II), Cd(II), and Pb(II) ions removal from aqueous solutions using activated carbon prepared from Cucumis melo peel. Fan and Anderson (2005) carried out a related study using granulated activated carbon to eradicate Cu(II) and Cd(II). Also, activated carbon has been applied in the decontamination of Cd(II) and Ni(II) as well as Pb(II), Hg(II), and As(III) as reported by many studies (Herrera-Barros *et al.*, 2018; Alghamdi *et al.*, 2019; Liu *et al.*, 2020; Sagharloo *et al.*, 2021).

Regardless of the capabilities and prolific application of commercial activated carbons, there are some constraints on usage attributable to their high cost. For that reason, attention has been directed towards the preparation and production of cost-effective adsorbents from natural materials that are readily available, carbonaceous, and easy to activate (Zhang *et al.*, 2020). To produce activated carbon, an organic material undergoes thermal degradation for subsequent decomposition into carbon granules (Jjagwe *et al.*, 2021).

2.5 Application of Agricultural Waste Materials in Heavy Metals Removal

Commercially activated carbons are expensive adsorbents regardless of their widespread use in water and wastewater treatments. This has generated an increased interest in the production

of safe, cheap, and economical adsorbents, which are more economical than commercially available activated carbon aimed at removing heavy metals from polluted resources (Liu *et al.*, 2020; Bayuo, 2021). Natural and waste materials from agriculture and industries are extensively being modified and converted into activated carbons aimed at heavy metals cleansing from wastewater (Zhang *et al.*, 2020). For instance, Fig. 5 demonstrates the application of activated carbons as adsorbents derived from agricultural wastes for water and wastewater treatment (Heidarinejad *et al.*, 2020).

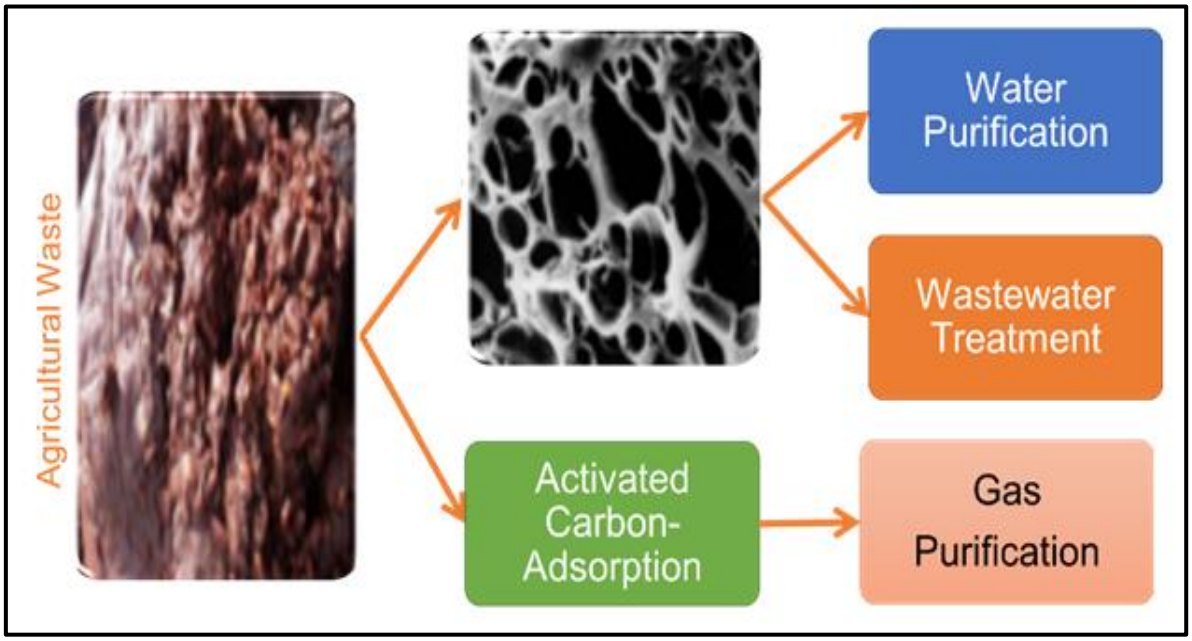

Figure 5: Application of activated carbon derived from biomass for environmental remediation

Activated carbon should have a wide capability, a fast rate of adsorption, be easy to regenerate or retrieve from water, have high porosity, and have a small pore diameter because adsorption ability is proportional to the amount of surface area available (Abegunde *et al.*, 2020). Typical adsorption properties of these sorbent materials are derived from polymer complexes such as lignin, simple sugars, hemicellulose, proteins, lipids, and starch with diverse functional groups (Alalwan *et al.*, 2020). These constituents play a vital role in the adsorption of heavy metal ions as they can form complexes and chelates with heavy metal ions. They are capable of replacing hydrogen ions with hazardous heavy metal ions dissolved in the aqueous media or donating a pair of an electrons to bind metal ions (Amar *et al.*, 2020).

The functional groups that are present in agricultural wastes include carbonyl, acetamido, phenolic, amido, carboxyl, amino, alcohols, esters, and sulphydryl (Baby *et al.*, 2019). It is

these groups, which possess an affinity for complexation with metals. During adsorption studies, various studies have confirmed the existence of functional groups and the binding ability of these groups with metal ions through spectroscopy analysis (Bayuo *et al.*, 2019; Parlayici & Pehlivan, 2019; Banchhor *et al.*, 2021).

Toxic heavy metals elimination by dint of low-cost biosorbents is regarded as more promising and cost-effective since there are numerous natural resources available locally and plentifully, that could be used as low-cost biosorbents (Dhiman, 2021). The development of agro-based materials into less expensive biosorbents is well acknowledged as a prospective and economical for the treatment of pollutants in water. The sources of agro-based biosorbents are presented in Fig. 6.

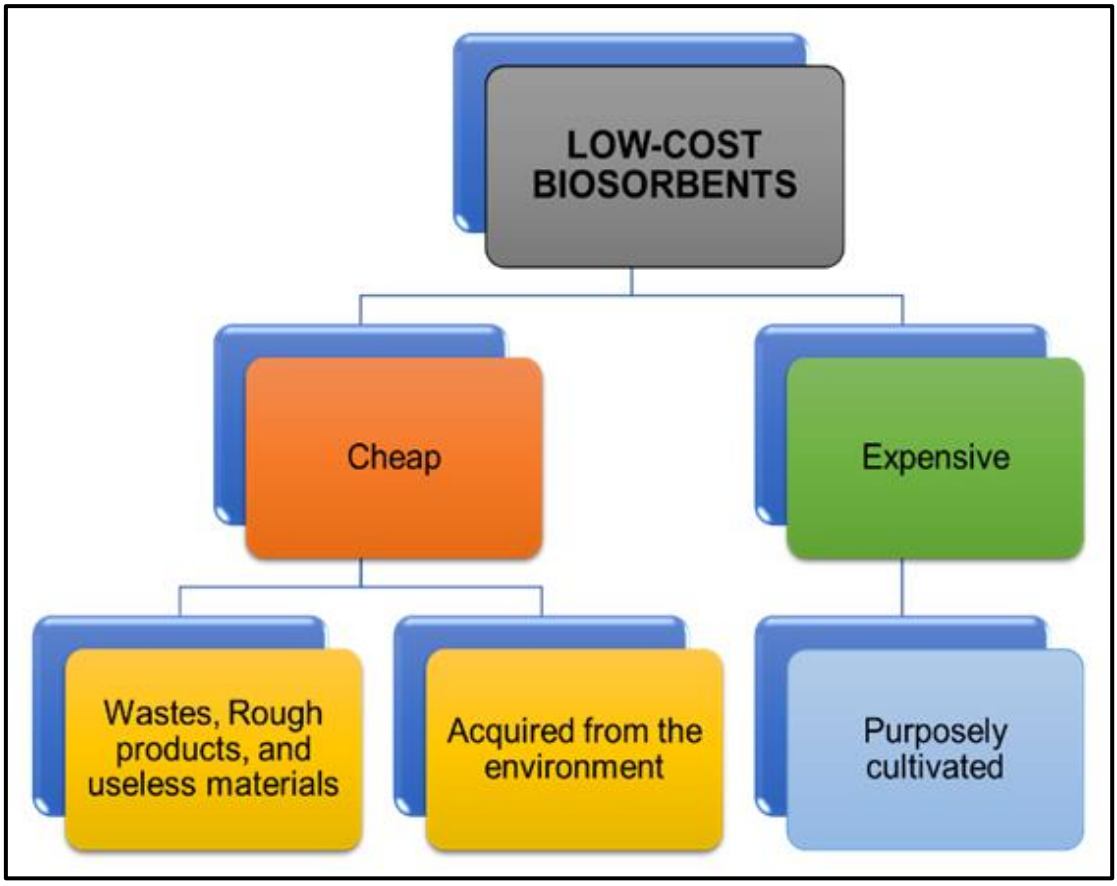

Figure 6: Different sources of agro-based biosorbents for adsorptive removal of heavy metals from aquatic environments

The increasing number of studies and publications on the adsorption-desorption process as shown in Fig. 7 using low-cost adsorbents conclude and recommend the increasing interest in the search for more low-cost adsorbents that are suitable for removing various pollutants from aqueous media. As a result, several studies have reported the uses of agro-based adsorbents in

eliminating heavy metals from water, wastewater, or effluents. Some of these studies are summarized in Table 2.

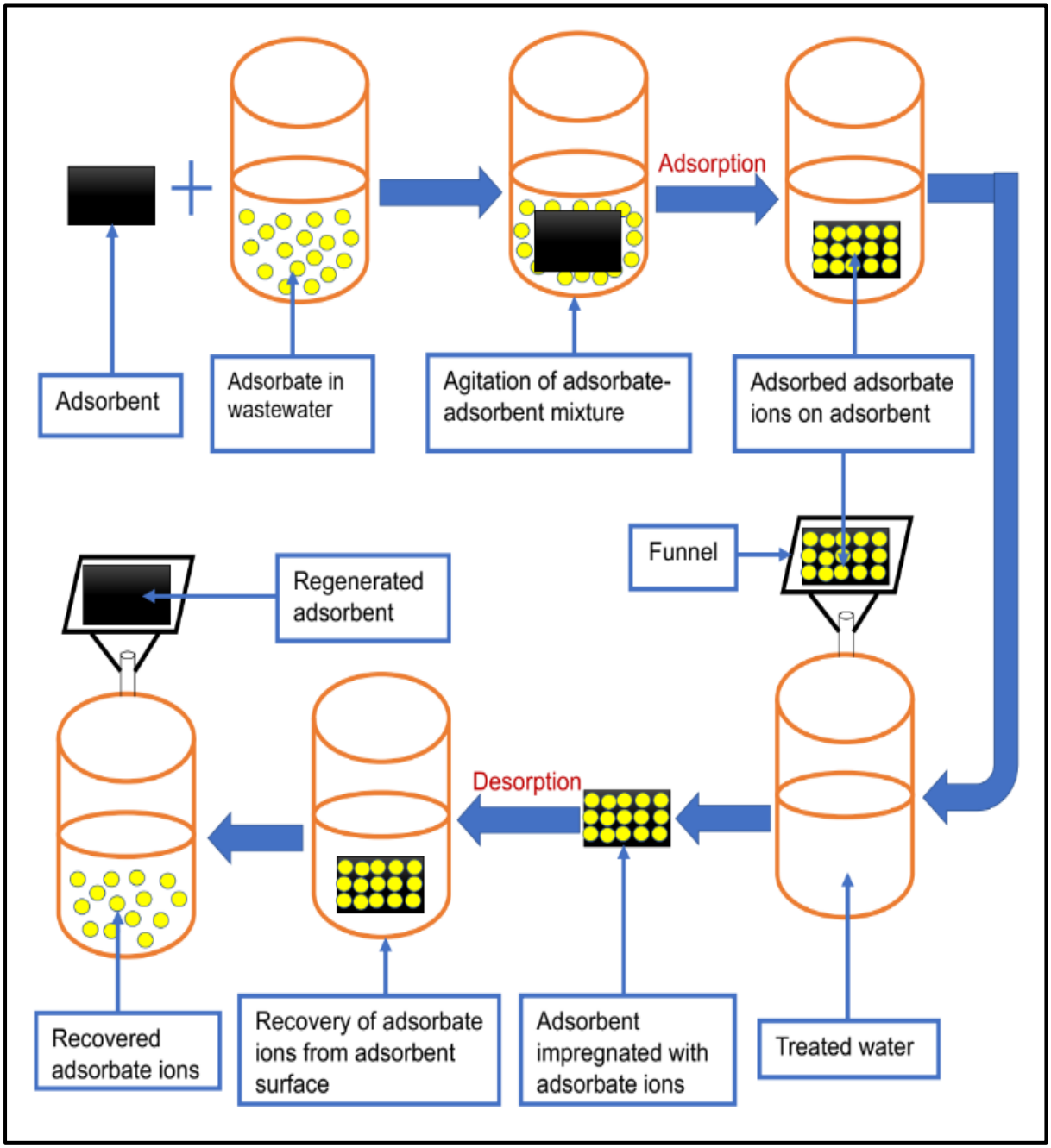

Figure 7: **A schematic diagram showing the adsorption-desorption process of heavy metals using non-conventional adsorbents derived from natural, agricultural, and industrial waste materials**

Table 2: Agricultural waste biosorbents for heavy metal ions sequestration

Bioadsorbent	Heavy metal	Removal efficiency (%)	Reference
Groundnut shell	Cr(VI) and Pb(II)	87.60 and 96.61	Bayuo *et al.* (2019a), Bayuo *et al.* (2018)
Shea fruit biomass	Cd(II)	76.86	Bayuo (2021)
Banana peels	Cu(II) and Pb(II)	99.79 and 88.94	Afolabi *et al.* (2021)
Spent tea leaves	As(V)	87.00	Dakhil *et al.* (2021)
Olive Stones	Cd(II), Cu(II), Pb(II) and Cr(VI)	77.40, 80.50, and 94.50	Amar *et al.* (2020)
Sunflower waste carbon	Cd(II)	99.80	Jain *et al.* (2021)
Saccharomyces cerevisiae	As(III) and As(V)	66.20 and 15.80	Hadiani *et al.* (2019)
Sugarcane bagasse	Hg(II)	61.00	Javidi & Esfandiari (2019)
Rice straw	As(V)	69.60	Mustapha *et al.* (2019)
Spent tea leaves	Cr(III)	95.42	Nur-E-Alam *et al.* (2018)
Bagasse biochar	Pb(II)	75.37	Poonam *et al.* (2018)
Corn and rice husks	Pb(II)	> 90.00	Rwiza *et al.* (2018)
Rice husk ash	Pb(II)	75.00	Chidozie *et al.* (2017)
Mung bean husk	As(V)	98.75	Mondal *et al.* (2017)
Typha angustifolia and *Salix matsudana* branches	Cd(II) and Pb(II)	90.00	Tang *et al.* (2017)
Mustard waste	Pb(II), Zn(II), and Cd(II)	94.56, 96.15 and 76.48	Nemeş & Bulgariu (2016)
Banana peel	Cd(II) and Pb(II)	93.2 and 83.78	Motaghi & Ziarati (2016)

2.6 Adsorption Isotherm and Kinetic Modeling

Adsorption isotherm describes how much adsorbate is adsorbed per unit weight of the sorbent material as a function of the equilibrium amount of the adsorbate in the bulk aqueous phase at constant temperature (Khan & Imteaz 2021). Therefore, the adsorption isotherms explain how the molecules of the adsorbate are distributed in the aqueous and solid phases when the sorption system reaches equilibrium (Farnane *et al.*, 2018). Thus, adsorption isotherms are crucial in determining the interactive behavior between the adsorbate molecules and the adsorbent material and help maximize the efficiency of sorbent material.

In addition to providing comprehensive insights on the uptake capacity of the investigated sorbent material, adsorption isotherm has a significant role in predicting the adsorption mechanisms (Mukherjee *et al.*, 2021). Also, the surface characteristics of the sorbent material, selectivity and affinity of adsorbate molecules for adsorption sites, and description of equilibrium sorption data are all frequently explained using isotherm models (Babapoor *et al.*, 2022). When the adsorption and desorption rates are the same, the dynamic equilibrium sorption is said to be established. To reach the sorption equilibrium, the concentration of adsorbate molecules at the sorbent interface must be in dynamic equilibrium with the concentration of the adsorbate molecules in the solute phase, and every active site on the sorbent material has the potential to interact with the molecules of the adsorbate.

The most common equilibrium models used to comprehend the mechanism of heavy metals adsorption include the Langmuir, Dubinin-Radushkevich (D-R), Freundlich, Temkin, Sips, and Redlich-Peterson isotherm models. The assumptions of the various adsorption isotherm models including their non-linearized equations are summarized in Table 3.

Table 3: Heavy metals adsorption isotherm models

Isotherm model	Isotherm model assumptions	Equation	Notation	Reference
Langmuir	Following the Langmuir model, the adsorbate accumulation can only take place at a limited number of discrete localized active sites on the adsorbent surfaces, which is homogeneous in nature leading to the occurrence of monolayer adsorption.	$q_e = \frac{q_{max} K_L C_e}{(1 + K_L C_e)}$	$\mathbf{K_L}$**:** Net adsorption enthalpy $\mathbf{q_e}$**:** Equilibrium uptake capacity $\mathbf{q_{max}}$**:** Maximum uptake capacity $\boldsymbol{C_e}$**:** Concentration at equilibrium	Wahid *et al*. (2022)
Freundlich	The Freundlich model presumes that the sequestration of heavy metals took place on the heterogeneous surface of the adsorbent leading to multi-layer adsorption. As the initial heavy metal ion concentration upsurges, more ions are adsorbed by the sorbent. The surface heterogeneity indicator is $\frac{1}{n}$ and the adsorbent surface becomes increasingly heterogeneous as $\frac{1}{n} \approx 0$. While favorable multilayer adsorption is achieved when n exceeds 1 ($n > 1$).	$\mathrm{q_e} = \mathrm{K_F C_e}^{\frac{1}{\mathrm{n}}}$	$\mathbf{K_F}$**:** Sorption capacity $\boldsymbol{n}$**:** Sorption intensity	Bayuo (2021)
Dubinin- Radushkevich (D-R)	The D-R model is analogous to the Langmuir model. However, this model assumes that the adsorptive elimination of heavy metal ions could take place on both heterogeneous and homogeneous surfaces of the adsorbent. The Dubinin-Radushkevich isotherm model is usually employed to identify the nature of heavy metal adsorption as being either physisorption or chemisorption.	$\mathrm{q_{e=}\ q_s \exp\left(-K_{DR}\mathcal{E}^2\right)}$	$\mathbf{q_s}$: Uptake capacity $\mathbf{K_{DR}}$: D-R constant $\boldsymbol{\mathcal{E}}$**:** Polanyi Potential	Alam *et al.* (2018)
Temkin	The Temkin isotherm model takes into consideration the interactive behavior between the adsorbent surface and heavy metal ions in the aqueous solutions as well as the non-uniform distribution of the adsorption heat.	$\mathrm{q_e} = \frac{\mathrm{RT}}{\mathrm{b}} \ln \mathrm{AC_e}$	$\boldsymbol{b}$ and $\boldsymbol{A}$: Temkin's constants **T:** Absolute temperature $\boldsymbol{R}$: Gas constant	Mohdee *et al.* (2018)

The efficiency and industrial applications of various sorbent materials in heavy metals as well as other contaminants removal from water systems required careful consideration of the process design, operational control, and sorption kinetics. This is because sorption kinetics is essential in providing knowledge about the adsorption mechanisms of various heavy metals, which is essential for the viability of the process (Nazerdeylami & Zare-Dorabei, 2019). The reaction time experimental data are employed to determine the rate-controlling step during the sorption process (Rahman *et al.*, 2021). Several adsorption kinetic models might be applied to analyze the sorption data obtained by a particular sorbent material during the adsorptive decontamination of heavy metals from aqueous media to explain the sorption mechanism and the rate-limiting step.

Generally, sorption in porous adsorbents is normally modeled using adsorption kinetic models. In the adsorption kinetic modeling, it is assumed that the rate of adsorption on an active site of the sorbent material is the rate-controlling step and this rate can be described by the three most common models including the pseudo-first-order, pseudo-second-order, and Elovich's kinetic models. As summarized in Table 4, the kinetic models are normally applied to study the adsorption of heavy metals removal from sorption systems and quantify the uptake capacity of the sorbent material (Velusamy *et al.*, 2021). However, neither the pseudo-first-order reaction nor the pseudo-second-order reaction explains the diffusion of the adsorbate molecules into the sorbent material. Therefore, adsorption mechanisms cannot be concluded without the investigation of the intraparticle diffusion model (Ajiboye *et al.*, 2021).

Table 4: Adsorption kinetic models

Kinetic model	Model description	Equation	Notation	Reference
Pseudo-first-order	This kinetic model presumes that the sequestration of adsorbates from sorption systems onto the adsorbent surface is reversible at equilibrium. Hence, this model describes the physisorption of various adsorbates onto the surface of the adsorbent for which diffusion is the rate-controlling step.	$\frac{dq_t}{dt} = k_{p_1}(q_e - q_t)$	$\mathbf{k_{p_1}}$**:** Pseudo-first-order rate constant **t:** Time $\mathbf{q_t}$**:** Adsorption capacity at a specific time	Ahmed *et al.* (2020)
Pseudo-second-order	This model assumes that during the adsorptive decontamination of adsorbates from aqueous media, electrons are shared between the adsorbates and the surface functional groups of the sorbent. The sharing of these electrons between the adsorbate molecules and the functional groups on the sorbent surface leads to the formation of a chemical bond, in which chemisorption is the rate-controlling step.	$\frac{dq_t}{dt} = k_{p_2}(q_e - q_t)^2$	$\mathbf{k_{p_2}}$: Pseudo-second-order rate constant	Memon *et al.* (2021)
Elovich	The Elovich kinetic model assumes a chemical reaction between the adsorbate molecules in the water systems and the sorbent surface functional groups.	$\frac{dq_t}{dt} = \alpha\exp(-\beta q_t)$	**α:** Initial rate of adsorption **β:** Constant of desorption	Labied *et al.* (2018)
Intra-particle diffusion	The adsorption mechanism of adsorbate molecules on the adsorbent surface is explained by the intra-particle diffusion model. The rate-controlling step is intra-particle diffusion if the graph between q_t and $t^{½}$ shows a straight line. Also, for the intra-particle diffusion to be the only rate-controlling step, the plot must pass through the origin.	$q_t = k_{id}t^{½} + C$	$\boldsymbol{k_{id}}$**:** Intra-particle diffusion constant **C:** Intercept	Olu *et al.* (2014)

The determination of an appropriate model among the various models presented in Tables 3 and 4 requires analyzing isothermal and kinetic data by fitting them to the different types of models. Generally, in selecting the best-fit adsorption isotherm and kinetic models, the coefficient of determination (R^2) and error functions such as sum square error, hybrid fractional error, the sum of absolute error, average relative error, the standard deviation of relative error, nonlinear chi-square value, and the sum of normalized errors are the most important parameters to take into consideration. When the coefficient of determination is close to unity and the smaller the error function values, the attained sorption data would be more compatible with the investigated adsorption isotherm and kinetic models (Shahrin *et al.*, 2018; Ameri *et al.*, 2020).

2.7 Optimization of Heavy Metal Removal by Central Composite Design of Response Surface Methodology

Over the years, one variable at a time is applied to track the influence of the operating factors on the adsorption of heavy metals onto sorbent materials. This method necessitates a large number of experiments, and it also fails to highlight the interactive behavior of the process factors (Karmaker *et al.*, 2021). Furthermore, when dealing with a high number of variables, this technique is time-consuming and costly (Cheng *et al.*, 2021). To overcome these limitations in terms of adsorption system scale-up, statistical analysis has various advantages, for instance, higher reliability and quicker than traditional methods, allowing us to better appreciate the interactions between the adsorbates and adsorbents and decreasing the total number of experiments required. Using the statistical design of experiments in the formulation of adsorption processes could lead to improved cleanup efficiency, lower process variability, and lower overall expenses in wastewater treatment (Çiçek *et al.*, 2012).

The Response Surface Methodology (RSM) is one of the applications of the Design of Experiments (DOE), which is a set of mathematical and statistical tools for designing, enhancing, and optimizing processes. It may be applied in assessing the relative importance of several influencing variables (Aslani *et al.*, 2018). This method can also be used to analyze studies in which one or more independent factors are influenced by a wide range of factors, with the goal of optimizing the responses. To attain the highest adsorption capacity and removal efficiency, the process factors must be optimized. Aside from lowering the number of adsorption tests, one of the benefits of this strategy is the ability to provide a mathematical correlation between the independent and dependent factors (Sagharloo *et al.*, 2021). In addition, this procedure allows users to study the effect of independent variables in relation to the

numerical variables (responses), and it allows them to collect vast volumes of data from a small number of tests (Jamileh *et al.*, 2020).

Several studies have been conducted on the removal of heavy metals from wastewater and the applicability of the RSM in optimizing the independent factors affecting the adsorption process of these heavy metals. For instance, the influence of the experimental variables on the competitive sorption of Ni(II) and Cu(II) ions by activated carbon derived from sewage sludge was evaluated using the CCD of the RSM (Khelifi *et al.*, 2022). The optimum Ni(II) concentration, Cu(II) concentration, adsorbent dose, contact time, and temperature were found to be 40.00 mg/L, 40.00 mg/L, 4.00 g/L, 100.00 min, and 30.00°C. The maximal adsorption rate of 7.48 and 4.04 mg/g for Ni(II) and Cu(II) ions, respectively was achieved under this optimized condition. In this study, aqueous solutions of Ni(II) and Cu(II) were used and no kinetics and thermodynamics adsorption were studied, which could have provided more insight into the adsorption behavior of these metal ions. Although desorption and regeneration studies were not conducted, it was concluded that the prepared activated carbon has the potential for Ni(II) and Cu(II) ions removal from aqueous solutions for environmental cleaning purposes.

Also, the expulsion of Ni(II) and Cu(II) from wastewater was tested by biochar-biopolymeric hybrid adsorbents by employing the CCD-RSM approach (Biswas *et al.*, 2019). At the optimized condition, Cu(II) maximal reduction capacity (47.05 mg/g) was obtained at baseline concentration of 84.80 mg/L, 1.40 g/L adsorbent dose, and temperature of 308.90 K, whereas Ni(II) uptake capacity (28.06 mg/g) was found at an initial concentration of 84.80 mg/L, adsorbent dose of 1.48 g/L, and temperature of 313.00 K. The Langmuir and pseudo-second-order models well explain the equilibrium and kinetic data, respectively. The process occurred endothermically and spontaneously, by the thermodynamic analyses. The recovery and reusability of the used adsorbent were not examined although the study concludes that the adsorbent is very prudent and demonstrates an excellent Ni(II) and Cu(II) ions removal.

In a study, Pb(II) and Cd(II) were removed from aqueous systems using an alumina-modified onion skin (AMOS) composite (Yusuff *et al.*, 2021). The CCD-RSM was utilized to optimize Pb(II) and Cd(II) removal onto AMOS, and the obtained best condition was Pb(II) and Cd(II) initial concentration of 200.00 mg/L, adsorbent dose of 1.20 g/L, and 75.59 min time of contact, with 92.05% and 94.89% removal efficiencies for Pb(II) and Cd(II), respectively. The Langmuir model gave the best fit to the equilibrium data with monolayer adsorption capacities of 9.74 mg/g and 14.17 mg/g for Pb(II) and Cd(II), respectively. The pseudo-second-order

model explains the adsorption data better. The desorption and regeneration of the exhausted adsorbent were studied and the reusability results suggest that AMOS is proficient and could be used and recycled in the wastewater treatment system. However, the thermodynamics parameters (Gibbs free energy, enthalpy, and entropy changes), which could have described the sorption characteristics of these heavy metals were not reported.

Furthermore more, the CCD of the RSM was being applied to study the reduction of Cd(II) and Pb(II) ions from effluents onto cow bone composite (Abdulrahman *et al.*, 2019). The ideal condition was achieved at a pH of 4.00, agitation speed of 50.00 rpm, 24.00 h time of shaking, particle size of 1.00 mm, and adsorbent dose of 12.50 g/L. The experimental results suited well to the Langmuir and Freundlich models for Cd(II) and Pb(II), respectively. Desorption and regeneration experiments were performed to make the sorption process more cost-effective. The eluting ability of Cd(II) and Pb(II) was realized as 88.00% and 84.00%, respectively. The thermodynamics parameters (Gibbs free energy, enthalpy, and entropy changes) were not reported so how the adsorptive removal of Cd(II) and Pb(II) have proceeded is not known.

The influence of the initial Pb(II) concentration, solution pH, and temperature on the fraction of Pb(II) adsorbed by phosphogypsum (PG) was studied (Lamzougui *et al.*, 2021). The experimental design approach was used to model the adsorption tests, and the CCD of the RSM was used to optimize the parameters. The findings reveal that the amount of Pb(II) removed upsurges with the initial Pb(II) concentration and reduces as the pH and temperature of the solution rise. At Pb(II) initial concentration of 109.64 mg/L, 5.25 pH, and 70.00^0C temperature, the optimal adsorption capacity of Pb(II) on the PG was attained. The kinetic data shows good representation with the pseudo-second-order model and it was discovered from the thermodynamic studies that the adsorption process was exothermic and spontaneous. In this study, the equilibrium isotherms were not investigated and so how well the adsorbate interacted with the adsorbent in the aqueous systems is not known. In addition, there is no information on the desorption, regeneration, and reusability of the used adsorbent. Yet, it was concluded that PG will be an effective adsorbent for Pb(II) sequestration from aqueous solutions since it is of low cost.

Similarly, Pb(II) was removed by two low-cost industrial products of ground granulated blast-furnace slag (GGBFS) and phosphorus slag (PS) (Shafaghat & Ghaemi, 2021). To compare the efficacy of both adsorbents in removing Pb(II) from an aqueous phase, the RSM based on the CCD approach was used. The initial Pb(II) concentration, rotation rate, and adsorbent weight

were all taken into account in the experimental design. The optimum adsorption capacity (6.41 mg/g) was determined using RSM models at the adsorbent weight (0.10 g/L), initial Pb(II) concentration (100.00 mg/L), and rotation rate (195.00 rpm). In this study, the adsorption equilibrium isotherms, kinetics, and thermodynamics were not conducted hence, the mechanism of Pb(II) decontamination by the adsorbents is not discussed. More so, there is no information on the desorption of the adsorbed ions and regeneration of the depleted adsorbents for reuse but the study indicates that GGBFS was more efficacious than PS adsorbent in removing Pb(II) under the same operating conditions.

Also, CCD of the RSM was applied in modeling batch experiments and optimized the impact of solution pH, contact time, adsorbent dosage, and initial concentration on Pb(II) decontamination by peanut hull-g-methyl methacrylate biopolymer (PH-g-MMA) (Chaduka *et al.*, 2020). The best condition for Pb(II) removal was achieved at 5.70 pH, 63.75 min time of contact, adsorbent dose of 4.50 g/L, and 76.25 mg/L Pb(II) initial concentration. Under this ideal condition, 99.30% of the Pb(II) in the aqueous media was extracted. The isothermal and kinetics analysis show that the experimental results matched well with the Langmuir and pseudo-second-order models, which describe the process as being chemisorptive. The thermodynamics parameters (Gibbs free energy, enthalpy, and entropy changes), suggest that the process happens spontaneously, endothermically, and upsurges the randomness on the adsorbent surface. The desorption and reusability tests reveal that PH-g-MMA could be regenerated up to 9 cycles and was capable of extracting over 75.00% of the Pb(II) from aqueous solutions.

Again, batch experiments were investigated to assess the ability to utilize activated carbon from *Manilkara Zapota* tree in Pb(II) decontamination from aqueous systems by CCD of the RSM (Sujatha *et al.*, 2020). The study examined the impact of individual and combination process variables, such as Pb(II) initial concentration, solution pH, and adsorbent dose, on Pb(II) depollution. At 0.837 desirability, the optimal uptake capacity (22.06 mg/g) of the adsorbent was obtained at the optimal condition of Pb(II) initial concentration (60.00 mg/L), pH (4.00), and adsorbent dose (0.2 g/L). The obtained data was completely fitted by the Langmuir and the pseudo-second-order models. The physisorption mechanism occurs in the elimination of Pb(II), according to the mean adsorption energy calculated with the use of the Dubinin-Radushkevich isotherm. In this study, the used-up carbon was regenerated through desorption processes, and about 91.00% of the adsorbed metal ions were recovered from the used carbon. Hence, the used

carbon is non-hazardous and can be used for the landfill, which is a safe disposal strategy. The thermodynamics parameters (Gibbs free energy, enthalpy, and entropy changes), which could also explain the adsorption process of Pb(II) were not discussed.

More so, the biosorption of Pb(II) from aqueous media onto Tamarind fruit shell powder (*Tamarinus Indica. L*) was studied (Bangaraiah & Sarathbabu, 2019). The operating factors such as agitation time, biosorbent dose, initial Pb(II) concentration, and solution pH were optimized by the CCD-RSM approach. The maximal removal efficiency of Pb(II) is 83.50% at the optimum process condition of 33.11 min of agitation time, 0.99 g/L biosorbent dose, 26.44 mg/L initial ion concentration, and pH of 6.98. The experimental data are best suited to Freundlich and pseudo-second-order models. The thermodynamics, desorption, and recyclability of the used adsorbent were not explored however, the study reveals the Tamarindus *Indica. L* was an effective biosorbent for Pb(II) remediation.

Likewise, the influence of three process factors on the decontamination of Pb(II) by groundnut shell was investigated using the CCD-RSM approach (Bayuo *et al.*, 2019). Applying the CCD, the optimized contact time (90.00 min), solution pH (8.00), and initial Pb(II) concentration (75.00 mg/L) gave a maximum uptake of 90.26% and adsorption capacity of 3.43 mg/g of Pb(II), respectively with the desirability of 0.966. The experimental results were better explained by the Langmuir and pseudo-second-order models. The adsorption thermodynamics, desorption, and reusability of the impregnated adsorbent were not investigated. Besides, the study reveals that the groundnut shell was efficient in Pb(II) removal from the aqueous phases.

In addition, a chitosan/rice husk ash/nano-γ alumina adsorbent was produced by Fooladgar *et al.* (2019) and used in the detoxification of Pb(II) from simulated wastewater. The CCD-RSM approach was employed to maximize operating factors such as solution pH, time of contact, initial Pb(II) concentration, and adsorbent dose, leading to 90.98% Pb(II) removal under the optimal condition of 5.00 pH, 105.00 min time of contact, 30.00 mg/L Pb(II) initial concentration, and adsorbent dosage of 0.01 g/L. The Langmuir model best represented the adsorption behavior of Pb(II), while the pseudo-second-order model best described the obtained experimental data. The thermodynamic results show that the Pb(II) adsorption was exothermic and spontaneous. The reusability of the used adsorbent in six subsequent adsorption-desorption cycles was conducted and the uptake capacity was maintained over 70.00% after six cycles, indicating that the nano-adsorbent demonstrates a high-level removal of Pb(II).

Further more, the influence of independent process variables namely the initial Pb(II) concentration, adsorbent dose, and contact time on Pb(II) decontamination by nickel ferrite-reduced graphene oxide nano-composite was studied by CCD of the RSM (Lingamdinne *et al.*, 2018). The removal of Pb(II) was observed to vary from 77.93 to 99.9%, which was influenced by the process variables. According to the numerical optimization, the best parameters for achieving Pb(II) removal with 0.953 desirability were 18.38 mg/L Pb(II) initial concentration, an adsorbent dose of 0.55 g/L, and an 83.00 min contact period. The equilibrium data matches the Langmuir among other models analyzed but the kinetics, thermodynamics, recovery, and regeneration of the adsorbent were not reported in this study.

For the extraction and purification of As(III) from wastewater, activated red mud-doped calcium-alginate beads were utilized (Naga *et al.*, 2021). The CCD of the RSM-based statistical modeling was applied in the optimization of the operational parameters (pH, sorbent dosage, contact time, and baseline concentration) for maximized As(III) removal. The highest adsorption of 92.00% of As(III) removal was found under the ideal operating parameters of pH 7.00-8.00, initial concentration of 10.00 mg/L, 0.80 g/L dosage, and 120 min time of contact at 303.00K. The thermodynamics and isothermal studies confirm the sorption process occurs non-spontaneously and endothermically with the Langmuir isotherm being the best fit to the As(III) equilibrium data. Furthermore, the kinetic analysis demonstrates that the experimental data best fits the pseudo-second-order model. In comparison to other adsorbents reported in several studies, the prepared adsorbent is efficient in sequestering As(III) up to an optimum capacity of 1.81 mg/g and it could be regenerated up to five cycles with 74.00% As(III) retrieval.

Similarly, an immobilized ZnO/TiO_2 activated carbon was developed for As(III) subtraction from wastewater and was modeled by the CCD of the RSM to find optimized conditions (Sagharloo *et al.*, 2021). According to optimized results, the best dosage, pH, contact time, and concentration to meet environmental regulations are 5.19 g/L, 6.76, 287.57 min, and 9.77 mg/L, respectively. The Langmuir isotherm and pseudo-second-order models show better agreement with the obtained data. The adsorption thermodynamics, retrieval, and reusability of the used adsorbent were not tested but the study infers that the new immobilized ZnO/TiO_2 activated carbon has a very superior efficiency in As(III) removal while being cost-effective, making it extremely useful for practical applications.

A study was carried out to find out if utilizing activated carbon prepared from teff husk may improve Cr(VI) removal from aqueous solutions (Adane *et al.*, 2020). To determine the effect

of the interactions of the process factors and optimize the process, a CCD-RSM approach was adopted. The optimum removal efficiency (95.60%) of the adsorbent was reached at a pH of 1.92, initial Cr(VI) concentration of 87.83 mg/L, adsorbent dose of 20.22 g/L, and 2.07 h time of contact. The best match models for the Cr(VI) adsorption data were the Langmuir and pseudo-second-order. The thermodynamics of Cr(VI) detoxification was not investigated and so how well the adsorption system proceeded is not known. In addition, there is no information on the desorption, regeneration, and reusability of the used adsorbent. Besides, the study recommends the teff husk as being effective and an economical adsorbent for Cr(VI) removal from contaminated water.

Likewise, in batch mode, CCD-RSM was used to remove Cr(VI) from the aqueous phase using an untreated biosorbent derived from *Arachis hypogea* husk (AHH) (Bayuo *et al.*, 2020b). The independent factors affecting the biosorption system were optimized and the optimal condition was attained as a contact time of 120.00 min, solution pH of 8.00, and an initial Cr(VI) concentration of 50.00 mg/L was achieved with a maximum uptake capacity of 2.36 mg/g. The equilibrium and kinetic data show good fitness to the Redlich–Peterson, and pseudo-second-order models. The thermodynamics parameters, which could have explained the sorption characteristics of Cr(VI) were not reported and no desorption and reusability of the adsorbent were studied. Besides, the AHH biosorbent was capable of detoxification Cr(VI) from the aqueous systems.

In another study, Javid *et al.* (2020) examined Cr(VI) removal ability with green-graphene nanosheets (GGN) synthesized using rice straw by the CCD-RSM approach. The interactive influence of two independent parameters such as KOH-to-raw rice ash ratio and temperature on the GGN surface area development was studied. The study indicates that the optimal condition was obtained at a KOH-to-raw rice ash ratio of 10.85 and a temperature of 749.61°C for the GGN preparation. The specific surface area achieved at the optimized operating condition for GGN was 551.14 m^2/g at Cr(VI) concentration (48.35 mg/L), adsorbent dose (1.46 g/L), contact time (44.30 min), and solution pH of 6.87. The Langmuir and pseudo-second-order models were the best fit for the obtained data. The adsorption thermodynamics, recovery, and reusability of the used adsorbent were not explored. However, the study suggests that the adsorbent is favorable and could be utilized in Cr(VI) reduction from wastewater.

Also, fly ash was modified chemically and used in removing Cr(VI) from aqueous environments (Jahangiri *et al.*, 2019). To develop models for response prediction and optimize

Cr(VI) process parameters, a CCD-RSM was used and 3.53 g/L adsorbent dose, 35.40 mg/L Cr(VI) initial concentration, 69.32 min time of contact, and pH of 2.77 were found as the optimal parameters values. The Freundlich and pseudo-second-order models best described the data obtained. According to the findings of the thermodynamic investigation, the sorption system was spontaneous, exothermic, and chemisorptive. The desorption and regeneration of the adsorbent were not conducted yet the study recommends fly ash as a great promising biosorbent for reducing Cr(VI) from aqueous solutions.

More so, the CCD of the RSM has been used to examine the extraction of Cr(VI) from aquatic systems by Amberlite XAD7 resin-loaded titanium dioxide (Ti-XAD7) (Sharifi *et al.*, 2019). An initial Cr(VI) concentration of 2.75 mg/L, 51.53 min time of contact, 8.70 pH, and a Ti-XAD7 dose of 5.05 g/L was found to be the best operating condition. The Langmuir and Sips models describe the experimental data well. The kinetic studies show that the Elovich kinetic model adequately explains the Cr(VI) adsorption characteristics. The adsorption thermodynamics, recovery, and reusability of the impregnated adsorbent were not investigated. In contrast to untreated XAD7, the modified XAD7 had a better Cr(VI) removal effectiveness, approximately 98.00% removal.

Likewise, a study was conducted to explore Cr(VI) removal using both chitosan modified with polyhexamethylene biguanide (Ch-PHMB NPs) and magnetic chitosan (M-Ch) from aqueous solutions by applying the CCD of the RSM (Aslani *et al.*, 2018). The impacts of four independent operating factors including solution pH, adsorbent dose, time of contact, and initial Cr(VI) concentration were optimized in Cr(VI) elimination. In contrast, all four factors investigated were found to have significant influences on Cr(VI) removal by Ch-PHMB NPs. However, for Cr(VI) removal by M-Ch NPs, only the interaction between solution pH and adsorbent dose indicates a significant effect. The Temkin and Freundlich models indicate a good representation of the obtained data for M-Ch and Ch-PHMB NPs, respectively. Both absorbents followed pseudo-second-order kinetics in extracting Cr(VI) from the aqueous systems. The thermodynamics investigations show Cr(VI) removal was non-spontaneous, exothermic, and decreased in randomness on the solid-liquid interface. The desorption and reusability of these adsorbents were not carried out. However, Ch-PHMBNPs adsorbent was found more efficient at removing Cr(VI), about 70.00% from the aqueous solutions than M-Ch adsorbent.

Additionally, a chemical activation was employed to produce activated carbon from the seed

shell of *Leucaena leucocephala* in extracting Cr(VI) from aqueous solutions through a batch system (Yusuff, 2018). Applying the CCD-RSM, the variables affecting the system including initial adsorbate concentration, solution pH, adsorbent dose, and temperature, were optimized. The results show that the optimum adsorption rate was found as 95.62 % at initial Cr(VI) concentration (71.49 mg/L), solution pH (4.22), adsorbent dose (0.57 g/L), and temperature (26.20°C). The Freundlich and pseudo-second-order models fit the obtained data well. The adsorption thermodynamics, recyclability, and reuse of the adsorbent were not investigated. However, the Cr(VI) sequestration was proven to be effective using the activated carbon from the seed shell of *Leucaena leucocephala*.

Nanodiopside was employed as a unique, green, and proficient adsorbent for removing Cd(II) ions from aqueous environments (Ghanavati *et al.*, 2021). The influence of sorption variables on the removal efficiency of the Cd(II) was examined by CCD-RSM and the best condition of the process variables for optimum Cd(II) decontamination was found to be pH of 5.60, adsorbent dose of 0.13 mg, Cd(II) initial concentration of 23.16 mg/L, 43.83 min time of contact time, and temperature of 34.75^0C. The adsorption data show a good correlation with the Freundlich and pseudo-second-order models. The thermodynamics parameters (Gibbs free energy, enthalpy, and entropy changes) that could have provided more insight into the sorption characteristics of Cd(II) were not reported. However, the desorption and regeneration tests were carried out, which showed that the adsorbent was still capable of being recycled and recovered 95.95% of Cd(II) in the sixth cycle.

More so, a zeolitic imidazolate framework (ZIF)-8 was prepared and treated with dimethylethylenediamine (ZIF-8-mmen) for Cd(II) removal (Binaeian *et al.*, 2020). The CCD-RSM was used to optimize the operations, which included three operational factors: pH of the solution, adsorbent dose, and contact time. With a maximum extraction efficiency of 85.38%, the best setting was reached at solution pH (2.00), dose (0.10 g/L), and time of contact (89.00 min). The equilibrium data best suited the Langmuir isotherm, indicating monolayer adsorption, whereas kinetic analyses of Cd(II) show a pseudo-first-order model. The Cd(II) sorption process was characterized by spontaneous, endothermic, and physisorption according to the thermodynamic studies. In the study, there is no information on the retrieval and reusability of the used adsorbent; so, the economic potential of the adsorbent is not known.

Similarly, a batch adsorption technique was applied to remove Cd(II) from synthetic solutions using eggshell powder (Sabah *et al.*, 2018). A CCD based on the RSM was utilized in the

process optimization, and the best condition was obtained at 44.00°C temperature, 2.98 g/L adsorbent dose, 36.74 mg/L Cd(II) initial concentration, and solution pH of 7.00. The cleanup yield of Cd(II) was 98.76% under this condition. The Freundlich model shows a good correlation with the isothermal data. The desorption results reveal that 45.60% of Cd(II) could be recovered and the reusability of the adsorbent was not tested to determine its economic prospects. Also, the adsorption kinetics and thermodynamics of the batch system were not performed in this study.

Ecer *et al.* (2020) investigated the influence of initial Hg(II) and As(V) concentrations, solution pH, adsorbent dose, and contact time in the sequestration of Hg(II) and As(V) by the CCD of the RSM onto Sulphur functionalized pumice. By applying numerical optimization, the optimal operating condition for Hg(II) removal was solution pH (6.33), initial metal concentration (36.94 mg/L), adsorbent dose (0.15 g/L), and time of contact (120.00 min) and the maximized condition for As(V) removal was solution pH (3.94), initial As(V) concentration (7.17 mg/L), adsorbent dose (0.15 g/L), and contact time (155.40 min). The adsorption yield of Hg(II) and As(V) in the attained optimized conditions were found as 92.14% and 88.02%, respectively. The equilibrium data for both metals were coherent with the Freundlich and Langmuir models, and the kinetic data of both metal ions were compatible with the pseudo-second-order model. In the study, the thermodynamics, retrieval, and reusability of the used adsorbent were not tested but from the findings, the adsorbent could be prudent for extracting various heavy metals from polluted aquatic systems.

Also, the CCD of the RSM was used to optimize the variables for removing Hg(II) from water with a novel nanostructured adsorbent (Azadegan *et al.*, 2019). Three process variables including contact time, pH of the solution, and sorbent dose were considered. The optimal condition was obtained as a pH of 4.50, 25.00 min of contact time, and sorbent dose of 0.06 g/L. The Langmuir and Freundlich models best agreed with the equilibrium data while both the pseudo-first and second-order models fitted well to the obtained data. The reusability and real wastewater samples tests were carried out and the results indicate high efficacy and promising capability of the adsorbent for actual environmental applications. However, the thermodynamics parameters such as Gibbs free energy, enthalpy, and entropy changes were not reported.

Likewise, the elimination of Hg(II) from aqueous systems by 3-mercaptopropyl trimethoxysilane-modified bentonite (B-SH) was conducted and the process was optimized

(Şahan *et al.*, 2018). The CCD-RSM findings reveal that the best condition was attained at a solution pH of 6.17, 36.95 mg/L Hg(II) initial concentration, a temperature of 37.28°C, and an adsorbent dose of 0.19 g/L. The maximum uptake capacity and percentage of removal were 19.30 mg/g and 99.23%, respectively, under the optimum condition established through the optimization method. The adsorption data fit the Langmuir model better than the other adsorption models. The adsorption process was discovered to be spontaneous, practical, and endothermic by the thermodynamics investigations. The desorption and regeneration of the used adsorbent were not reported in this study. Besides, the study shows that the B-SH has a high Hg(II) adsorptive removal capacity and could also be used to remove other metal ions from aqueous environments.

The optimization of Cu(II) elimination from wastewater by fly ash utilizing CDD-RSM was studied by Maiti *et al.* (2020). The interactive effects of the following process factors namely initial Cu(II) concentration, solution pH, and fly ash dose were determined and optimized. With an optimized initial Cu(II) concentration of 43.00 mg/L, pH 6.00, and a fly ash dosage of 63.00 g/L, the maximum Cu(II) removal efficiency (93.80%) was reached. In this study, the equilibrium isotherms, kinetics, and thermodynamics as well as the regeneration of exhausted adsorbent were not discussed and this could have offered more insight into the sorption behavior of Cr(VI). Besides, according to the results, fly ash can be utilized to remediate wastewater from a variety of sectors, including copper smelting, electroplating, and fertilizer manufacturing industries.

The CCD of the RSM was applied to explore and maximize the mono-component removal of Cu(II), Co(II), and Ni(II) onto trimellitated sugarcane bagasse adsorbent in a continuous fixed-bed column (Xavier *et al.*, 2018). The Cu(II), Co(II), and Ni(II) ions had maximal uptake capacities of 1.06, 0.80, and 1.03 mmol/g, respectively, at the optimum operating conditions of initial metal ion concentration and spatial time. The Thomas and Bohart-Adams models were used to model the breakthrough curves, with the Bohart-Adams model predicting the experimental results more precisely. The enthalpy, Gibbs free energy, and entropy changes of adsorption onto the adsorbent indicate the process was endothermic, spontaneous, and improved with increasing disorderliness at the solid-liquid interface. The recovery and reuse of the used adsorbent were not discussed.

The review of the relevant literature indicates that the design of experiments can be considered a useful and strong technique for designing, modeling, and optimizing heavy metals removal

using diverse adsorbents. The literature review reveals that the application of the central composite design of the response surface methodology led to the development of accurate and valid quadratic models. Consequently, the developed quadratic models were utilized in predicting the response variables and optimization of the independent adsorption variables for the effective removal of heavy metals from the aqueous systems using various sorbent materials.

CHAPTER THREE

MATERIALS AND METHODS

3.1 Samples Collection

The dry maize plants (*Zea mays*) containing three different parts such as stalks, cobs, and tassels from which the hybrid granular activated carbon was produced were obtained from farms through farmers in Nambala-Tengeru in the Arusha Region of Tanzania. Consequently, these maize residues were pretreated separately before the novel hybrid granular activated carbon was prepared from these three parts.

3.2 Chemicals and Reagents

All the chemicals and reagents used in this study were of laboratory analytical grade and were purchased and used as received from Alpha Chemika located in Mumbai, India. These chemicals and reagents include sodium hydroxide (NaOH, 97%), sodium arsenite ($NaAsO_2$, 98%), mercuric chloride ($HgCl_2$, 99%), sodium borohydride ($NaBH_4$), Ethylenediaminetetraacetic acid (EDTA, 99%), hydrochloric acid (HCl, 37%), nitric acid (HNO_3, 68%), sulphuric acid (H_2SO_4, 98%), starch, phosphoric acid (H_3PO_4, 85%), sodium thiosulphate ($NaSO_4$, 99%), iodine solution (I, 99%), sodium chloride (NaCl, 99%), calcium chloride ($CaCl_2$, 99%), deionized and distilled water.

3.3 Equipment and Apparatus

The analytical equipment that was used in this study includes the following tubular furnace, chemical balance, oven, cold vapour atomic absorption spectrophotometer (CVAAS), rotary shaker, Fourier transform infrared spectrometer (FT-IR), scanning electron microscope joined with energy-dispersive spectrometre (SEM-EDS), X-ray diffractometer (XRD), transmission electron microscope (TEM), thermogravimetric analyzer (TGA), Brunauer-Emmett-Teller (BET), and pH meter.

Also, some of the apparatus used in the study are desiccators, mortar, pestle, sieves (90-450 µm), beakers, watch glasses, filter papers, polythene bags, ceramic crucibles, measuring cylinders, separatory funnels, spatula, conical and volumetric flasks, pipettes, graduated cylinders, sample bottles, and plastic containers.

3.4 Preparation of Hybrid Granular Activated Carbon

The different parts of the dry maize plant including stalks, cobs, and tassels were washed thoroughly, repeatedly, and rinsed using double distilled water to remove dust and any insoluble contaminants. The three different parts were air-dried at room temperature (20±0.50 ℃) and later dried at 105 ℃ for 24 h in an oven (Labtech AVI-413, China) to constant weight. The different parts were then ground into powder separately and the equal weight of each part was measured and mixed thoroughly.

The mixed powder of the different parts of the dry maize plant was activated chemically, which involved a two-step process. Lower activation temperatures, shorter treatment times, less energy consumption, and a higher output of activated carbon with more surface area and pore volume are the benefits of chemical activation over physical activation (Supong *et al.*, 2019). This, however, results in more steps and chemical expenses (Bergna *et al.*, 2020).

The first step was the carbonization of the powdered maize residues at an optimum temperature of 500 ℃ in an inert atmosphere and the second step was the activation of the biochar obtained from the carbonization process with the presence of nitrogen gas (N_2). The optimum temperature of 500 ℃ was selected from a tested temperature range of 350-550 ℃, in 500 ℃ which produced a biochar of good quality, high biochar yield, and carbon content. In the activation process, the biochar was mixed with an impregnating agent, phosphoric acid, and starch as a binder in a proper ratio of 1:3 and 1:1, respectively, and then heated up to an optimum temperature of 800 ℃ using a tubular furnace (Carbolite CTF 12/65/550, UK) and then cool. This optimum temperature of 800 ℃ was selected from a tested temperature range of 600-850 ℃ because it produced activated carbon of high quality, yield, carbon cotent, and numerous surface functional groups. The resulting product was leached with distilled water to remove the residual impregnating agent until it became neutral and dried again at 105 ℃ in the oven for 24 h to a consistent weight. The ultimate hybrid granular activated carbon (HGAC) was produced after mechanical crushing and sieving to mesh sizes of 90-450 µm using the American Society for Testing and Materials (ASTM) standard sieves. The biosorbent was then stored in airtight plastic containers and then used for the biosorption experiments. The granular activated carbon was required because recycling of the exhausted activated carbon can be achieved by using mineral acids and bases but the powdered biosorbents are very difficult to regenerate (Akhter *et al.*, 2021).

3.5 Preparation of Stock Solutions and Sample Solutions Analysis

The stock solutions of the single-metal [As(III) and Hg(II)] as well as binary-metal ions [As(III)+Hg(II)] for the batch tests were prepared up to 1000 mg/L. In preparing the stock solutions of the metal ions, procedures listed in APHA (1989) were followed. To prepare the stock solution of As(III), 1.732 g of sodium arsenite ($NaAsO_2$) was dissolved in de-ionized water and diluted to the 1000 mL mark with de-ionized water. Similarly, 1.354 g of mercuric chloride ($HgCl_2$) was dissolved in 200 mL of distilled water, then 10 mL of concentrated nitric acid (HNO_3) was added, and the resulting solution was diluted to the 1000 mL mark using de-ionized water.

For the binary-metal solutions, the desired combinations of As(III)+Hg(II) ions were obtained by diluting 1000 mg/L of stock solutions of single-metal ions and mixing them in the test medium. The initial concentration of the ions in the binary-metal system was in the ratio of 1:1 and working concentrations ranging from 5-100 mg/L were prepared from the stock solutions to the desired concentrations using the dilution method. The CVAAS (Rayleigh WFX 210, China) was employed for the determination of the residual concentrations after the adsorption-desorption of As(III) and Hg(II) ions from the non-competitive and competitive aqueous solutions.

3.6 Physicochemical Parameters and Characterization of the Biosorbent

The physicochemical parameters of the biosorbent that were determined include the following moisture content, bulk density, pH of biosorbent, volatile matter, ash content, pH of point of zero charge, carbon yield, fixed carbon content, and iodine number. The background concentrations of As(III) and Hg(II) in the prepared HGAC were also assessed. Furthermore, the characterization of the biosorbent was carried out using FT-IR (PerkinElmer Spectrum, USA), BET (ASAP 2460 Micro metrics, USA), SEM (Tescan Vega3, USA), EDS (Oxford), XRD (Rigaku, Japan), XRF (EZ5001XSV, USA), TEM (JOEL-2010, Japan), and TGA (SDT Q600, USA).

3.6.1 Determination of Moisture Content (MC)

A crucible was filled with 2 g of the activated carbon precursor, which was then dried continuously at 110 ℃ in the oven. The drying sample was repeatedly reweighed using an analytical chemical balance (KERN PLS 1200-3A, USA) at intervals of 10 min until a

consistent weight was attained. The moisture content is determined by the ratio of the change in weight to the initial weight, expressed as a percentage (Eq. 1) (Agbajelola *et al.*, 2015).

$$\mathrm{MC} = \frac{(W_3 - W_1)}{(W_2 - W_1)} \times 100 \quad (1)$$

Where $W_1 =$ empty crucible weight, $W_2 =$ crucible and sample weight before oven drying and $W_3 =$ crucible and sample weight after oven drying.

3.6.2 Determination of Bulk Density (BD)

The density of granular activated carbon was found by filling the activated carbon into a 10 mL measuring cylinder and then weighing it using an analytical chemical balance. The weight noted as the bulk weight was then divided by the volume of the measuring cylinder used. The bulk density is expressed in Eq. (2) (Pachaiyappan *et al.*, 2012).

$$\mathrm{BD} = \frac{W_2 - W_1}{\mathrm{V}} \quad (2)$$

Where $W_1 =$ empty measuring cylinder weight, $W_2 =$ measuring cylinder filled with sample weight, and $V =$ measuring cylinder volume.

3.6.3 Determination of Volatile Matter (VM)

A closed crucible containing 2 g of oven-dried activated carbon precursor was heated for 10 min at 900 ℃ in a muffle furnace (Labtech AVI-418, China). Volatile solids were calculated using Eqs. (3) and (4), respectively after the crucible had been cooled in a desiccator (Akpen *et al.*, 2016).

$$W_L = \frac{\text{Initial mass} - \text{Final mass}}{\text{Initial mass}} \times 100 \quad (3)$$

$$VM = W_L - MC \quad (4)$$

Where W_L is weight loss in % and MC is moisture content in % as defined in Eq.(1).

3.6.4 Determination of Ash Content (AC_{Ash})

A crucible containing 10 g of the dry activated carbon samples was placed in a muffle furnace heated to 600 °C. The crucible and its contents were then moved into a desiccator and allowed to cool after the furnace had been running for 3 h. The crucible and its contents were reweighed, and the new weight was recorded and the percentage of ash content was determined using Eq. (5) (Otaru *et al.*, 2013; Mukoko *et al.*, 2015).

$$AC_{Ash} = \frac{(W_3 - W_1)}{(W_2 - W_1)} \times 100 \quad (5)$$

Where W_1 is the empty crucible weight, W_2 is the crucible and carbon samples weight and W_3 is the crucible and carbon samples' weight after heating at 600 ℃.

3.6.5 Determination of Carbon Yield (CY) and Fixed Carbon Content (FCC)

A 2 g of the dried activated carbon samples kept in a crucible were heated in a muffle furnace to a temperature of 850 ℃ for 10 min. The crucible with the samples was then removed and cooled using a desiccator. The activated carbon yield was determined using Eq. (6) (Akpen *et al.*, 2016).

$$CY = \frac{W_1}{W_0} \times 100 \quad (6)$$

Where W_0 is the dried carbon sample weight and W_1 is the carbon samples' weight after retrieving from the furnace.

Also, the fixed carbon content (FCC) was determined using Eq. (7).

$$FCC = 100 - \mathrm{MC} + AC_{Ash} + \mathrm{VM} \quad (7)$$

Where CY is carbon yield, MC is moisture content, VM is volatile matter, and AC_{Ash} is ash content.

3.6.6 Determination of Iodine Number (IN)

To determine the iodine number, 0.1 g of activated carbon was put in a conical flask that contained 25 mL of iodine solution. The activated carbon was then mixed thoroughly with the iodine solution by swirling the flask for one minute. After the mixing, the activated carbon-iodine solution was filtered and 10 mL of the filtrate was then pipetted and kept in a conical flask, which was titrated with 0.04 N sodium thiosulphate ($NaSO_4$) solution until it became clear. The iodine number was obtained from Eq. (8) (Mukoko *et al.*, 2015).

$$IN = \frac{V_I C_I M_I (V_{i(NaSO_4)} - V_{(fNaSO_4)})}{W_0 V_{i(NaSO_4)}} \quad (8)$$

Where V_I is the volume of iodine (25 mL), $V_{i(NaSO_4)}$ is the initial volume of $NaSO_4$ solution (11.3 mL), $V_{(fNaSO_4)}$ is the final volume of $NaSO_4$ solution after titration, W_0 is sample weight (0.1 g), M_I is iodine molar weight (126.9 g/mol), and C_I is the iodine concentration (0.046 N).

3.6.7 Determination of pH and pH of Point of Zero Charge (pH_{pzc}) of the Biosorbent

The activated carbon produced was washed with tap water severally and then followed with distilled water. The pH of the aqueous extract was then determined by a pH meter (Hanna HI 2211, Romania) until a neutral pH was achieved. Also, the pH of the point of zero charge (pH_{zpc}) of the activated carbon was carried out using the solid addition technique (Ahmad & Haseeb, 2015; Bayuo *et al.*, 2019). This is done by adding 0.1 g of the biosorbent to 50 mL of distilled water using a variable initial pH from 1-12 and stirring for 24 h. The adjustment of the initial pH was carried out using either 0.1 M NaOH or 0.1 M HCl solutions. The pH was measured once again after stirring for 24 h. The change in pH was determined as the difference between the final and initial pH values as given in Eq. (9). The change in pH (ΔpH) was then plotted versus the initial pH (pH_0) and point of intersection gives the pH_{pzc} of the biosorbent.

$$\Delta pH = pH_f - pH_0 \quad (9)$$

Where ΔpH is the change in pH, pH_0 is the initial pH and pH_f is the final pH.

3.7 One-Factor-At-A-Time Batch Biosorption Experiments

The batch biosorption experiments were performed to assess the adsorptive performance of As(III) and Hg(II) ions onto the biosorbent from the non-competitive and competitive aqueous solutions, respectively. The batch biosorption technique was selected to obtain the equilibrium data because of its simplicity and reliability (Al-Qodah *et al.*, 2017; Aigbe *et al.*, 2021).

The single-metal [A(III) and Hg(II)]; non-competive biosorption experiments were carried out by varying contact time (10-180 min), pH of the solution (2.00-14.00), particle size (90-450 µm, biosorbent dosage (0.5-5 g/L), initial As(III) and Hg(II) concentration (5-100 mg/L), and reaction temperature (10-85 ℃) while maintaining other experimental conditions constant. A known amount of the biosorbent was added to 250 mL Erlenmeyer flasks containing 100 mL aqueous solutions after pH adjustment. The initial pH of the solution was adjusted by adding 0.1 M NaOH or 0.1 M HCl solutions before the biosorption test. The Erlenmeyer flasks were subsequently capped and shaken at 120 rpm for a predetermined time using a rotary shaker until equilibrium conditions were achieved. After shaking at the stipulated time, the sample solutions were filtered using the Whatman 42 filter paper. The collected filtrate was then analyzed by the CVAAS.

More so, the competitive removal of As(III) and Hg(II) ions onto the biosorbent from the

binary-metal component system [As(III)+Hg(II)] was performed by preparing aqueous solutions of each metal ion containing the same concentration in 50 mL volumetric flasks and combining them to obtain 100 mL mixed binary-metal solutions. The 100.00 mL mixed binary-metal solutions were placed in 250 Erlenmeyer flasks with a 1:1 ratio of the initial concentration of each metal ion ranging from 5-100 mg/L. Similarly, the solution pH was controlled by 0.1 M HCl or 0.1 M NaOH followed by the addition of a known amount of the biosorbent and shaken at 120 rpm, filtered, and analyzed after attaining the equilibrium time. All the batch experiments were conducted in triplicates using the same biosorption parameters and conditions used for the removal of As(III) and Hg(II) from the non-competitive biosorption system. The removal efficiency and uptake capacities were calculated using Eqs. (10-12), respectively (Rahman *et al.*, 2021; Teng *et al.*, 2021).

$$\text{Removal efficiency } (\%) = \frac{(C_0 - C_e)}{C_0} \times 100 \tag{10}$$

The biosorption capacity at a specific time, q_t (mg/g) is given by Eq. (11):

$$q_t = \frac{(C_0 - C_t) \times V}{m} \tag{11}$$

The biosorption capacity, q_e (mg/g) at equilibrium time is also expressed as in Eq. (12):

$$q_e = \frac{(C_0 - C_e) \times V}{m} \tag{12}$$

Where C_0 and C_e are As(III) and Hg(II) initial and equilibrium As(III) and Hg(II) concentrations (mg/L), respectively; C_t is the initial As(III) and Hg(II) concentration (mg/L) at time t, V is the volume (mL) of As(III) and Hg(II) solutions, and m is the weight (g) of the biosorbent.

3.7.1 Effect of Contact Time

The effect of contact time was carried out by mixing a 1.5 g/L biosorbent dose of 125 µm particle size with 100 mL single-metal ion solutions in 250-mL Erlenmeyer flasks containing 25 mg/L initial concentration of As(III) and Hg(II) ions. The Erlenmeyer flasks were then shaken at various time intervals ranging from 10-180 min (10, 20, 30, 40, 60, 90, 120, 150, and 180 min) at 120 rpm. The experiment was operated at a solution pH of 5 and room temperature $(20 \pm 0.5\ ℃)$. For the binary-component biosorption system, 100 mL mixed metal ions [As(III)+Hg(II)] solutions of the same concentration (25 mg/L) were used, and all the experimental conditions were the same as in the single-biosorption system. After agitating the

setups for each time interval, the suspension was filtered using 42 µm Whatman filter paper. The residual concentrations of the As(III) and Hg(II) ions in both the single and binary biosorption systems were analyzed, respectively alongside the blanks using CVAAS. The blank solutions served as a control for the presence of the metal ions in both single-metal and binary-metal biosorption systems which may be adsorbed after the treatment.

3.7.2 Effect of the Initial pH of the Solutions

Non-competitive and competitive aqueous solutions of different pH values ranging between 2-14 (2, 4, 6, 8, 10, 12, and 14) were prepared to determine the effect of solution pH on the removal of As(III) and Hg(II) ions from single-metal and binary-metal biosorption systems, respectively. A fixed amount of biosorbent dose (1.5 g/L) of particle size (125 µm) was added to 100 mL single-metal and binary-metal solutions with an initial concentration of 25 mg/L. The pH of the solutions was adjusted by either 0.1 M HCl or 0.1 M NaOH solution. The mixture was agitated at 120 rpm for the predetermined contact time under room temperature (20 ± 0.5 ℃) . After shaking to the equilibrium time, the residual As(III) and Hg(II) ions concentration in the blanks and solution samples were measured by CVAAS.

3.7.3 Effect of Biosorbent Particle Size

To evaluate the effect of biosorbent particle sizes on the removal of As(III) and Hg(II) ions from the single-metal and binary-metal biosorption systems, the experiments were conducted by using varying particle sizes of the biosorbent from 90-450 µm (90, 125, 180, 355, and 450 µm and 25 mg/L initial concentration of each metal ion in 100 mL solution at room temperature (20 ± 0.5 ℃). The mixture was agitated with 1.5 g/L of biosorbent dosage and shaken at 120 rpm for the equilibrium time. The residual concentrations of As(III) and Hg(II) in the single-metal and binary-metal solutions as well as in the blanks were examined using CVAAS.

3.7.4 Effect of Biosorbent Dosage

The effect of biosorbent dosage was conducted by varying the biosorbent doses from 0.5-5 g/L (0.5, 1, 1.5, 2, 2.5, 3, 3.5, 4, 4.5, and 5 g/L) with optimum pH and biosorbent particle size attained for both single-metal and binary-metal biosorption systems, respectively. A 100 mL aqueous solution containing 25 mg/L single-metal and binary-metal ions was agitated with the different doses and stirred for the equilibrium time achieved for both biosorption systems at 120 rpm under room temperature (20 ± 0.5 ℃). At the end of the predetermined contact time,

the residual concentration of As(III) and Hg(II) ions in the single and binary component systems, respectively, and those of the blanks were analyzed using CVAAS.

3.7.5 Effect of Initial Single-Metal and Binary-Metal ions Concentration

The effect of the initial concentration on the biosorbent efficiency for the decontamination of As(III) and Hg(II) ions in 100 mL solutions of the single-metal component system was conducted at different concentrations of As(III) and Hg(II) ranging from 5-100 mg/L (5, 10, 15, 25, 30, 45, 60, 75, and 100 mg/L). For the binary-component biosorption system, 100 mL mixed As(III)+Hg(II) ions solutions of the same concentrations were used, and all the experimental conditions were the same as in the single-biosorption system. The mixture was shaken at 120.00 rpm for the equilibrium contact time at room temperature (20 ± 0.5 ℃). The experiment was operated at optimum pH, biosorbent particle size, and dosage. At the equilibrium time, the residual amount of As(III) and Hg(II) ions in the non-competitive and competitive solutions together with the blanks were determined using CVAAS.

3.7.6 Effect of Reaction Temperature

The effect of reaction temperature on the decontamination of As(III) and Hg(II) ions from non-competitive and competitive aqueous solutions was investigated at varying temperatures from 10-85 ℃ (10, 15, 25, 35, 45, 55, 65, 75, and 85 ℃). The consistency of the temperature was retained using an accuracy of $\pm$ 0.5 ℃. The biosorption experiments were performed in 100 mL solutions with the optimum initial metal ion concentrations, solution pH, biosorbent particle size, and dosage achieved for both single- and binary-component systems. The adsorbate-biosorbent mixtures were placed in a water bath and shaken using a rotary shaker at 120 rpm for the optimum contact time obtained for both single-component and bicomponent systems. At the end of the respective equilibrium time, the residual concentrations of As(III) and Hg(II) ions in the sample solutions and the blanks were determined using CVAAS.

3.7.7 Desorption of As(III) and Hg(II) ions and Regeneration of Spent Biosorbent

To perform the recovery and regeneration experiments, the optimum dosage of the biosorbent with the optimum particle size obtained for both single- and binary-component systems was introduced into 100 mL of the optimum initial concentration attained from single-metal and binary-metal biosorption systems in separate 250 mL Erlenmeyer flasks. After equilibration for the optimum contact times and optimum temperatures attained for both biosorption systems,

the biosorbent was filtered and the amount of the As(III) and Hg(II) ions in the liquid phase was measured. The residual single-metal and binary-metal ions loosely attached to the biosorbent surface were removed through washing using distilled water and then dried in an oven at 105 ℃ to obtain a constant weight.

Subsequently, a known amount of single-metal and binary-metal treated biosorbent was added to separate Erlenmeyer flasks containing 100 mL of the desorption eluents after pH adjustments. Five diverse desorption eluents including distilled water, 0.1 M of H_2SO_4, HNO_3, HCl, and EDTA were tested in the recovery of As(III) and Hg(II) ions from the spent biosorbent and testing its renewability and reusability. The regeneration and reusability of the spent biosorbent were investigated by performing ten successive biosorption-desorption cycles for As(III) and Hg(II) ions removal by the biosorbent. The biosorption-desorption experiments were performed using a rotary shaker with an agitation speed of 120 rpm and operated at optimum conditions of contact time, solution pH, reaction temperature, biosorbent particle size, and dosage. The residual As(III) and Hg(II) concentrations in the non-competitive and competitive aqueous solutions after the biosorption-desorption experiments were measured using CVAAS.

The desorption efficiency was calculated using Eq. (13) below (Bayuo *et al.*, 2020):

$$\text{Desorption efficiency} = \frac{C_{de}}{C_{ad}} \times 100 \qquad (13)$$

Where C_{ad} and C_{de} are the concentrations of As(III)) and Hg(II) ions adsorbed and desorbed, respectively.

3.8 Experimental Design by Central Composite Design

The design of an experiment is a statistical technique for identifying both cause and effect relationships. The design of the experiment aims to gather data on common relationships between biosorption process independent variables to identify optimum operating conditions. The design of experiments using a statistical tool such as Design Expert of Stat-Ease is less time-consuming and efficient in modeling and optimizing heavy metals removal from aquatic systems at the lowest possible cost (Ghosh *et al.*, 2021). Additionally, a proper selection of design and optimization models in a statistical tool enables the concurrent study of the effects of significant factors during empirical investigations (Ghaee *et al.*, 2012). The RSM is a design of experiment in the Design Expert, Stat-Ease that employs numerical data from appropriate experiments to develop regression model equations to investigate the interactive behavior

among independent factors as a function of dependent variables (responses) and find the optimum operating condition for a process (Djaghout *et al.*, 2015). Hence, response surface methodology is generally used in experimental design, process modeling, and optimization of a system.

In the present study, the CCD, a component of the RSM, was used to examine the single and interactive effects of three independent factors namely (A)-Contact time, (B)-Biosorbent dosage, and (C)-Initial metal ion concentration on two dependent factors (responses) including (Y1)-Removal efficiency (%) and (Y2)-Biosorption capacity (mg/g). This is because among all the designs in RSM including the central composite design, Box-Behnken design, and three-level full factorial design, the central composite design offers high-quality significant predictions of linear and quadratic interactive effects of the operating parameters influencing the process (Afolabi *et al.*, 2021). The central composite design comprises three types of space points including $2k$ factorial, $2k$ axial and N_c center experimental runs, where k is the number of independent factors. The experimental runs needed for the modeling and the process optimization are determined by Eq. (14) (Khelifi *et al.*, 2022).

$$N = 2^k + 2k + N_c \quad (14)$$

The factor levels of the independent variables in this study are coded as -1.00 (Low), 0.00 (Centre), and +1.00 (High). The range and the levels of the independent factors, which were obtained from the preliminary batch biosorption studies and used by the central composite design for designing the experiments statistically are displayed in Tables 5 and 6, respectively.

Table 5: As(III) biosorption process influencing variables and levels

Independent factor	Symbol	Unit	Factor level		
			Low	**Middle**	**High**
			-1.00	**0.00**	**+1.00**
Contact time	A	min	40	65	90
Biosorbent dosage	B	g/L	0.5	1.75	3
Initial concentration	C	mg/L	10	20	30

Table 6: Hg(II) biosorption process influencing variables and levels

Independent factor	Notation	Unit	Factor level		
			Low	Centre	High
			-1.00	0.00	+1.00
Contact time	A	min	30	60	90
Biosorbent dosage	B	g/L	0.5	2	3.5
Initial concentration	C	mg/L	15	30	45

The HGAC was used to carry out the batch biosorption tests following the layout given by the CCD-RSM in Design Expert software version 13 of Stat-Ease, which assessed the interacting effects of three independent adsorption process variables, involving A: Contact time, B: Biosorbent dosage, and C: Initial concentration. These three independent biosorption factors, their ranges, and the response variables listed in Tables 5 and 6, respectively were chosen from the one-factor-at-a-time experimental design. These three parameters were selected because they were found to be the most influencing parameters on the adsorptive removal of As(III) and Hg(II) from the synthetic wastewater. As a result, the CCD-RSM was adopted to improve the removal rate of As(III) and Hg(II) ions from the aqueous solutions utilizing these biosorption process variables.

The CCD-RSM statistically generated a set of twenty (20) experimental runs with varying configurations of these biosorption variables with respect to the response variables, required for the modeling and optimization processes. In developing the regression model equations, each response variable including (Y1)-Removal efficiency and (Y2)-Biosorption capacity was used. The developed model equation for each response variable, which is in the form Eq. (15) was then, used to optimize the responses as a function of the independent factors (Kumari *et al.*, 2021).

$$Y = b_0 + \sum_{i=1}^{n} b_i X_i + \sum_{i=1}^{n} b_{ii} {X_i}^2 + \sum_{i=1}^{n-1} \sum_{j=i+1}^{n} b_{ij} X_i X_j \quad (15)$$

Where Y denotes the predicted response, b_0 is the constant of coefficient, b_i is the linear regression coefficient, b_{ij} is the regression coefficient for two-factor interaction effects, b_{ii} represents the regression coefficient for quadratic main effects, X_i, and X_j are the levels of factors.

3.8.1 Optimization of Biosorption System Factors

In the optimization process, the desirability function in the central composite design of the response surface methodology was employed to explain the effects of the independent variables, and their interactions and to obtain optimum responses and exact values for the independent variables.

Specifically, the following steps are required in the optimization of the independent operating factors using the central composite design based on the response surface methodology (Shafaghat & Ghaemi, 2021):

(i) Select the number of independent and dependent factors, then statistically design the experiments.

(ii) Carry out the laboratory investigations according to the design matrix

(iii) Choose the significant independent factors that have an influence on the efficiency of the process during the course of the experimentations.

(iv) Develop regression model equations from the dependent factors (responses) as a function of the independent factors.

(v) Check the accuracy, validity, and agreement of the developed regression models to the experimental data.

(vi) Finally, carry out numerical optimization to determine optimum conditions by employing the desirability function.

3.8.2 Models Validation

In the post-optimization analysis, the selected quadratic models applied to determine the optimum conditions for maximum remediation of As(III) and Hg(II) from the synthetic wastewater using HGAC were validated at a two-sided 95% confidence level. Five confirmatory laboratory experimental runs were performed at the optimum operating conditions predicted by the quadratic models.

3.9 Biosorption Isotherm and Kinetic Modeling

The biosorption equilibrium isotherms and kinetics of the mono-metal [As(III) and Hg(II)] and

binary-metal [As(III)+Hg(II)] biosorption systems were conducted by adding a known amount of the biosorbent dose of 90 µm particle size to 250 mL Erlenmeyer flasks containing 100 mL aqueous solutions with varying initial concentration (5-100 mg/L) and contact time (10-180 min) after pH adjustment while maintaining other parameters constant. Tables 7 and 8, respectively summarized the other experimental conditions that remained constant during the isotherm and kinetics studies of As(III) and Hg(II) in the monocomponent and bicomponent sorption systems. The Erlenmeyer flasks containing the sample solutions were subsequently capped and shaken at 120 rpm for a predetermined time using a rotary shaker until equilibrium conditions were achieved. After shaking at the stipulated time, the sample solutions were filtered using the Whatman 42 filter paper. The collected filtrate was subjected to metal ions analysis using the CVAAS. While the equilibrium isothermal data was applied to four isotherm models including the Langmuir, Freundlich, Dubinin-Radushkevich, and Temkin, the kinetic data was analyzed by four models such as the pseudo-first-order, pseudo-second-order, Elovich, and intra-particle diffusion kinetic models.

Table 7: Constant experimental conditions of equilibrium isotherm studies for As(III) and Hg(II) removal in mono-metal [As(III) and Hg(II)] and binary-metal [As(III)+Hg(II)] biosorption systems

Parameter	Equilibrium operating conditions		
	As(III)	Hg(II)	As(III)+Hg(II)
Contact time (min)	60	90	120
pH of solution	6	4	4
Biosorbent dose (g/L)	3	3.5	2.5
Temperature (℃)	35	45	55

Table 8: Constant experimental conditions of kinetics studies for As(III) and Hg(II) removal in mono-metal [As(III) and Hg(II)] and binary-metal [As(III)+Hg(II)] biosorption systems

Parameter	Equilibrium operating conditions		
	As(III)	Hg(II)	As(III)+Hg(II)
pH of solution	6	4	4
Biosorbent dose (g/L)	3	3.5	2.5
Initial concentration (mg/L)	30	45	25
Temperature (℃)	35	45	55

3.10 Biosorption Thermodynamics Studies

The biosorption thermodynamic studies provide insightful information on the biosorption process including its exothermic or endothermic nature, spontaneity, and randomness at the liquid-solid interface. To investigate the thermodynamic parameters such as enthalpy (ΔH^0), Gibbs free energy (ΔG^0), and entropy (ΔS^0) of the biosorption process, the equilibrium data from the effect of temperature was used.

The biosorption thermodynamics of the mono-metal [As(III) and Hg(II)] and binary-metal [As(III)+Hg(II)] biosorption systems were conducted by adding a known amount of the biosorbent dose of 90 µm particle size to 250 mL Erlenmeyer flasks containing 100 mL aqueous solutions with varying temperature (10-85 ℃) after pH adjustment. Other parameters were kept constant as summarized in Table 9. The Erlenmeyer flasks were subsequently capped and shaken at 120 rpm for a predetermined time using a rotary shaker until equilibrium conditions were achieved. After shaking at the stipulated time, the sample solutions were filtered using the Whatman 42 filter paper. The collected filtrate was subjected to metal ions analysis using the CVAAS.

The following Eqs. (16-18) were applied in computing the thermodynamic parameters from the experimental data attained by the biosorbent (Narayanasamy *et al.*, 2022).

$$\Delta G^0 = -RT \ln K_L \quad (16)$$

Where K_L is the distribution coefficient expressed as $K_L = \frac{q_e}{C_e}$, R is the gas constant and T is the absolute reaction temperature.

Also, the ΔG^0 is related to ΔH^0 and ΔS^0 at fixed temperature as given in Eq. (17).

$$\Delta G^0 = \Delta H^0 - T\Delta S^0 \quad (17)$$

Combining Eqs. (16) and (17), an Eq. (18) is formed.

$$\ln K_L = \frac{\Delta S^0}{R} - \frac{\Delta H^0}{RT} \quad (18)$$

Table 9: Constant experimental conditions of thermodynamics studies for As(III) and Hg(II) removal in mono-metal [As(III) and Hg(II)] and binary-metal [As(III)+Hg(II)] biosorption systems

Parameter	Equilibrium operating conditions		
	As(III)	Hg(II)	As(III)+Hg(II)
Contact time (min)	60	90	120
pH of solution	6	4	4
Biosorbent dose (g/L)	3	3.5	2.5
Initial concentration (mg/L)	30	45	25

3.11 Application of the Biosorbent in Treating Real Industrial Wastewater

Real wastewater was sampled from the A to Z textile industry in the Arusha region of Tanzania to test the applicability of the HGAC in the competitive adsorptive removal of different heavy metals from the wastewater. The wastewater collected was pretreated based on the protocols for water and wastewater analysis (Gilcreas, 1967). The water samples collected in the plastic containers were acidified using HNO_3 to a pH < 2 and then transported to the laboratory at a temperature of 4 ℃ within 4 h and then stored until analysis.

Subsequently, the wastewater samples were characterized using an atomic absorption spectrophotometer (AAS) following the standard methods documented in APHA (1989) to determine the number of pollutants and the concentration of each present in the wastewater before subjecting it to a batch biosorption test.

3.11.1 Batch Biosorption Experiments

The textile wastewater was subjected to biosorption by the HGAC using the batch technique in which a known dosage of the biosorbent was added to 100 mL of the wastewater in 250 mL

Erlenmeyer flasks. The batch experimental setups were operated at varying contact times (10-240 min), pH of the solution (2-14), particle size (63-450 µm), biosorbent dose (0.5-5 g/L), and temperature (20-65 ℃). The sample solutions were agitated at varied speeds (25-400 rpm) using a flask rotary shaker. The sample solutions were centrifuged and filtered through 0.42 µm Whatman filter paper after the agitation time had elapsed. The supernatant was analyzed by AAS at the wavelength of 193.70, 253.70, 283.31, 396.00, and 357.90 nm for total As, Hg, Pb, Cd, and Cr, respectively to measure the amount of each heavy metal ion adsorbed on the HGAC.

3.11.2 Desorption and Regeneration Studies

To test the recoverability of the adsorbed As, Hg, Pb, Cd, and Cr ions and regeneration of the HGAC, the spent HGAC was pretreated by drying in an oven at 105 ℃ to a constant mass and utilized in the desorption studies. Ten (10) different desorption eluents including H_2O, H_3PO_4, H_2SO4, HNO_3, HCl, EDTA, NaOH, NaCl, KOH, and $CaCl_2$ were tested for stripping off the adsorbed metal ions from the spent HGAC and in testing its reusability and safe disposal.

In the desorption process, the previously used HGAC was transferred into 250-mL Erlenmeyer flasks containing the different desorption eluents and were shaken on a rotary flask shaker operating at a speed of 120 rpm and room temperature of $20 \pm 0.5\ ^0C$ for a contact time of 120 min. After agitating to the predetermined time interval, the sample mixtures were then filtered through Whatman number 42 filtering paper, and the concentration of As, Hg, Pb, Cd, and Cr ions released into the liquid phase was analyzed by AAS, and the desorption efficiency as well as the quantity of metal ions desorbed were calculated.

3.12 Experimental Design and Process Optimization Using Central Composite Design

To optimize the biosorption process, batch experiments were statistically designed by CCD-RSM of the Design Expert Software Version 13, Stat-Ease using five independent desorption factors, and each factor was set at three levels (-1.00, 0.00, +1.00) as listed in Table 10. As stated previously, these five independent adsorption factors and their levels were chosen from the one-factor-at-a-time biosorption studies. The batch biosorption was carried out according to the CCD-RSM experimental design matrix using a series of Erlenmeyer flasks holding 100 mL of the textile wastewater.

Table 10: Biosorption process independent factors and their levels

Independent factor	Symbol	Unit	Factor level		
			Low	Middle	High
			-1.00	0.00	+1.00
Contact time	A	min	30	75	120
Solution pH	B	-	3	5	7
Dosage	D	g/L	0.5	1.25	2
Agitation speed	C	rpm	100	200	300
Temperature	E	℃	30	37.5	45

3.12.1 Models Validation

In the post-optimization analysis, the selected quadratic models applied to determine the optimum conditions for maximum remediation of As and Hg from the competitive textile wastewater using HGAC were validated at a two-sided 95% confidence level. Five confirmatory laboratory experimental runs were performed at the optimum operating conditions predicted by the quadratic models.

3.13 Biosorption Isotherm, Kinetic, and Thermodynamic Studies

The biosorption isotherm, kinetic, and thermodynamic studies were carried out using Erlenmeyer flasks of 250 mL containing 100 mL of the textile wastewater. A known amount of the biosorbent was then added to the wastewater after pH adjustment. For the biosorption isotherm and kinetic studies, the experiments were performed under room temperature (20 ± 0.5 ℃) at varying biosorbent dosage (0.5-5 g/L) and contact time (10-240 min), respectively. After shaking the solid-liquid mixtures to the respective contact time, the residual concentrations of the metal ions in the blanks and sample solutions were determined using AAS. The isothermal and kinetic data attained for the adsorptive removal of As, Hg, Pb, Cd, and Cr ions from the wastewater onto the HGAC were fitted by four isotherm and kinetic models, respectively. To determine the thermodynamic parameters and thermal effects on the removal of the As, Hg, Pb, Cd, and Cr ions from the wastewater, temperature variation experiments were conducted between 20-65 ℃.

3.14 Method of Data Analysis

The analysis of variance (ANOVA) and statistical tools under the CCD-RSM for instance probability (p-value), coefficient of determination (R-squared), Fisher value (F-value), and residuals were used in the analysis of the data. OriginPro software and Microsoft Excel were also used in the organization of the data as well as in performing descriptive statistics including histograms, percentages, and linear regressions.

3.15 Quality Assurance and Control Measures

The following set of quality assurance and control measures were adopted to help yield results that are reliable and secure as well as ensure safety in the laboratory and the environment at large:

(i) All containers containing arsenic, mercury, and other heavy metal salts, as well as solutions, were kept tightly sealed and kept in a dry, well-ventilated area at all times, and the storage space was clearly labeled as 'Keep Off, Highly Toxic'.

(ii) Direct contact with arsenic and mercury, as well as other heavy metals, was avoided, and proper personal protective equipment (PPE), such as a laboratory coat with full long sleeves, a face shield and safety glasses, gloves, a respirator mask, and closed-toed shoes, were mandatory.

(iii) All secondary sludge or wastes created, especially the spent/used biosorbent containing arsenic, mercury, and other heavy metals were properly managed by disposing of them safely into a designated incinerator. In the event that arsenic, mercury, and other heavy metals solutions or salts were spilled, the spill was cleaned up as soon as possible, and the materials used in the clean-up were placed in a clear double plastic bag with the waste labeled and disposed of properly into the designated incinerator.

(iv) Absolutely no eating, drinking, or chewing gum where arsenic and mercury as well as other heavy metals were used. Also, hands and forearms were washed thoroughly with soap and water each time gloves were removed.

(v) All activities involving open sources of liquid arsenic and mercury, as well as any heavy metal-containing organic/inorganic compounds, were performed in a certified

chemical fume hood.

(vi) All sample containers and glassware were treated with 10% nitric acid, then washed thoroughly with tap water and rinsed with distilled water before being used.

(vii) All of the chemicals and reagents used in the experiments were of analytical quality. Besides, every analytical instrument was calibrated with commercially available chemicals and validated with standard reference materials and approved reference materials.

(viii) The stock solutions containing arsenic, mercury, and other heavy metals were freshly prepared and diluted for each biosorption study to minimize errors in the experimental data. Also, sample solutions collected after the biosorption process were provided with identification labels before they were sent for analysis.

CHAPTER FOUR

RESULTS AND DISCUSSION

4.1 Physicochemical Parameters of the Biosorbent

The physiochemical parameters including moisture content, bulk density, volatile matter, ash content, carbon yield, pH of biosorbent, fixed carbon content, iodine number, and pH of point of zero charge of the biosorbent were investigated and the results are summarized in Table 11.

The physicochemical characteristics of the prepared hybrid granular activated carbon, as presented in Table 11, are consistent with results reported in the literature for activated carbon derived from various agricultural waste materials. This includes activated maize cob (Agbajelola *et al.*, 2015), activated *Albizia saman* (Akpen *et al.*, 2016), and rice hull activated carbon (Mukoko *et al.*, 2015), which have all been effectively applied for the adsorptive removal of heavy metals from aqueous systems. Also, arsenic [As(III)] and mercury [Hg(II)] background concentrations were determined in the activated carbon precursor before the biosorption process. It was found that both As(III) and Hg(II) ions were not present in activated carbon precursor and thus had no effect on the results of the study.

Table 11: Physiochemical parameters of the prepared hybrid granular activated carbon

Physiochemical parameter	Parameter value
Moisture content (%)	2.15 ± 0.03
Bulk density (g/cm^3)	0.38 ± 0.08
Volatile matter (%)	25.60 ± 0.02
Ash content (%)	1.05 ± 0.05
Carbon yield (%)	85.75 ± 0.06
pH of biosorbent	7.20 ± 0.01
Fixed carbon content (%)	71.20 ± 0.03
Iodine Number (mg/g)	952.36 ± 0.04
Point of zero charge pH (pH_{pzc})	3.20 ± 0.01
Arsenic (mg/L)	Not detected (N.D.)
Mercury (mg/L)	Not detected (N.D.)

4.1.1 Moisture Content

A moisture level of 30% or less is required for biomass to be carbonized since vaporizing biomass with a high moisture content would require more heat energy and time (Menya *et al.*, 2018; Janković *et al.*, 2019). According to Table 11, the results of the current study revealed that the activated carbon had a moisture content of 2.15%. It has been discovered that a moisture level of less than 20% is ideal for the preparation of granular activated carbons from biomass, with lower values causing the granules to disintegrate and higher values lowering their longevity and strength (Missagia *et al.*, 2011). By strengthening hydrogen bonds and van der Waals forces, granular activated carbons prepared at the right moisture content also promote the bonding nature of particles (Rizhikovs *et al.*, 2012; Hu *et al.*, 2016). The ideal granulation pressure, use, kind of binder, and energy consumption during granulation are all affected by the moisture content as well (Smith *et al.*, 2012).

4.1.2 Bulk Density

When choosing the precursor materials for activated carbon, bulk density and hardness are crucial factors. These factors affect the mechanical strength and attrition resistance of the resulting granular activated carbon needed for use in high-pressure aqueous solutions (Smith *et al.*, 2012; Hernández *et al.*, 2014). Granular activated carbon's resilience to attrition is a crucial quality since it enables the preservation of the material's physical integrity and resistance to frictional forces experienced during water treatments (Qiu & Guo, 2010). The 0.38 g/cm^3 bulk density obtained in this study was found to be greater than 0.25 g/cm^3 suggesting better filterability of the biosorbent (Bayuo *et al.*, 2020c). The amount of water contaminants that can be treated by the activated carbon per unit of time shows dependence on the bulk density (Dzigbor & Chimphango, 2019).

4.1.3 Volatile Matter

A high volatile matter percentage encourages high porosity, which results in a large surface area of the developed activated carbon (Dzigbor & Chimphango, 2019). The volatile matter of the carbon precursor determined in the current study was 25.6%, which resulted in a high carbon yield and an increase in the fixed carbon. For the manufacture of activated carbon, it has been discovered that a volatile matter percentage > 70% (on a dried basis) is preferable (Menya *et al.*, 2018). However, larger levels of volatile matter lead to lower levels of fixed carbon (Olupot *et al.*, 2016) and with a corresponding reduction in the biochar and activated

carbon yields (Acevedo-Páez *et al.*, 2020). When compared to their inorganic counterparts, organic binding agent granules often contain more volatile matter, less ash, and fixed carbon (Hu *et al.*, 2015). However, the continual emission of organic carbon during water purification caused by the utilization of organic binders can alter the structural morphology of the manufactured granular activated carbon, impairing its adsorption capabilities (Ogata *et al.*, 2012).

4.1.4 Ash Content

Depending on how much ash is present in the biomass and subsequently, in the activated carbon, the existence of ash in particular biomass could be beneficial or detrimental to the adsorption process. For example, silica in the ash combines with the activating agent during chemical activation, lowering the desired ideal activating agent/precursor ratio that would otherwise be required to develop activated carbons with higher adsorption characteristics (Menya *et al.*, 2018). In addition, the high ash concentration may prevent pore formation, resulting in activated carbon with a low specific surface area (Bandara *et al.*, 2020). The precursor for activated carbon (dry basis) needs to have an ash level of less than 5% to minimize these complications (Jjagwe *et al.*, 2021). In this study, the ash content was determined to be 1.05% indicating the suitability of using the carbon precursor in producing high-quality granular activated carbon.

4.1.5 Carbon Yield

Chemical activation, which is regulated by the impregnation ratio of the activator to the precursor, has a significant impact on the carbon yield of the precursor. The carbon yield, surface area, adsorption capacity, and activation energy are all affected by the impregnation ratio. The carbon yield of the precursor was found to be high representing 85.75%. The chemical activation leads to higher carbon yields due to lower activation temperatures and the dehydrating effects of activators, which prevent the formation of tar (Jjagwe *et al.*, 2021). Due to the restrictions in the synthesis of tars and volatiles, chemical activation produces higher carbon yields than physical activation through de-polymerization, dehydration, and condensation (Bedia *et al.*, 2020). In contrast to physical activation, chemical activation results in uniformly produced interior micropores with minimal morphological alterations. Physical activation carbon yields are reduced due to non-homogeneity in pore formation and morphology as well as the increase in weight losses (Ideta *et al.*, 2020).

4.1.6 Fixed Carbon Content

Fixed carbon content gives information on the amount of biochar formation in the carbonization process and it is usually the remains of solid combustible residues after the volatile matter drives off. The fixed carbon content of the precursor was found to be 71.45%. The higher the fixed carbon, the higher the biochar production in the thermochemical conversion process as a product yield. However, to increase activated carbon yield, the carbon component of the precursor should be between 40 and 90% (Nieto-Delgado *et al.*, 2011).

4.1.7 Iodine Number

The pore volume that is accessible in the activated carbon of interest can be determined by the iodine number, which is a measurement of the iodine adsorbed in the pores (Al-Rub *et al.*, 2003). The most essential measure for characterizing the effectiveness of activated carbon is its iodine number, which is typically utilized as a quick commercial test for determining the adsorbent's quality. It provides details regarding the internal surface of the adsorbent, with 1.0 mg of the iodine absorbed being equivalent to a 1.00 m^2 internal surface (El-Hendawy *et al.*, 2001; Machrouhi *et al.*, 2019). In this study, the iodine number was obtained as 952.36 mg/g, which falls within the suggested range of 600-1100 mg/g (Mukoko *et al.*, 2015). The iodine number obtained suggests a higher degree of carbon precursor activation and high adsorptive capacity of the produced biosorbent for the removal of As(III) and Hg(II) as well as other heavy metal ions from single-component and multi-component biosorption systems.

4.1.8 pH and Point of Zero Charge (pH_{pzc}) of the Biosorbent

The pH of the prepared hybrid granular activated carbon was found to be neutral with a pH value of 7.20 and the pH of the point of zero charge of the biosorbent was determined to be 3.2 as shown in Fig. 8. In most adsorption experiments, the pH of the point of zero charge (pH_{pzc}) should be compared with the pH of the adsorption system as pH_{pzc} determined the limitations of the solution pH (Aeisyah *et al.*, 2014). At a pH value below pH_{pzc}, the surface of the biosorbent will be positively charged, whereas at a pH above the pH_{pzc}, the surface of the biosorbent will be negatively charged (Sellaoui *et al.*, 2017). Generally, the negatively charged biosorbent surface charge enhances the uptake of metal cations from the aqueous solutions.

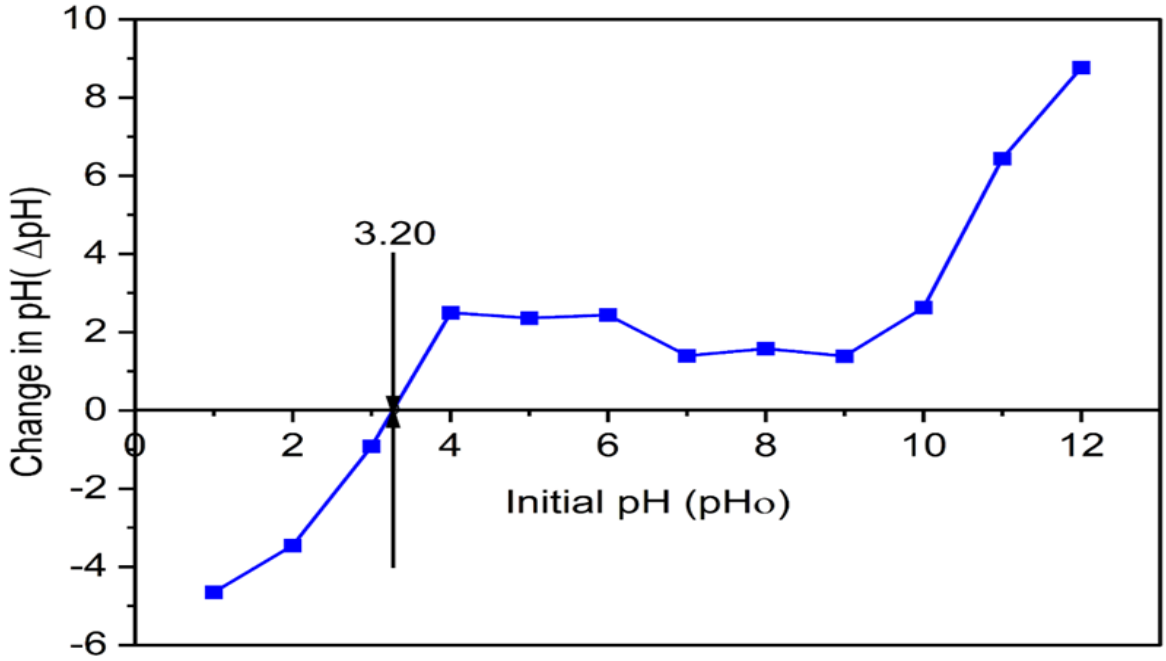

Figure 8: pH of the point of zero charge (pHpzc) of the hybrid granular activated carbon

4.2 Characterization of the Biosorbent

4.2.1 Thermogravimetric Analysis (TGA)

The thermogravimetric analysis (TGA) makes it feasible to discover potential weight or constituent losses due to temperature action while also determining the sorbent material stability throughout a range of temperatures. Figures 9 (a) and (b) represent the TGA curves of the thermal degradation process of the carbon precursors attained at 10 °C min^{-1} heating rate from 25-1000 °C in an inert (nitrogen) environment to prevent combustion.

Figure 9 (a), which depicts the unmodified carbon precursor, demonstrates that the TGA took place in two steps. The first stage, which occurred between 25 and 230 °C, had a weight loss of 4.18% that was attributable to water loss in the carbon precursor. The second stage, which took place between 230 and 900 °C and resulted in 69.02% weight loss, was attributable to lignocellulose degradation. However, the TGA curve of the activated carbon presented in Fig. 9 (b) can be divided into three stages of weight losses in the temperature ranges of 50-500 °C, 500-830 °C, and 830-975 °C, respectively. The first weight loss of 20.90% at the temperature range of 50-500 °C is due to the desorption of physically adsorbed and interlamellar water molecules as well as the devolatilization of organic matter from the activated carbon (Zhao *et al.*, 2019). In phase two, the weight loss of 28.55% from 500-830 °C is a result of the

degradation of hemicellulose, cellulose, lignin, and surface functional groups. The third weight loss of 22.76% which occurred at 830-975 °C is attributed to the disappearance of the carbon skeleton. More importantly, it was found that there is an increase in weight loss starting at 500-975 °C suggesting the existence of carbonyls, basic, and phenols groups in the hybrid activated carbon (Labied *et al.*, 2018). The TGA results showed that the hybrid granular activated carbon is thermally stable than the biochar and can be applied as a potential biosorbent for the decontamination of As(III) and Hg(II) ions from aquatic environments without losing its microstructure.

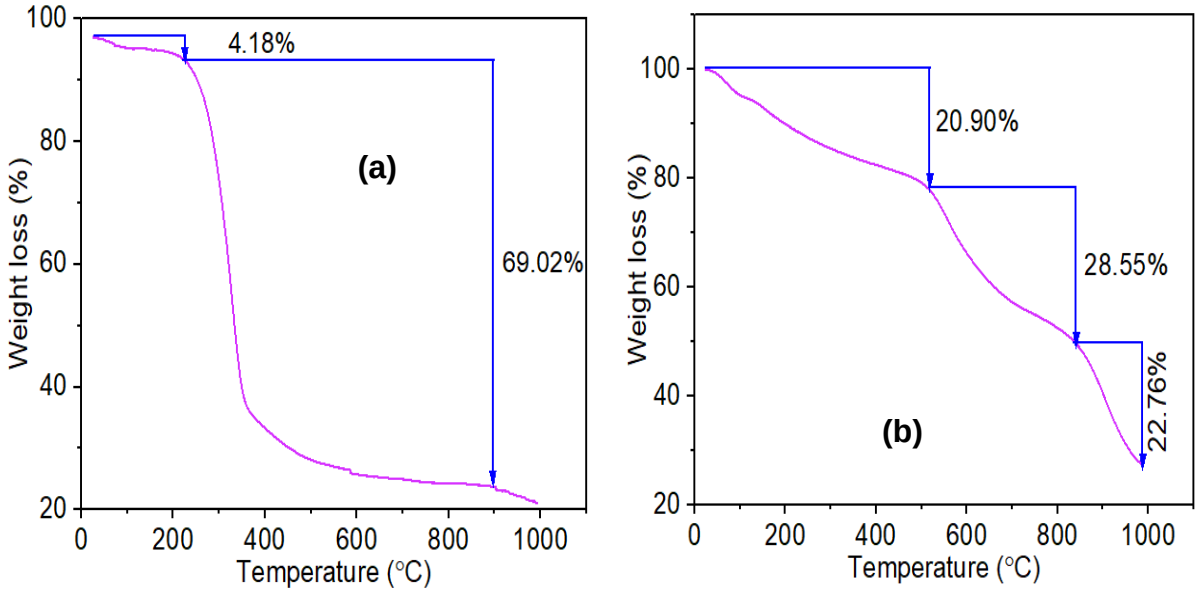

Figure 9: TGA of the raw carbon precursor (a) and the hybrid granular activated carbon (b)

4.2.2 Scanning Electron Microscopy (SEM) and Energy Dispersive Spectroscopy Analysis

The SEM was utilized to study the morphological features and surface properties of the HGAC, while the EDS was utilized in the determination of the elemental compositions in the HGAC. The SEM micrograph of the pristine HGAC was determined at a scale of 50 µm before the abatement of the As(III) and Hg(II) ions from the non-competitive and competitive sorption systems as presented in Fig. 10 (a). In Fig. 10 (a), the rough microstructure, intergranular pores, and presence of numerous voids, and fissures in the SEM image may make it easier for As(III) and Hg(II) ions to interact with the biosorbent surface, resulting in the efficient elimination of As(III) and Hg(II) ions from the non-competitive and competitive sorption systems. The micro- and mesopores development in the HGAC might be triggered by the volatilization of various

constituents including hemicellulose, cellulose, lignin, and other organic components found in the maize residues during the impregnation and activation process of the carbon precursor using H_3PO_4. The EDS results displayed in Fig. 10 (b) showed the elemental composition of the HGAC before the sorption process of As(III) and Hg(II) ions from the non-competitive and competitive sorption systems. The major elements found in the HGAC with the highest percentage weight composition (wt%) include carbon (C, 88.71%), oxygen (O, 31.49%), phosphorus (P, 6.90%), silicon (Si, 2.13%), sodium (Na, 0.47%), potassium (K, 0.21%), and calcium (Ca, 0.08%).

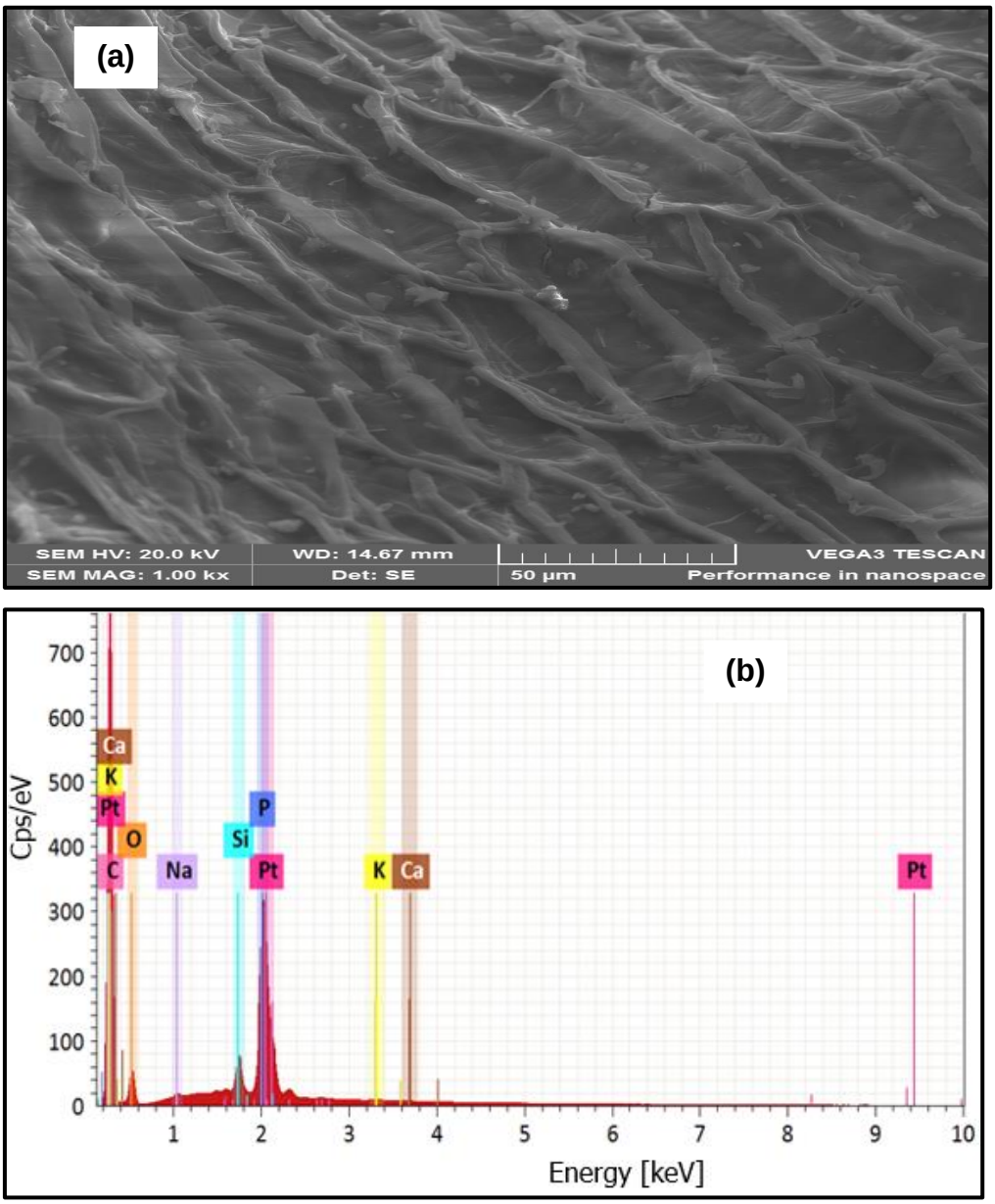

Figure 10: **SEM image (a) and EDS spectrum (b) of the biosorbent before the biosorption of As(III) and Hg(II) ions from the non-competitive and competitive sorption systems**

4.2.3 Transmission Electron Microscopy (TEM) Analysis

The TEM micrograph of the HGAC before the decontamination of As(III) and Hg(II) ions from the non-competitive and competitive sorption systems is displayed in Fig. 11. The TEM image of the untreated biosorbent with the heavy metal ions presented in Fig. 11, shows that the biosorbent is transparent, porous, rough, and highly aggregated with wrinkles loosely distributed on the surface. The wrinkles on the surface of the biosorbent and its porous nature could increase the biosorbent surface area and favor As(III) and Hg(II) ions removal from the non-competitive and competitive aqueous media.

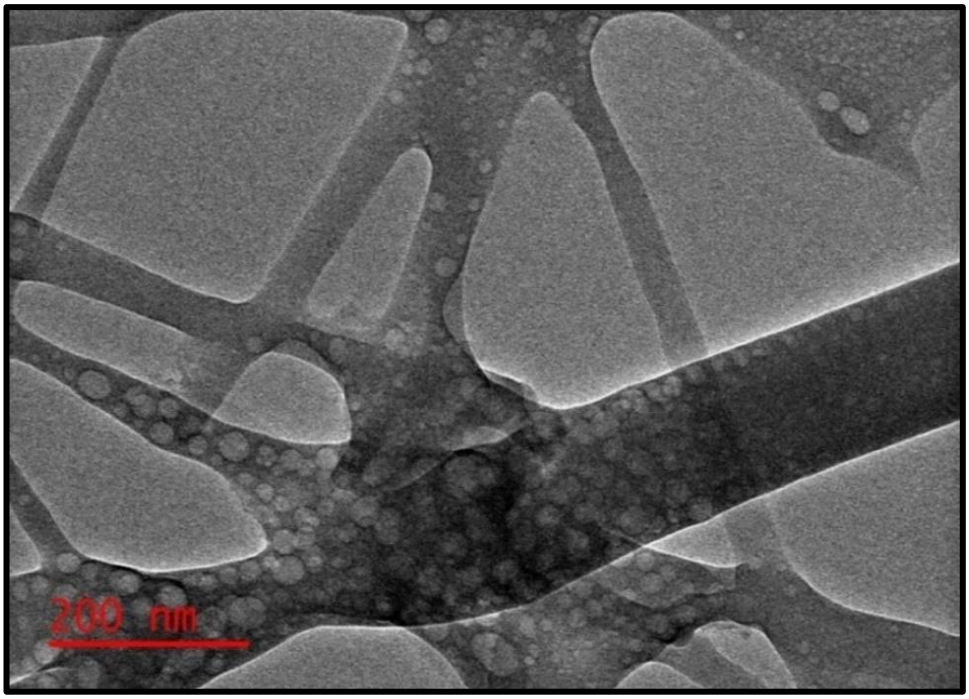

Figure 11: TEM image of the biosorbent before the biosorption of As(III) and Hg(II) ions from the non-competitive and competitive sorption systems

4.2.4 X-Ray Diffraction (XRD) analysis

The X-ray diffraction pattern of the as-prepared biosorbent before the removal of As(III) and Hg(II) ions from the non-competitive and competitive biosorption systems is presented in Fig. 12. It was observed that there is a broad diffraction peak located at $2\theta = 28.27°$, which indicates the presence of carbon structure in the biomaterial (Yusuff, 2018). The existence of the broad peak also suggests that the prepared granular activated carbon obtained from the maize residues was mainly amorphous and porous in nature (Mukoko *et al.*, 2015).

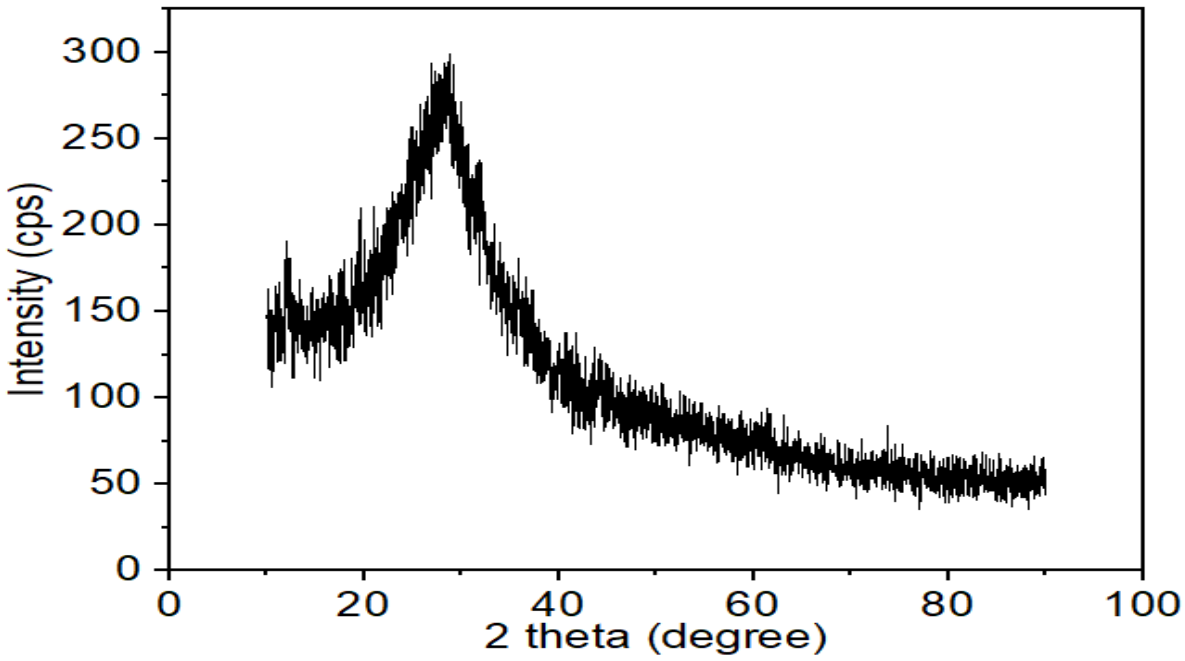

Figure 12: XRD spectrum of the biosorbent before the biosorption of As(III) and Hg(II) ions from the non-competitive and competitive sorption systems

4.2.5 Brunauer-Emmett-Teller (BET) Analysis

The Brunauer-Emmett-Teller (BET) specific surface area of biosorbent was determined from nitrogen gas (N_2) adsorption/desorption isotherms obtained using ASAP 2460 Micro metrics, USA. The pore size distribution and BET-specific surface area were determined based on the adsorption-desorption of nitrogen at -196.00 ^{0}C by the Barrett-Joyner-Halenda (BJH) technique (Tang *et al.*, 2018). The micropore area and micropore volume were also computed by the application of the t-plot method (Labied *et al.*, 2018). At a relative pressure of $\frac{P}{P_0} =$ 0.989, the total pore volume was determined from the liquid phase of adsorbate adsorbed. As shown in Fig. 13, both the biochar (BC) and the activated carbon (AC) exhibited type-II isotherm according to the International Union of Pure and Applied Chemistry (IUPAC) classification (Labied *et al.*, 2018). In the type-II isotherm, the nitrogen adsorption and desorption branch coincided, indicating a characteristic of non-porous or microporous biosorbent and the knee of the isotherm was an indication of completion of monolayer adsorption and initiation of multilayer adsorption (Drweesh *et al.*, 2016).

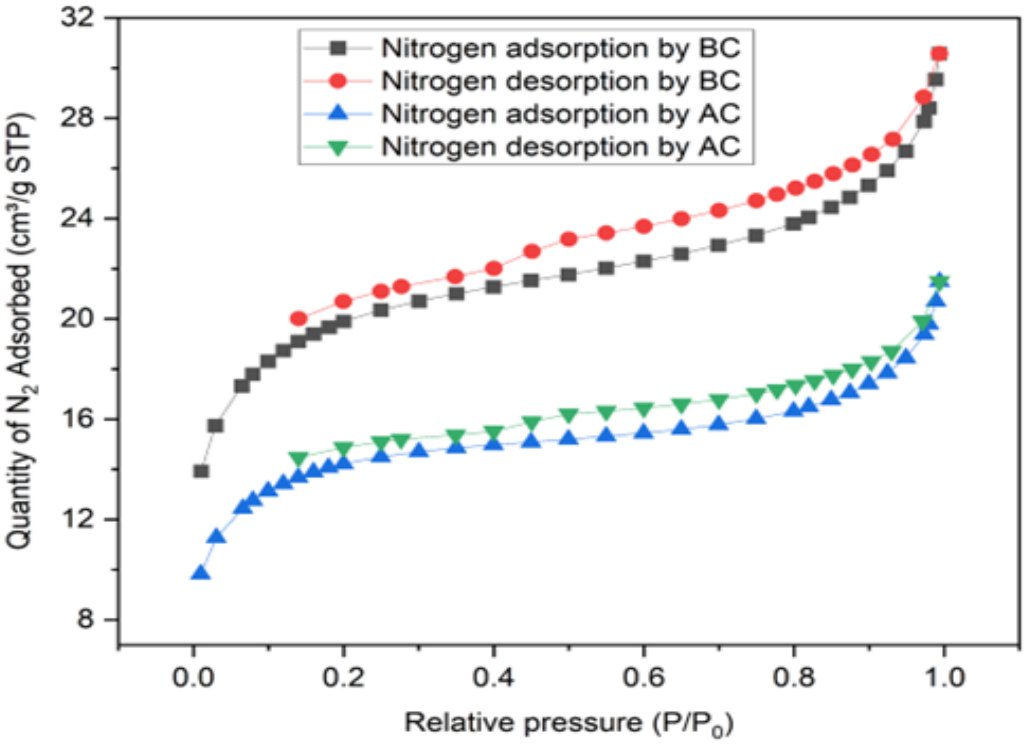

Figure 13: Nitrogen adsorption-desorption isotherms of the biochar (BC) and H_3PO_4-activated carbon (AC) derived from maize residues

Due to either chemisorption or physisorption or both taking place at the surface and in the pore structure of porous materials, these textural parameters are crucial when applying them in sorption processes (Omri & Benzina, 2012). Hence, the textural properties of the prepared granular activated carbon before and after surface modification are given in Table 12. As summarized in Table 12, the BET surface area of the biochar obtained after the maize residues were carbonized at 500 ℃ was relatively small, which was only 473.6 m^2/g, and the total pore volume was 0.0286 cm^3/g.

Table 12: Textural properties of the biochar before and after chemical activation

Textural parameter	Biochar (BC)	Activated carbon (AC)
BET surface area (m^2/g)	473.6	1254.8
Micropore surface area (m^2/g)	124.3	312.7
Total pore volume (cm^3/g)	0.0286	0.0813
Micropore volume (cm^3/g)	0.0119	0.0450

However, the BET surface area of the biochar after H_3PO_4 activation (hybrid granular activated carbon) was obvious, reaching 1254.9 m^2/g, and the proportion of micropores was extremely

large, which might play a significant role in the adsorptive removal of As(III) and Hg(II) from the wastewater (Liu *et al.*, 2021). At the same time, the pore volume of the activated carbon also increased to 0.0450 cm^3/g. The increase in pore volume could provide more adsorption sites and promote the decontamination of As(III) and Hg(II) ions from the non-competitive and competitive sorption systems.

4.2.6 Fourier Transform Infrared Spectrometry (FT-IR) Analysis

Surface functional group analysis of the biosorbent was conducted by Fourier Transform Infrared Spectrophotometer operating between 400 and 4000 cm^{-1}. The FT-IR spectra of the biosorbent before the biosorption process as well as after the biosorption of As(III) and Hg(II) ions from non-competitive and competitive sorption systems are shown in Fig. 14. Figure 14 shows the FT-IR spectrum of the biosorbent before the biosorption process and spectral bands were observed at 3341.60, 2849, 2921.90, 1734, 1597, 1317.80, 1370.40, 1241, and 1034.23 cm^{-1}.

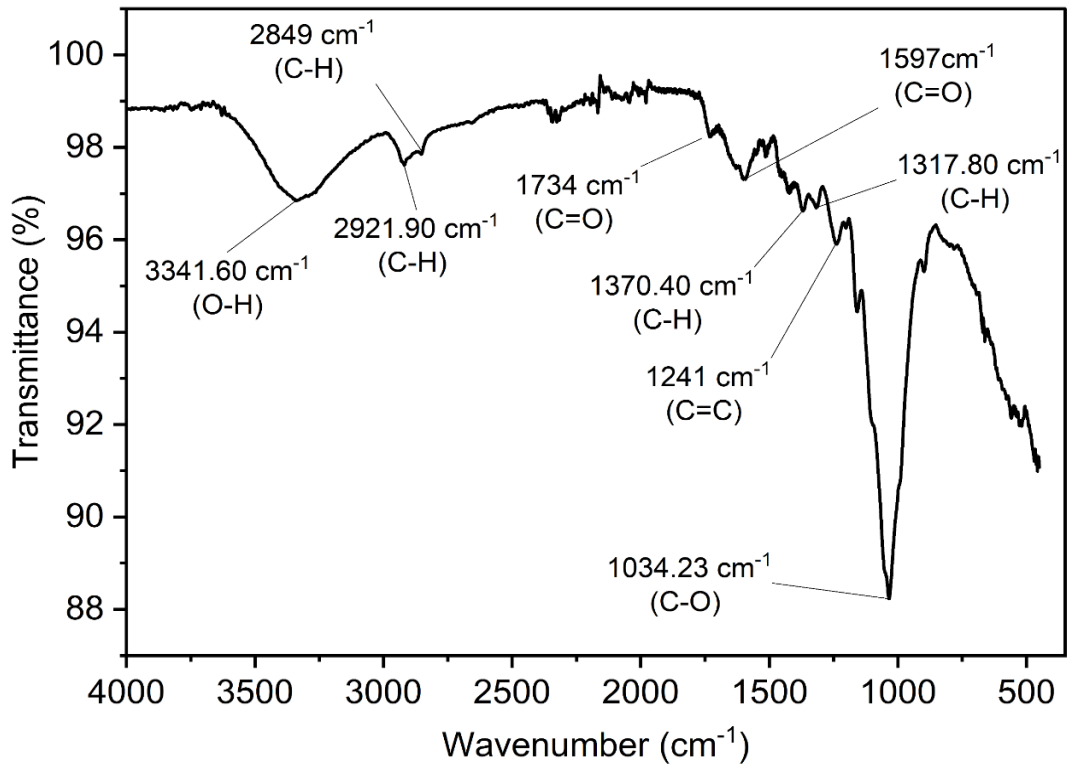

Figure 14: FT-IR spectra of the biosorbent before the sorption process of As(III) and Hg(II) ions from the non-competitive and competitive sorption systems

The broad stretching absorption peak at around 3341.60 cm^{-1} represents the stretching vibration of the hydroxyl (O-H) as well as amino (N-H) functional groups (Fooladgar *et al.*, 2019). The

absorption bands at 2849 and 2921.90 cm^{-1} correspond to the (C-H) asymmetric and symmetric stretching vibrations, respectively (Siddiqui *et al.*, 2020). The spectral band around 1597-1734 cm^{-1} is a result of the stretching of the carbonyl (C=O) functional groups due to the hemicelluloses and lignin aromatic groups (Bayuo *et al.*, 2019). The peaks around 1317.80 and 1370.40 cm^{-1} are due to aromatic (C-H) and carboxyl-carbonate structures (Mukoko *et al.*, 2015). Also, the absorption bands around 1241 and 1034.23 cm^{-1} correspond to the stretching of unsaturated aliphatic (C=C) and (C-O) functional groups, respectively (Sun *et al.*, 2019).

4.3 Independent Factors Influencing As(III) and Hg(II) Removal from Sorption Systems

4.3.1 Effect of Contact Time

The biosorption of As(III) and Hg(II) ions from monocomponent (non-competitive) and bicomponent (competitive) sorption systems onto the hybrid activated carbon by varying contact time as a function of removal efficiency and biosorption capacity is shown in Fig. 15, respectively.

The biosorption process of As(III) and Hg(II) ions from the monocomponent and bicomponent sorption systems was observed to take place in two stages. While the percentage removal and uptake capacity of As(III) and Hg(II) ions by the HGAC from the monocomponent and bicomponent media was observed to increase with increasing contact time during the initial stage, the second stage represented a slow progressive biosorption process as displayed in Figs. 15 (a-d), respectively. The rapid detoxification of the As(III) and Hg(II) ions from both biosorption systems during the first phase suggests the availability and large active biosorbent surface phenomena for the adsorptive removal of As(III) and Hg(II) ions from the wastewater (Alam *et al.*, 2018). Furthermore, the presence of hydroxyl groups in biosorbent facilitates the formation of complexes between As(III) and Hg(II) ions and the biosorbent surface causing faster biosorption (Ahmad & Haseeb, 2015).

In Figs. 15 (a) and (c), the equilibrium biosorption of As(III) from the monocomponent and bicomponent sorption systems was achieved at 60 and 120 min with removal efficiencies of 92.26 and 84.93%; and biosorption capacities of 15.38 and 14.16 mg/g, respectively (Appendix 1). Also, at contact times of 90 and 120 min, optimum percentage elimination of 96.09 and 95.84% as well as uptake capacity of 16.02 and 15.97 mg/g was attained by the HGAC for Hg(II) removal from the monocomponent and bicomponent sorption media as displayed in Figs.

15 (b) and (d), respectively (Appendix 2). Comparatively, the maximum removal efficiency and uptake capacity of As(III) and Hg(II) ions from the bicomponent sorption systems were found to be relatively smaller than those in the monocomponent systems. This implies that the coexistence of both As(III) and Hg(II) ions in the bicomponent system inhibited the removal of each heavy metal ion indicating an antagonistic effect.

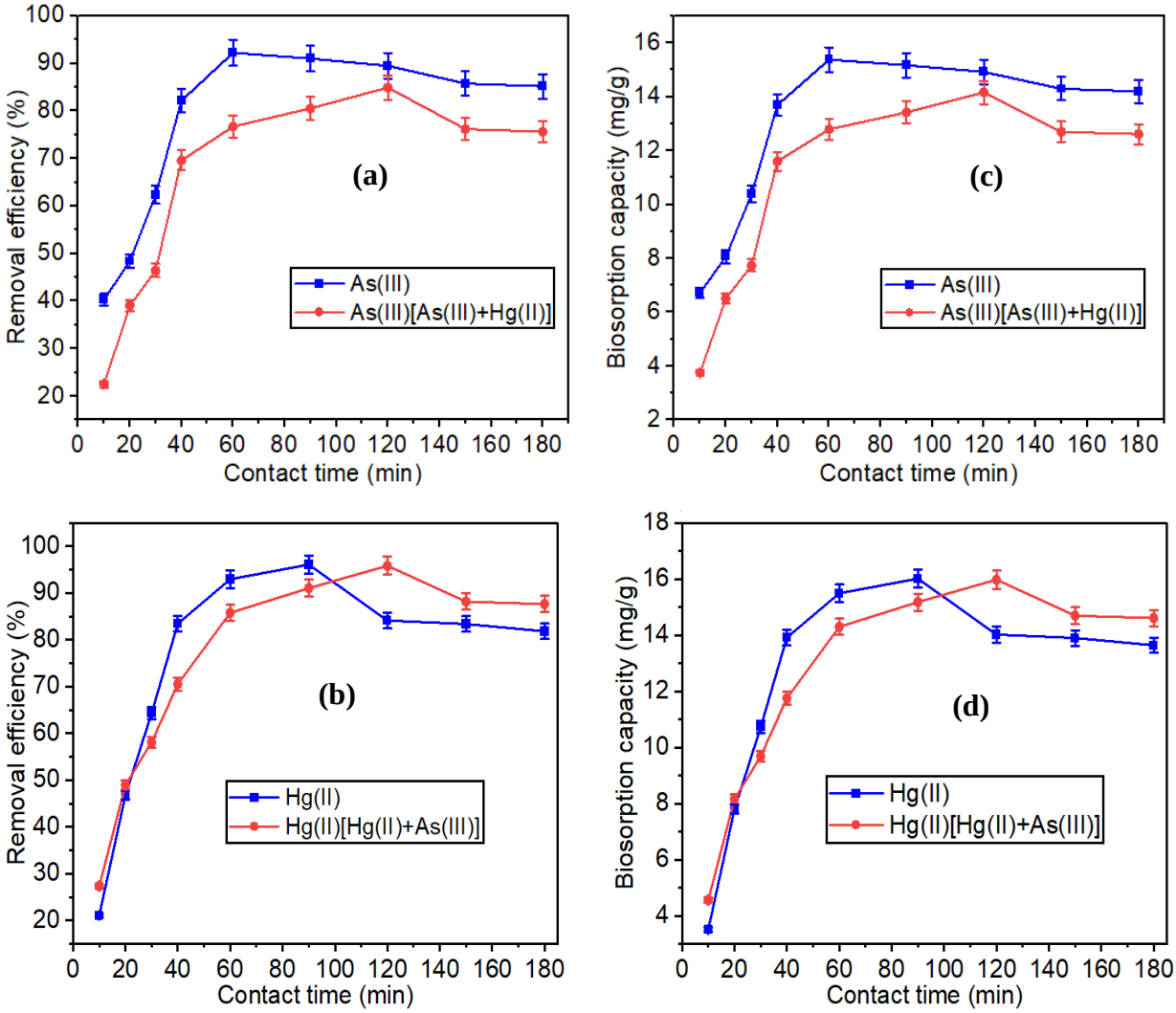

Figure 15: Effect of contact time on removal efficiency (a and b) and biosorption capacity (c and d) on As(III) and Hg(II) removal from monocomponent and bicomponent sorption systems, respectively

4.3.2 Effect of Initial pH of the Solution

The effect of solution pH on the decontamination of As(III) and Hg(II) ions from the monocomponent and bicomponent sorption systems onto the biosorbent at different pH values is shown in Figs. 16 (a-d), respectively. Figures 16 (a) and (c) show that the removal efficiency and uptake capacity of As(III) ions from the monocomponent sorption system are augmented

by increasing the pH of the solution (Appendix 3).

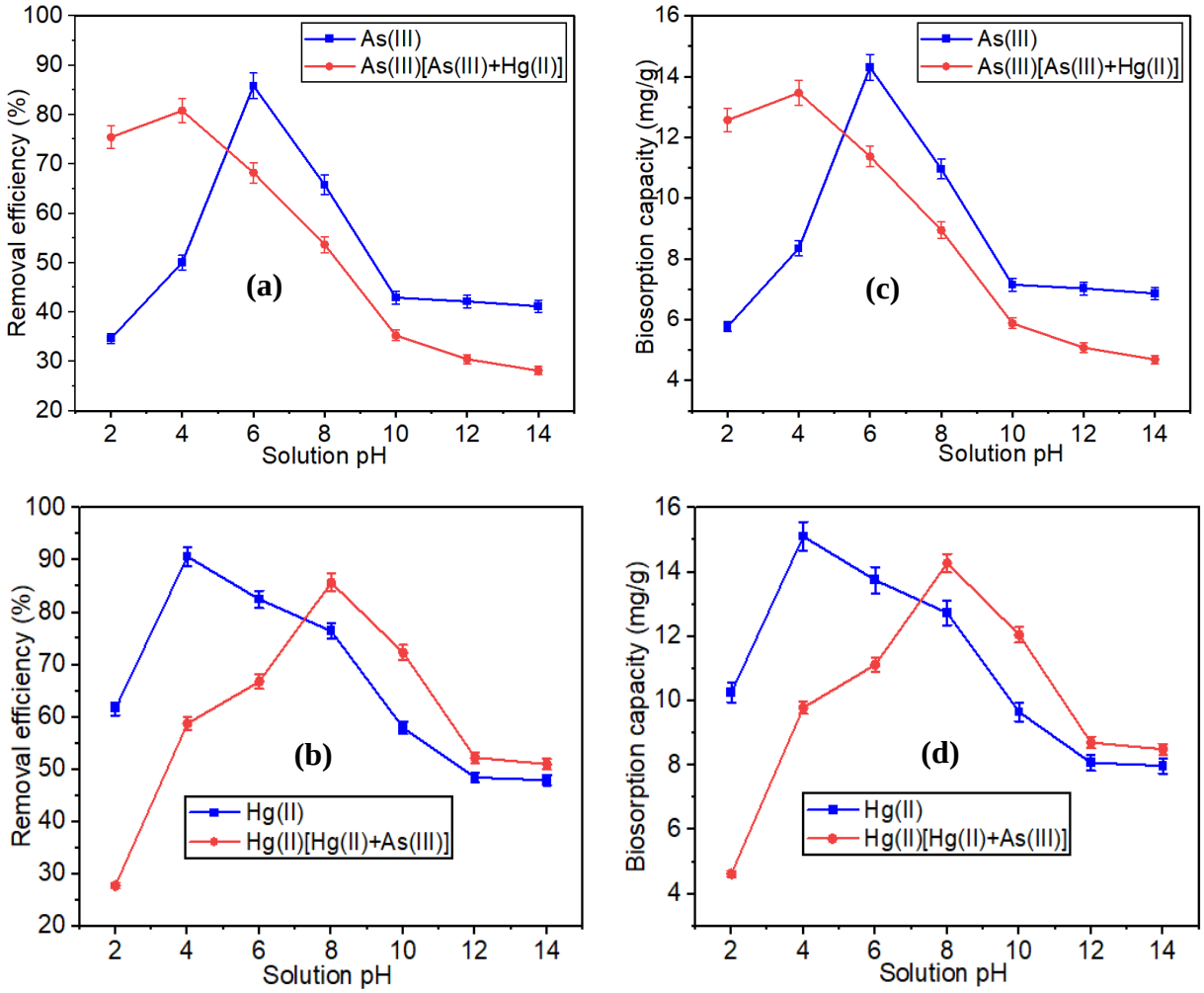

Figure 16: Effect of pH of solution on removal efficiency (a and b) and biosorption capacity (c and d) on As(III) and Hg(II) removal from monocomponent and bicomponent sorption systems, respectively

Whilst, the removal efficiency and uptake capacity of As(III) ions by the biosorbent in the binary component system all decreased with the increasing pH of the solution. At about solution pH of 6 and 4, the equilibrium biosorption of As(III) ions from the single-metal and binary-metal systems was achieved with a maximum removal efficiency of 85.83 and 80.81% and biosorption capacity of 14.30 and 13.47 mg/g, respectively. The removal rate of As(III) ions from both the monocomponent and bicomponent sorption systems decreased sharply after the pH of 6 and 4, respectively because of the high competition of excessive OH^- and the As(III) ions in the solution (Kango & Kumar, 2016; Yang *et al.*, 2020).

In Figs. 16 (b) and (d), it was found that the removal rate and sorption capacity of Hg(II) by the HGAC in the monocomponent sorption medium increased with decreasing pH of the

aqueous solution. It was observed that the percentage removal and uptake capacity of the Hg(II) ions by the biosorbent increased during the first stage because there is no precipitation of the metal ions but at higher pH values, the metal ions will precipitate in the form of hydroxyl ions, which will compete for the binding sites on the biosorbent surface. Meanwhile, the decontamination of Hg(II) from the bicomponent sorption system augmented at higher pH values and this is because the solution pH facilitated the Hg(II) ions to bind to the available functional groups present on the HGAC surface. The active HGAC sorption sites were better able to deprotonate when the solution pH increased and created a more negative charge on the HGAC surface, which has a strong affinity for the Hg(II) ions (Egirani *et al.*, 2021). While maximum removal efficiency of 90.67% and uptake rate of 15.11 mg/g was accomplished at the pH of 4 from the monocomponent sorption system, optimal elimination of Hg(II) from the bicomponent system was attained using a pH of 8 with removal rate and uptake capacity of 85.68% and 14.28 mg/g, respectively (Appendix 4).

In contrast, the biosorption of As(III) and Hg(II) ions from the monocomponent system was higher than that in the bicomponent sorption system. This is because as the amount of biosorbent dose and concentration of the As(III) and Hg(II) is the same in the bicomponent system, the heavy metal ions will compete with each other for the limited adsorption sites, which exert an antagonistic effect on the removal of the single heavy metal ions.

The surface charge of every biosorbent plays a vital role in heavy metal ions adsorption and this is determined by the pH point of zero charge (pHpzc). The pHpzc is the pH at which the biosorbent surface is universally neutral with the same number of negatively and positively charged surface functions. At solution pH values below the pHpzc, the bio-adsorbent surface is positively charged, and at solution pH values beyond the pHpzc, the bio-adsorbent is negatively charged (Sajjadi *et al.*, 2018). The pHpzc of the HGAC was found to be 3.2, which is below the optimum solution pH values obtained for the monocomponent and bicomponent sorption systems thereby creating a negatively charged surface. Therefore, it was much easier to adsorb metal cations such as the As(III) and Hg(II) ions on the negatively charged biosorbent surface. A similar trend was observed by Bashir *et al.* (2019).

4.3.3 Effect of Biosorbent Particle Size

The effect of the biosorbent particle size on the detoxification of As(III) and Hg(II) ions from non-competitive and competitive biosorption systems is presented in Fig. 17. In Figs. 17 (a-d),

an upsurge in the biosorbent particle size caused a decrease in the removal efficiency and uptake capacity of As(III) and Hg(II) ions by the biosorbent from both monocomponent and bicomponent sorption systems, respectively.

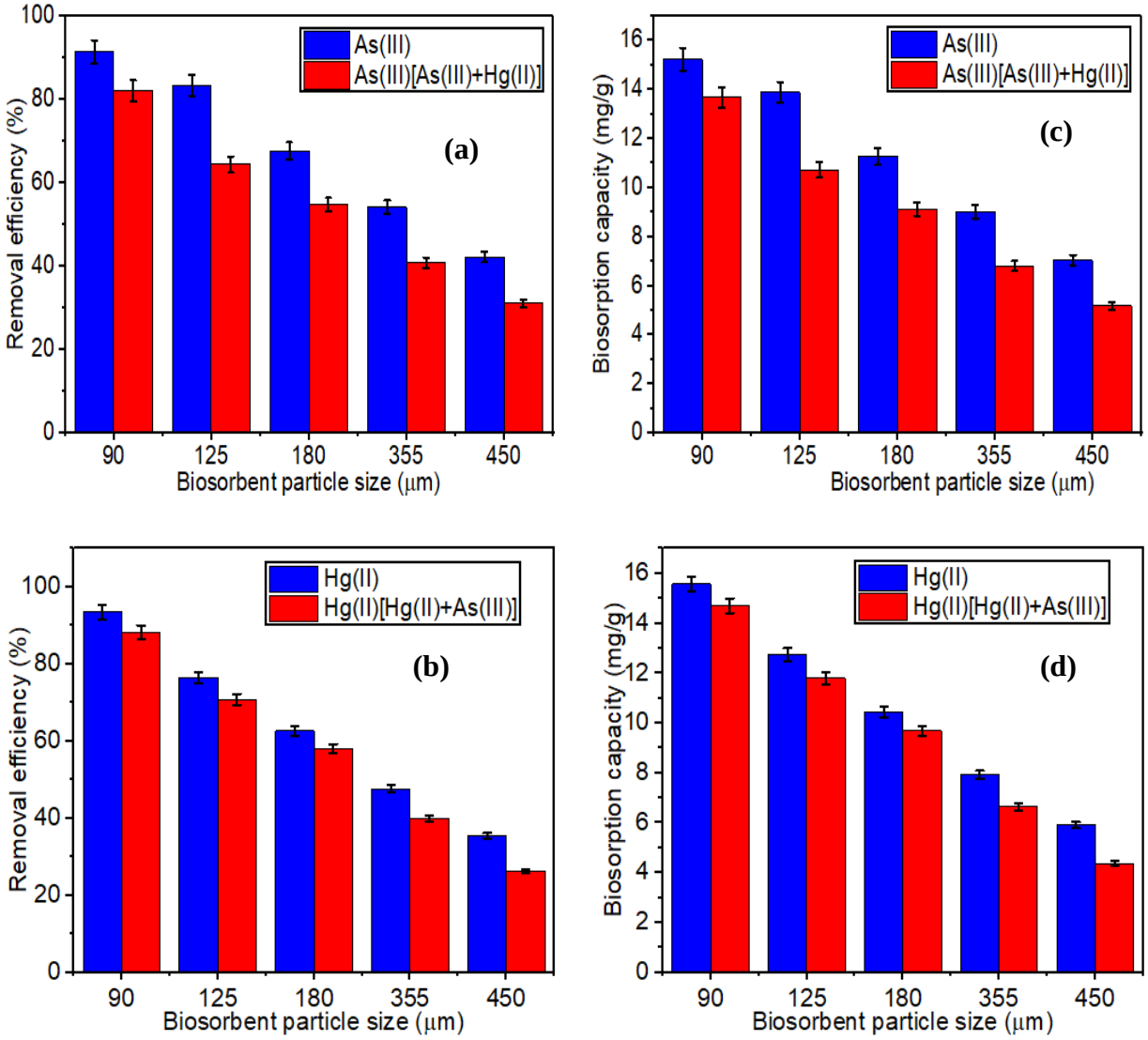

Figure 17: Effect of biosorbent particle size on removal efficiency (a and b) and biosorption capacity (c and d) on As(III) and Hg(II) removal from monocomponent and bicomponent sorption systems, respectively

At a biosorbent particle size of 90 µm, there was maximum removal of As(III) and Hg(II) ions from both monocomponent and bicomponent sorption systems. The optimum removal efficiency and biosorption capacity of As(III) ions at 90 µm best particle size were found to be 91.43 and 82.09% and 15.24 and 13.68 mg/g for non-competitive and competitive systems, respectively (Appendix 5). Similarly, the Hg(II) maximum removal efficiencies of 93.45 and 88.25% and uptake capacities of 15.58 and 14.71 mg/g, respectively were accomplished for the

non-competitive and competitive systems at a bio-adsorbent particle size of 90 µm (Appendix 6). Studies have shown that as particle size decreases, the surface area of the biosorbent improves, increasing the uptake of the metal ions by the biosorbent (Krika *et al.*, 2016; Nagy *et al.*, 2023). Besides, due to higher access to pores and larger surface area for bulk sorption per unit weight of the biosorbent, decreasing particle size enhances As(III) and Hg(II) ions uptake at a constant biosorbent dosage (Memon *et al.*, 2021; Krishna & Swamy, 2012).

In comparison, the relative biosorption efficiency of As(III) and Hg(II) ions from the non-competitive and competitive aqueous solutions were similar except that the removal efficiency and uptake capacity of As(III) and Hg(II) ions by the biosorbent in the bicomponent sorption systems were less than those determined from the monocomponent system. This is because the coexistence of both As(III) and Hg(II) ions lowered the uptake capacity of each heavy metal ion from the competitive system, which suggests an antagonistic effect.

4.3.4 Effect of Biosorbent Dosage

The effect of biosorbent dosage as presented in Fig. 18 shows that the decontamination of As(III) and Hg(II) ions from the monocomponent and bicomponent sorption systems increased rapidly as the biosorbent dosage upsurges and declined sharply afterward, respectively. In Fig. 18 (a) and (b), As(III) and Hg(II) removal efficiencies attained from the monocomponent and bicomponent sorption systems, respectively increased when the biosorbent concentration increased. It is possible that as the dosage increased, more active sites for binding the metal ions became available, leading to a rise in the amount of As(III) and Hg(II) ions removed from the monocomponent and bicomponent sorption systems (Dawodu *et al.*, 2020). Additionally, the greater uptake efficiency observed may have been caused by an increase in the surface area brought on by a comparable increase in the biosorbent loads (Adio *et al.*, 2019). A similar trend was observed by Hiew *et al.* (2021), in which a corresponding upsurge in biosorbent active sites and surface area due to increasing the biosorbent loads led to an increase in the percentage removal of heavy metal ions.

At biosorbent dosages of 3 and 2.5 g/L, the optimum removal rate of As(III) ions from the monocomponent and bicomponent sorption systems was 98.63 and 93.75%, respectively (Appendix 7). Whilst, the optimal Hg(II) decontamination efficiencies from the monocomponent and bicomponent sorption media were 98.13 and 94.63% attained at 3.5 and 2 g/L, respectively as best bio-adsorbent loads (Appendix 8). However, the sharp decline in the

percentage removal of As(III) and Hg(II) ions from both the monocomponent and bicomponent sorption systems after reaching equilibrium, respectively is due to particle stacking at excess adsorbent dosage, which reduces the active sites on the biosorbent surfaces leading lower uptake of the As(III) and Hg(II) ions by the biosorbent (Memon *et al.*, 2021). Likewise, Peng *et al.* (2018) observed that at excessive doses, particle agglomeration is likely to occur leading to lower removal efficiency of the heavy metal ions on the active sites of the bio-adsorbent.

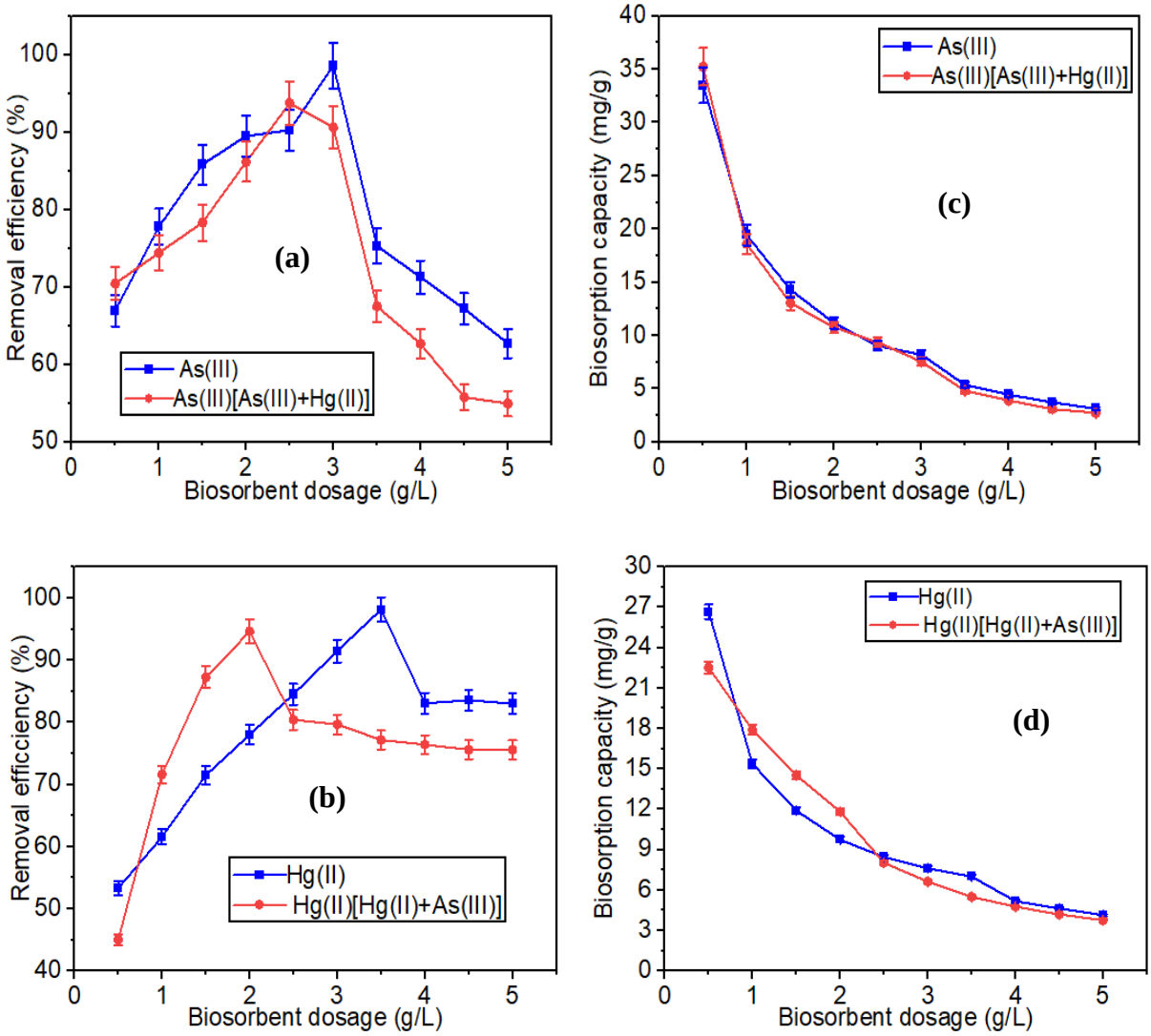

Figure 18: Effect of biosorbent dosage on removal efficiency (a and b) and biosorption capacity (c and d) on As(III) and Hg(II) removal from monocomponent and bicomponent sorption systems, respectively

On the contrary, the biosorption capacities of As(III) and Hg(II) ions from the monocomponent and bicomponent sorption systems increased with decreasing biosorbent loads in which maximum uptake rates of 33.47 and 35.23 mg/g; and 26.67 and 22.54 mg/g, respectively were achieved at a biosorbent dosage of 0.5 g/L as shown in Figs. 18 (c) and (d), respectively. The

decrease in biosorption capacity as the biosorbent dosage increases could be due to the overlapping of available sorption sites because of overfilling of pores on the biosorbent (Essomba *et al.*, 2014). It was also found that the uptake capacity of As(III) ions from the bicomponent sorption system by the biosorbent was higher than that in the monocomponent system due to the synergistic interactive effect between As(III) and Hg(II) ions in the competitive solutions at higher biosorbent loads. In contrast, the Hg(II) ions uptake rate by the HGAC was lower in the bicomponent sorption system than that of the monocomponent system because of the antagonistic effect among Hg(II) and As(III) species in the competitive aqueous solution.

4.3.5 Effect of Initial Metal Ion Concentration

The experimental results of the influence of initial metal ions concentration on the detoxification of As(III) and Hg(II) ions from the monocomponent and bicomponent sorption systems are presented in Fig. 19. As can be seen in Figs. 19 (a) and (b), the removal efficiency increased gradually by decreasing As(III) and Hg(II) initial concentrations in the monocomponent and bicomponent sorption systems, respectively. In Fig. 19 (a), it was found that the removal rate of As(III) ions from the monocomponent and bicomponent sorption systems decreased rapidly after reaching optimum at initial concentrations of 30.00 and 25.00 mg/L with optimum removal efficiencies of 93.26 and 90.65%, respectively (Appendix 9).

Also, in Fig. 19 (b), at initial metal ions concentrations of 45 and 15 mg/L, maximum Hg(II) ions removal rates of 96.78 and 95.13% were achieved by the biosorbent from the monocomponent and bicomponent sorption media, respectively (Appendix 10). The percentage removal of As(III) and Hg(II) ions from the monocomponent and bicomponent sorption systems decreased at elevated initial concentrations due to surface-reactive sites getting occupied steadily and reaching saturation point (Pasgar *et al.*, 2022). Likewise, Igberase *et al.* (2017) investigated the removal of Pb(II), Zn(II), Cu(II), Ni(II), and Cd(II) by modified ligand as an adsorbent and it was observed that at lower initial concentrations, Pb(II), Zn(II), Cu(II), Ni(II), and Cd(II) removal efficiencies were very high. However, at higher initial concentrations, lower removal efficiencies were recorded for all heavy metals. This was because as the initial concentration upsurges, more metal ions are present in the aqueous solution, which leads to more ions being adsorbed to the same amount of adsorbent. This causes the biosorbent to become saturated, which lowers the removal efficiencies of the heavy metals. Similar trends were observed by Hosseini-Bandegharaei *et al.* (2011) and Chen *et al.* (2017),

in which a decrease in concentration increased the removal efficiency.

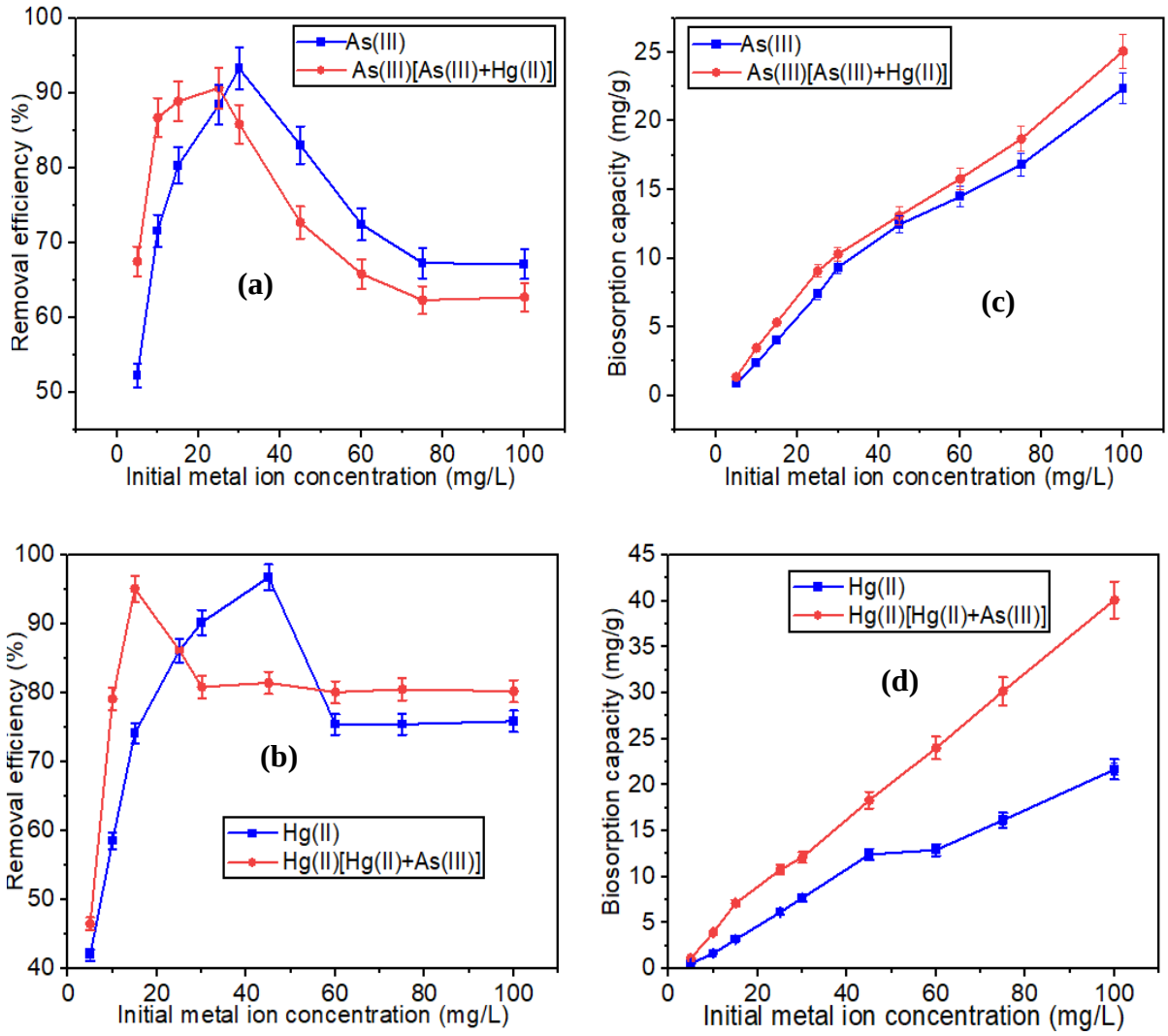

Figure 19: Effect of initial concentration on removal efficiency (a and b) and biosorption capacity (c and d) on As(III) and Hg(II) removal from monocomponent and bicomponent sorption systems, respectively

In Figs. 19 (c) and (d), the biosorption capacity of As(III) and Hg(II) ions increased with increasing initial metal ions concentration in both monocomponent and bicomponent sorption systems. This is because the mass transfer resistance decreased due to the enhanced driving force at increasing initial concentration allowing more As(III) and Hg(II) species to be adsorbed onto the biosorbent (Hiew *et al.*, 2021). Similarly, Sha *et al.* (2018) observed that at low concentrations, there are fewer heavy metal ions to occupy the active sites on the biosorbent surface and as the concentration of the heavy metal upsurges, the driving force generated by the concentration gradient improved as well as the area between the metal ions and biosorbent surface also enhances. This therefore leads to more frequent collisions of the

heavy metal ions with the active biosorption sites, causing an increase in the uptake capacity of the heavy metal ions ions by the biosorbent. The present study found that at 100 mg/L, the optimum biosorption capacities of As(III) and Hg(II) in the monocomponent and bicomponent sorption systems were 22.38 and 25.09 mg/g; and 21.69 and 40.13 mg/g, respectively. Hence, there exists a synergistic effect in which the uptake capacity of As(III) and Hg(II) ions by the biosorbent in the bicomponent sorption system was higher than that in the monocomponent sorption system.

4.3.6 Effect of Reaction Temperature

The removal efficiency and biosorption capacity of As(III) and Hg(II) ions from monocomponent and bicomponent sorption systems augmented rapidly as an initial reaction temperature increased respectively, and suddenly decreased sharply as shown in Fig. 20. It was observed that at higher levels of reaction temperature, both the removal and uptake rates decreased drastically and this might be because of the deterioration of the surface chemistry of the biosorbent through excessive heating (Dhabab *et al.*, 2012). Similarly, the weakening of adsorptive interactions between the biosorbent active sites and the As(III) and Hg(II) ions could be the cause of the decline in the removal rate at higher reaction temperatures (Lashkenari *et al.*, 2011).

In Figs. 20 (a) and (c), the maximum decontamination of As(III) ions from the monocomponent and bicomponent sorption systems was accomplished at optimum reaction temperatures of 35.00 and 55.00 ℃ with removal efficiencies of 93.98 and 89.28% and biosorption capacities of 9.40 and 8.93 mg/g, respectively (Appendix 11). Also, at a temperature of 45 and 55 ℃, Hg(II) maximum removal efficiencies of 95.91 and 90.20% and uptake capacities of 12.33 and 6.77 mg/g were attained from the monocomponent and bicomponent sorption systems as displayed in Figs. 20 (b) and (d), respectively (Appendix 12). The upsurge of temperature in the sorption systems increased As(III) and Hg(II) removal efficiencies and uptake capacities due to the enhanced kinetic energy of the ionic species through the biosorbent and the subsequent biosorption on the active surface (Lenka *et al.*, 2021). Labied *et al.* (2018) found that at low temperatures, heavy metal ions have low kinetic energy as they approach the active sites of the biosorbent, which causes ion agglomeration and reduces the interaction between the adsorbate and the active sites. Therefore, the decontamination of As(III) and Hg(II) species in both sorption media with rising temperature suggested that the removal of As(III) and Hg(II) ions by the HGAC is an endothermic process, which also indicates the mechanism of As(III)

and Hg(II) biosorption from the monocomponent and bicomponent sorption systems was mainly chemisorption (Mondal *et al.*, 2019).

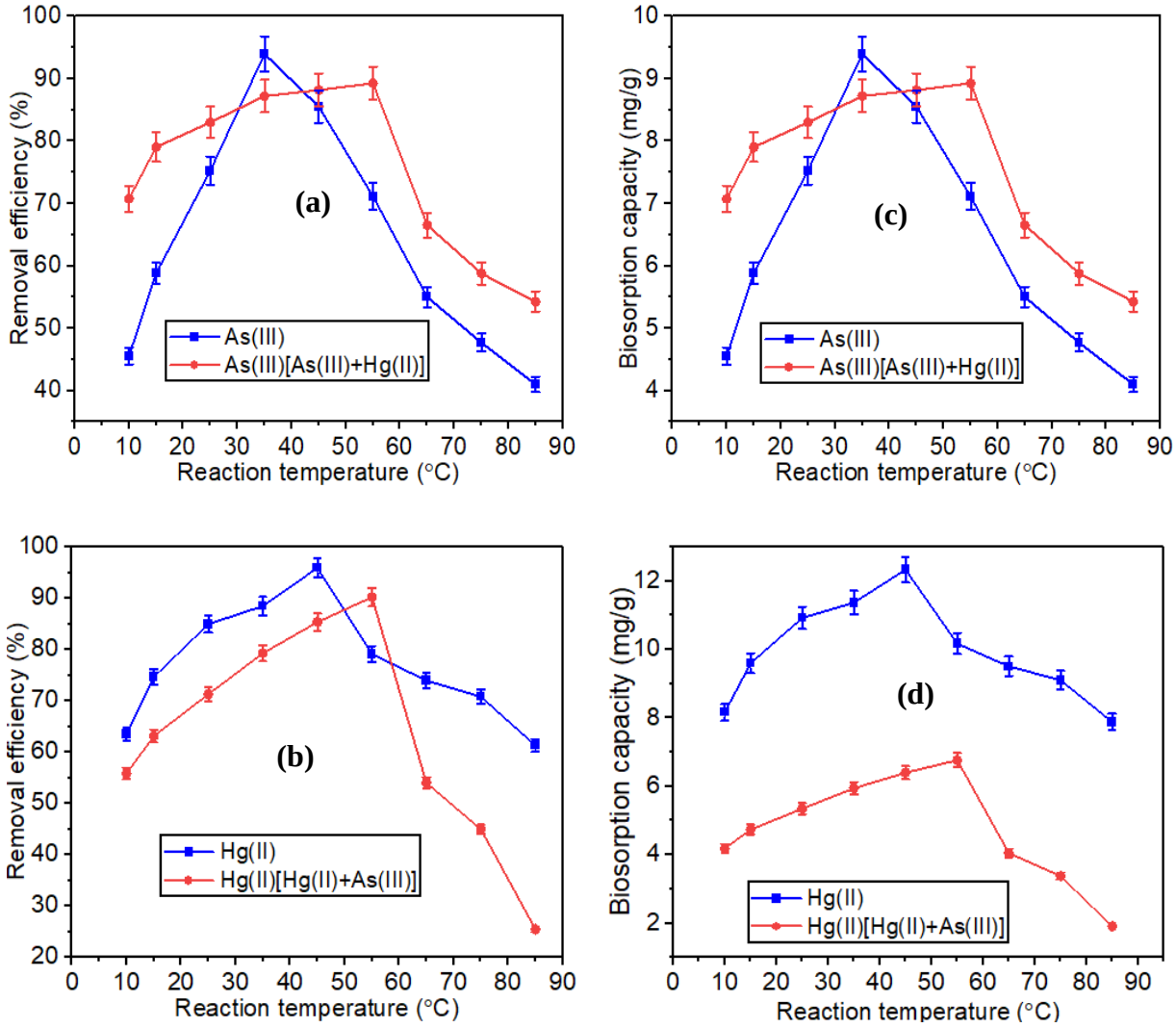

Figure 20: Effect of reaction temperature on removal efficiency (a and b) and biosorption capacity (c and d) on As(III) and Hg(II) removal from monocomponent and bicomponent sorption systems, respectively

Comparatively, the decontamination of As(III) and Hg(II) ions from the monocomponent and bicomponent sorption systems were similar though higher removal efficiency and uptake capacity could be observed in the monocomponent sorption system. Hence, the biosorption of As(III) and Hg(II) ions in the bicomponent sorption system was highly inhibited implying an antagonistic effect.

To determine the overall efficiency of the HGAC, biosorption tests were performed using the best operating conditions attained for the independent factors during the removal of As(III) and Hg(II) ions from the single-metal and binary-metal sorption systems, respectively. For As(III),

overall removal efficiencies of 95.33 and 91.74% were achieved in the single-metal and binary-metal sorption systems, respectively. Also, overall removal efficiencies of 97.06 and 93.58% for Hg(II) were accomplished in the single-metal and binary-metal sorption systems, respectively. This shows that the HGAC is found to be a promising biosorbent and could be employed in the remediation of heavy metals from water and wastewater.

4.4 Desorption, Regeneration, and Reusability of Spent Biosorbent

4.4.1 Desorption Studies

The efficiency of any sorbent material is largely assessed based on its recyclability and reusability. Hence, it is indispensable that the adsorbent maintains its original sorption capacity even after multiple cycles of adsorption-desorption studies (Dahake *et al.*, 2021). Furthermore, renewability and reusability are imperative to safeguard the economic viability of using the bio-adsorbent for sorption process scale-up and industrial applications.

The desorption experiments as presented in Fig. 21 (a) indicate that the 0.1 M HCl and EDTA acids have the highest degree of desorption, which allows for the recovery of As(III) ions adsorbed on the biosorbent surface from monocomponent and bicomponent sorption systems at the level of 93.71 and 84%, respectively (Appendix 13). Similarly, Gerard *et al.* (2016) used 0.1 M HCl as the best desorption agent to extract As(III) ions accumulated on the surface of chitosan/iron oxide nano-composite from a single component system to recycle the spent nano-composite. It was observed that the HCl could desorb about 99% of the adsorbed As(III) ions on the nano-composite surface. In another study, the desorption of modified chitosan beads loaded with Cd(II) and Pb(II) ions was assessed by Igberase and Osifo (2015) using different extraction eluents. However, among the eluents that were investigated 0.5 M HCl was successfully used in desorbing the spent adsorbent, and percentage desorption of 98.94% and 97.50% was obtained for Cd(II) and Pb(II) ions, respectively. Besides, Filote *et al.* (2019) studied the possibility of using 0.1 M of NaCl, HNO_3, and EDTA for the recovery of Pb(II) ions from the spent biosorbent derived from *Fucus spiralis* seaweed. It was observed that 0.10 M EDTA was the most efficient desorbing eluent to recover Pb(II) ions on the biosorbent surface.

Also, among all the desorption eluents tested as shown in Fig. 21 (b), it was found that 0.1 M HNO_3 and HCl acids are the best desorption eluents and could retrieve about 91.47 and 80.85% of Hg(II) ions adsorbed onto the biosorbent surface in the monocomponent and bicomponent

sorption media, respectively (Appendix 14). The HNO_3 and HCl acids are the best desorption eluents because, in an HNO_3 solution, H^+ can replace adsorbed ions on the surface of bio-adsorbent while Cl^- from HCl can easily form a complex with Hg(II) ions and then release to the solution (Kim *et al.*, 2011; Vakili *et al.*, 2019). However, distilled water was observed not to be a suitable desorption eluent in desorbing Hg(II) ions adsorbed onto the surface of the bio-adsorbent in both mono- and bi-solutes sorption systems and have the lowest desorption efficiencies of 2.65 and 4.13%, respectively.

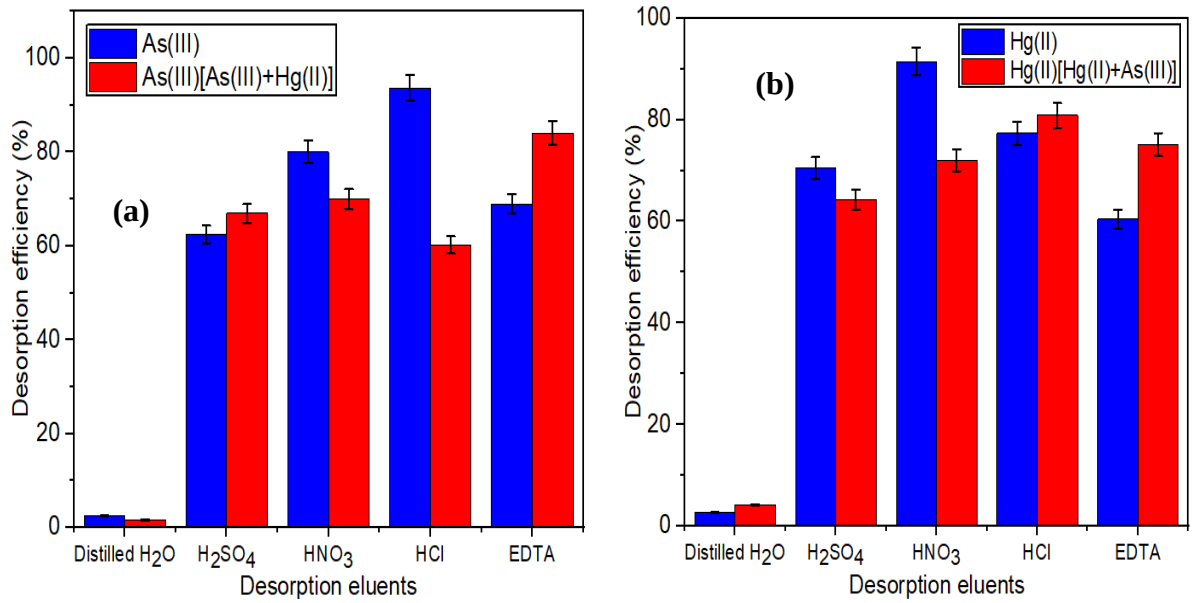

Figure 21: Desorption eluents for adsorbed As(III) ions (a) and Hg(II) ions (b) recovery on spent biosorbent surface from monocomponent and bicomponent sorption systems, respectively

The weakest desorption eluent was distilled water with desorption efficiency of 2.45 and 1.64%; and of 2.65 and 4.13% for As(III) and Hg(II) ions retrieval from mono- and binary metal-loaded biosorbents, respectively. This suggests that the distilled water has no significant effect on the recovery of As(III) and Hg(II) ions from the biosorbent surface. The effective desorption of As(III) and Hg(II) ions from the spent biosorbent surface by HCl, HNO_3, and EDTA acids for the monocomponent and bicomponent sorption systems, respectively suggests an ion-exchange mechanism (Vijayalakshmi *et al.*, 2017).

4.4.2 Regeneration and Reusability of Spent Biosorbent

It was found that after the biosorption of As(III) and Hg(II) ions from both monocomponent and bicomponent sorption systems, the FT-IR spectra of the impregnated biosorbent nearly

coincided with that of the original spectra of the biosorbent before the biosorption. This means that the basic structure and properties of the biosorbent remained relatively stable during the process of the metal ions biosorption suggesting the renewability of the biosorbent for further use.

Figure 22 (a) shows the adsorption-desorption cycles of the As(III) ions from both monocomponent and bicomponent sorption systems were repeated ten times using 0.1 M HCl and 0.1 M EDTA solutions, respectively, as desorption eluents for the retrieval of As(III) ions from the biosorbent surface to evaluate the sorbent's renewability and reusability. The regeneration and reusability studies indicate that the uptake capacity of the biosorbent slightly reduces with increasing regeneration cycles, in which the removal efficiencies of As(III) ions from the monocomponent and bicomponent sorption systems decreased from 90.45-60.95% and 88.74-61.42%, respectively when the regeneration cycles increased from one to eight (Appendix 15). This could be due to the acid treatment causing slight damage to the sorbent's original outer surface layer (Gupta *et al.*, 1997). It was found that after the eight-cycle, there was no significant recovery of As(III) ions on the biosorbent surface suggesting that some of the metal ions adsorbed on the biosorbent were due to chemisorption, which is irreversible (Bayuo *et al.*, 2020).

Also, in Fig. 22 (b), the removal efficiencies of Hg(II) ions from the mono- and binary-metal ions-loaded biosorbent using 0.1 M HNO_3 and HCl decreased slowly from 92.31-68.48% and 86.88-36.77%, respectively as the regeneration cycles were elevated from one up to eight (Appendix 16). This could be due to the decrease in the availability of binding sites for Hg(II) ions uptake and partial desorption of Hg(II) ions chemically adsorbed on the HGAC surface (Hiew *et al.*, 2021). Since there was no noticeable weight loss in the biosorbent load even after the fifth cycle, this suggests good mechanical stability of the bio-adsorbent as supported by the TGA analysis presented in Fig. 22 (b) (Gupta *et al.*, 2021). However, the percentage removal of Hg(II) ions reduced drastically after the sixth to tenth regeneration cycles. This was probably due to the collapse of the HGAC microstructure and continuous pore microstructure distortion owing to repeated adsorption-desorption cycles (Gupta *et al.*, 2021; Liu *et al.*, 2020).

Considering the economic potential of the biosorbent, the adsorption-desorption results suggest that the biosorbent could be recycled for multiple reuses and retrieval of As(III) and Hg(II) ions without significantly losing its biosorption properties. However, the observed reduction of the biosorbent performance for the uptake of As(III) and Hg(II) ions over time could be due

to the blocking of some binding sites as well as changes in the sorbent's chemistry and structure (Vijayalakshmi *et al.*, 2017).

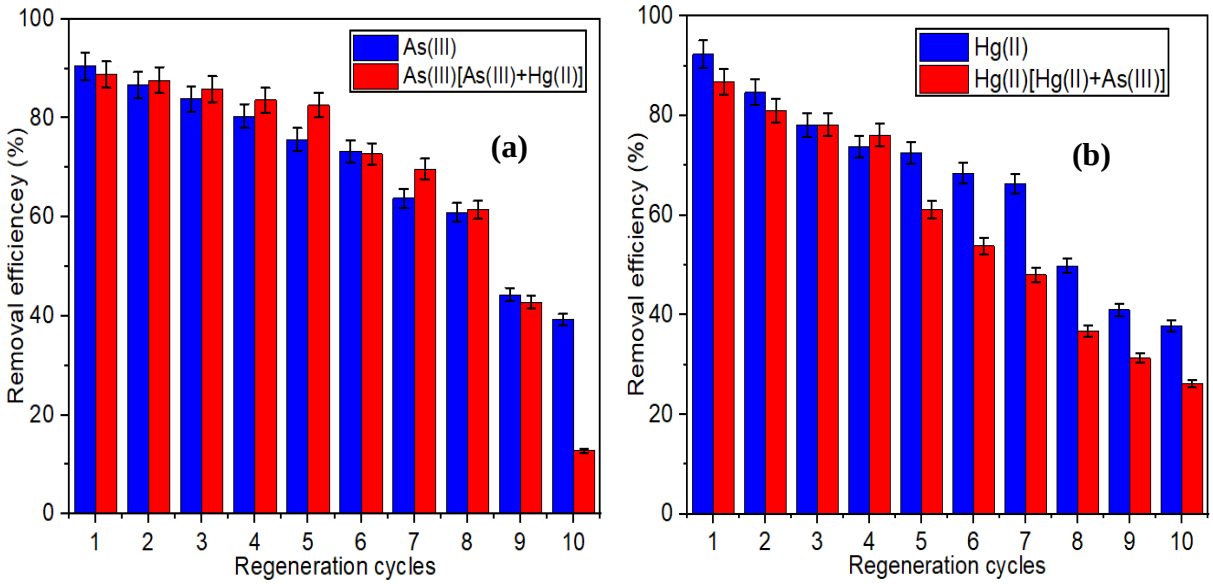

Figure 22: Regeneration and reusability of the biosorbent spent in the removal of As(III) ions (a) and Hg(II) ions (b) from monocomponent and bicomponent sorption systems, respectively

4.5 Experimental Design and Modeling of As(III) and Hg(II) Removal from Non-Competitive Sorption System

The effects of three independent biosorption process variables, namely A- contact time, B- biosorbent dosage, and C- initial heavy metal ion concentration on the removal and uptake rates were scrutinized according to CCD-RSM. The CCD matrix of the biosorption factors influencing As(III) and Hg(II) removal from aqueous systems in coded form with corresponding response parameters such as Y1-removal efficiency (%) and Y2- biosorption capacity (mg/g) are listed in Tables 13 and 14, respectively. Tables 13 and 14 show the CCD has factorial points with the sign of ± 1.000, axial points (±1.682), and center points (0.00). Out of the twenty (20) experimental runs, eight (8) were factorial runs, six (6) were center runs and the other six (6) were axial runs.

In Table 13, it was observed that the experimental run 10 with operating conditions of contact time = 90 min, biosorbent dosage = 0.5 g/L, and initial concentration = 10 mg/L was found to have the highest removal rate of 99.9%, and biosorption capacity of 8.0 mg/g. Whilst lower biosorption of As(III) was attained at experimental run 19 with operating conditions of contact time = 65 min, biosorbent dosage = 1.75 g/L, and initial As(III) concentration = 20 mg/L with

(Y1)-removal efficiency and (Y2)-biosorption capacity of 61% and 1.18 mg/g, respectively. Moreover, the results displayed in Table 14 indicate that Hg(II) maximum (Y1)-removal efficiency and (Y2)-biosorption capacity of 99.2% and 12.00 mg/g, respectively were attained at experimental run 6 with operating conditions of contact time = 30 min, biosorbent dosage = 0.5 g/L and initial Hg(II) concentration = 15 mg/L. Also, the lowest removal and biosorption rates of 67% and 2.00 mg/g, correspondingly were accomplished at contact time = 60 min, biosorbent dosage = 2 g/L, and initial Hg(II) concentration = 30 mg/L of the experimental run 20.

Table 13: Design matrix of As(III) biosorption factors in coded form with corresponding response variables

Run	Space Type	Biosorption influencing factors			Responses	
		A-Contact time (min)	B-Biosorbent dosage (g/L)	C-Initial concentration (mg/L)	Y1-Removal efficiency (%)	Y2-Biosorption capacity (mg/g)
1	Center	0.000	0.000	0.000	73.15	2.98
2	Factorial	-1.000	1.000	1.000	94.24	6.92
3	Factorial	-1.000	-1.000	-1.000	98.80	7.05
4	Factorial	1.000	1.000	-1.000	88.50	3.47
5	Center	0.000	0.000	0.000	73.48	3.11
6	Factorial	1.000	1.000	1.000	95.58	6.87
7	Center	0.000	0.000	0.000	74.34	3.18
8	Factorial	-1.000	-1.000	1.000	85.26	3.56
9	Center	0.000	0.000	0.000	75.00	3.00
10	Factorial	1.000	-1.000	-1.000	99.90	8.00
11	Factorial	1.000	-1.000	1.000	79.82	3.20
12	Factorial	-1.000	1.000	-1.000	82.35	2.43
13	Axial	1.682	0.000	0.000	77.87	3.97
14	Axial	0.000	0.000	1.682	65.44	2.24
15	Axial	0.000	0.000	-1.682	71.73	2.40
16	Axial	0.000	-1.682	0.000	84.29	4.10
17	Axial	-1.682	0.000	0.000	76.22	3.30
18	Axial	0.000	1.682	0.000	83.00	3.19
19	Center	0.000	0.000	0.000	61.00	1.18
20	Center	0.000	0.000	0.000	60.21	1.20

Table 14: Design matrix of Hg(II) biosorption factors in coded form with corresponding response variables

Run	Space Type	Biosorption influencing factors			Responses	
		A-Contact time (min)	B-Biosorbent dosage (g/L)	C-Initial concentration (mg/L)	Y1-Removal efficiency (%)	Y2-Biosorption capacity (mg/g)
1	Factorial	-1.000	-1.000	0.000	75.75	3.85
2	Center	0.000	0.000	1.000	72.40	4.24
3	Factorial	-1.000	1.000	-1.000	72.62	2.46
4	Factorial	1.000	-1.000	-1.000	88.30	7.16
5	Center	0.000	0.000	0.000	72.34	4.37
6	Factorial	-1.000	-1.000	1.000	99.15	12.00
7	Factorial	1.000	-1.000	0.000	84.20	7.90
8	Center	0.000	0.000	1.000	71.93	4.40
9	Center	0.000	0.000	0.000	72.56	4.06
10	Factorial	1.000	1.000	-1.000	87.55	8.16
11	Factorial	-1.000	1.000	1.000	80.15	5.84
12	Factorial	1.000	1.000	-1.000	76.35	3.32
13	Axial	1.682	0.000	0.000	79.24	4.17
14	Center	0.000	0.000	1.682	68.44	2.76
15	Axial	0.000	0.000	-1.682	81.10	5.25
16	Axial	0.000	-1.682	0.000	88.48	7.08
17	Axial	-1.682	0.000	0.000	73.74	3.11
18	Axial	0.000	0.000	0.000	71.4	3.47
19	Axial	0.000	1.682	0.000	76.90	2.51
20	Center	0.000	0.000	0.000	67.00	2.01

4.5.1 Development of Response Surface Quadratic Models

Following the biosorption process, the experimental data attained by the HGAC for As(III) and Hg(II) ions elimination from the wastewater were fitted to various models, including linear, logarithmic, quadratic, and cubic models in the CCD-RSM of the Design Expert software. A stepwise regression analysis was then conducted to select the regression models that would best predict the response variables. Thus, the response parameters, Y1-removal efficiency, and Y2-biosorption capacity in Tables 13 and 14, respectively were employed by the CCD-RSM to generate regression models as functions of all the independent influencing biosorption factors as shown in the generalized Eq. (19) (Shafaghat & Ghaemi, 2021). The analysis of variance (ANOVA) was done to verify the quadratic models' suitability, significance, and compatibility.

$$Y = b_0 + \sum_{i=1}^{n} b_i X_i + \sum_{i=1}^{n} b_{ii} {X_i}^2 + \sum_{i=1}^{n-1} \sum_{j=i+1}^{n} b_{ij} X_i X_j + \varepsilon \quad (19)$$

Where Y stands for the predicted response variable, b_0 is the constant coefficient, b_i stands for a linear coefficient, b_{ij} for an interaction coefficient, b_{ii} for a quadratic coefficient, X_i and X_j for coded values of variables, and ε for the unpredicted response variables on the experimental data (Mourabet *et al.*, 2017).

The quadratic models were recommended and chosen as statistically significant with sequential p-values < 0.0001 above the other regression models (cubic, 2FI, and Linear) for As(III) and Hg(II) removal efficiency as displayed in Tables 15 and 16, respectively and As(III) and Hg(II) uptake capacity as shown in Tables 17 and 18, respectively. The Cubic model was observed to be aliased, making it unsuitable for modeling and optimizing As(III) and Hg(II) biosorption process factors (Sujatha *et al.*, 2020).

Table 15: Quadratic model fitness summary for As(III) removal efficiency

Source	Sequential p-value	Lack of Fit P-value	Adjusted R^2	Predicted R^2	Remark
Linear	0.9286	< 0.0001	0.1652	0.6717	
2FI	0.3745	< 0.0001	0.1348	0.2781	
Quadratic	< 0.0001	0.9695	0.9968	0.9951	Suggested
Cubic	0.9231	0.8065	0.9950	0.9793	Aliased

Table 16: Quadratic model fitness summary for Hg(II) removal efficiency

Source	Sequential p-value	Lack of Fit P-value	Adjusted R^2	Predicted R^2	Remark
Linear	0.1736	< 0.0001	0.1300	0.2751	
2FI	0.1157	< 0.0001	0.3235	0.3663	
Quadratic	< 0.0001	0.4138	0.9945	0.9826	Suggested
Cubic	0.4138	-	0.9952	-	Aliased

Table 17: Quadratic model fitness summary for As(III) biosorption capacity

Source	Sequential p-value	Lack of Fit P-value	Adjusted R^2	Predicted R^2	Remark
Linear	0.9323	< 0.0001	0.1665	0.8264	
2FI	0.0071	< 0.0001	0.4477	0.1311	
Quadratic	< 0.0001	0.9524	0.9988	0.9980	Suggested
Cubic	0.8755	0.8975	0.9982	0.9974	Aliased

Table 18: Quadratic model fitness summary for Hg(II) biosorption capacity

Source	Sequential p-value	Lack of Fit P-value	Adjusted R^2	Predicted R^2	Remark
Linear	0.1022	0.0005	0.1963	0.2851	
2FI	0.0012	0.0035	0.7206	0.4127	
Quadratic	< 0.0001	0.7708	0.9886	0.9708	Suggested
Cubic	0.7708	-	0.9841	-	Aliased

From Tables 15-18, it was found that the discrepancy between the adjusted and predicted correlation coefficients of the developed quadratic models for the responses [(Y1)-Removal efficiency and (Y2)-Biosorption capacity] attained for the decontamination of As(III) and Hg(II) ions from non-competitive aqueous solutions was less than 0.20. This implies that the developed quadratic models were accurate and adequate and could be used in the prediction of the responses (Shafaghat & Ghaemi, 2021). Also, the As(III) and Hg(II) removal efficiency

and uptake capacity Lack of Fit p-values were found to be greater than 0.10 showing that the lack of fit of the quadratic models was not significant, further indicating strong fitness and robustness of the developed models (Bayuo *et al.*, 2022).

Tables 19 and 20, respectively, provide an overview of the quadratic model fitness statistics for As(III) and Hg(II) removal performance and uptake capacity by the HGAC. The quadratic models of As(III) and Hg(II) removal efficiency and uptake capacity had coefficients of determination (R^2) nearly equal to one indicating that the quadratic models were accurate and exhibited good fitness (Ecer *et al.*, 2020).

Table 19: Fit statistics for As(III) removal efficiency and biosorption capacity

Statistics	**Removal efficiency**	**Biosorption capacity**
Correlation coefficient (R^2)	0.9984	0.9994
Standard deviation (Std. Dev.)	0.56	0.06
Mean	80.01	3.77
Percentage coefficient of variance (C.V%)	0.71	1.61
Adequate Precision	93.22	150.57

Table 20: Fit statistics for Hg(II) removal efficiency and biosorption capacity

Statistics	**Removal efficiency**	**Biosorption capacity**
Correlation coefficient (R^2)	0.9972	0.9943
Standard deviation (Std. Dev.)	0.60	0.25
Mean	77.98	4.91
Percentage coefficient of variance (C.V%)	0.77	5.13
Adequate Precision	68.56	50.58

Also, the quadratic models generated for As(III) and Hg(II) removal and uptake rates were found to have good mean and minimal standard deviation values, which imply that the models were accurate and reliable for modeling purposes. The ratio of signal to noise is determined by adequate precision, and a value higher than 4.00 is preferred (Sagharloo *et al.*, 2021). In Tables 19 and 20, respectively, the adequate precision values of As(III) and Hg(II) percentage removal and uptake rate were greater than 4.00 indicating the good suitability and reliability of the

selected quadratic models in predicting the responses (Uddin & Baig, 2019; Meshram *et al.*, 2023). The As(III) and Hg(II) removal efficiency and uptake capacity percentage coefficients of variations (C.V%) were much less than 5.00% suggesting that the models are desirable and credible and might be applied to a variety of future phenomena. Studies have shown that a developed quadratic model is regarded as repeatable and reproducible if the coefficient of variation (CV%) value is much less than 10.00% (Agarwal *et al.*, 2016; Jain *et al.*, 2021).

4.5.2 Analysis of Variance of Developed Response Surface Quadratic Models

The ANOVA of the quadratic models was explored to identify the statistical significance and interacting influences of the sorption parameters on the maximum abatement of As(III) and Hg(II) ions from water systems (Yılmaz *et al.*, 2019; Najafpour *et al.*, 2020; Zhou *et al.*, 2020). The quadratic models were subjected to an ANOVA, and the model's fitness as well as the significance levels for the independent parameters and their interactions were determined using the p- and F-values for As(III) and Hg(II) ions biosorption on the HGAC. While the ANOVA for the quadratic models of As(III) removal efficiency and biosorption capacity is displayed in Tables 21 and 22, respectively, the quadratic models of Hg(II) removal efficiency and biosorption capacity are presented in Tables 23 and 24, respectively. The ANOVA results of the quadratic models of As(III) and Hg(II) removal efficiency and biosorption capacity as displayed in Tables 21-24 were observed to be significant because their F-values were relatively high and had smaller p-values (< 0.0001) (Anupam *et al.*, 2011).

Table 21: ANOVA of the quadratic model developed for As(III) removal efficiency

Source	Sum of Squares	df	Mean Square	F-value	p-value	Remark
Block	757.82	1	757.82	-	-	-
Model	1765.47	9	196.16	614.72	< 0.0001	significant
A-Contact time	2.57	1	2.57	8.06	0.0195	significant
B-Biosorbent dosage	2.04	1	2.04	6.40	0.0323	significant
C-Initial concentration	46.60	1	46.60	146.05	< 0.0001	significant
AB	17.49	1	17.49	54.82	< 0.0001	significant
AC	16.10	1	16.10	50.46	< 0.0001	significant
BC	345.71	1	345.71	1083.37	< 0.0001	significant
A^2	478.49	1	478.49	1499.46	< 0.0001	significant
B^2	944.29	1	944.29	2959.14	< 0.0001	significant
C^2	110.76	1	110.76	347.09	< 0.0001	significant
Residual	2.87	9	0.3191	-	-	-
Lack of Fit	0.4517	5	0.0903	0.1493	0.9695	not significant
Pure Error	2.42	4	0.6051	-	-	-
Cor Total	2526.16	19	-	-	-	-

Table 22: ANOVA of the quadratic model developed for As(III) biosorption capacity

Source	Sum of Squares	df	Mean Square	F-value	p-value	Remark
Block	15.27	1	15.27	-	-	-
Model	55.38	9	6.15	1668.88	< 0.0001	significant
A-Contact time	0.5365	1	0.5365	145.51	< 0.0001	significant
B-Biosorbent dosage	0.9757	1	0.9757	264.65	< 0.0001	significant
C-Initial concentration	0.0328	1	0.0328	8.89	0.0154	significant
AB	0.0200	1	0.0200	5.42	0.0448	significant
AC	0.7200	1	0.7200	195.28	< 0.0001	significant
BC	32.72	1	32.72	8875.68	< 0.0001	significant
A^2	10.69	1	10.69	2900.67	< 0.0001	significant
B^2	10.78	1	10.78	2924.51	< 0.0001	significant
C^2	2.27	1	2.27	615.15	< 0.0001	significant
Residual	0.0332	9	0.0037	-	-	-
Lack of Fit	0.0063	5	0.0013	0.1878	0.9524	not significant
Pure Error	0.0269	4	0.0067	-	-	-
Cor Total	70.68	19	-	-	-	-

Table 23: ANOVA for response surface quadratic model for Hg(II) removal efficiency

Source	Sum of Squares	df	Mean Square	F-value	p-value	Remark
Block	64.09	1	64.09	-	-	-
Model	1183.15	9	131.46	361.25	< 0.0001	significant
A-Contact time	23.67	1	23.67	65.05	< 0.0001	significant
B-Biosorbent dosage	184.56	1	184.56	507.18	< 0.0001	significant
C-Initial concentration	118.00	1	118.00	324.26	< 0.0001	significant
AB	22.88	1	22.88	62.88	< 0.0001	significant
AC	180.79	1	180.79	496.79	< 0.0001	significant
BC	121.45	1	121.45	333.73	< 0.0001	significant
A^2	124.75	1	124.75	342.81	< 0.0001	significant
B^2	379.76	1	379.76	1043.57	< 0.0001	significant
C^2	117.66	1	117.66	323.33	< 0.0001	significant
Residual	3.28	9	0.3639	-	-	-
Lack of Fit	2.02	5	0.4045	1.29	0.4138	not significant
Pure Error	1.25	4	0.3132	-	-	-
Cor Total	1250.52	19	-	-	-	-

Table 24: ANOVA for response surface quadratic model for Hg(II) biosorption capacity

Source	Sum of Squares	df	Mean Square	F-value	p-value	Remark
Block	16.46	1	16.46	-	-	-
Model	99.52	9	11.06	174.25	< 0.0001	significant
A-Contact time	1.27	1	1.27	20.09	0.0015	significant
B-Biosorbent dosage	25.92	1	25.92	408.50	< 0.0001	significant
C-Initial concentration	5.86	1	5.86	92.29	< 0.0001	significant
AB	1.97	1	1.97	31.04	0.0003	significant
AC	36.59	1	36.59	576.64	< 0.0001	significant
BC	9.83	1	9.83	154.97	< 0.0001	significant
A^2	3.05	1	3.05	48.08	< 0.0001	significant
B^2	10.87	1	10.87	171.22	< 0.0001	significant
C^2	7.36	1	7.36	115.96	< 0.0001	significant
Residual	0.5711	9	0.0635	-	-	-
Lack of Fit	0.2180	5	0.0436	0.4939	0.7708	not significant
Pure Error	0.3531	4	0.0883	-	-	-
Cor Total	116.55	19	-	-	-	-

If the p-value is less than 0.05, the Lack of Fit (LOF) score is statistically significant at the 95% confidence level. However, if the p-value is more than 0.05, the LOF is insignificant. In general, if the chosen quadratic model well fits the experimental data, the LOF test would not be significant. The As(III) and Hg(II) removal and uptake rates Lack of Fit p-values were greater than 0.05 indicating that the LOF test is not statistically significant compared to the pure error, signifying strong adaptability of the quadratic models (Karmaker *et al.*, 2021). A valid LOF test for the response variables was further supported by the five (5) LOF degrees of freedom (df) and four (4) df for the pure error as listed in Tables 21-24.

Furthermore, as summarized in Tables 21-24, the quadratic model terms of As(III) and Hg(II) removal efficiency and biosorption capacity have values of $p < 0.05$, indicating that all these

terms are significant statistically. Thus, it was observed that the As(III) and Hg(II) removal and uptake efficiencies achieved by the HGAC were significantly influenced by all of the uni-factors, interaction factors, and quadratic effect factors including A, B, and C; AB, AC, and BC; and A^2, B^2, and C^2, respectively. There may be numerous inconsequential terms in the quadratic model if there is a considerable discrepancy between the determination coefficients (R^2) and adjusted correlation coefficient (R^2) (Elbah *et al.*, 2016; Jain *et al.*, 2021).

Comparatively, the initial concentration and biosorbent dosage produce the main interactive effect on the percentage removal and biosorption capacity of As(III) species by the HGAC among the three independent biosorption factors studied, based on the ANOVA results displayed in Tables 21-24, with $p < 0.0001$ and very high F-values. It has been found that the higher the F-values and the lower the p-values, the greater the influence of the model terms on the response (Rahimi *et al.*, 2015).

The second-order polynomial Eqs. (20)-(23), in which all the quadratic model terms were found to be statistically significant, were obtained from the regression analysis of the responses, respectively. Thus, synergism and antagonism during the optimization of As(III) and Hg(II) biosorption processes are indicated by positive and negative coefficient values in the second-order polynomial Eqs. (20)-(23), respectively. For As(III) removal rate and uptake capacity by the HGAC, only three model terms, B, C, and AC, were found to have antagonistic consequences on the optimization of As(III) percentage removal and uptake capacity as shown in Eqs. (20) and (21), respectively although the majority of model terms favored the optimization of As(III) biosorption. The process factors A, AB, BC, A^2, B^2, and C^2 were found to have a positive impact on As(III) biosorption.

$$Y1 = +67.33 + 0.43A - 0.39B - 1.85C + 1.48AB - 1.42AC + 6.57BC + 5.76\,A^2 + 8.10B^2 + 2.77C^2 \quad (20)$$

$$Y2 = +2.13 + 0.20A - 0.27B - 0.05C + 0.05AB - 0.30AC + 2.02BC + 0.86A^2 + 0.87B^2 + 0.40C^2 \quad (21)$$

Similarly, the positive sign before the model terms in regression model Eqs. (22) and (23), respectively suggest a synergistic effect indicating that those factors promoted detoxification of Hg(II) ions from the aqueous media. Whilst, a negative sign implies the antagonistic effect of the independent factor(s), which negatively influences the detoxification of Hg(II) ions from the wastewater (Sujatha *et al.*, 2020).

$$Y1 = +70.10 + 1.32\mathrm{A} - 3.68\mathrm{B} - 294\mathrm{C} + 1.69\mathrm{AB} + 4.75\mathrm{AC} + 390\mathrm{BC} + 2.94\mathrm{A}^2 + 5.14\mathrm{B}^2 + 2.86\mathrm{C}^2 \quad (22)$$

$$Y2 = +3.32 + 0.31\mathrm{A} - 1.38\mathrm{B} - 0.65\mathrm{C} + 0.50\mathrm{AB} + 2.14\mathrm{AC} + 1.11\mathrm{BC} + 0.46\mathrm{A}^2 + 0.87\mathrm{B}^2 + 0.71\mathrm{C}^2 \quad (23)$$

4.5.3 Quadratic Models Suitability and Adequacy Testing

The diagnostic test in the CCD-RSM was used to verify the models' appropriateness and adequacy before the quadratic models were utilized in assessing the observed data. To determine the suitability and appropriateness of the proposed quadratic models, diagnostic plots for As(III) and Hg(II) removal rate and uptake capacity were evaluated.

The best acceptable graphical tool for evaluating residuals normality and validating multivariate regression models is the normal % probability plot of studentized residuals as shown in Fig. 23. The normal % probability versus externally studentized residuals plots for As(III) and Hg(II) removal efficiency and uptake capacity by the HGAC are displayed in Figs. 23 (a and b) and (c and d), respectively. The quadratic models were found to be realistic because the residual distribution of the As(III) and Hg(II) percentage removal and uptake rate by the HGAC demonstrate that the residual data sets are spread evenly on both sides of the diagonal line (Cheng *et al.*, 2021). The residual data points fell within the straight line with minimal variations in the normal % probability plots, indicating a normal error distribution of the response variables (Shafaghat & Ghaemi, 2021).

The externally studentized residuals are utilized to search for unusual or significant data points. Figs. 24 (a and b) and (c and d), respectively, show the externally studentized residuals versus the predicted As(III) and Hg(II) removal efficiency and uptake capacity by the HGAC. These plots demonstrate that the internally and externally studentized residuals for As(III) and Hg(II) removal efficiency and uptake capacity, respectively, are within the recommended minimum and maximum values of precisely +4.00 or - 4.00 sigma. This meant that there were no misfits or data points that were beyond the red horizontal lines. The residuals were also seen to be randomly distributed about the zero line and without any discernible pattern (Chaduka *et al.*, 2020).

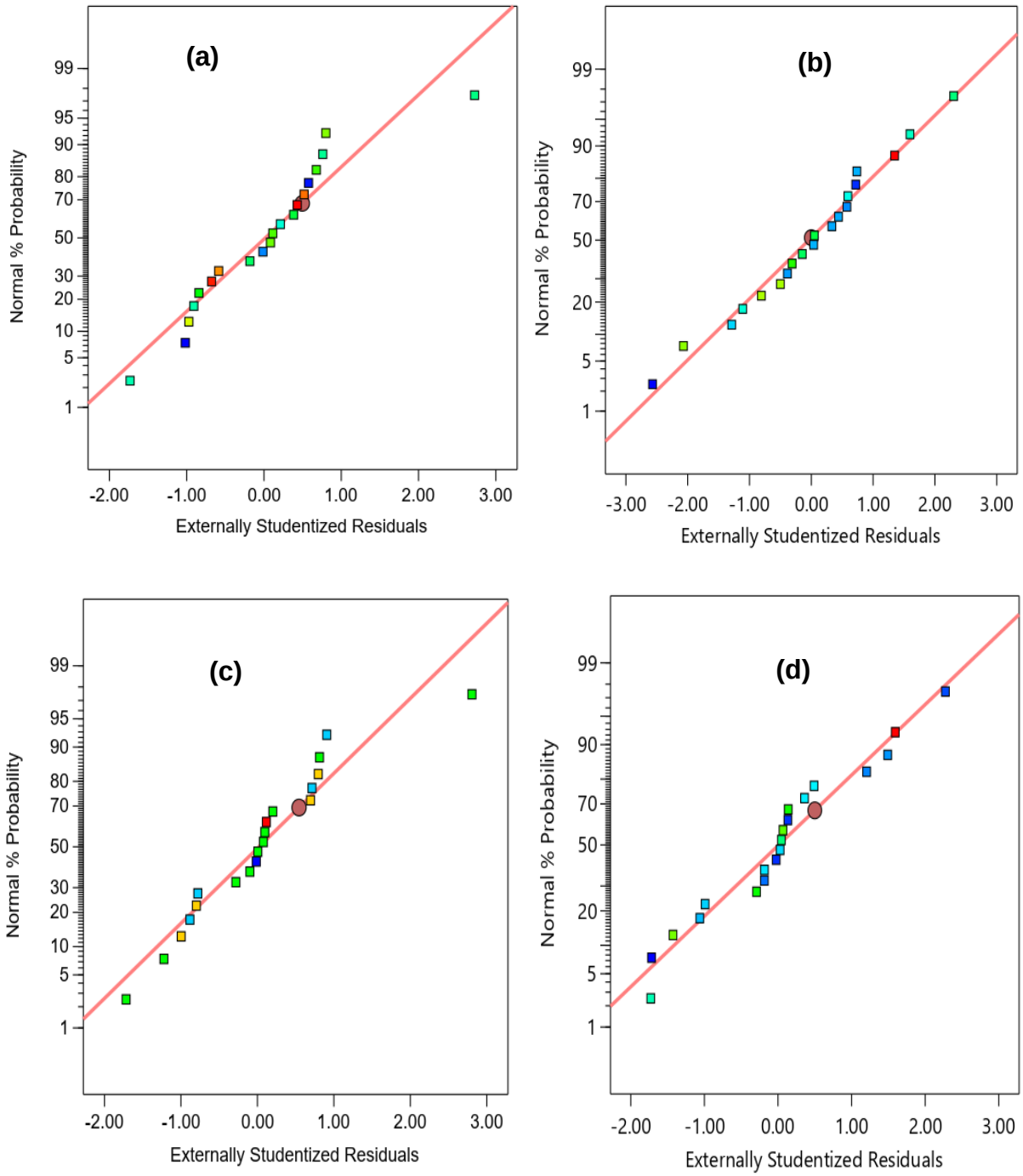

Figure 23: **Normal % probability versus externally studentized residuals for As(III) and Hg(II) removal efficiency (a and b) and biosorption capacity (c and d), respectively**

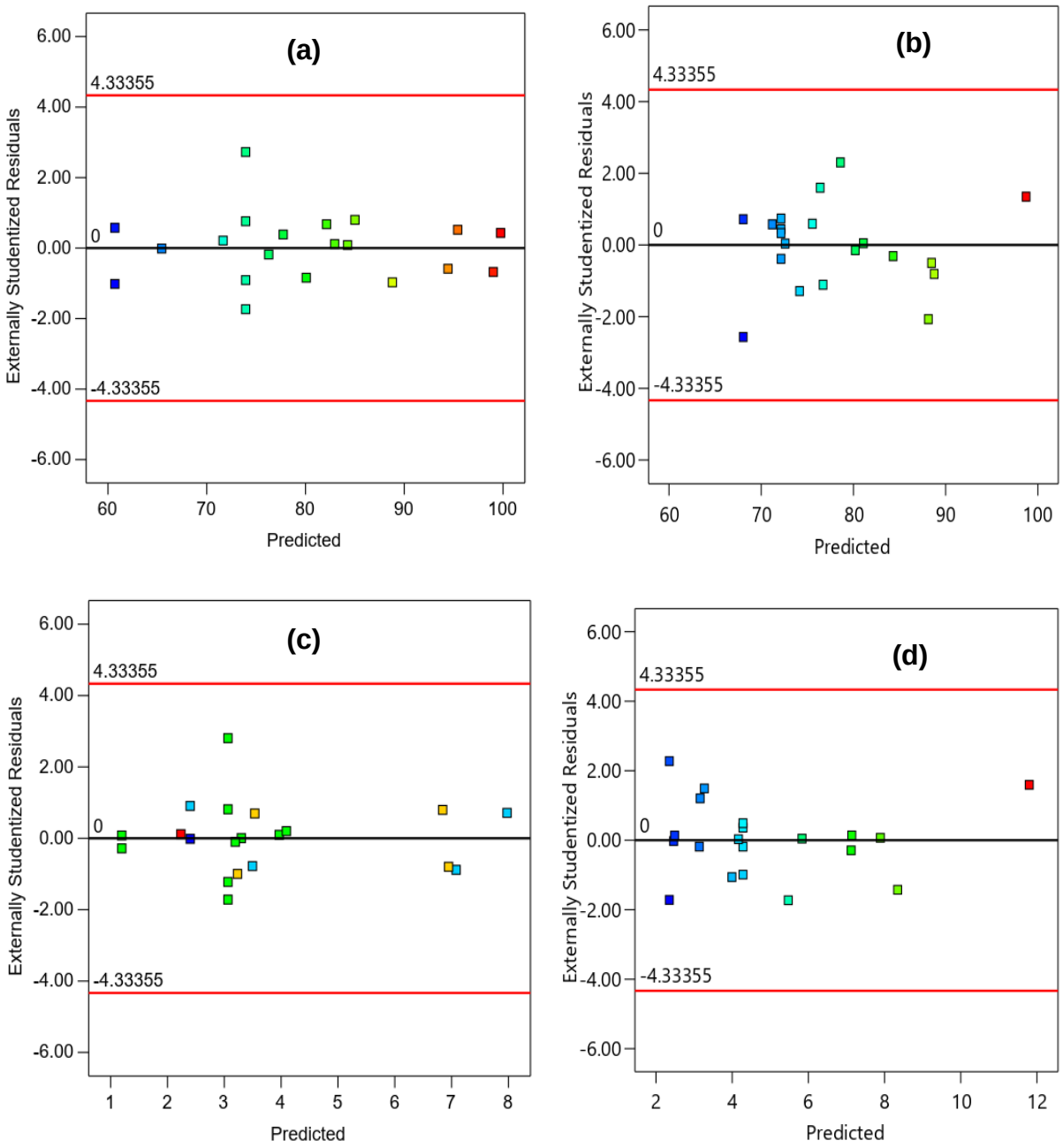

Figure 24: Externally studentized residuals versus predicted for As(III) and Hg(II) removal efficiency (a and b) and biosorption capacity (c and d), respectively

The Box-Cox normality plot in Fig. 25 is utilized to identify a transformation that will generally normalize the data if they are not normally distributed. The Lambda values for As(III) and Hg(II) removal efficiency and biosorption capacity were found to be within the value of 1.00 as displayed in Figs. 25 (a and b) and (c and d), respectively, suggesting that the quadratic models were accurate and required no transformation (Sujatha *et al.*, 2020). Meanwhile, Figs. 26 (a and b) and (c and d), respectively, show the leverage versus run number plots for removal efficiency and uptake capacity of As(III) and Hg(II). The plots revealed that the leverage values

are between 0.00 and 1.00, signifying that no data points will unreasonably affect the fitness of the quadratic models (Das, 2017).

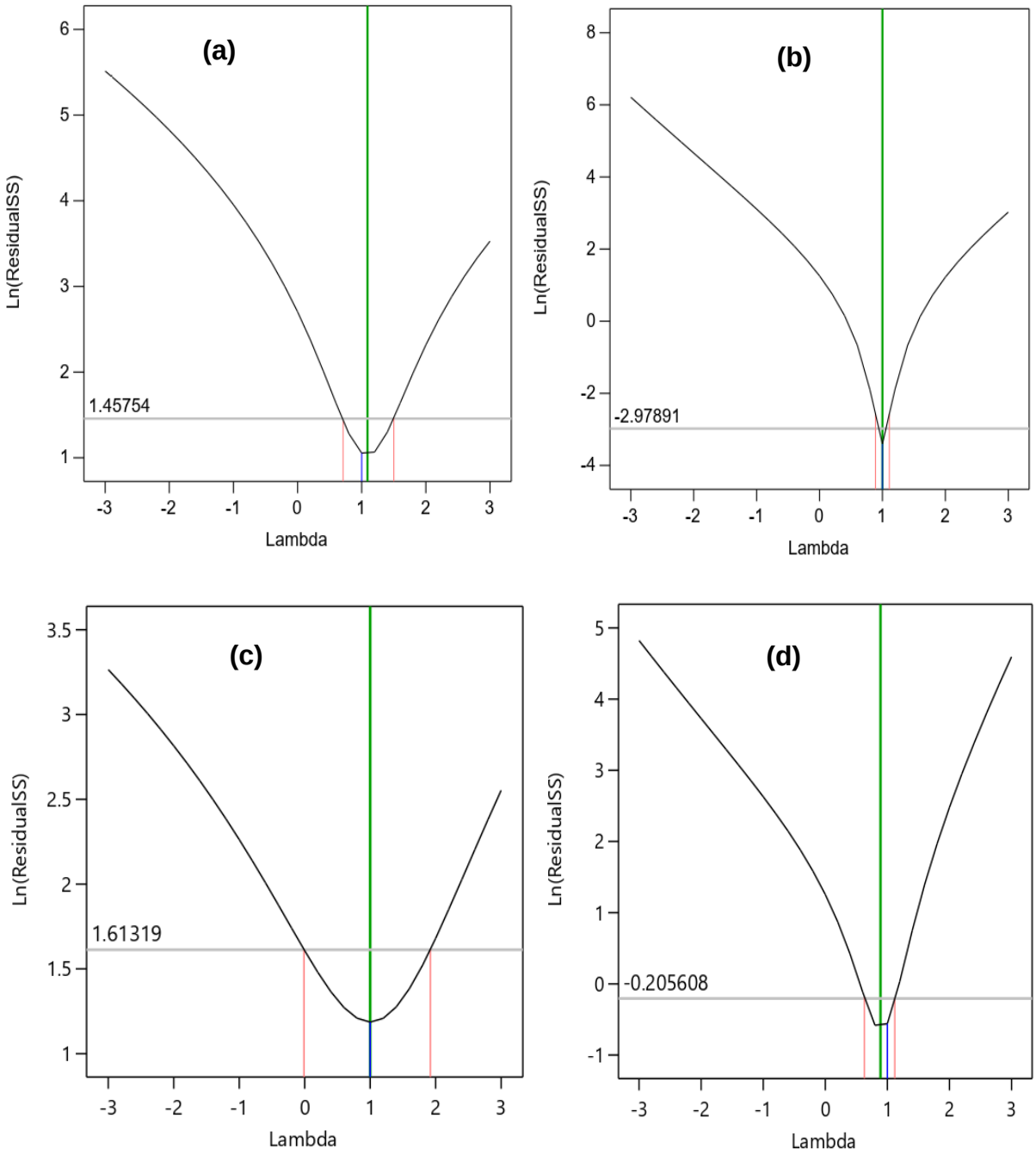

Figure 25: Box-Cox normality plot for As(III) and Hg(II) removal efficiency (a and b) and adsorption capacity (c and d), respectively

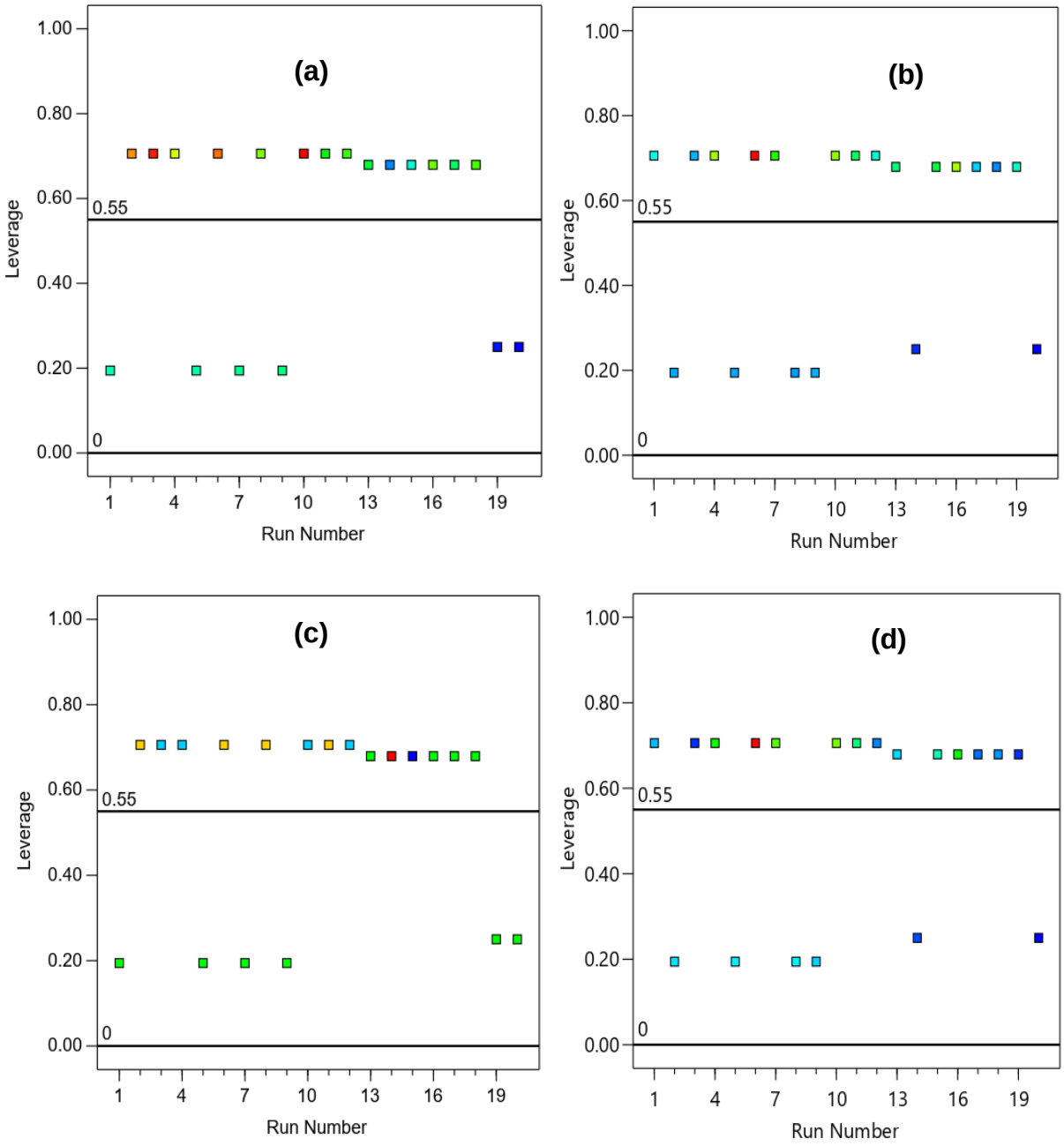

Figure 26: Leverage versus run number for As(III) and Hg(II) removal efficiency (a and b) and biosorption capacity (c and d), respectively

The proposed quadratic models as expressed in Eqs. (20)-(23) were applied to fit the observed data as well as to predict data of As(III) and Hg(II) percentage removal and uptake rate, respectively. Figure 27 shows the relationship between the actual and predicted values of As(III) and Hg(II) removal efficiency (a and b) and uptake capacity (c and d), respectively. The plots demonstrate a significant correlation between actual (experimental) data and quadratic models' predicted data for As(III) and Hg(II) optimal depollution from aqueous systems. The actual and projected data for the As(III) and Hg(II) removal and biosorption rates are

summarized in Tables 25 and 26, respectively. The difference between the actual and predicted responses is significant for determining which regression models fit the data the best.

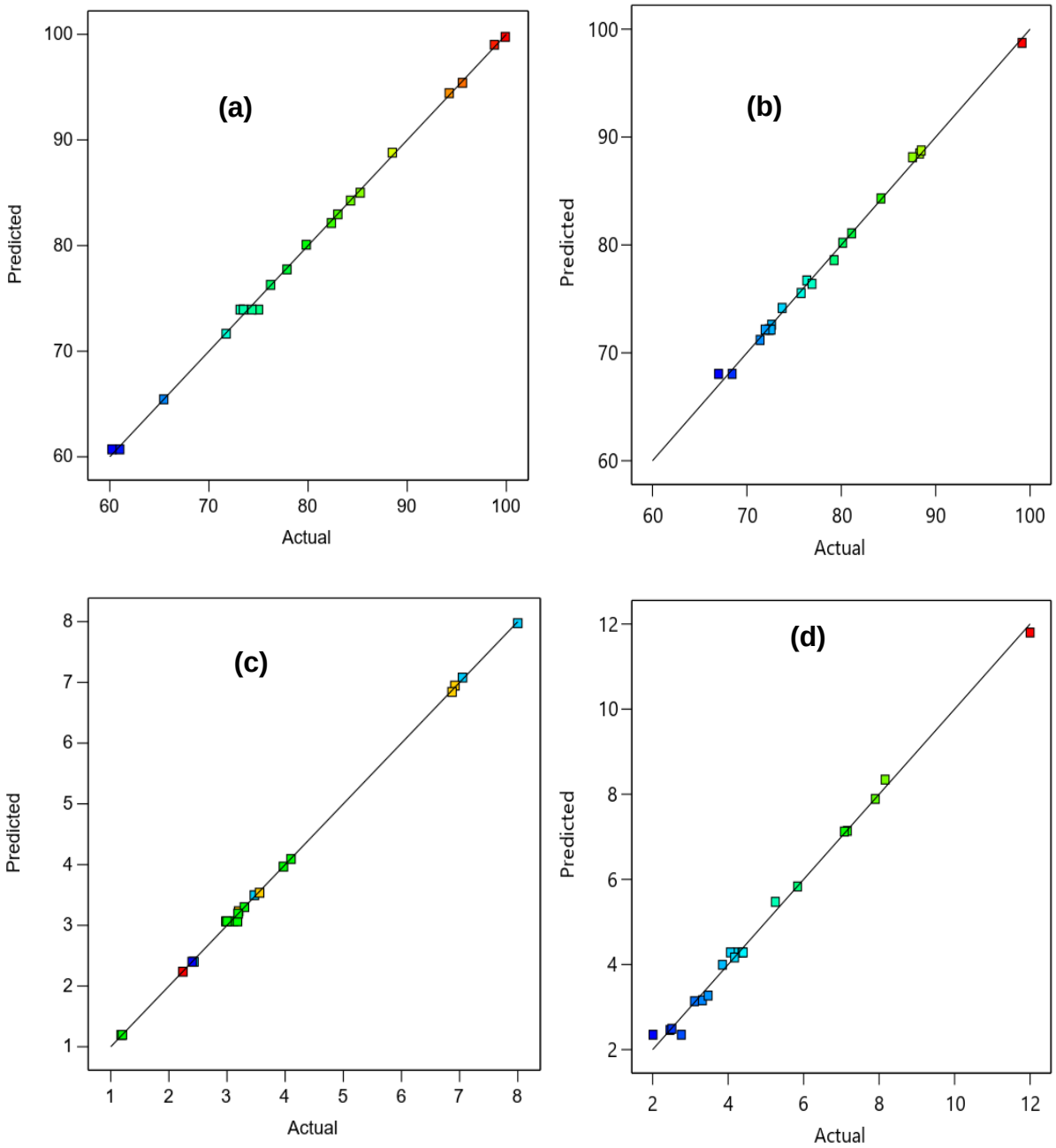

Figure 27: Predicted versus actual for As(III) and Hg(II) removal efficiency (a and b) and biosorption capacity (c and d), respectively

In Tables 25 and 26, respectively, it was found that the variations between the actual and predicted data for both response variables: removal and uptake rates were minimal as can be seen from the residuals. This suggests that the response surface quadratic models were accurate and valid in the response predictions (Nyangi, 2021). Also, the leverages were observed to be far less than 1.0 indicating the suitability of the developed quadratic models. Therefore, it could

be inferred that the quadratic models developed in this study were accurate and showed a better correlation between the adsorption-influencing parameters and the response variables.

Table 25: Actual and predicted values of As(III) removal efficiency and biosorption capacity

Removal efficiency (%)				Biosorption capacity (mg/g)			
Actual Value	Predicted Value	Residual	Leverage	Actual Value	Predicted Value	Residual	Leverage
73.15	73.94	-0.79	0.19	2.98	3.06	-0.08	0.19
94.24	94.43	-0.19	0.71	6.92	6.95	-0.03	0.71
98.80	99.01	-0.21	0.71	7.05	7.08	-0.03	0.71
88.50	88.80	-0.30	0.71	3.47	3.50	-0.03	0.71
73.48	73.94	-0.46	0.19	3.11	3.06	0.05	0.19
95.58	95.41	0.17	0.71	6.87	6.84	0.03	0.71
74.34	73.94	0.40	0.19	3.18	3.06	0.12	0.19
85.26	85.01	0.25	0.71	3.56	3.54	0.02	0.71
75.00	73.94	1.06	0.19	3.00	3.06	-0.06	0.19
99.90	99.76	0.14	0.71	8.00	7.98	0.02	0.71
79.82	80.08	-0.26	0.71	3.20	3.23	-0.03	0.71
82.35	82.14	0.21	0.71	2.43	2.40	0.03	0.71
77.87	77.74	0.13	0.68	3.97	3.97	0.00	0.68
65.44	65.44	0.00	0.68	2.24	2.24	0.00	0.68
71.73	71.66	0.07	0.68	2.40	2.40	0.00	0.68
84.29	84.26	0.03	0.68	4.10	4.09	0.01	0.68
76.22	76.28	-0.06	0.68	3.30	3.30	0.00	0.68
83.00	82.96	0.04	0.68	3.19	3.19	0.00	0.68
61.00	60.71	0.29	0.25	1.18	1.20	-0.02	0.25
60.21	60.71	-0.50	0.25	1.20	1.20	0.00	0.25

Table 26: Actual and predicted values of Hg(II) removal efficiency and biosorption capacity

Removal efficiency (%)				Biosorption capacity (mg/g)			
Actual Value	Predicted Value	Residual	Leverage	Actual Value	Predicted Value	Residual	Leverage
75.75	75.55	0.20	0.71	3.85	3.99	-0.14	0.71
72.40	72.15	0.25	0.19	4.24	4.28	-0.04	0.19
72.62	72.61	0.01	0.71	2.46	2.46	0.00	0.71
88.30	88.47	-0.17	0.71	7.16	7.14	0.02	0.71
72.34	72.15	0.19	0.19	4.37	4.28	0.09	0.19
99.15	98.73	0.42	0.71	12.00	11.80	0.20	0.71
84.20	84.31	-0.11	0.71	7.90	7.89	0.01	0.71
71.93	72.15	-0.22	0.19	4.40	4.28	0.12	0.19
72.56	72.15	0.41	0.19	4.06	4.28	-0.22	0.19
87.55	88.13	-0.58	0.71	8.16	8.34	-0.18	0.71
80.15	80.20	-0.05	0.71	5.84	5.83	0.01	0.71
76.35	76.71	-0.36	0.71	3.32	3.16	0.16	0.71
79.24	78.59	0.65	0.68	4.17	4.17	0.00	0.68
68.44	68.05	0.39	0.25	2.76	2.35	0.41	0.25
81.10	81.08	0.02	0.68	5.25	5.47	-0.22	0.68
88.48	88.76	-0.28	0.68	7.08	7.12	-0.04	0.68
73.74	74.16	-0.42	0.68	3.11	3.14	-0.03	0.68
71.40	71.20	0.20	0.68	3.47	3.27	0.20	0.68
76.90	76.40	0.50	0.68	2.51	2.49	0.02	0.68
67.00	68.05	-1.05	0.25	2.01	2.35	-0.34	0.25

4.5.4 Biosorption Process Factors Interaction and Response Surface Modeling

The 3D response surface plots are displayed in Figs. 28-33 for As(III) percentage removal and biosorption capacity, respectively are the graphical representation of the regression quadratic

models.

In Fig. 28 (a), the removal efficiency increased with rising contact time and biosorbent dosage. Giri *et al.* (2021) and Ranjan *et al.* (2021) observed the same trend when java plum and amaltash seed biomass-based bio-adsorbents and maghemite-loaded pumice composite were used, respectively in removing As(III) from spiked wastewater. Also, the biosorption capacity improved with increasing contact time and at lower biosorbent dosage as shown in Fig. 28 (b). The upsurge in As(III) uptake capacity with declining HGAC dosage is due to less saturation in the liquid phase, which resulted in more biosorption of the As(III) ions on the HGAC surface (Choudhary & Bhattacharyya, 2020).

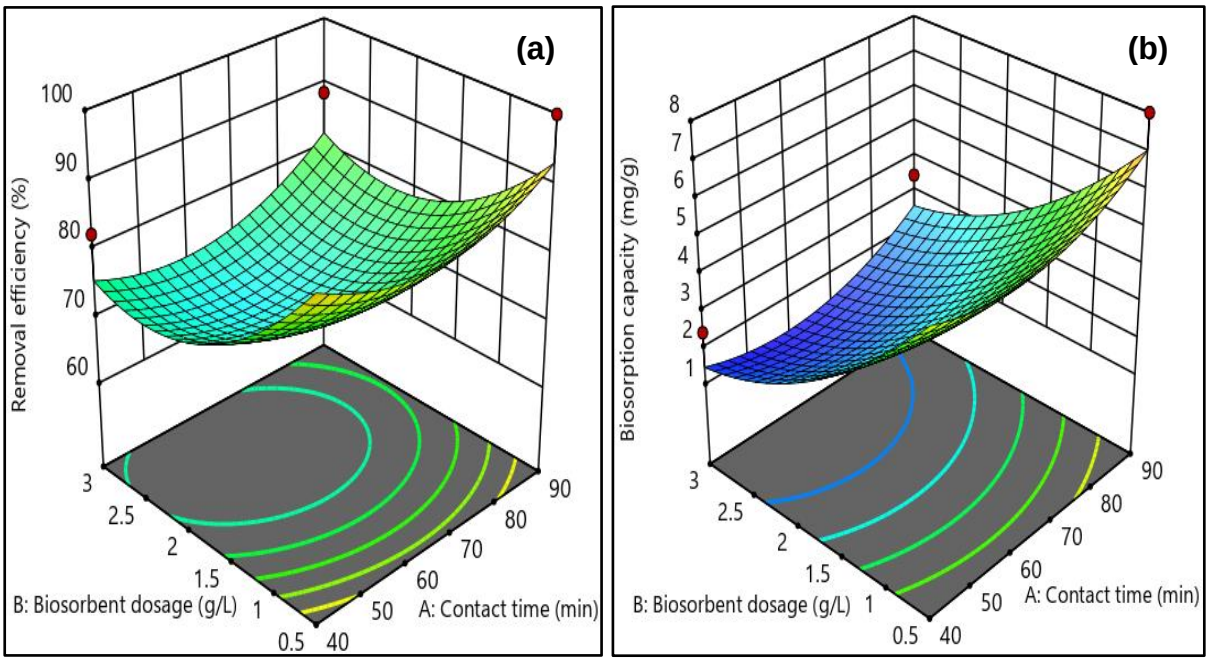

Figure 28: Response surface 3D plots of interaction model terms: A and B for As(III) removal efficiency (a) and biosorption capacity (b), respectively

Also, the combined influence of contact time and the biosorbent dosage on (Y1)-Removal efficiency and (Y2)-Biosorption capacity of Hg(II) from the aqueous media at a constant initial Hg(II) concentration are presented in Figs. 29 (a) and (b), respectively. It was found that the two independent biosorption factors have a significant impact on removal efficiency. In Fig. 29 (a), an upsurge in the numerical values of both biosorption factors increased the removal efficiency significantly and in reverse due to the net negative interactive influence between the two process variables. This implies that the removal rate of Hg(II) ions by the biosorbent is dependent on the time of contact and biosorbent dose. However, the interactive influence of the contact time and biosorbent dosage on Hg(II) ions uptake capacity by the biosorbent

suggests that the two variables have a mutual effect on biosorption capacity and an increase in one factor decreased the biosorption capacity due to the antagonistic interactive effect between the two system factors as shown in Fig. 29 (b).

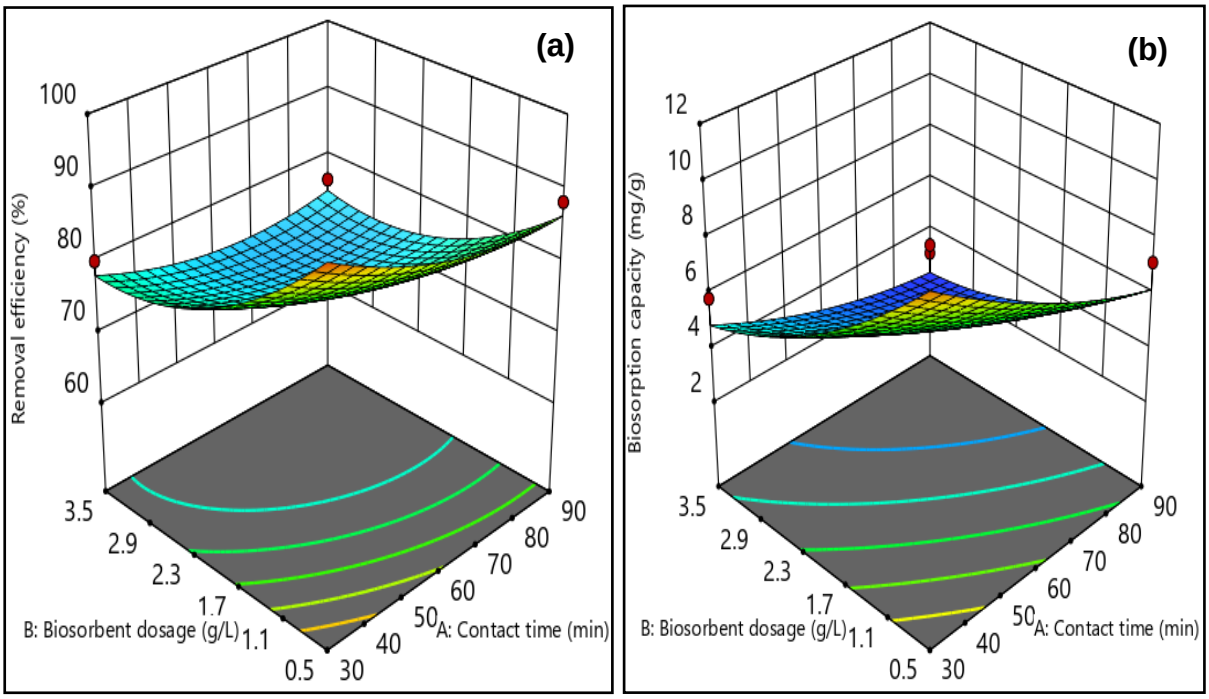

Figure 29: Response surface 3D plots of interaction model terms: A and B for Hg(II) removal efficiency (a) and biosorption capacity (b), respectively

The interaction between contact time and As(III) initial concentration at a constant biosorbent dosage is presented in Fig. 30. As shown in Fig. 30 (a), respectively, it was discovered that the removal efficiency increased at a longer contact time and smaller initial As(III) concentrations. The As(III) ions had a great chance to diffuse and be adsorbed onto the surface and into the pores of HGAC as the contact time progressed until the adsorption attained equilibrium at the ideal agitation time (Anyika *et al.*, 2017). Similarly, according to Bordoloi *et al.* (2022), the removal rate of arsenic species was observed to decrease at elevated initial concentration levels because of the saturation of the sorption sites on the biosorbent. Likewise, it was discovered that the biosorption capacity improved as the contact time and initial As(III) concentration increased as presented in Fig. 30 (b), respectively. However, this observation is more evident at higher initial As(III) concentrations, which might be because, at lower concentration levels, the active spots on the bio-adsorbent surface could not be occupied by As(III) species. The collision of the As(III) species with the active adsorption sites increases as the initial concentration rises, increasing the amount of As(III) that is adsorbed by the biosorbent (Sha *et al.*, 2018).

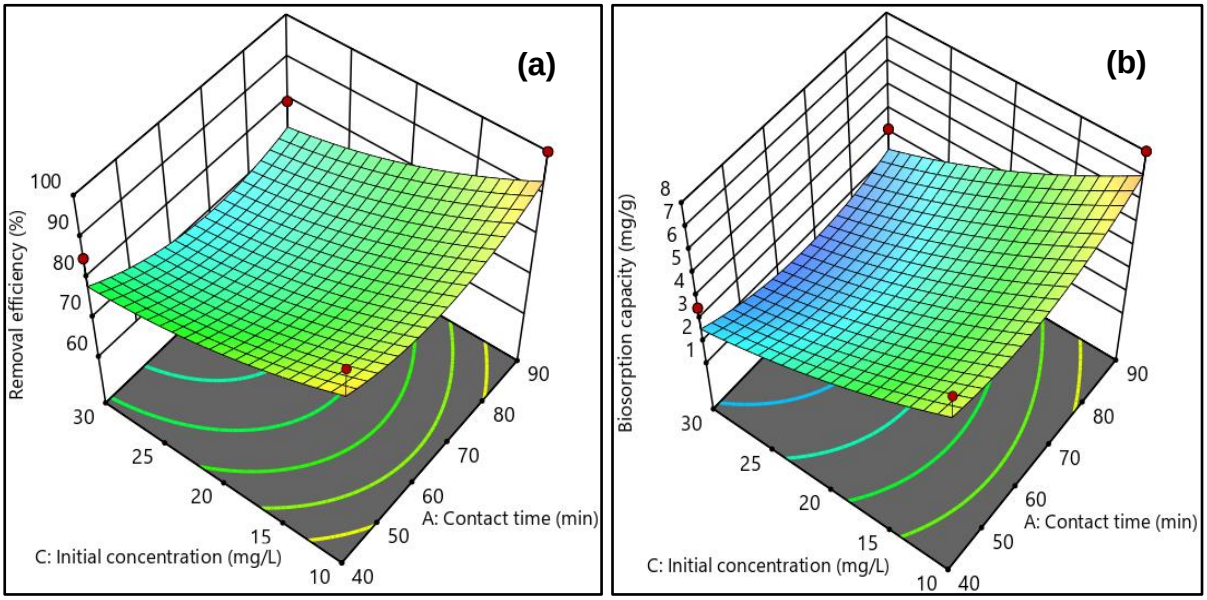

Figure 30: Response surface 3D plots of interaction model terms: A and C for As(III) removal efficiency (a) and biosorption capacity (b), respectively

Similarly, the interactive consequences of the contact time and initial Hg(II) concentration on the percentage removal and uptake capacity at a constant biosorbent dosage are displayed in Figs. 31 (a) and (b), respectively. The increase in contact time and initial Hg(II) concentration resulted in a reduction in the removal efficiency while Hg(II) ions uptake capacity by the biosorbent from the monocomponent sorption system increases with rising initial Hg(II) concentration and time of contact. The collective interactive effect was found to be at maximum at higher values of these two independent biosorption factors.

Figure 32 (a) shows the interactive effect between the biosorbent dosage and As(III) initial concentration at constant contact time, which indicates that the removal percentage upsurges with increasing biosorbent dosage and declining initial As(III)concentration. Also, in Figure 32 (b), the biosorption capacity was observed to upsurge with an increasing initial concentration of As(III) and decreasing biosorbent dosage. In another study, Meshram *et al.* (2022) observed that when the biosorbent dosage was increased, the biosorption of Pb(II) by the activated carbon was reduced. This may be because there are more un occupied sorption sites available to bind the limited amount of the Pb(II) ions in the aqueous solution.

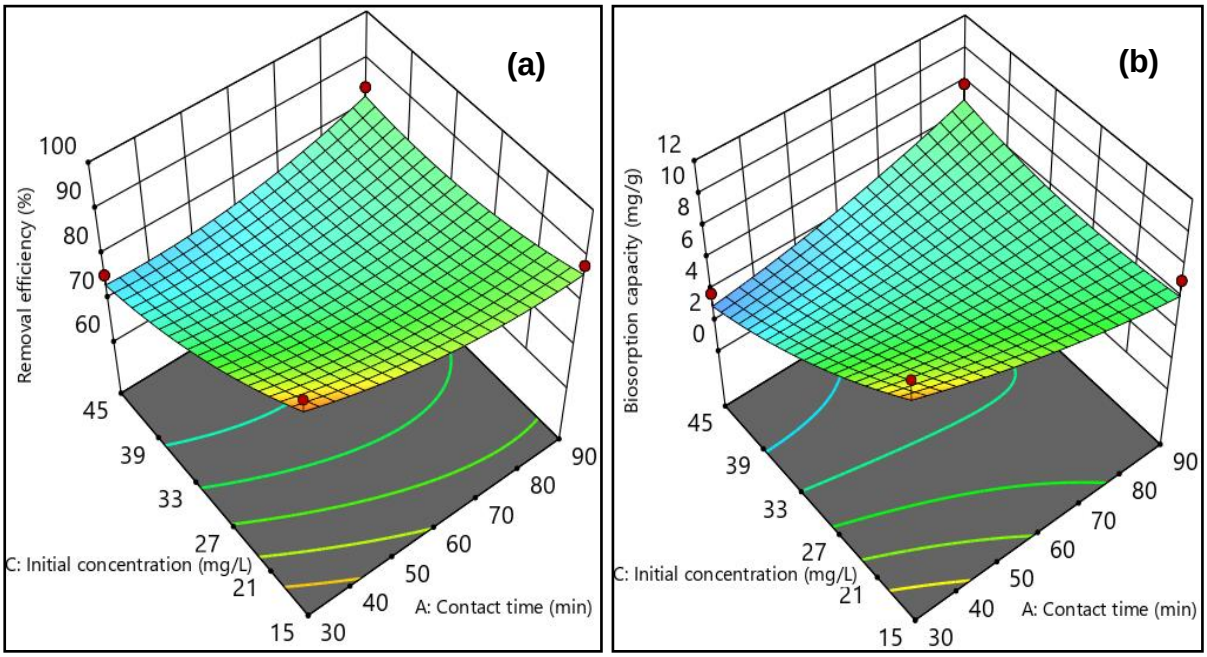

Figure 31: Response surface 3D plots of interaction model terms: A and C for Hg(II) removal efficiency (a) and biosorption capacity (b), respectively

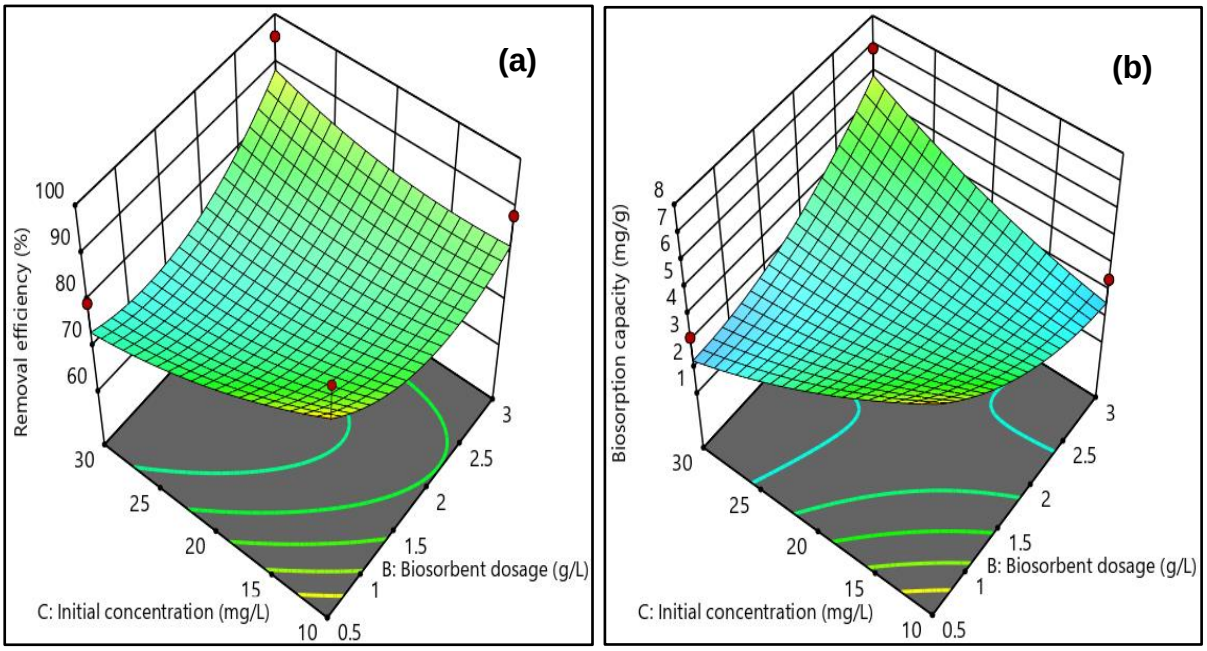

Figure 32: Response surface 3D plots of interaction model terms: B and C for As(III) removal efficiency (a) and biosorption capacity (b), respectively

Likewise, the combined influence of biosorbent dosage and initial Hg(II) concentration on the percentage removal and uptake capacity at a constant contact time is displayed in Figs. 33 (a) and (b), respectively. It was observed that biosorbent dosage and initial Hg(II) concentration at a constant contact time have a resultant effect on both Hg(II) removal rate and uptake

capacity by the biosorbent from the monocomponent system. The removal efficiency was found to decrease when the biosorbent dosage and initial Hg(II) concentration increased while the biosorption capacity increased with rising initial concentration and decreasing biosorbent dosage. Similarly, the collective interactive influence on the responses was obvious at higher values of the studied factors.

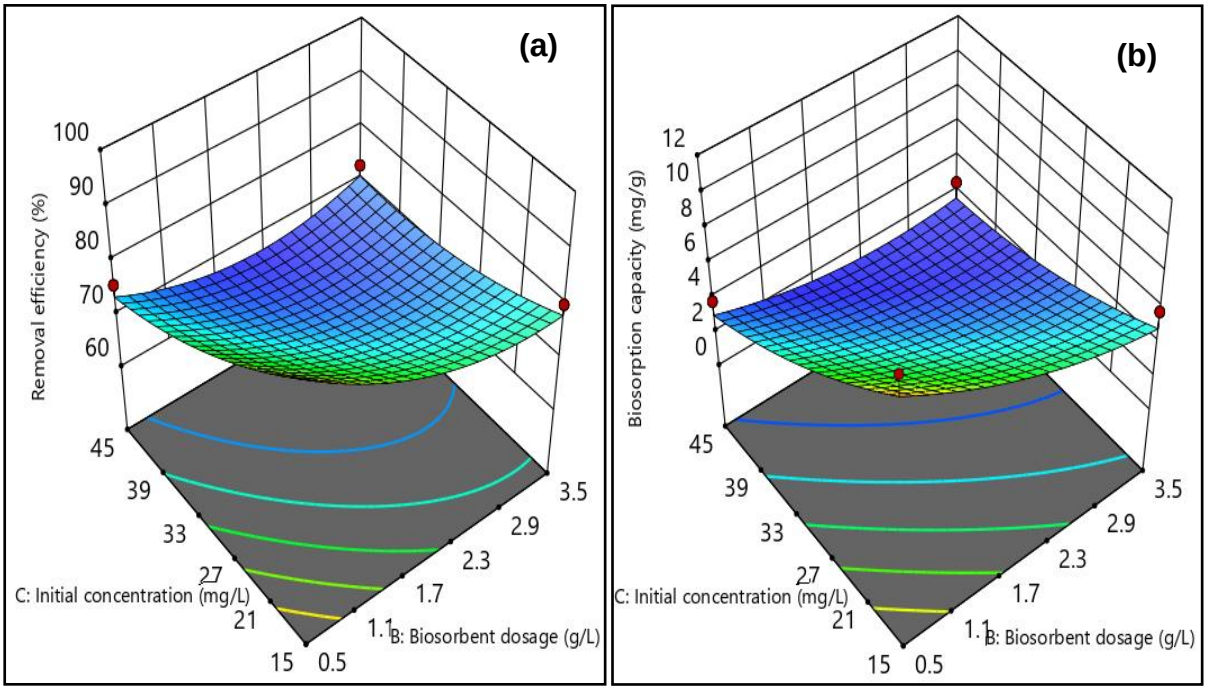

Figure 33: Response surface 3D plots of interaction model terms: B and C for Hg(II) removal efficiency (a) and biosorption capacity (b), respectively

4.5.5 Numerical Optimization of Adsorption Process Parameters Using CCD-RSM

The main benefit of numerically optimizing the removal of heavy metals using sorbent materials is that it helps to reduce the cost of the process in subsequent steps and for industrial uses (Khalifa *et al.*, 2019). The CCD-RSM enables simultaneous optimization of the independent adsorption process factors influencing the response variables, while simultaneously enhancing performance requirements and lowering error with the fewest possible runs (Mondal *et al.*, 2019). The desirability function in CCD-RSM was applied to investigate the optimum sorption conditions for As(III) and Hg(II) detoxification from the aqueous systems (Archin *et al.*, 2019). The criteria employed to achieve the maximum removal and biosorption capacity of As(III) and Hg(II) by CCD-RSM using the HGAC are listed in Tables 27 and 28, respectively where all of the investigated biosorption process variables are "in range" and the response variables are "in maximize".

According to the selected criteria, 20 solutions containing optimal experimental operating conditions of the independent factors for As(III) and biosorption on the HGAC were provided as presented in Tables 29 and 30, respectively. Under the selected optimum experimental conditions of 90 min contact time, 0.5 g/L biosorbent dosage, and 10 mg/L initial As(III) concentration shown in Fig. 34, maximum As(III) removal and biosorption capacity were 93.14% and 7.04 mg/g with the desirability of 0.844. For the optimal decontamination of Hg(II) ions from the wastewater, the best operating conditions of 30 min contact time, 0.5 g/L biosorbent dosage, and 15 mg/L initial concentration were found at 0.903 desirability with maximum removal rate and uptake capacity of Hg(II) of 96.68% and 10.83 mg/g, respectively as shown in Fig. 35.

Table 27: Criteria set for independent and response factors to optimize As(III) biosorption from aqueous systems

Name	Goal	Lower Limit	Upper Limit
A: Contact time	is in range	40	90
B: Biosorbent dosage	is in range	0.5	3
C: Initial concentration	is in range	10	30
Removal efficiency	maximize	60.21	99.90
Biosorption capacity	maximize	1.18	8.00

Table 28: Criteria set for independent and response factors to optimize Hg(II) biosorption from aqueous systems

Name	Goal	Lower Limit	Upper Limit
A: Contact time	is in range	30	90
B: Biosorbent dosage	is in range	0.5	3.5
C: Initial concentration	is in range	15	45
Removal efficiency	maximize	67.00	99.15
Biosorption capacity	maximize	2.01	12.00

Table 29: As(III) optimization solutions for independent parameters and response variables

Number	Contact time	Biosorbent dosage	Initial concentration	Removal efficiency	Biosorption capacity	Desirability	Remark
1	90.00	0.500	10.000	93.143	7.041	0.844	Selected
2	90.00	0.500	10.094	92.999	7.012	0.840	
3	89.54	0.500	10.000	92.927	7.002	0.839	
4	89.33	0.500	10.000	92.828	6.984	0.836	
5	88.82	0.500	10.000	92.593	6.940	0.830	
6	90.00	0.500	10.614	92.208	6.848	0.819	
7	87.63	0.500	10.000	92.065	6.843	0.816	
8	90.00	0.568	10.011	91.979	6.826	0.814	
9	86.93	0.500	10.001	91.768	6.787	0.809	
10	86.70	0.500	10.000	91.671	6.769	0.806	
11	85.23	0.500	10.000	91.082	6.658	0.790	
12	84.84	0.500	10.000	90.931	6.629	0.786	
13	84.36	0.500	10.000	90.752	6.595	0.782	
14	40.00	0.500	10.000	92.395	6.145	0.768	
15	40.00	0.500	10.151	92.205	6.106	0.763	
16	41.44	0.500	10.000	91.772	6.074	0.755	
17	40.00	0.500	10.425	91.866	6.036	0.754	
18	81.17	0.500	10.001	89.655	6.381	0.752	
19	42.44	0.500	10.000	91.361	6.029	0.747	
20	42.88	0.500	10.000	91.186	6.009	0.743	

Table 30: Hg(II) optimization solutions for independent parameters and response variables

Number	Contact time (min)	Biosorbent dosage (g/L)	Initial concentration (mg/L)	Removal efficiency (%)	Biosorption capacity (mg/g)	Desirability	
1	30.000	0.500	15.000	96.679	10.832	0.903	Selected
2	30.449	0.500	15.002	96.513	10.782	0.898	
3	30.000	0.500	15.143	96.515	10.781	0.898	
4	30.000	0.516	15.000	96.471	10.781	0.897	
5	30.000	0.500	15.270	96.369	10.736	0.893	
6	30.000	0.529	15.000	96.308	10.742	0.893	
7	30.947	0.500	15.005	96.329	10.728	0.892	
8	30.000	0.500	15.431	96.184	10.679	0.888	
9	31.604	0.500	15.000	96.099	10.659	0.885	
10	30.000	0.550	15.000	96.029	10.674	0.885	
11	32.096	0.500	15.000	95.924	10.607	0.880	
12	30.523	0.556	15.000	95.772	10.602	0.877	
13	30.000	0.500	15.747	95.821	10.567	0.876	
14	32.486	0.500	15.000	95.787	10.565	0.876	
15	30.000	0.577	15.000	95.685	10.590	0.875	
16	33.155	0.500	15.000	95.554	10.495	0.869	
17	30.000	0.601	15.000	95.388	10.518	0.867	
18	30.000	0.500	16.323	95.175	10.367	0.856	
19	34.546	0.500	15.000	95.078	10.350	0.854	
20	31.474	0.500	16.100	94.908	10.293	0.848	

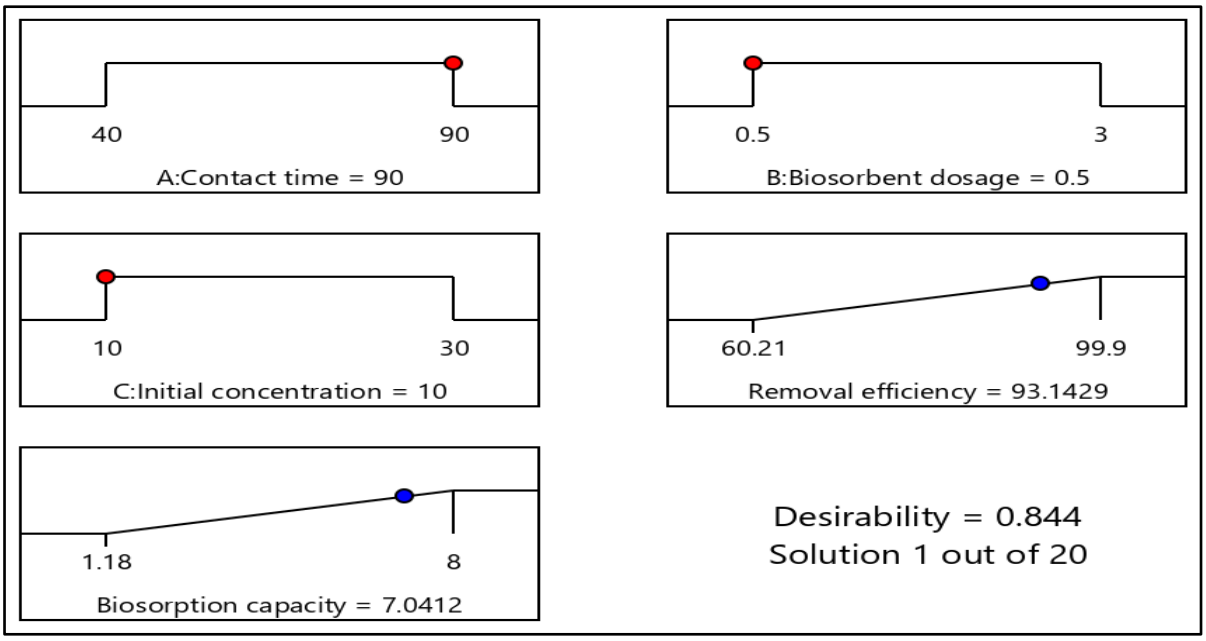

Figure 34: Optimization ramps containing optimum operating conditions for maximum removal and uptake capacity of As(III) ions from the wastewater

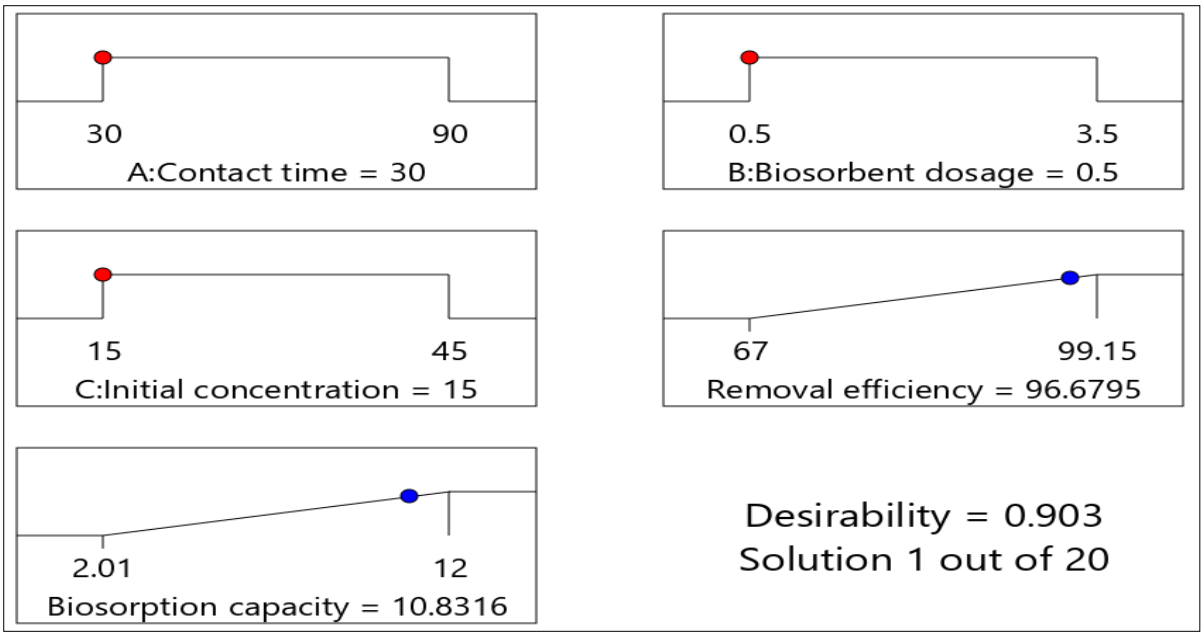

Figure 35: Optimization ramps containing optimum operating conditions for maximum removal and uptake capacity of Hg(II) ions from the wastewater

4.5.6 Validation of Quadratic Models and Confirmation of Optimization Results

In the post-optimization analysis, the proposed quadratic models applied to figure out the optimal conditions for maximum remediation of As(III) and Hg(II) from the water systems using HGAC were validated. To verify the precision of the quadratic models and optimized

results, five different experimental runs were performed under the optimum operating conditions determined by the desirability function during the optimization process as displayed in Figs. 34 and 35, respectively. In Table 31, the validation of the optimization results at a 95% confidence level using the selected operating conditions gave a maximum removal efficiency of 94.33% and an uptake rate of 7.15 mg/g for As(III), which are reasonably close to the maximum predicted data obtained by the CCD-RSM confirming the accuracy and validity of the response surface quadratic models. Similarly, the confirmatory experimental results presented in Table 32 show that the optimum removal efficiency of 97.93% and biosorption capacity of 11.15 mg/g attained for Hg(II) is within the prediction intervals suggesting the validity of the quadratic models. Comparatively, in both Tables 31 and 32, respectively, there exists a good correlation between the confirmatory experimental and the predicted results of As(III) and Hg(II) removal efficiency and biosorption capacity with minimal residuals and standard deviations indicating that the developed quadratic models have been validated and could be used in predicting future cases.

Table 31: Quadratic models validation and confirmation of optimization results

Response variable	Predicted Mean	Predicted Median	Std Dev	n	SE Pred	95% PI low	Data Mean	95% PI high
Removal efficiency	93.14	93.14	0.56	5	0.53	91.95	94.33	94.34
Biosorption capacity	7.04	7.04	0.06	5	0.06	6.91	7.15	7.17

Table 32: Quadratic models validation and confirmation of optimization results

Response	Predicted Mean	Predicted Median	Std Dev	n	SE Pred	95% PI low	Data Mean	95% PI high
Removal efficiency	96.68	96.68	0.60	5	0.56	95.41	97.93	97.95
Biosorption capacity	10.83	10.83	0.25	5	0.24	10.30	11.15	11.36

4.6 Biosorption Modeling and Thermodynamics Studies

4.6.1 Biosorption Isotherm Modeling

The fitness of the equilibrium data attained for the removal of As(III) and Hg(II) from the monocomponent sorption systems to four types of two-parameter biosorption isotherm models including Langmuir, Temkin Freundlich, and Dubinin-Radushkevich (D-R) was tested. The two-parameters isotherm plots are presented in Figs. 36-39 while the models' constant parameters are summarized in Table 33.

Table 33: Two-parameter biosorption isotherm models parameters for As(III) and Hg(II) removal

Isotherm model	Parameter	Heavy metal	
		As(III)	Hg(II)
Langmuir	q_m (mg/g)	155.42	112.46
	K_L (L/mg)	0.2088	0.2398
	R_L	0.0387	0.0551
	R^2	0.9995	0.9998
	SSE	4.90×10^{-7}	1.60×10^{-7}
Temkin	A (L/g)	0.2863	0.3361
	b (kJ/mol)	8.6727	12.5952
	B	2.9526	2.0991
	R^2	0.9806	0.9854
	SSE	0.0008	0.0004
Freundlich	K_F (mg/g)	1.0021	0.9124
	n	2.1455	2.3635
	$\frac{1}{n}$	0.4661	0.4231
	R^2	0.9251	0.8893
	SSE	0.0114	0.0253
Dubinin-Radushkevich (D-R)	K_{DR} (mol^2/k-J^2)	8.00×10^{-6}	1.00×10^{-5}
	q_s (mg/g)	9.0866	7.3839
	E (kJ/mol)	2.5000	2.2222
	R^2	0.6995	0.7722
	SSE	0.1849	0.1056

In Fig. 36, the coefficient of determination (COD) obtained for the non-competitive removal of As(III) and Hg(II) ions are 0.9995 and 0.9998 with a very small coefficient of non-determination (CND) of 0.0005 and 0.0002, respectively. It was also observed that there was

no significant difference between the COD and the adjusted COD. The adjusted COD of 0.9994 and 0.9997, and Pearson's r of 0.9997 and 0.9999 for As(III) and Hg(II), respectively were found to be close to one indicating a good fit. In addition, the small residual sum of squares (RSS) of 0.6488 and 0.7385 obtained for As(III) and Hg(II), respectively indicate that the Langmuir model best fits the equilibrium data achieved by the biosorbent. The agreement of the equilibrium data attained for the removal of As(III) and Hg(II) ions from mono-metal systems indicates that the mechanism of biosorption proceeded through monolayer sorption on the homogeneous surfaces of the bio-adsorbent with a uniform distribution of the adsorption energy for all sites (Saadi *et al.*, 2015).

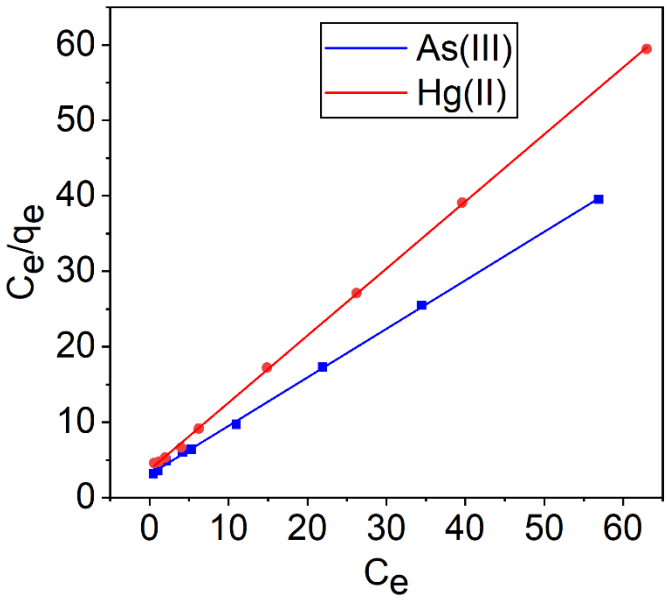

Linear fitting parameters of As(III)

Equation	y = a + b*x
Plot	As(III)
Intercept	3.08171 ± 0.13248
Slope	0.64338 ± 0.00558
Residual Sum of Squares	0.64879
Pearson's r	0.99974
R-Square (COD)	0.99947
Adj. R-Square	0.9994

Linear fitting parameters of Hg(II)

Equation	y = a + b*x
Plot	Hg(II)
Intercept	3.70823 ± 0.14274
Slope	0.88919 ± 0.00531
Residual Sum of Squares	0.73851
Pearson's r	0.99988
R-Square (COD)	0.99975
Adj. R-Square	0.99971

Figure 36: Linear fitting of two-parameter Langmuir biosorption isotherm models for As(III) and Hg(II) removal from monocomponent systems

Therefore, the adsorptive removal of As(III) and Hg(II) ions by the hybrid granular activated carbon was mainly chemisorption on the monolayer. As summarized in Table 33, the Langmuir monolayer uptake capacity (q_m) obtained for non-competitive removal of As(III) and Hg(II) ions is 155.42 and 112.46 mg/g, respectively suggesting the high uptake capacity of the prepared biosorbent. Furthermore, the dimensionless separation factor (R_L) obtained for detoxification of As(III) and Hg(II) ions from the mono-metal system was between 0.00 and 1.00, which suggests that the biosorption process was favorable under all the studied conditions (Liu *et al.*, 2020).

The two-parameter Temkin isotherm plot of As(III) and Hg(II) as presented in Fig. 37 has a high COD of 0.9806 and 0.9854 and small CND of 0.0194 and 0.0146, respectively. The

adjusted COD of 0.9778 and 0.9833 and Pearson's r of 0.9902 and 0.9927 for As(III) and Hg(II), respectively were also found to be high implying good conformity. However, in the Temkin model, the RSS of 3.5927 and 1.3965 for As(III) and Hg(II) were found to be higher than those obtained in the Langmuir model indicating that the Langmuir model provides a better fit for the biosorption of As(III) and Hg(II) on the biosorbent. From Table 33, the high heat of sorption parameter, *b* obtained for the decontamination of As(III) and Hg(II) ions individually from the mono-metal systems implies chemisorption (Bayuo *et al.*, 2018). The Temkin isotherm model assumes that the heat of adsorption of all the molecules in the layer as a function of temperature will decrease linearly with the active attachment sites, ignoring the lower and upper limit concentration sets (Tekin & Açikel, 2022).

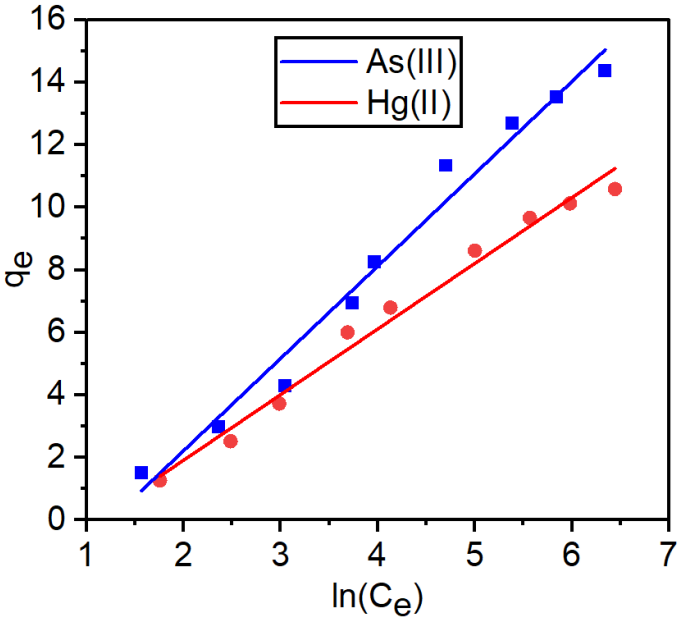

Linear fitting parameters of As(III)

Equation	y = a + b*x
Plot	As(III)
Intercept	-3.69233 ± 0.68795
Slope	2.9526 ± 0.15713
Residual Sum of Squares	3.59265
Pearson's r	0.99023
R-Square (COD)	0.98056
Adj. R-Square	0.97778

Linear fitting parameters of Hg(II)

Equation	y = a + b*x
Plot	Hg(II)
Intercept	-2.28852 ± 0.43476
Slope	2.0991 ± 0.09663
Residual Sum of Squares	1.39645
Pearson's r	0.99266
R-Square (COD)	0.98538
Adj. R-Square	0.98329

Figure 37: Linear fitting of two-parameter Temkin biosorption isotherm models for As(III) and Hg(II) removal from monocomponent systems

Figure 38 depicts that the equilibrium data of the mono-metal [As(III) and Hg(II)] are less represented by the Freundlich empirical model with COD of 0.9251 and 0.8893, respectively in comparison to the Langmuir and Temkin models. The level of fitness of the sorption data of As(III) and Hg(II) can also be seen from the other good fitting parameters such as adjusted COD, Pearson's r, and RSS displayed in Fig. 38. The representation of the sorption data obtained from the adsorptive removal of As(III) and Hg(II) individually to the Freundlich isotherm suggests multilayer sorption of the heavy metal ions on the heterogeneous surfaces of the bio-adsorbent with a non-uniform dispersion of the heat of sorption (Batool *et al.*, 2019). From Table 33, the adsorption intensity (n) of the biosorbent is higher than unity indicating

that the chemisorption is predominant and there exists heterogeneity at the biosorbent surface (Guo *et al.*, 2017). The calculated values of n for As(III) and Hg(II) were 2.146 and 2.364 respectively, which satisfied the heterogeneity condition of $1.00 < n < 10.00$ (Chigondo & Nyamunda, 2013). Also, the values of $\frac{1}{n}$ for As(III) and Hg(II) were below unity. The larger the value of n and the smaller the value of $\frac{1}{n}$ signifies stronger interaction between the biosorbent surface and As(III) and Hg(II) ions in the non-competitive aqueous media (Bazrchi *et al.*, 2018).

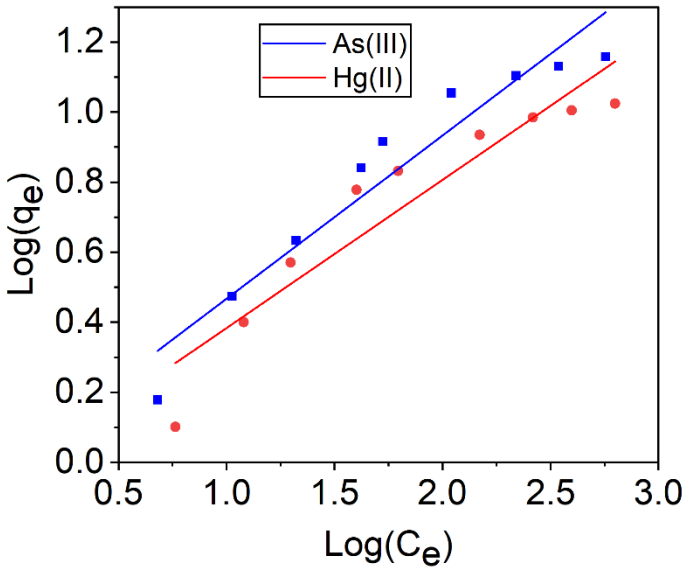

Linear fitting parameters of As(III)

Equation	y = a + b*x
Plot	As(III)
Intercept	9.46597E-4 ± 0.09535
Slope	0.4661 ± 0.05015
Residual Sum of Squares	0.06901
Pearson's r	0.9618
R-Square (COD)	0.92505
Adj. R-Square	0.91435

Linear fitting parameters of Hg(II)

Equation	y = a + b*x
Plot	Hg(II)
Intercept	-0.03979 ± 0.11026
Slope	0.42308 ± 0.05643
Residual Sum of Squares	0.08982
Pearson's r	0.94301
R-Square (COD)	0.88926
Adj. R-Square	0.87344

Figure 38: Linear fitting of two-parameter Freundlich biosorption isotherm models for As(III) and Hg(II) removal from monocomponent systems

Based on the linear fitting parameters shown in Fig. 39, the D-R isotherm model was also found to describe the sorption data of As(III) and Hg(II) attained from the mono-metal systems, respectively though it was the least fit among all the tested two-parameter isotherm models. The Dubinin-Radushkevich (D-R) model was found to have the lowest correlation coefficients of 0.6995 and 0.7722, which are far from unity for As(III) and Hg(II), respectively. The fitness of the equilibrium sorption data of As(III) and Hg(II) to the D-R model reveals that the elimination of As(III) and Hg(II) ions took place on both the homogeneous and heterogeneous surfaces of the biosorbent. In Table 33, the mean sorption energy determined for the detoxification of As(III) and Hg(II) ions is 2.50 and 2.22 kJ/mol, respectively, which indicates the physisorption process. Physisorption is described when E ranges from 1.00-8.00 kJ/mol and chemisorption occurs when E is between 8.00-16.00 kJ/mol (Dada *et al.*, 2021).

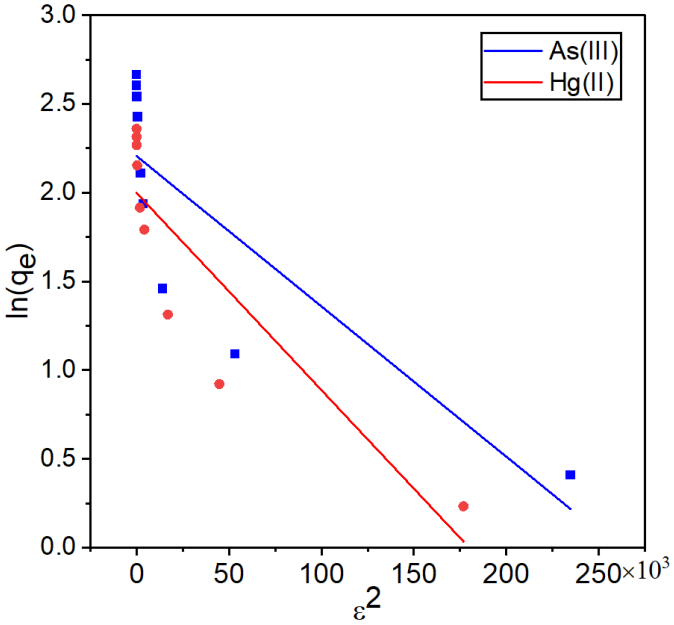

Linear fitting parameters of As(III)

Equation	y = a + b*x
Plot	As(III)
Intercept	2.20683 ± 0.16876
Slope	-8.47026E-6 ± 2.09849E-6
Residual Sum of Squares	1.46721
Pearson's r	-0.83634
R-Square (COD)	0.69947
Adj. R-Square	0.65654

Linear fitting parameters of Hg(II)

Equation	y = a + b*x
Plot	Hg(II)
Intercept	1.99934 ± 0.13929
Slope	-1.11076E-5 ± 2.27998E-6
Residual Sum of Squares	0.97946
Pearson's r	-0.87877
R-Square (COD)	0.77224
Adj. R-Square	0.73971

Figure 39: Linear fitting of two-parameter Dubinin-Radushkevich (D-R) biosorption isotherm models for As(III) and Hg(II) removal from monocomponent systems

4.6.2 Biosorption Kinetic Modeling

In this study, As(III) and Hg(II) biosorption kinetic data obtained from monocomponent sorption systems by the biosorbent was modeled using pseudo-second-order, Elovich, Weber-Morris intraparticle diffusion, and pseudo-first-order kinetic models. The four kinetic model plots are shown in Figs. 40-43 and the models' constant parameters are summarized in Table 34. These kinetic models were envisaged to investigate the mechanism and the sorption process of As(III) and Hg(II) ions individually onto the hybrid granular activated carbon.

Figure 40 reveals that the elimination of As(III) and Hg(II) ions by the biosorbent in the non-competitive biosorption systems was proficiently explained by the pseudo-second-order model with good COD, adjusted COD, and Pearson's r. The COD and CND attained from the kinetic data were found to be 0.9880 and 0.0120 for As(III) as well as 0.9712 and 0.0288 for Hg(II), respectively. From the kinetic models' constant parameters summarized in Table 34, it was observed that there was no discernible variation between the calculated equilibrium uptake capacity ($q_{e,cal}$) and the experimental equilibrium biosorption capacity ($q_{e,exp}$) implying that the pseudo-second-order kinetic model fitted well with both As(III) and Hg(II) sorption data. This also suggests the efficiency of the prepared biosorbent in the elimination of As(III) and Hg(II) ions from the mono-metal sorption systems.

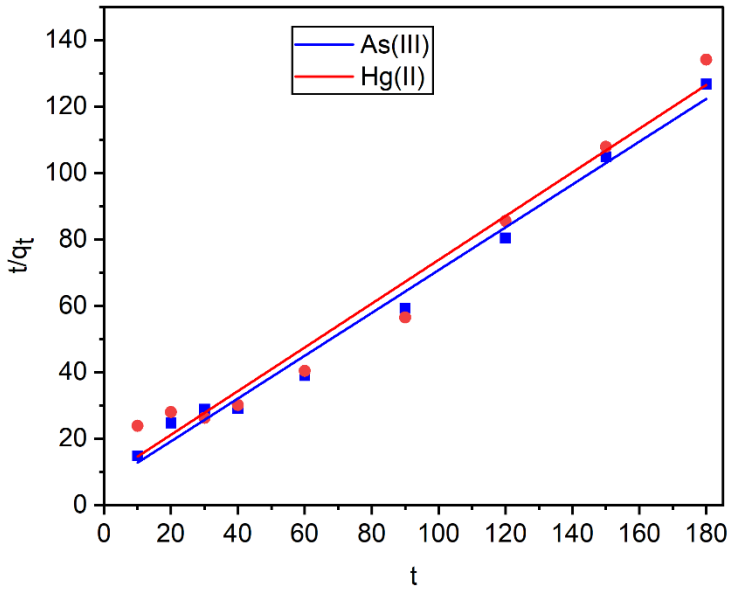

Linear fitting parameters of As(III)

Equation	y = a + b*x
Plot	As(III)
Intercept	6.36819 ± 2.59258
Slope	0.64421 ± 0.02684
Residual Sum of Squares	148.99287
Pearson's r	0.99398
R-Square (COD)	0.988
Adj. R-Square	0.98628

Linear fitting parameters of Hg(II)

Equation	y = a + b*x
Plot	Hg(II)
Intercept	8.05094 ± 4.13919
Slope	0.65824 ± 0.04284
Residual Sum of Squares	379.77848
Pearson's r	0.98549
R-Square (COD)	0.9712
Adj. R-Square	0.96708

Figure 40: Linear fitting of pseudo-second-order biosorption kinetic model for As(III) and Hg(II) removal from monocomponent systems

Table 34: Biosorption kinetic models parameters for As(III) and Hg(II) removal

Kinetic model	Parameter	Heavy metal	
		As(III)	Hg(II)
Pseudo-second-order	Kp_2 (L/min)	0.0652	0.0538
	q_e (mg/g)	1.5523	1.5193
	$q_{e,cal}$ (mg/g)	1.5533	1.5223
	R^2	0.9880	0.9712
	SSE	0.0003	0.0017
Elovich	α (mg/g.min)	0.2224	0.3610
	β (g/mg)	3.4060	3.0003
	R^2	0.7658	0.7114
	SSE	0.1120	0.1700
Intraparticle diffusion	K_{id} (g/mg.min)	0.0718	0.0787
	C	0.6689	0.5591
	R^2	0.6165	0.5341
	SSE	0.3003	0.4430
Pseudo-first-order	Kp_1 (1/min)	0.0134	0.0074
	q_e (mg/g)	0.5054	0.5721
	$q_{e,cal}$ (mg/g)	0.5210	0.0281
	R^2	0.4135	0.2468
	SSE	0.7021	1.1580

The fitness of the experimental data to the pseudo-second-order model explained the mechanism of the individual biosorption of As(III) and Hg(II) ions onto the biosorbent to be due to the chemisorption process where the adsorbate share valence electrons with the biosorbent surface and forms a weak chemical bond (Ahmed *et al.*, 2020; Batool *et al.*, 2019). This was confirmed by the surface functional groups analysis using FT-IR, which showed the possible engagement of functional groups on the surface of the biosorbent during As(III) and Hg(II) sequestration by sharing electrons between the biosorbent and heavy metal ions (Bayuo *et al.*, 2019).

The chemical reaction taking place between the surface functional groups on the sorbent and the adsorbate in the aqueous solution is kinetically expressed by the Elovich kinetic model. As shown in Fig. 41, the Elovich kinetic model fits less to the experimental data obtained for As(III) and Hg(II) in comparison to the pseudo-second-order with relatively high COD values of 0.7658 and 0.7114, respectively. The other fitted parameters include adjusted COD, Pearson's r, and RSS and the fitness of the equilibrium data to the Elovich kinetic model suggests that the decontamination of As(III) and Hg(II) ions from the mono-metal sorption system was due to chemisorption, which occurred on the heterogeneous surface of the biosorbent (Liu *et al.*, 2021).

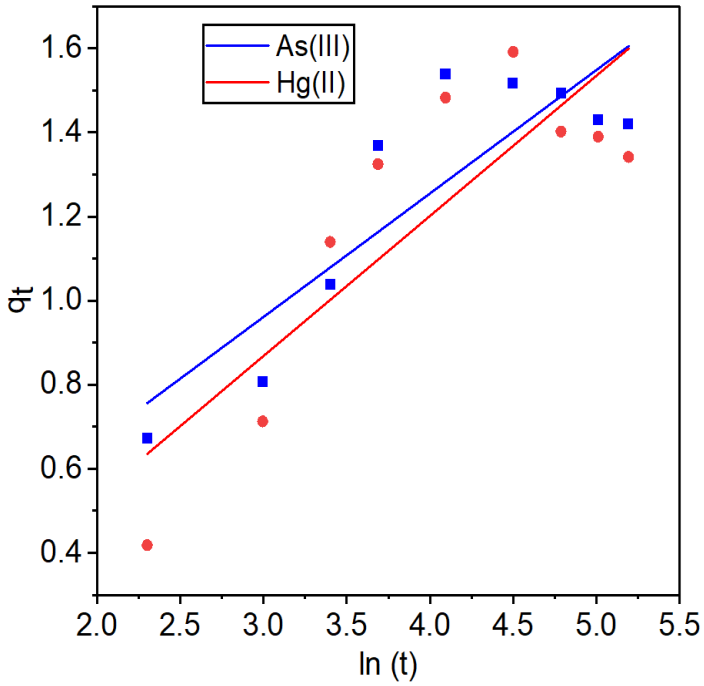

Linear fitting parameters of As(III)

Equation	y = a + b*x
Plot	As(III)
Intercept	0.07995 ± 0.2518
Slope	0.29362 ± 0.06138
Residual Sum of Squares	0.20224
Pearson's r	0.87508
R-Square (COD)	0.76576
Adj. R-Square	0.73229

Linear fitting parameters of Hg(II)

Equation	y = a + b*x
Plot	Hg(II)
Intercept	-0.13221 ± 0.32921
Slope	0.33335 ± 0.08025
Residual Sum of Squares	0.3457
Pearson's r	0.84344
R-Square (COD)	0.71139
Adj. R-Square	0.67016

Figure 41: Linear fitting of Elovich biosorption kinetic model for As(III) and Hg(II) removal from monocomponent systems

The Weber-Morris intraparticle diffusion kinetic model becomes the rate-controlling step when a straight-line graph of q_t versus $t^{½}$ passes through the origin (Olu-Owolabi *et al.*, 2014). Figure 42 indicates the Weber-Morris intra-particle diffusion kinetic model plot of As(III) and Hg(II) exhibited a relatively low fit to the kinetic data than the pseudo-second-order and Elovich models with low COD of 0.6165 and 0.5341, respectively, and other low fitted parameters. It was found that the linear plots generated on the adsorptive removal of As(III) and Hg(II) ions from the non-competitive biosorption systems failed to pass through the origin as shown in Fig. 42. This depicts that the rate is controlled by mass transfer across the boundary layer, which takes place in slowly agitated batch biosorption systems (Bastami *et al.*, 2020).

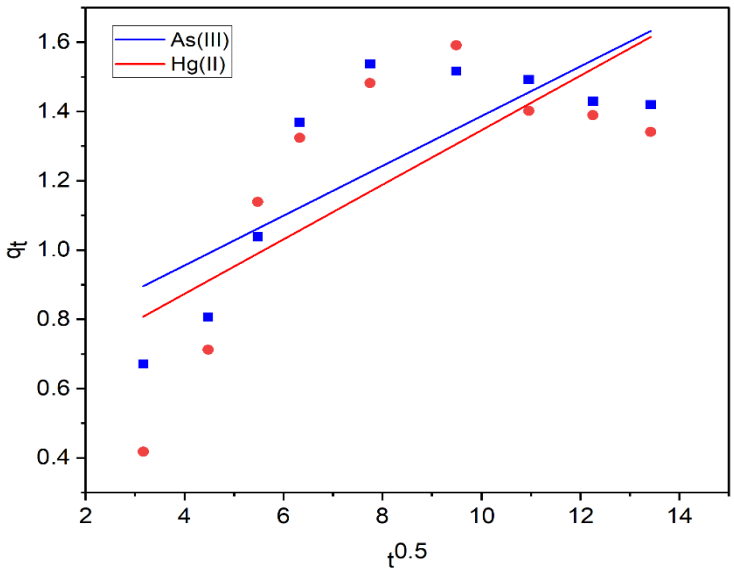

Linear fitting parameters of As(III)

Equation	y = a + b*x
Plot	As(III)
Intercept	0.66885 ± 0.1888
Slope	0.07181 ± 0.0214
Residual Sum of Square	0.33114
Pearson's r	0.78515
R-Square (COD)	0.61646
Adj. R-Square	0.56166

Linear fitting parameters of Hg(II)

Equation	y = a + b*x
Plot	Hg(II)
Intercept	0.55914 ± 0.2451
Slope	0.07873 ± 0.02779
Residual Sum of Squares	0.55808
Pearson's r	0.73081
R-Square (COD)	0.53409
Adj. R-Square	0.46753

Figure 42: Linear fitting of Weber-Morris intra-particle diffusion biosorption kinetic model for As(III) and Hg(II) removal from monocomponent systems

To describe liquid-solid sorption systems based on the solid capacity, the pseudo-first-order kinetic model was developed. Figure 43 reveals that the pseudo-first-order model could not describe the experimental data of As(III) and Hg(II) as deduced from the very low COD values of 0.4417 and 0.3516, respectively, and other non-fitted parameters. Hence, the biosorption mechanism achieved by the biosorbent through the single removal of As(III) and Hg(II) ions from the non-competitive aqueous solutions could not be explained to be due to physisorption. According to the pseudo-first-order kinetic model, the molecules of the adsorbate are physically adsorbed (physisorption) to the sorbent surface at equilibrium, which is based on the reversibility of the sorption process (Memon *et al.*, 2021).

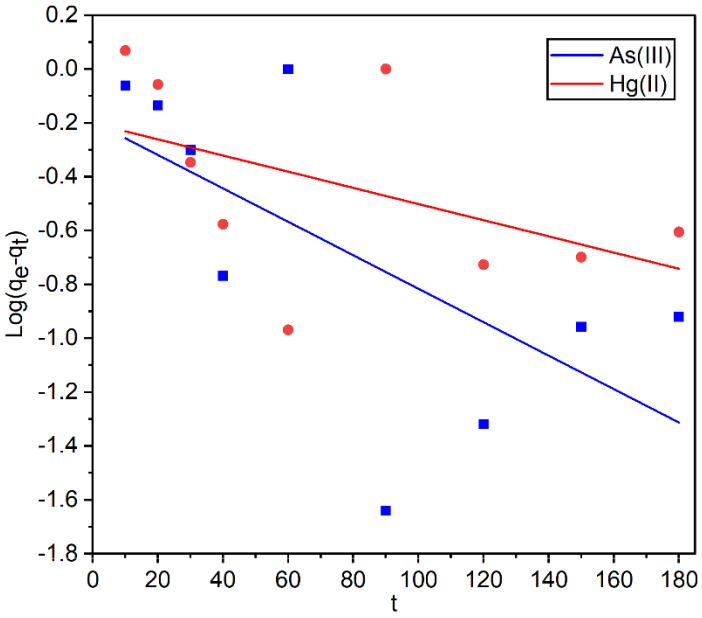

Linear fitting parameters of As(III)

Equation	y = a + b*x
Plot	As(III)
Intercept	-0.19445 ± 0.27019
Slope	-0.00621 ± 0.0028
Residual Sum of Squares	1.61826
Pearson's r	-0.64304
R-Square (COD)	0.4135
Adj. R-Square	0.32971

Linear fitting parameters of Hg(II)

Equation	y = a + b*x
Plot	Hg(II)
Intercept	-0.20047 ± 0.19168
Slope	-0.003 ± 0.00198
Residual Sum of Squares	0.81444
Pearson's r	-0.49675
R-Square (COD)	0.24677
Adj. R-Square	0.13916

Figure 43: Linear fitting of pseudo-first-order biosorption kinetic model for As(III) and Hg(II) removal from monocomponent sorption systems

4.6.3 Biosorption Thermodynamics Studies

Temperature is a key variable in heavy metal ions sequestration from aqueous systems that is linked to the thermodynamics of the biosorption mechanism. Mostly, there are two main types, endothermal and exothermal biosorption processes that are always examined due to a rise or fall in the temperature during biosorption (Aeisyah *et al.*, 2014). The thermodynamic variables that ought to be studied before the spontaneity of the system can be inferred include standard Gibbs free energy (ΔG^0), entropy (ΔS^0), and enthalpy changes (ΔH^0).

In Fig. 44, the higher R^2 of 0.9919 and 0.9741 and low RSS values attained during the removal of As(III) and Hg(II) indicate a good fit of the thermodynamic sorption data. The thermodynamic parameters (ΔG^0, ΔH^0 and ΔS^0) that explained the feasibility, spontaneity, and nature of adsorbate-biosorbent interactions were determined as displayed in Table 35. The values of the thermodynamic parameters in Table 35 show that the ΔG^0 values obtained during the removal of As(III) first increased from -8.423 to -1.674 kJ/mol at the temperature range of 283-308 *K* and later decreased from -1.674 to -11.207 kJ/mol at 308-358 K. For Hg(II), the ΔG^0 values initially augmented from -7.061 to -1.058 kJ/mol at 283-318 *K* and then declined from -1.058 to -9.214 kJ/mol at 318-358 K. It was observed that negative values of ΔG^0 were obtained from all the temperature ranges of 10-85 ℃ (283-358 K) indicating the spontaneous nature of As(III) and Hg(II) ions removal from non-competitive biosorption systems by the

biosorbent (Mondal *et al.*, 2017).

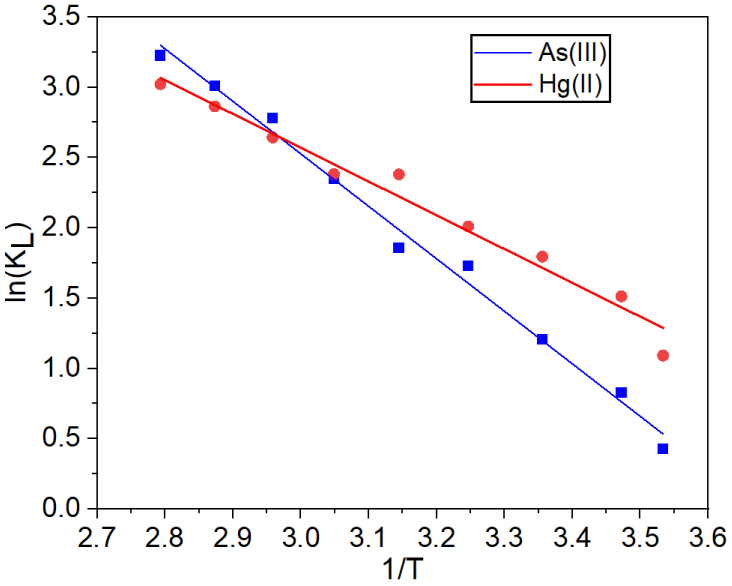

Linear fitting parameters of As(III)

Equation	y = a + b*x
Plot	As(III)
Intercept	13.72707 ± 0.40363
Slope	-3.7337 ± 0.1274
Residual Sum of Squares	0.06277
Pearson's r	-0.99595
R-Square (COD)	0.99192
Adj. R-Square	0.99076

Linear fitting parameters of Hg(II)

Equation	y = a + b*x
Plot	Hg(II)
Intercept	9.77778 ± 0.4691
Slope	-2.98976 ± 0.4691
Residual Sum of Squares	0.08479
Pearson's r	-0.98697
R-Square (COD)	0.97411
Adj. R-Square	0.97041

Figure 44: Linear fitting of thermodynamic parameters for As(III) and Hg(II) removal from monocomponent sorption systems

The ΔH^0 values computed for the adsorptive removal of As(III) and Hg(II) ions from the non-competitive biosorption systems were found to be +31.042 and +24.857 kJ/mol, respectively, and the positive values of ΔH^0indicate endothermic biosorption (Syafiqah & Yussof, 2018). Therefore, the individual detoxification of As(III) and Hg(II) ions from the mono-metal systems increased with increasing reaction temperature (Zeng *et al.*, 2020). In Table 35, the fact that the values of ΔH^0 obtained during the removal of As(III) and Hg(II) ions were found to be in the range 20.90-418.40 $kJmol^{-1}$ the mechanism of biosorption was due to chemisorption (Ma *et al.*, 2019; Sun *et al.*, 2012).

Besides, positive ΔS^0 values of +11.413 and +8.129 kJ/mol.K were determined for the sequestration of As(III) and Hg(II) ions, respectively from the mono-metal systems. The positive values of the ΔS^0 is suggestive of the upsurge in randomness at the adsorbate-biosorbent interface during the adsorptive removal of As(III) and Hg(II) ions (Yeo *et al.*, 2021). Therefore, the positive values of ΔS^0 can be an indication that the biosorbent had a high affinity towards As(III) and Hg(II) ions in the non-competitive aqueous solutions.

Table 35: Thermodynamic parameters for removal of As(III) and Hg(II) ions from non-competitive biosorption systems

Temperature (K)	As(III)					Hg(II)				
	ΔG^0 (kJmol^{-1})	ΔH^0 (kJmol^{-1})	ΔS^0 (kJmol^{-1}K^{-1})	R^2	SSE	ΔG^0 (kJmol^{-1})	ΔH^0 (kJmol^{-1})	ΔS^0 (kJmol^{-1}K^{-1})	R^2	SSE
283.000	-8.423	+31.042	+11.413	0.9919	1.346×10^{-4}	-7.061	+19.976	+8.129	0.9741	1.369×10^{-3}
288.000	-7.291					-5.930				
298.000	-5.669					-4.521				
308.000	-1.674					-3.893				
318.000	-4.301					-1.058				
328.000	-6.817					-6.063				
338.000	-8.994					-7.059				
348.000	-10.107					-7.723				
358.000	-11.207					-9.214				

4.7 Application of the Biosorbent in Treating Real Industrial Wastewater

Real wastewater was sampled from the A to Z textile industry in the Arusha region of Tanzania to test the applicability of the HGAC in the simultaneous multicomponent adsorption of different heavy metals. The wastewater collected was pretreated based on the protocols for water and wastewater analysis (Gilcreas, 1967). The water samples collected in the plastic containers were acidified using HNO_3 to a pH < 2 and then transported to the laboratory at a temperature of 4 ℃ within 4 h and then stored until analyses. Subsequently, the wastewater samples were characterized using CVAAS following the standard methods documented in APHA (1989) to determine the number of pollutants and the concentration of each present in the wastewater before subjecting it to a batch adsorption test. The physicochemical properties of wastewater collected from the textile industry are summarised in Table 36. In Table 36, the total heavy metal ions detected in the textile industrial wastewater include the following: arsenic, mercury, chromium, lead, iron, and cadmium, which were all found to be beyond the maximum allowable limits as recommended by the World Health Organization (Joseph *et al.*, 2019).

Table 36: Physiochemical characterization of textile industrial wastewater

Physiochemical parameter	Parameter value
pH	6.95
Conductivity (ms/cm)	11.33
Total hardness as $CaCO_3$ (mg/L)	346
Total dissolved solids (mg/L)	494
Total suspended solids (mg/L)	234
Turbidity (FTU)	76
Chemical oxygen demand [COD (mg O_2/L)]	540
Biochemical oxygen demand [BOD (mg O_2/L)]	268
Chlorides (mg Cl^-/L)	85
Sulfates (mg SO_4^{2-}/L)	247
Chromium (Cr) [mg/L]	2.5423
Cadmium (Cd) [mg/L]	1.3576
Lead (Pb) [mg/L]	1.8272
Mercury (Hg) [mg/L]	0.2528
Arsenic (As) [mg/L]	0.9615
Iron (Fe) [mg/L]	0.2867

4.8 Batch Biosorption Experiments

In the batch studies, the effect of several independent biosorption factors including agitation speed, contact time, pH of the solution, biosorbent particle size, biosorbent dosage, initial heavy metal ion concentration, and temperature influencing the removal efficiency and biosorption capacity of As, Hg, Pb, Cd, and Cr species in real industrial wastewater was investigated.

4.8.1 Effect of Agitation Speed

Figure 45 shows the influence of agitation speed on the decontamination of As, Hg, Pb, Cd, and Cr species from real industrial wastewater (Appendix 17). It is observed that as the agitation speed increases the removal efficiency and biosorption capacity upsurges as well. Initially, at low agitation speed the rate of removal of heavy metals is very small because, at low speed, the biosorbent settles at the bottom. At an agitation speed of 250 rpm, maximum removal efficiencies of 99.73, 98.85, 98.33, 98.13, and 97.95% with corresponding uptake capacities of 19.18, 5.05, 35.93, 26.64, and 49.81 mg/g for As, Hg, Pb, Cd, and Cr ions, respectively were attained by the biosorbent.

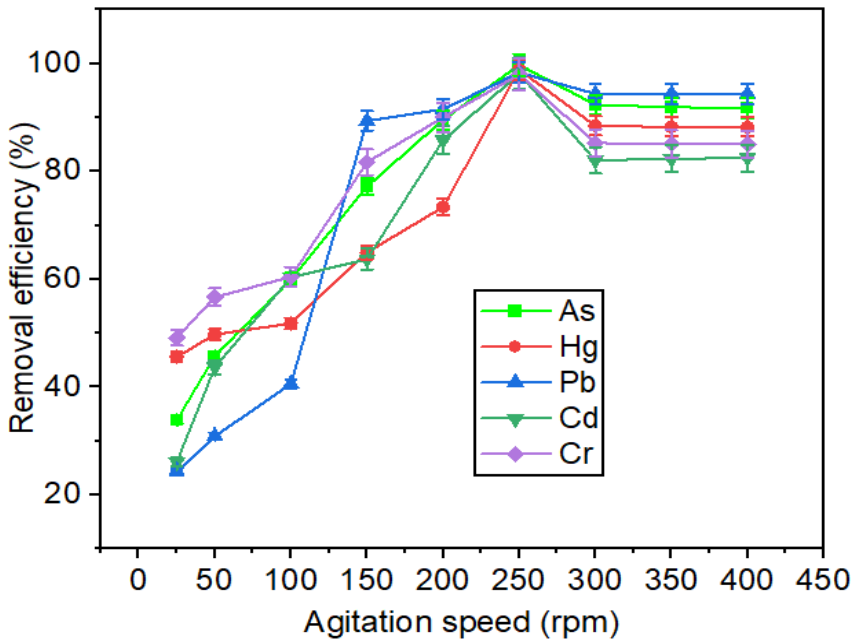

Figure 45: Effect of agitation speed on the removal efficiency of As, Hg, Pb, Cd, and Cr ions from the real textile wastewater

Jayakumar *et al.* (2019) also observed that at a high speed, Zn removal efficiency increases, because the diffusion of Zn ions onto the biosorbent is very less at lower agitation speeds.

Similarly, Jalees *et al.* (2019) found that increasing agitation speed prevents the settling of biosorbent leading to proper mixing between the heavy metal ions (Pb, Cd, Ni, Cr) and biosorbent and enhancing removal efficiency and uptake capacity of metal ions due to effective binding onto active biosorbent sites. In another study, a higher shaking rate promoted the transfer of Cr ions from the total solution to the surface of the adsorbent and shortened the equilibrium time for adsorption (Singh *et al.*, 2021).

4.8.2 Effect of Contact Time

The percentage removal and uptake capacity of As, Hg, Pb, Cd, and Cr ions by the HGAC from industrial wastewater was observed to increase with increasing contact time during the initial stage and later plateaued as presented in Fig. 46 (Appendix 18).

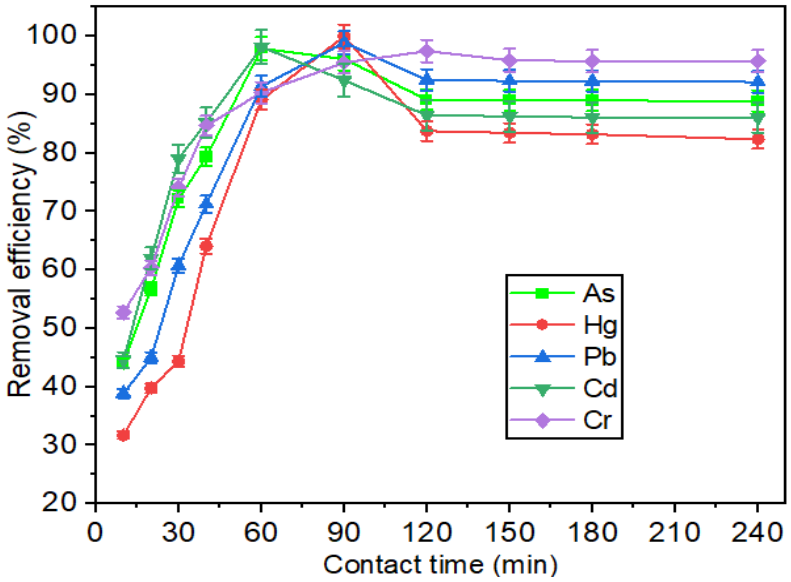

Figure 46: Effect of contact time on the removal efficiency of As, Hg, Pb, Cd, and Cr ions from the real textile wastewater

The fast uptake of As, Hg, Pb, Cd, and Cr ions by the HGAC from the industrial wastewater during the initial stages of the sorption process was attributable to the existence and accessibility of active binding sites on the biosorbent surface and the initial high amount of As, Hg, Pb, Cd, and Cr ions present in the sorption media (Adio *et al.*, 2019). However, as contact time increased, the percentage removal and uptake capacity decreased because the metal ions covered the active binding sites of the biosorbent, causing repulsion as agitation time increased (Igberase *et al.*, 2017). At an optimum contact time of 60 min, maximum removal efficiencies of 97.94 and 98.16% and biosorption capacities of 18.83 and 26.65 mg/g were achieved for As and Cd, respectively. Whilst, at an optimum contact time of 90 min, maximum removal

efficiencies of 99.96 and 98.92% and biosorption capacities of 5.05 and 36.15 mg/g were achieved for Hg and Pb, respectively. For Cr, the maximum removal efficiency of 97.48% and biosorption capacity of 49.56 mg/g were attained at an optimum contact time of 120 min. Similarly, an iron oxide/nano-porous carbon magnetic composite was applied by Joshi *et al.* (2019) for the detoxification of As ions from wastewater, and equilibrium was reached at 60 min. On the contrary, Memon *et al.* (2021) investigated the decontamination of As species from wastewater using chemically activated hematite (Fe_2O_3) iron ore, and the optimum percentage removal was achieved at an equilibrium time of 120 min. In a study conducted by Sheikh *et al.* (2021), using *Allium cepa* seeds as a novel biosorbent for the adsorptive removal of heavy metal ions, the equilibrium biosorption time was 90 min for Cd, Pb, and Cu, and 120 min for Cr and Zn, respectively.

4.8.3 Effect of pH of the Solution

The sequestration of As, Hg, Pb, Cd, and Cr ions from industrial wastewater at different solution pH values is shown in Fig. 47 (Appendix 19). In Fig. 47, it was found that the removal rate and sorption capacity of As, Hg, Pb, Cd, and Cr ions by the HGAC from the wastewater increased with decreasing pH of the aqueous solution. The percentage removal and uptake capacity of the As, Hg, Pb, Cd, and Cr ions ions by the biosorbent increased during the first stage because there is no precipitation of the metal ions but at higher pH values, the metal ions will precipitate in the form of hydroxyl ions, which will compete for the binding sites on the biosorbent surface. Therefore, due to the high competition between the metal and hydroxyl ions in the industrial wastewater, the removal rate and sorption capacity of As, Hg, Pb, Cd, and Cr ions by the HGAC declines at higher pH values as displayed in Fig. 47, respectively.

The pH of the point of zero charges of the biosorbent was determined to be 3.2, and it was discovered that when the pH of the solution rises, the positive surface charge reduces, leading to a decrease in the electrostatic repulsion between the metal ions and the surface biosorbent and higher removal efficiency (Giraldo *et al.*, 2020). At about solution pH of 4, the equilibrium biosorption of As and Cr ions from the wastewater was achieved with a maximum removal efficiency of 96.77 and 98.38% and biosorption capacity of 18.61 and 50.02 mg/g, respectively. While at optimum solution pH of 6, the maximum removal efficiency of 99.80 and 98.63% and biosorption capacity of 5.05 and 36.04 mg/g for Hg and Pb ions, respectively were achieved, the maximum Cd removal rate of 99.46% and uptake capacity of 27.01 mg/g was accomplished at pH of 5.

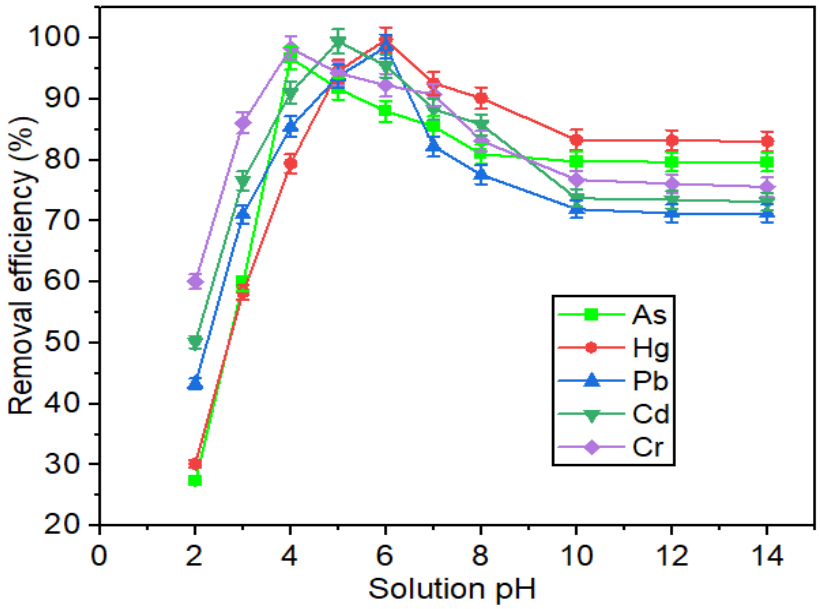

Figure 47: Effect of pH of the solution on the removal efficiency of As, Hg, Pb, Cd, and Cr ions from the real textile wastewater

The optimum pH of 6 obtained in this present study for the detoxification of Hg and Pb ions from wastewater is consistent with the pH value determined in the removal of As and Cd ions from aqueous systems by a novel calcium-based magnetic biochar (Wu *et al.*, 2018). Similarly, Bhatti (2021) studied the removal of As species from wastewater using iron ore adsorbent, and a maximum removal rate was attained at pH 6.

4.8.4 Effect of Biosorbent Particle Size

The impact of biosorbent particle size on the competitive depollution of As, Hg, Pb, Cd, and Cr species from industrial wastewater was investigated at different biosorbent particle sizes ranging from 63-450 µm and the experimental results are displayed in Fig. 48 (Appendix 20). The results demonstrated that the percentage removal and uptake rate of As, Hg, Pb, Cd, and Cr ions by the HGAC from the wastewater decreased with increasing the biosorbent particle size of the HGAC as presented in Fig. 48. However, when the biosorbent particle size decreases, the surface area increases, as well as the number of active biosorption sites (Flores-Trujillo *et al.*, 2021). Maximum removal efficiencies of 99.84, 98.34, 97.91, 99.51, and 97.54% and uptake capacities of 19.20, 4.97, 35.78, 27.02, and 49.60 mg/g were accomplished for As, Hg, Pb, Cd, and Cr at a biosorbent particle size of 63 µm, respectively.

Similarly, Oguz (2022) explored the decontamination of Cu(II) from wastewater and it was observed that removal efficiency and biosorption capacity increased with the reduction of

biosorbent particle size. Likewise, Nagy *et al.* (2023) investigated different particle sizes of biosorbents prepared from cotton stalks and date palm stone residues on the removal of Cd(II), Pb(II), and Zn(II) ions from wastewater. It is found that the sequestration of Cd(II), Pb(II), and Zn(II) ions from the aqueous solutions increased with decreasing biosorbent particle size. Furthermore, Rahaman *et al.* (2021) observed an increase in the removal efficiency and uptake capacity for Cr, Cd, and Pb ions from wastewater as biosorbent particle size decreased.

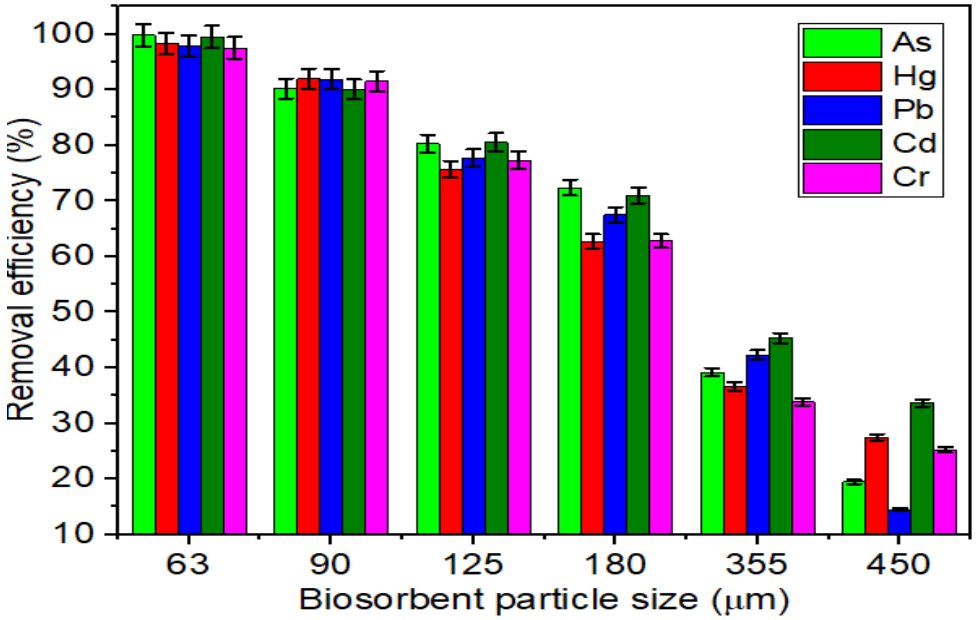

Figure 48: Effect of biosorbent particle size on the removal efficiency of As, Hg, Pb, Cd, and Cr ions from the real textile wastewater

4.8.5 Effect of Biosorbent Dosage

The influence of the biosorbent dosage on the detoxification of As, Hg, Pb, Cd, and Cr ions competitively from the industrial wastewater was conducted at different loads of the HGAC in the range of 0.5-5 g/L. In Fig. 49, it is observed that upon increasing the biosorbent dosage, As, Hg, Pb, Cd, and Cr ions removal rate increased while the uptake capacity decreased (Appendix 21). It has been found that when the biosorbent load is augmented, there is a corresponding upsurge in the available active sites and the biosorbent surface area leading to an increase in the removal efficiency of As, Hg, Pb, Cd, and Cr ions (Hiew *et al.*, 2021). The optimum decontamination efficiencies of 98.07, 99.68, and 97.06% with corresponding biosorption capacities of 6.29, 1.68, and 11.82 mg/g were attained at 1.5 g/L for As, Hg, and Pb, respectively. Whilst, optimum removal efficiencies of 98.85 and 99.74% with uptake capacities of 6.71 and 12.68 mg/g were attained at 2 g/L for Cd and Cr, respectively.

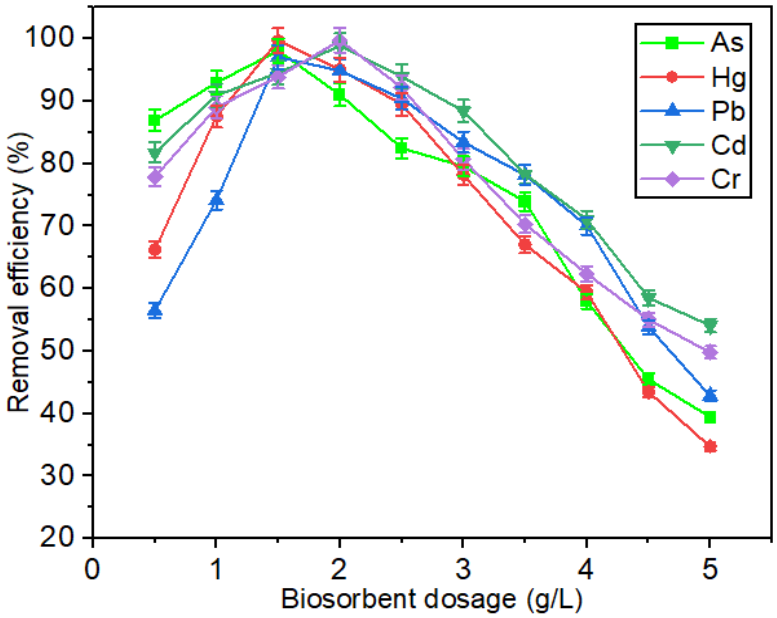

Figure 49: Effect of biosorbent dosage on the removal efficiency of As, Hg, Pb, Cd, and Cr ions from the real textile wastewater

It was found that the removal efficiencies of As, Hg, Pb, Cd, and Cr ions from the wastewater attained by biosorbent decreased at higher dosages. This is because, at excessive biosorbent dosages, particle agglomeration is likely to occur leading to the availability of fewer As, Hg, Pb, Cd, and Cr ions to be adsorbed on the active sites of the biosorbent. As a result, the uptake rate is reduced by the non-occupancy of the biosorbent active binding sites by the As, Hg, Pb, Cd, and Cr ions (Peng *et al.*, 2018). In Fig. 49, maximum As, Hg, Pb, Cd, and Cr ions uptake capacities of 16.71, 3.35, 20.64, 22.20, and 39.60 mg/g were realized at the lowest biosorbent dosage of 0.50 g/L.

Maity *et al.* (2021) investigated the adsorptive removal of As, Cr, and Cd ions using biosorbent produced from *Colocasia esculenta* stem and it was observed that the percentage removal of As, Cr, and Cd ions increased at higher biosorbent loads. Similarly, Gerard *et al.* (2016) investigated the impact of adsorbent dosage on As ions detoxification from wastewater using chitosan-coated iron-oxide nanocomposites, and the optimum adsorbent dosage was found to be 2.00 g/L. Similarly, Nguyen *et al.* (2019) used sludge from an iron-ore processing area as an adsorbent to remove As, Mn, Zn, Cd, and Pb ions from competitive aqueous solutions, and 20.00 g/L was observed to be the best adsorbent dosage for the maximum adsorptive removal of all the five heavy metals.

4.8.6 Effect of Solution Temperature

The influence of solution temperature on the confiscation of As, Hg, Pb, Cd, and Cr ions from the industrial wastewater by the biosorbent was studied within the temperature range of 20-65 ℃ as shown in Fig. 50, respectively (Appendix 22). The decontamination efficiency and uptake capacity of As, Hg, Pb, Cd, and Cr ions from the wastewater were augmented with rising temperature. With the rise of temperature, the biosorption process increases, which can be due to an increase of strong interaction forces between biosorbent and As, Hg, Pb, Cd, and Cr ions (Saeed *et al.*, 2020). Therefore, the removal of As, Hg, Pb, Cd, and Cr ions by the biosorbent is an endothermic process, which also implies the mechanism of As, Hg, Pb, Cd, and Cr ions removal from the wastewater is due to chemical biosorption. The maximum removal efficiencies of 98.98, 98.22, and 97.92% and biosorption capacities of 6.34, 1.66, and 6.00 mg/g were attained at 40 ℃ for As, Hg, and Cd, respectively.

Whilst, optimum removal efficiencies of 99.70 and 99.57% with uptake capacities of 12.14 and 12.66 mg/g were attained at 45 ℃ for Pb and Cr, respectively. The upsurge of temperature in the sorption system increases the As, Hg, Pb, Cd, and Cr ions uptake rate due to the high diffusion rate of As, Hg, Pb, Cd, and Cr ions through the biosorbent and the subsequent biosorption on the active surface of the biosorbent (Mohubedu *et al.*, 2019).

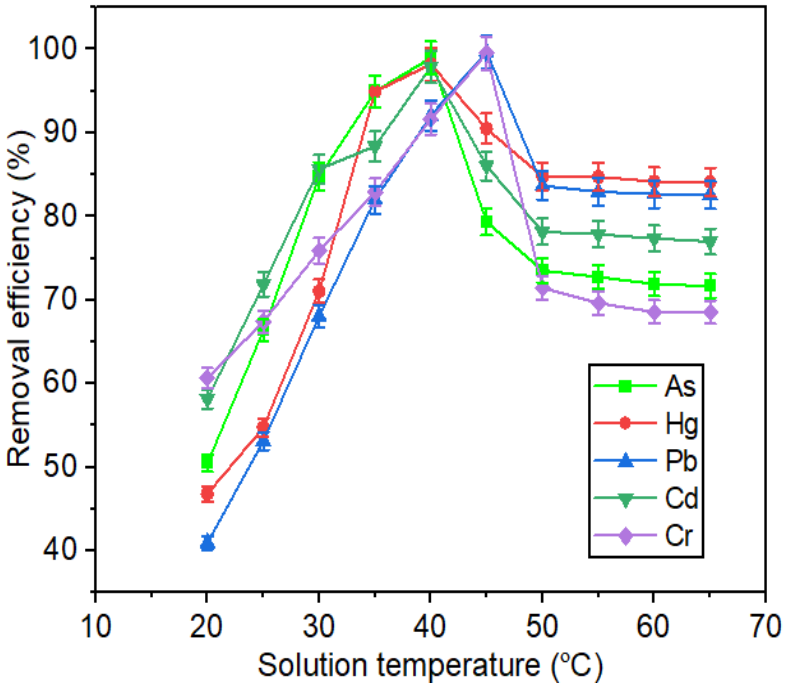

Figure 50: Effect of solution temperature on the removal efficiency of As, Hg, Pb, Cd, and Cr ions from the real textile wastewater

However, it was observed that at higher levels of solution temperature, both the removal and uptake rates decreased drastically and this might be because of the deterioration of the surface chemistry of the adsorbent through excessive heating. Gaur *et al.* (2018) observed maximum biosorption of As and Pb ions using soya bean biosorbent at a temperature of 37 ℃ and the removal rate was found to decline rapidly with further increase in temperature above 37 ℃. Also, Mandal *et al.* (2013) studied the effect of temperature on As species removal from industrial wastewater using zirconium polyacrylamide hybrid material and the study showed that the highest As species removal efficiency was observed at 50 ℃. On the contrary, Adelaja *et al.* (2019) observed that a temperature above 40 °C, leads to a decrease in Hg ions uptake which was due to the increase in the retarding forces acting on the diffusing ions.

4.8.7 Desorption and Biosorbent Regeneration Studies

The recycling of the adsorbent through the desorption process is the most important aspect from an economic point of view. Desorption is an indispensable part of the adsorption process and the aim is to estimate the reuse of any adsorbent industrially, for ecological interests and sustainable development (Bessaha *et al.*, 2019). For large-scale industrial applications, regeneration and reusability are vital biosorbent characteristics, since the ability to reuse a biosorbent is a crucial parameter for the decontamination process from the economic point of view. The adsorption-desorption cycles of the As, Hg, Pb, Cd, and Cr ions from the industrial wastewater were conducted on consecutive times using 0.1 M of H_3PO_4, H_2SO_4, HNO_3, HCl, EDTA, NaOH, NaCl, KOH, $CaCl_2$, and H_2O solutions, respectively, as desorption eluents for the retrieval of As, Hg, Pb, Cd, and Cr ions from the biosorbent surface to evaluate the biosorbent's recyclability and reusability is shown in Fig. 51 (Appendix 23).

Among all the desorption eluents tested, the study found that 0.1 M HCl acid solution was the best desorption eluents and could retrieve about 98.17, 99.56, 98.71, 97.14, and 99.54% of As, Hg, Pb, Cd, and Cr ions adsorbed onto the biosorbent surface, respectively. Therefore, 0.1 M HCl solution was selected for the regeneration of the spent biosorbent for its reusability in successive biosorption-desorption cycles. Similarly, a desorption test was carried out by Díaz *et al.* (2022) for the recovery of Ni(II) and Co(II) ions using several eluents and it was observed that 0.1 M HCl was the best desorption agent with recovery efficiencies of 85 and 70%, respectively.

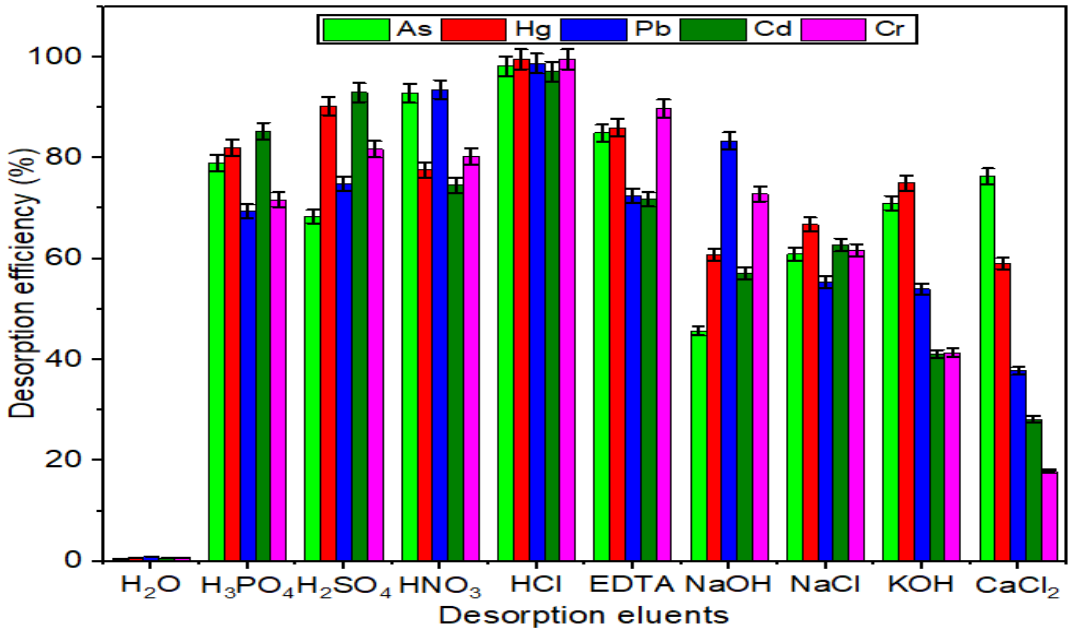

Figure 51: Desorption eluents for adsorbed As, Hg, Pb, Cd, and Cr ions recovery on spent biosorbent surface from the textile wastewater

The regeneration and reusability studies revealed that the removal efficiency of the biosorbent decreases with each subsequent regeneration cycle as shown in Fig. 52 (Appendix 24). The removal efficiencies decreased from 98.22-53.98%, 99.84-51.30%, 97.35-57.83%, 96.73-57.83%, and 98.07-53.27% for As, Hg, Pb, Cd, and Cr ions, respectively when the regeneration cycles increased from one to ten.

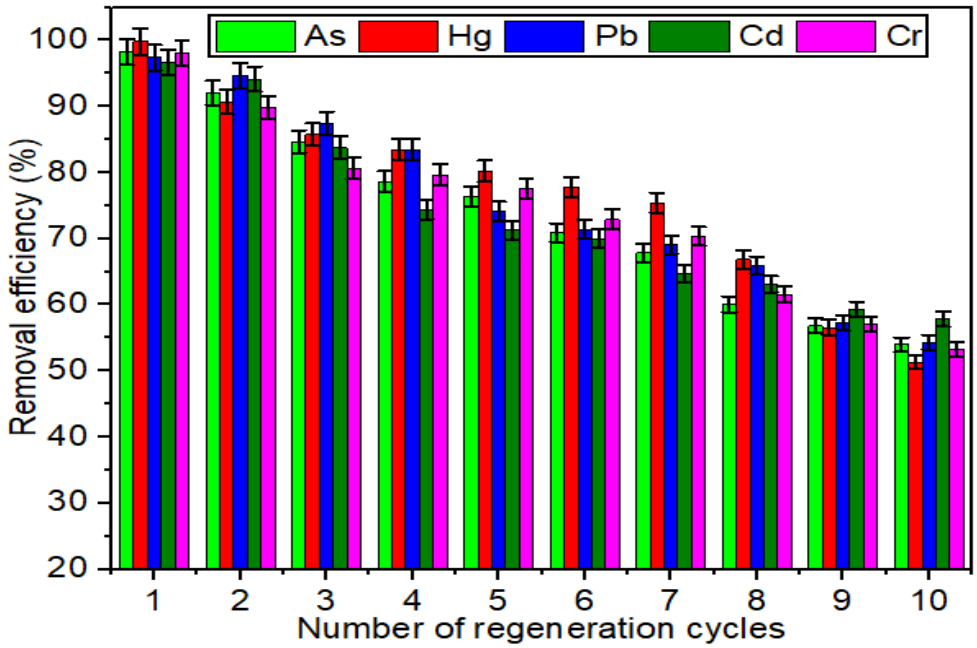

Figure 52: Regeneration and reusability of the spent biosorbent in the removal of As, Hg, Pb, Cd, and Cr ions from the textile wastewater

The biosorption-desorption of As, Hg, Pb, Cd, and Cr ions on the metal ions-loaded biosorbent surface was found to be highest at the first regeneration cycle with recovery efficiencies of 98.22, 99.84, 97.35, 96.73, and 98.07%, respectively. It may be concluded that 0.1 M HCl has the potential to desorb the As, Hg, Pb, Cd, and Cr ions due to H^+ biosorption and pH shift, however, in turn, this also changes the chemistry of the surface functional groups leading to reduction in the capacity of the biosorbent in next biosorption-desorption cycle (Gupta *et al.*, 2022). The results of the spent biosorbent regeneration suggest that the biosorbent is capable of being used effectively, recycled, and reused severally and even up to the ten cycle implying the economic potential and the sustainability of the biosorbent in environmental pollutants remediation, especially heavy metals.

4.9 Experimental Design and Process Optimization Using Central Composite Design

4.9.1 Experimental Design and Modeling of Heavy Metal Removal

To determine the interactive effects, model, and optimize the independent factors for As and Hg ions removal from the industrial wastewater in the coexistence of other three heavy metals, 50 batch experiments with varying combinations of the factors were conducted according to the central composite design. The experimental design matrix and the responses for As and Hg ions biosorption are presented in Table 37. The results displayed in Table 37 indicate that As species maximum (X1)-removal efficiency of 99.36% was attained at experimental run 6 with operating conditions of contact time $= 30$ min, solution pH $=$ 7, biosorbent dosage $= 0.5$ g/L, agitation speed $= 300$ rpm, and tenperature$= 30$ ℃. Whilst Hg maximum (X2)-removal efficiency of 99.98% was attained at experimental run 38 with operating conditions of contact time $= 75$ min, solution pH $= 5$, biosorbent dosage $=$ 2.37 g/L, agitation speed $= 200$ rpm, and tenperature$= 37.5$ ℃.

Table 37: Design matrix of As and Hg biosorption factors in coded form with corresponding response variables

Run	Space Type	Biosorption influencing Factors					Responses	
		A: Contact time (min)	B: Solution pH	C: Dosage (g/L)	D: Agitation speed (rpm)	E: Temperature (℃)	X1: Removal efficiency (%)	X2: Removal efficiency (%)
1	Axial	0.000	1.495	0.000	0.000	0.000	95.54	97.80
2	Factorial	-1.000	-1.000	-1.000	1.000	1.000	93.19	91.84
3	Factorial	-1.000	1.000	-1.000	-1.000	1.000	95.62	97.96
4	Center	0.000	0.000	0.000	0.000	0.000	77.43	94.85
5	Center	0.000	0.000	0.000	0.000	0.000	76.81	97.06
6	Factorial	-1.000	1.000	-1.000	1.000	-1.000	99.36	90.11
7	Axial	0.000	0.000	-1.495	0.000	0.000	96.03	98.20
8	Center	0.000	0.000	0.000	0.000	0.000	76.72	96.98
9	Factorial	-1.000	1.000	-1.000	1.000	1.000	92.34	88.86
10	Center	0.000	0.000	0.000	0.000	0.000	77.51	95.84
11	Factorial	-1.000	1.000	1.000	-1.000	1.000	91.45	91.72
12	Center	0.000	0.000	0.000	0.000	0.000	77.29	95.24
13	Factorial	-1.000	1.000	1.000	1.000	-1.000	94.72	92.86
14	Axial	0.000	0.000	0.000	0.000	1.495	79.76	89.95
15	Factorial	-1.000	-1.000	1.000	1.000	1.000	88.62	95.88
16	Axial	0.000	0.000	0.000	0.000	-1.495	82.95	90.36
17	Factorial	1.000	-1.000	1.000	-1.000	-1.000	92.75	96.25
18	Factorial	1.000	1.000	1.000	-1.000	-1.000	94.98	98.95
19	Factorial	1.000	1.000	-1.000	-1.000	-1.000	92.71	97.46
20	Factorial	1.000	1.000	-1.000	-1.000	1.000	91.89	98.76
21	Factorial	1.000	-1.000	-1.000	1.000	-1.000	93.65	81.68
22	Factorial	-1.000	-1.000	-1.000	-1.000	-1.000	97.84	94.42
23	Axial	0.000	0.000	0.000	1.495	0.000	73.73	83.76
24	Factorial	-1.000	-1.000	1.000	-1.000	-1.000	90.83	97.53
25	Axial	-1.495	0.000	0.000	0.000	0.000	78.34	98.24
26	Factorial	-1.000	1.000	1.000	-1.000	-1.000	93.28	95.48
27	Factorial	1.000	1.000	-1.000	1.000	1.000	89.04	90.43
28	Axial	0.000	0.000	0.000	-1.495	0.000	73.27	93.12
29	Center	0.000	0.000	0.000	0.000	0.000	77.81	95.76
30	Factorial	1.000	1.000	-1.000	1.000	-1.000	93.17	88.77

Table 37 (continued)

Run	Space Type	Biosorption influencing Factors					Responses	
		A: Contact time (min)	B: Solution pH	C: Dosage (g/L)	D: Agitation speed (rpm)	E: Temperature (℃)	X1: Removal efficiency (%)	X2: Removal efficiency (%)
31	Factorial	1.000	1.000	1.000	1.000	-1.000	96.64	94.12
32	Factorial	-1.000	-1.000	1.000	-1.000	1.000	91.00	98.43
33	Factorial	1.000	1.000	1.000	-1.000	1.000	95.49	97.15
34	Factorial	-1.000	-1.000	-1.000	-1.000	1.000	96.37	98.82
35	Axial	1.495	0.000	0.000	0.000	0.000	77.77	96.47
36	Factorial	1.000	-1.000	1.000	1.000	1.000	94.76	93.27
37	Factorial	-1.000	-1.000	1.000	1.000	-1.000	93.31	95.89
38	Axial	0.000	0.000	1.495	0.000	0.000	95.75	99.98
39	Center	0.000	0.000	0.000	0.000	0.000	77.74	95.53
40	Axial	0.000	-1.495	0.000	0.000	0.000	95.03	97.64
41	Factorial	-1.000	1.000	-1.000	-1.000	-1.000	98.25	96.56
42	Factorial	1.000	1.000	1.000	1.000	1.000	95.23	92.55
43	Factorial	-1.000	-1.000	-1.000	1.000	-1.000	98.22	87.34
44	Factorial	1.000	-1.000	1.000	1.000	-1.000	96.51	93.20
45	Factorial	1.000	-1.000	-1.000	-1.000	1.000	92.66	94.64
46	Factorial	1.000	-1.000	1.000	-1.000	1.000	95.02	98.00
47	Factorial	1.000	-1.000	-1.000	-1.000	-1.000	92.08	90.63
48	Center	0.000	0.000	0.000	0.000	0.000	77.59	95.50
49	Factorial	1.000	-1.000	-1.000	1.000	1.000	90.73	85.42
50	Factorial	-1.000	1.000	1.000	1.000	1.000	89.08	88.65

4.9.2 Selection of Models and Responses Prediction

The quadratic models were preferred and selected by the Design Expert to investigate the interactive behavior among the selected independent factors as a function of the removal efficiency and biosorption capacity as summarized in Tables 38 and 39, respectively. The cubic model was shown to be aliased and could not be applied for subsequent modeling of any experimental data as reported in Tables 38 and 39, respectively (Khelifi *et al.*, 2022).

Table 38 shows that the quadratic model selected for As species (X1)-removal efficiency has high correlation coefficients of 0.9984, 0.9974, and 0.9952 for R^2, adjusted $R^{2,}$ and predicted

R^2, respectively. Whilst for the (X2)-removal efficiency of Hg by the biosorbent, the selected quadratic model has high R^2, adjusted $R^{2,}$ and predicted R^2 of 0.9834, 0.9719, and 0.9506, respectively, as summarized in Table 39. It was found that the discrepancy between the adjusted and predicted correlation coefficients of the developed quadratic models for the removal efficiency attained for the decontamination of As and Hg ions from the wastewater was less than 0.20. This implies that the developed quadratic models were accurate and adequate and could be used in the prediction of the responses (Shafaghat & Ghaemi, 2021). More so, the adequate precision, which determines the signal-to-noise ratio obtained from the quadratic models developed for all the responses was greater than 4.00 as summarized in Tables 38 and 39, respectively. This further suggests that the selected quadratic models are suitable and desirable and could be applied effectively in design space navigation (Sagharloo *et al.*, 2021).

Table 38: Quadratic model fitness summary for As removal efficiency

Source	Sequential p-value	Lack of Fit P-value	R^2	Adjusted R^2	Predicted R^2	Adequate precision	Remark
Linear	0.9773	< 0.0001	-	0.0943	0.1695	-	
2FI	0.9918	< 0.0001	-	0.3280	0.5232	-	
Quadratic	< 0.0001	0.5413	0.9984	0.9974	0.9952	97.37	Suggested
Cubic	0.3276	0.6406	-	0.9977	0.9881	-	Aliased

Table 39: Quadratic model fitness summary for Hg removal efficiency

Source	Sequential p-value	Lack of Fit P-value	R^2	Adjusted R^2	Predicted R^2	Adequate precision	Remark
Linear	< 0.0001	0.0002	-	0.3849	0.2858	-	
2FI	0.0045	0.0007	-	0.5951	0.6279	-	
Quadratic	< 0.0001	0.7383	0.9834	0.9719	0.9506	43.10	Suggested
Cubic	0.4869	0.7667	-	0.9722	0.8454	-	Aliased

4.9.3 ANOVA for responses quadratic models

The model significance as well as the interactive and quadratic effects of the independent factors on the removal efficiency of As and Hg species from the competitive aqueous solutions

were investigated through the analysis of variance (ANOVA) as summarized in Tables 40 and 41, respectively. The acceptability, suitability, and significance of a model are established by examining the model F-value, p-value, level of precision, and the discrepancy between the predicted and adjusted R-squared (Sun *et al.*, 2019).

According to the ANOVA results displayed in Tables 40 and 41, respectively for the quadratic models, a factor having a p-value less than 0.05 indicates the significance of that factor at a 95% confidence level (Abedpour *et al.*, 2020). Tables 40 and 41 show that the fitted quadratic models to the responses are significant with p-values smaller than 0.05 ($p < 0.001$). The level of significance and the interaction of the biosorption factors during As and Hg ions removal from the competitive biosorption system are dependent on the F-value. The higher the F-value, the lower the p-value and the more significant the model term (Sabah *et al.*, 2018). The model terms with p-values smaller than ($p < 0.05$) are indicative that the developed quadratic models are highly significant and could accurately be used for the prediction of the responses (Adetokun *et al.*, 2019).

Table 40 shows that all the model terms for As removal efficiency are significant with p-values less than 0.05 and insignificant model terms include D, AB, and BD. Also, in Table 41, all the model terms for Hg removal efficiency are significant with p-values less than 0.05 and insignificant model terms include B, AE, BD, and DE. It was also found that the Lack of Fit test for the As and Hg ions removal efficiencies have p-values bigger than 0.05, suggesting the Lack of fit of the models is not significant (Alimohammadi *et al.*, 2017; Dehghani *et al.*, 2017). Hence, the quadratic models were valid for the prediction of the responses required for the decontamination of As and Hg ions from industrial wastewater.

Table 40: ANOVA for response surface quadratic model for As removal efficiency

Source	Sum of Squares	df	Mean Square	F-value	p-value	Remark
Model	3057.88	20	152.89	934.02	< 0.0001	significant
A-Contact time	1.35	1	1.35	8.26	0.0075	significant
B-Solution pH	1.15	1	1.15	7.02	0.0129	significant
C-Dosage	5.27	1	5.27	32.22	< 0.0001	significant
D-Agitation speed	0.24	1	0.24	1.47	0.2352	not significant
E-Temperature	45.15	1	45.15	275.82	< 0.0001	significant
AB	0.43	1	0.43	2.66	0.1140	not significant
AC	129.40	1	129.40	790.52	< 0.0001	significant
AD	1.98	1	1.98	12.07	0.0016	significant
AE	13.09	1	13.09	79.99	< 0.0001	significant
BC	3.40	1	3.40	20.77	< 0.0001	significant
BD	0.64	1	0.64	3.92	0.0573	not significant
BE	3.21	1	3.21	19.59	0.0001	significant
CD	4.34	1	4.34	26.54	< 0.0001	significant
CE	3.83	1	3.83	23.39	< 0.0001	significant
DE	26.96	1	26.96	164.67	< 0.0001	significant
A^2	0.73	1	0.73	4.46	0.0435	significant
B^2	740.95	1	740.95	4526.44	< 0.0001	significant
C^2	792.21	1	792.21	4839.57	< 0.0001	significant
D^2	37.41	1	37.41	228.52	< 0.0001	significant
E^2	34.86	1	34.86	212.94	< 0.0001	significant
Residual	4.75	29	0.1637	-	-	-
Lack of Fit	3.60	22	0.1638	1.00	0.5413	not significant
Pure Error	1.14	7	0.1634	-	-	-
Cor Total	3062.63	49	-	-	-	-

Table 41: ANOVA for response surface quadratic model for Hg removal efficiency

Source	Sum of Squares	df	Mean Square	F-value	p-value	Remark
Model	840.50	20	42.02	85.66	< 0.0001	significant
A-Contact time	5.16	1	5.16	10.52	0.0030	significant
B-Solution pH	1.50	1	1.50	3.05	0.0912	not significant
C-Dosage	65.54	1	65.54	133.60	< 0.0001	significant
D-Agitation speed	307.41	1	307.41	626.63	< 0.0001	significant
E-Temperature	3.03	1	3.03	6.18	0.0189	significant
AB	57.92	1	57.92	118.06	< 0.0001	significant
AC	19.80	1	19.80	40.36	< 0.0001	significant
AD	5.21	1	5.21	10.62	0.0029	significant
AE	1.62	1	1.62	3.29	0.0799	not significant
BC	52.76	1	52.76	107.55	< 0.0001	significant
BD	0.38	1	0.38	0.78	0.3856	not significant
BE	23.79	1	23.79	48.49	< 0.0001	significant
CD	44.44	1	44.44	90.58	< 0.0001	significant
CE	25.19	1	25.19	51.34	< 0.0001	significant
DE	0.87	1	0.87	1.77	0.1939	not significant
A^2	7.78	1	7.78	15.86	0.0004	significant
B^2	11.21	1	11.21	22.84	< 0.0001	significant
C^2	29.64	1	29.64	60.41	< 0.0001	significant
D^2	117.79	1	117.79	240.10	< 0.0001	significant
E^2	67.71	1	67.71	138.02	< 0.0001	significant
Residual	14.23	29	0.49	-	-	-
Lack of Fit	9.88	22	0.45	0.72	0.7383	not significant
Pure Error	4.35	7	0.62	-	-	-
Cor Total	854.72	49	-	-	-	-

4.9.4 Suitability and Accuracy of Responses Quadratic Models

The suitability and accuracy of the developed response surface models for the prediction of the responses required for the decontamination of As and Hg ions from the industrial wastewater by performing diagnostics tests. A key tool for assessing the suitability of a model is its residuals from least squares. Residuals are the discrepancy between predicted and observed data. While Figs. 53 (a) and (b), depict the normal % probability versus the externally studentized residuals of As and Hg species removal efficiencies, respectively, Figs. 54 (a) and (b) show the predicted versus the actual removal efficiencies of As and Hg species, respectively.

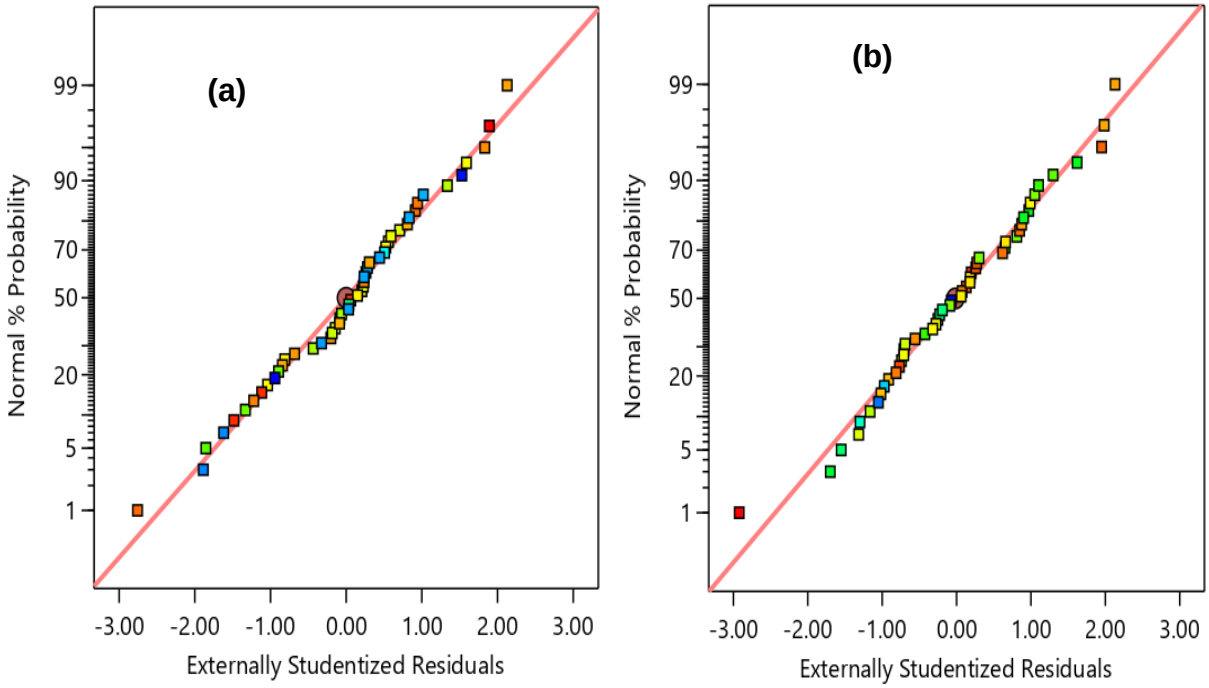

Figure 53: Normal % probability versus externally studentized residuals for As ions removal efficiency (a) and Hg species removal efficiency (b), respectively

As shown in the normal plot of residuals as well as the predicted versus actual removal efficiencies of As and Hg ions displayed in Figs. 53 and 54, respectively, all the data points are oriented along and close to the diagonal line and this means that the experimental data originating from the study is normally distributed (Gottipati & Mishra, 2010). This suggests that the developed quadratic models are accurate and valid for the prediction of the percentage removal of As and Hg by the biosorbent from industrial wastewater. More so, the plots of externally studentized residuals versus predicted presented in Figs. 55 (a) and (b), respectively for As and Hg ions removal efficiencies show random data point distribution between -4.00 and +4.00 with no any obvious trend confirming the reliability and adequacy of the model for

predicting both the responses (Shafaghat & Ghaemi, 2021). Besides, the leverage plots, which are presented in Figs. 56 (a) and (b) for As and Hg ions removal efficiencies, respectively show that the data points appear to be arranged horizontally suggesting the adequacy of the responses for fitted quadratic models. The leverage of all the experimental runs was found to be minimal ranging between 0.00-0.84, which is less than 1.00 suggesting that the predicted responses generated by the quadratic models are accurate and correlated well with the experimental values.

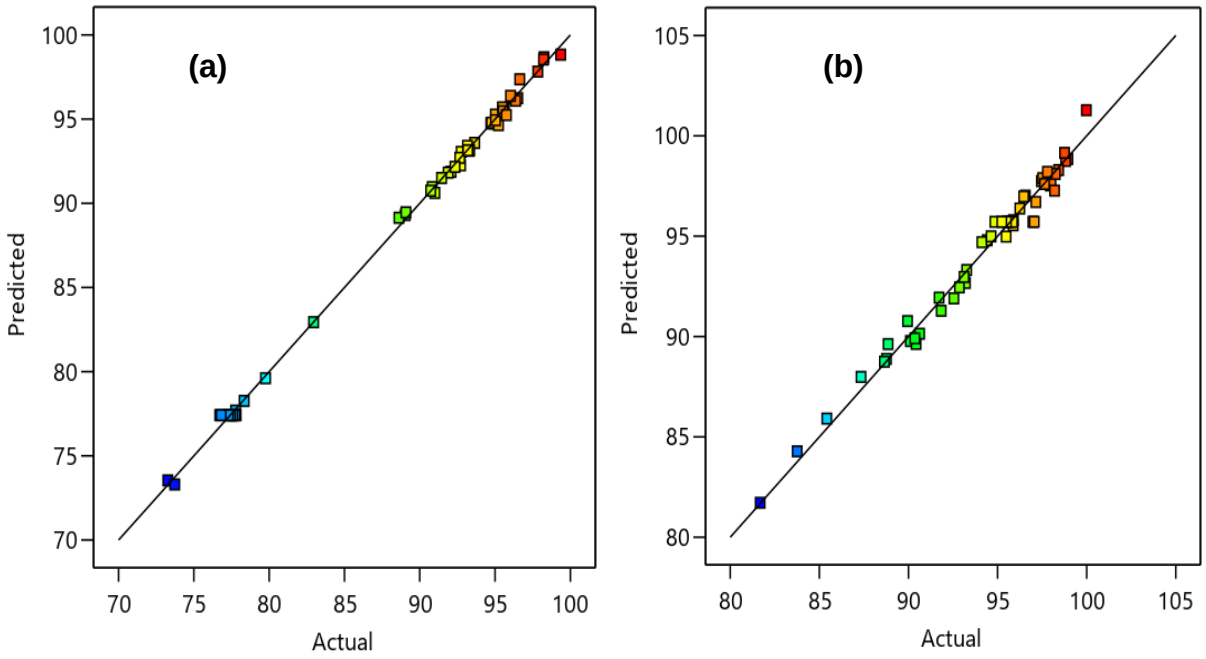

Figure 54: Predicted versus actual values for As ions removal efficiency (a) and Hg ions removal efficiency (b), respectively

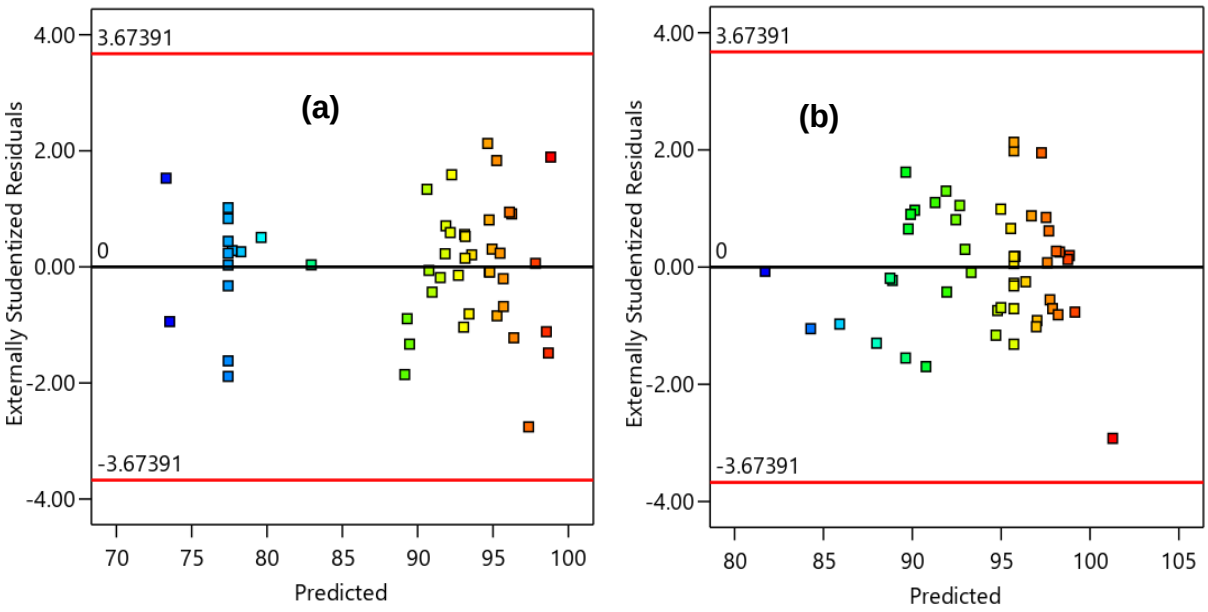

Figure 55: Externally studentized residuals versus predicted values for As ions removal efficiency (a) and Hg ions removal efficiency (b), respectively

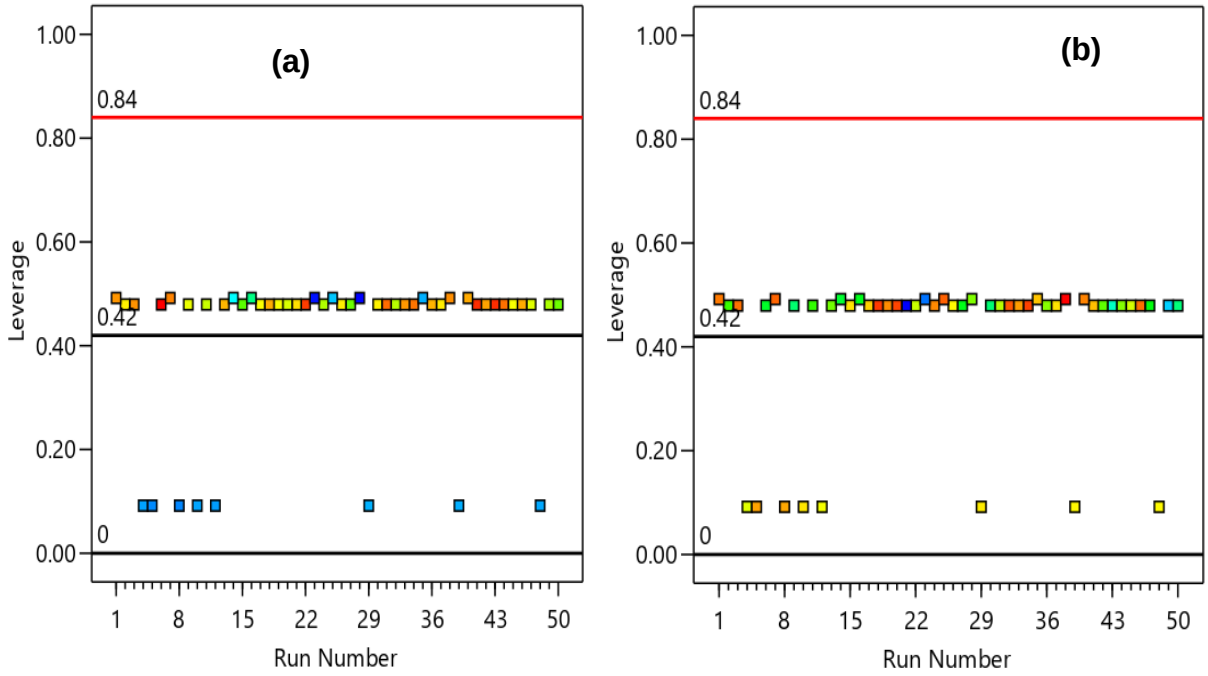

Figure 56: Leverage versus run number for As ions removal efficiency (a) and Hg ions removal efficiency (b), respectively

4.9.5 Optimization of the Biosorption Process Factors and Validation of Quadratic Models

The final step in the central composite design of the response surface methodology is to obtain the best-operating conditions for the optimum detoxification of As and Hg ions from the textile

wastewater using the biosorbent.

In this study, the desirability function was applied to identify the maximum experimental condition for which optimum removal rate and uptake capacity could be attained for effective sequestration of As and Hg ions from the competitive biosorption system using the prepared novel HGAC. For the optimal decontamination of As and Hg ions from the industrial wastewater, the maximum operating condition was found at contact time = 119 min, solution pH = 7, biosorbent dosage = 2 g/L, agitation speed = 194 rpm, and tenperature= 30 ℃. In Fig. 57, after seeking 20 optimization solutions at 0.968 desirability, the maximum removal efficiencies of As and Hg species under the optimum experimental condition were 97.72 and 99.99%, respectively.

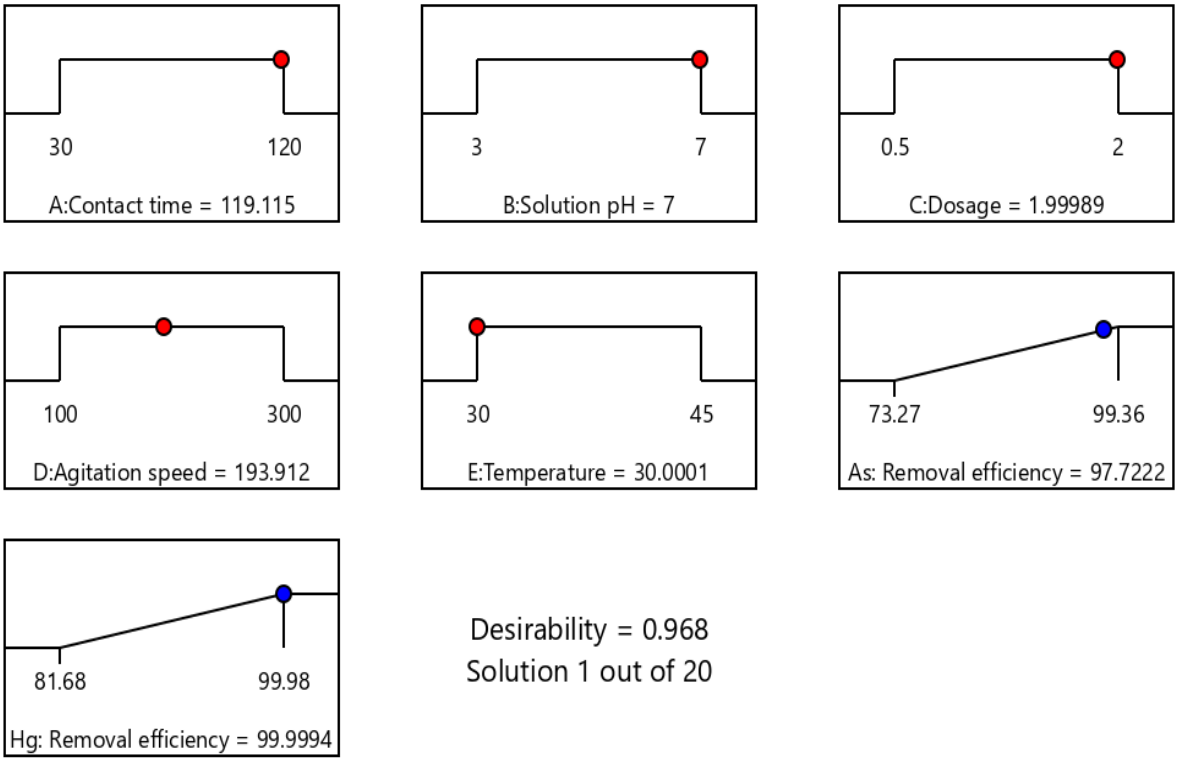

Figure 57: Desirability ramps containing optimum operating conditions for As and Hg ions removal from the industrial wastewater

To confirm the quadratic models developed for the dependent factors (responses) as a function of the independent factors, confirmatory experimental runs were performed at the optimum operating conditions. Table 42 shows the data mean of five confirmatory experimental runs conducted at a two-sided 95% confidence level using the best-operating conditions achieved for the decontamination of As and Hg ions from the textile wastewater. The confirmatory experimental results show that at the optimal setting identified for As and Hg ions sequestration,

the optimum removal efficiencies of 98.16 and 99.13%, were attained, which is within the prediction intervals. Comparatively, there exists a good correlation between the confirmatory experimental and the predicted results with minimal residuals and standard deviations indicating that the developed quadratic models have been validated and could be used in predicting future cases.

Table 42: Confirmation of optimum responses obtained for As and Hg ions decontamination from industrial wastewater

Response	Predicted Mean	Std Dev	n	SE Pred	95% PI low	Data Mean	95% PI high
As: Removal efficiency (%)	97.60	0.40	5	0.29	97.00	98.16	98.20
Hg: Removal efficiency (%)	99.58	0.70	5	0.51	98.55	99.13	100.62

4.10 Biosorption Modeling and Thermodynamic Studies

4.10.1 Biosorption Isotherm Modeling

In this study, the equilibrium sorption data obtained at different biosorbent dosage during the competitive biosorption of As, Hg, Pb, Cd, and Cr ions from the industrial wastewater were modeled with the Langmuir, Freundlich, Dubinin-Radushkevich, and Temkin biosorption isotherm models, which plots are given in Figs. 58 (a, b, c, and d, respectively) and with the isotherm constants values summarized in Table 43. Among the four biosorption isotherm models analyzed, the sorption data was found to show a good fit for all the biosorption isotherm models. However, the Langmuir isotherm model best correlated with the equilibrium sorption data of As, Hg, Pb, Cd, and Cr attained by the biosorbent with the highest correlation coefficients of 0.9998, 0.9993, 0.9995, 0.9993, and 0.9991, respectively as shown in Fig. 58.

Therefore, it could be explained that the biosorption of As, Hg, Pb, Cd, and Cr ions was mainly chemical biosorption forming a monolayer on the surface of the hybrid granular activated carbon. The Langmuir maximum monolayer sorption capacity attained by the biosorbent was 30.26, 90.71, 50.81, 80.14, and 120.44 mg/g for the adsorptive removal of As, Hg, Pb, Cd, and Cr ions from the industrial wastewater, respectively. Also, the dimensionless separation factor

(R_L) of the Langmuir isotherm have values, that all fall in the range between $0.00 < R_L > 1.00$ attained by the biosorbent indicating favorable monolayer biosorption (Bhatti, 2021).

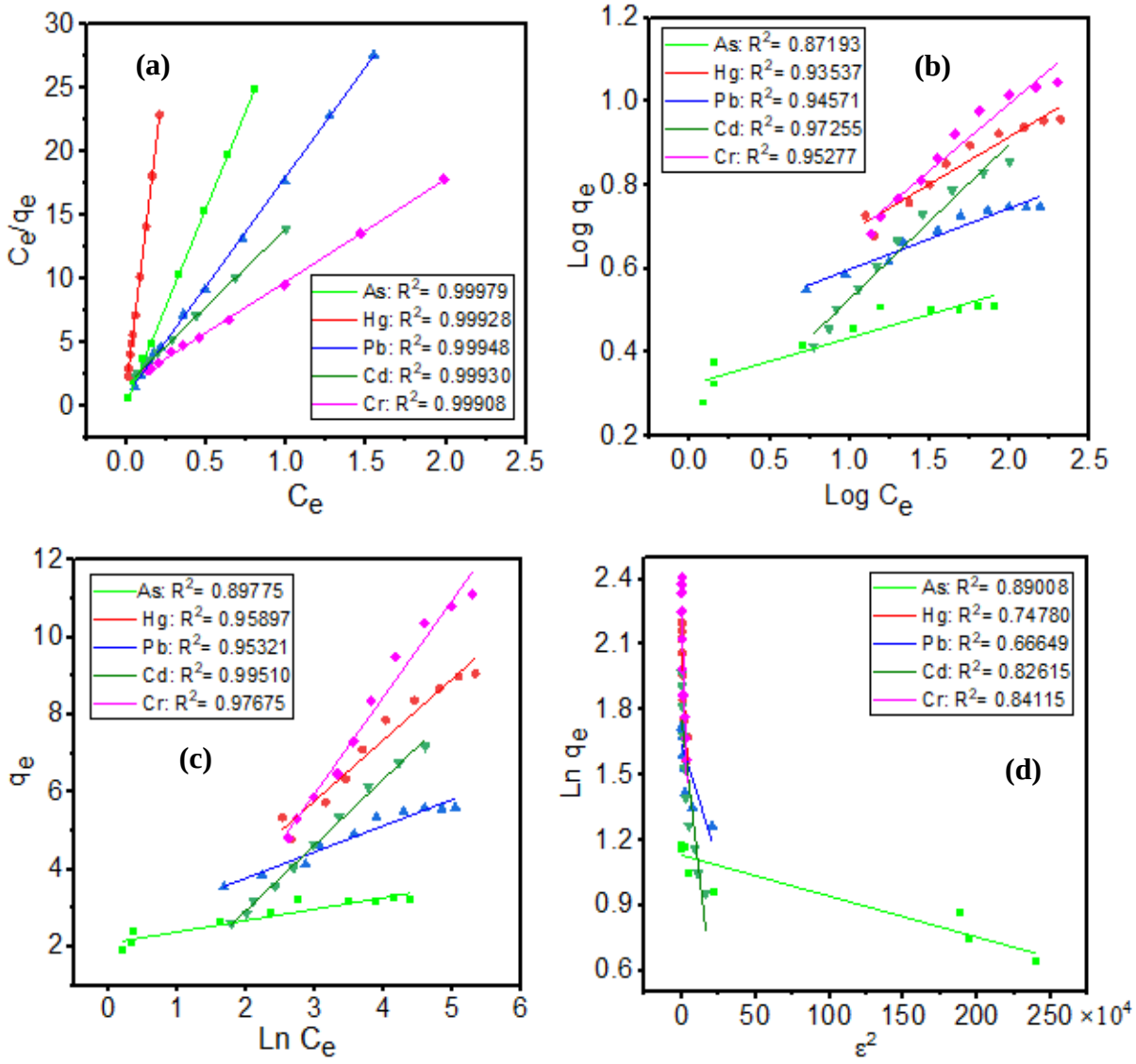

Figure 58: Biosorption isotherm plots, (a) Langmuir, (b) Freundlich, (c) Temkin, and (d) Dubinin-Radushkevich models for As(III) and Hg(II) removal from multicomponent sorption systems

Similarly, amaltash and java plum seeds (Giri *et al.*, 2021), sugarcane bagasse activated carbon composite (Joshi *et al.*, 2019), potato peel and rice husk ash (Bibi *et al.*, 2017), mulberry wood (Zama *et al.*, 2017), chitosan and nano-chitosan (Kwok *et al.*, 2018), activated hematite (Fe_2O_3) iron ore (Memon *et al.*, 2021), iron ore adsorbent (Bhatti, 2021), and ferrihydrite-modified biochar (Tian *et al.*, 2022) was explored for heavy metals removal from aqueous solutions and their equilibrium sorption data correlated well with the Langmuir isotherm model.

Table 43: Biosorption isotherm models parameters for heavy metals removal from the industrial wastewater

Isotherm model	Parameter	Heavy metal				
		As	**Hg**	**Pb**	**Cd**	**Cr**
Langmuir	q_m (mg/g)	30.26	90.71	50.81	80.14	120.44
	K_L (L/mg)	1.12	0.07	0.20	0.07	0.04
	R^2	0.99979	0.99928	0.99948	0.99930	0.99908
	R_L	0.21	0.38	0.47	0.52	0.29
Temkin	A (L/g)	1.35	1.94	3.56	0.76	0.54
	b (kJ/mol)	8543.33	1568.08	3643.49	1457.40	991.03
	B	0.29	1.58	0.68	1.70	2.50
	R^2	0.89775	0.95897	0.95321	0.99510	0.97675
Freundlich	K_F (mg/g)	2.10	2.89	2.83	1.44	2.25
	n	8.90	4.40	6.82	2.70	3.11
	$\frac{1}{n}$	0.11	0.23	0.15	0.37	0.32
	R^2	0.87193	0.93537	0.94571	0.97255	0.95277
Dubinin-Radushkevich	K_{DR} (mol^2/kJ^2)	2.00×10^{-7}	1.00×10^{-5}	2.00×10^{-6}	6.00×10^{-6}	2.00×10^{-5}
	q_s (mg/g)	3.10	8.10	5.15	5.77	9.61
	E (kJ/mol)	1581.14	223.61	500.00	288.68	158.11
	R^2	0.89008	0.74780	0.66649	0.82615	0.84115

4.10.2 Biosorption Kinetic Modeling

To better elucidate the kinetics of As, Hg, Pb, Cd, and Cr ions biosorption from the industrial wastewater onto the biosorbent, the pseudo-first-order, pseudo-second-order, Elovich, and intra-particle diffusion kinetic models were applied. The experimental data of As, Hg, Pb, Cd, and Cr attained by the biosorbent at different biosorption times were used for the kinetic analysis. The linear fitting results and parameters of the biosorption kinetic models are shown in Figs. 59 (a, b, c, and d, respectively) and Table 44, respectively.

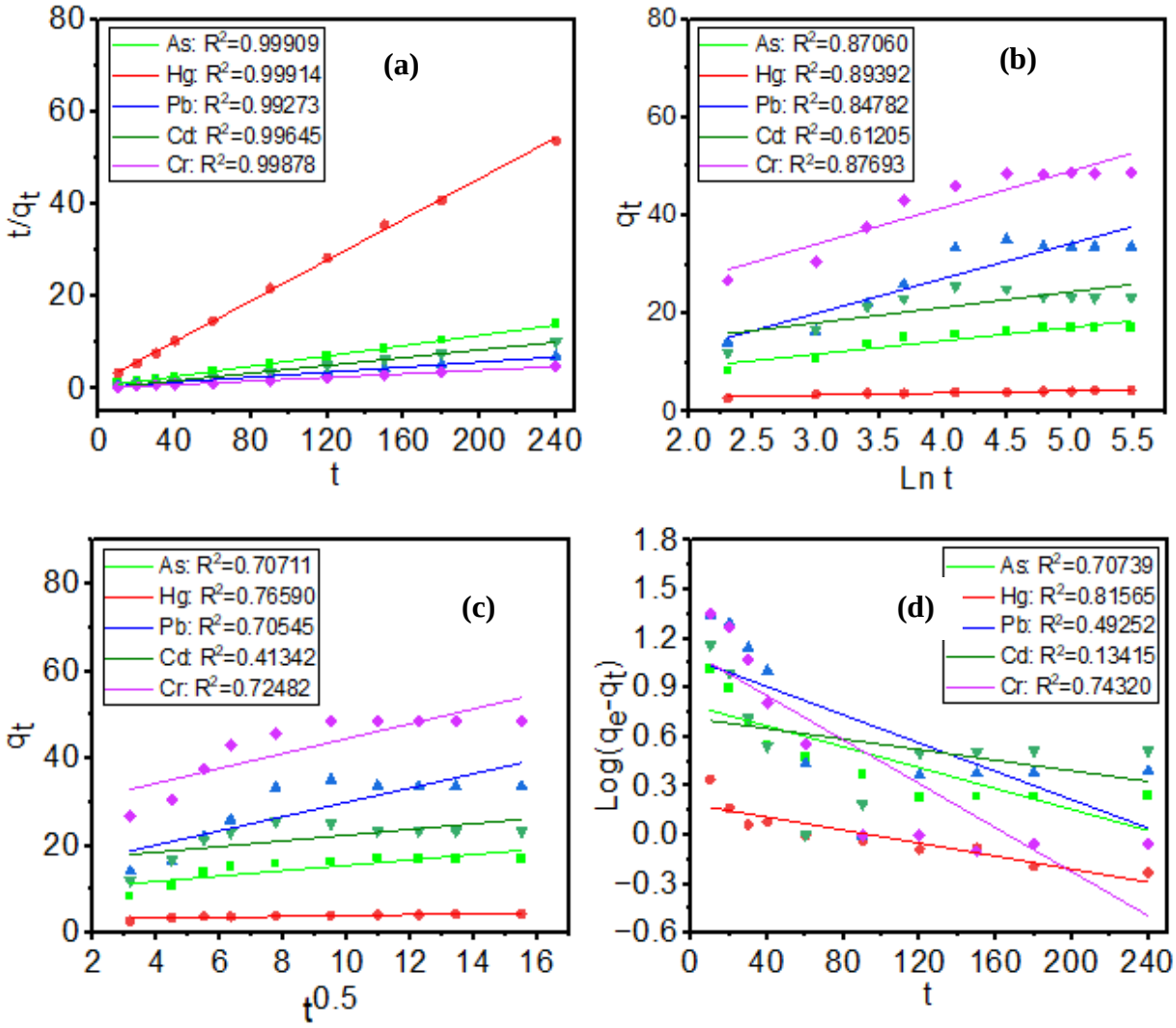

Figure 59: Biosorption kinetic plots, (a) Pseudo-second-order, (b) Elovich, (c) Intra-particle diffusion, and (d) Pseudo-first-order kinetic models

According to Table 44 and Fig. 59 (a), the pseudo-second-order kinetic model was observed to be well-fitted to the experimental data of As, Hg, Pb, Cd, and Cr better than those of the other three biosorption kinetic models. The pseudo-second-order kinetic model was found to have

the highest correlation coefficients of 0.9991, 0.9991, 0.9927, 0.9965, and 0.9988, which are close to unity for As, Hg, Pb, Cd, and Cr, respectively. Therefore, the kinetic data attained from the competitive sorption systems were best described by the pseudo-second-order model indicating that the biosorptive removal of As and Hg by the biosorbent was mainly chemisorption (Liu *et al.*, 2021).

Similarly, the removal of As and Cd ions from aqueous systems using modified wheat straw biochar was studied by Zhu *et al.* (2020), and the kinetic data were well described by the pseudo-second-order kinetic model. Also, Wang *et al.* (2021) found that the sorption data of heavy metals attained by magnetic biochar-microbe biochemical composite best fitted the pseudo-second-order kinetic model. More so, Soni and Shukla (2019) and Salih *et al.* (2019) reported similar results using fly ash-based zeolite-reduced graphene oxide composite and chitosan to decontaminate heavy metals from aqueous systems, respectively.

Table 44: Biosorption kinetic models parameters for heavy metals removal from industrial wastewater

Kinetic model	Parameter	Heavy metal				
		As	Hg	Pb	Cd	Cr
Pseudo-first-order	Kp_1 (L/min)	7.37×10^{-3}	4.61×10^{-3}	9.90×10^{-3}	3.68×10^{-3}	1.54×10^{-3}
	q_e (mg/g)	6.23	1.55	12.03	5.20	13.15
	R^2	0.70739	0.81565	0.49252	0.13415	0.74320
Pseudo-second-order	Kp_2 (L/min)	6.17×10^{-3}	6.08×10^{-3}	1.85×10^{-3}	1.27×10^{-2}	2.28×10^{-3}
	q_e (mg/g)	17.98	24.54	36.76	23.98	51.02
	R^2	0.99909	0.99914	0.99273	0.99645	0.99878
Elovich	α (mg/g)	11.47	68.03	6.01	0.32	36.96
	$\beta\ (g/mg)$	0.36	2.32	0.14	52.79	0.13
	R^2	0.87060	0.89392	0.84782	0.61205	0.87693
Intraparticle diffusion	K_{id} (g/mg.min)	0.60	0.10	1.64	0.65	1.72
	C	10.08	3.07	13.82	16.15	27.59
	R^2	0.5355	0.7745	0.6914	0.3861	0.7221

4.10.3 Thermodynamic Studies

The decontamination of heavy metals shows dependence on the solution temperature. Hence, the effect of temperature on As, Hg, Pb, Cd, and Cr ions removal from the competitive aqueous systems was studied by varying temperatures of the solutions. The experimental data obtained from the industrial wastewater was applied to determine the thermodynamic parameters including the change in Gibbs free energy (ΔG^0), entropy (ΔS^0) and enthalpy (ΔH^0) as summarized in Table 45. The negative and positive values of ΔG^0 and ΔH^0, respectively indicating the spontaneity and endothermic nature of the adsorption process (Zaimee *et al.*, 2021). While the positive values of ΔS^0 suggests an increase in randomness at the biosorbent-adsorbate interface (Batool *et al.*, 2019).

Similarly, Dhoble *et al.* (2018) explored the ability of bark-based magnetic iron oxide particles as an adsorbent to remove As species, and the thermodynamic parameters evaluated indicated the sorption process was spontaneous and feasible at negative values of the ΔG^0, endothermic at positive values of the ΔH^0, and with increasing randomness on the liquid-solid interface at the positive values of the ΔS^0. Also, Alimohammady *et al.* (2017) investigated the simultaneous adsorptive removal of As, Cd, and Hg ions from industrial wastewater by chemically modified graphene oxide and computed the thermodynamic parameters including ΔG^0, ΔH^0 and ΔS^0. The study found that for all the temperature ranges studied, the ΔG^0 values were negative suggesting the feasibility and spontaneous sorption of the heavy metals. Also, the ΔH^0 and ΔS^0 values were positive implying that the adsorption process is endothermic and at the solid-solution interface, randomness increases during the sorption process.

Table 45: Biosorption thermodynamic parameters for the removal of heavy metals from industrial wastewater

Temp (K)	As			Hg			Pb			Cd			Cr		
	ΔG^0 (kJ/mol)	ΔH^0 (kJ/mol)	ΔS^0 (J/mol.K)	ΔG^0 (kJ/mol)	ΔH^0 (kJ/mol)	ΔS^0 (J/mol.K)	ΔG^0 (kJ/mol)	ΔH^0 (kJ/mol)	ΔS^0 (J/mol.K)	ΔG^0 (kJ/mol)	ΔH^0 (kJ/mol)	ΔS^0 (J/mol.K)	ΔG^0 (kJ/mol)	ΔH^0 (kJ/mol)	ΔS^0 (J/mol.K)
283	-7.42	75.34	271.72	-2.72	63.93	268.17	-0.23	58.18	212.31	-17.29	23.98	139.79	-19.00	56.10	255.71
288	-7.97			-2.90			-0.39			-17.72			-20.38		
298	-8.43			-3.03			-0.50			-18.03			-21.31		
308	-8.81			-3.14			-0.59			-18.40			-21.82		
318	-9.14			-3.23			-0.66			-18.86			-22.65		
328	-9.43			-3.31			-0.72			-19.15			-23.39		
338	-9.69			-3.38			-0.77			-19.60			-24.15		
348	-9.93			-3.44			-0.81			-19.94			-25.19		
358	-10.14			-3.49			-0.85			-20.10			-26.09		

4.10.4 Determination of the Mechanism of Biosorption

To determine the mechanisms of of heavy metal ions biosorptive removal from the non-competitive and competitive sorption systems, the spent HGAC was characterized using SEM-EDS, TEM, XRD, BET, and FT-IR. The disappearance of the cavities or the pores from the SEM image of the pristine HGAC [Fig. 10 (a)] is an indication that the depollution of heavy metal ions from the non-competitive and competitive sorption media has taken place as displayed in Figs. 60 (a, b, c, and d), correspondingly. Also, after the application of the HGAC for the adsorptive sequestration of the heavy metal ions from the non-competitive and competitive sorption systems, it was observed that the elemental As, Hg, Pb, Cd, and Cr were present in the EDS spectra as shown in Figs. 61 (a, b, c, and d), respectively. These observations show that the biosorption of the heavy metal ions on the pristine HGAC [Fig. 10 (b)] were successful. More so, in Figs. 62 (a, b, c, and d), respectively, it was observed that after the detoxification of heavy metal ions from the non-competitive and competitive sorption system, the pores that were observed in the TEM image of pristine HGAC (Fig. 11) were filled up and the presence of the smooth spherical shapes in the microstructure confirmed the detoxification of the As, Hg, Pb, Cd, and Cr ions by the biosorbent.

Furthermore, after the decontamination of heavy metal ions from the non-competitive and competitive sorption systems, there were changes in the appearance of the peaks in the XRD spectrum (Fig. 12), and new diffraction peaks were observed in the spent activated carbon as presented in Figs. 63 (a, b, c, and d), respectively. The changes and appearances of the new peaks in the XRD spectra confirm the presence and uptake of As, Hg, Pb, Cd, and Cr ions by the biosorbent from the non-competitive and competitive biosorption systems onto the surface of the HGAC (Sellaoui *et al.*, 2017). As summarized in Table 46, the BET surface area, micropore surface area, micropore volume, and total pore volume of the activated carbon decreased after the biosorption of As, Hg, Pb, Cd, and Cr ions from the non-competitive and competitive sorption systems. The decrease in the textural parameters of the activated carbon loaded with the heavy metal ions was significant in comparison to the pristine HGAC (Table 12), indicating that these parameters played an important role in the heavy metal biosorption process. Hence, it can be concluded that the As, Hg, Pb, Cd, and Cr ions were adsorbed to the outer surface and the pore surface of H_3PO_4-modified hybrid granular activated carbon (Dong & Lin, 2017; Liu *et al.*, 2021).

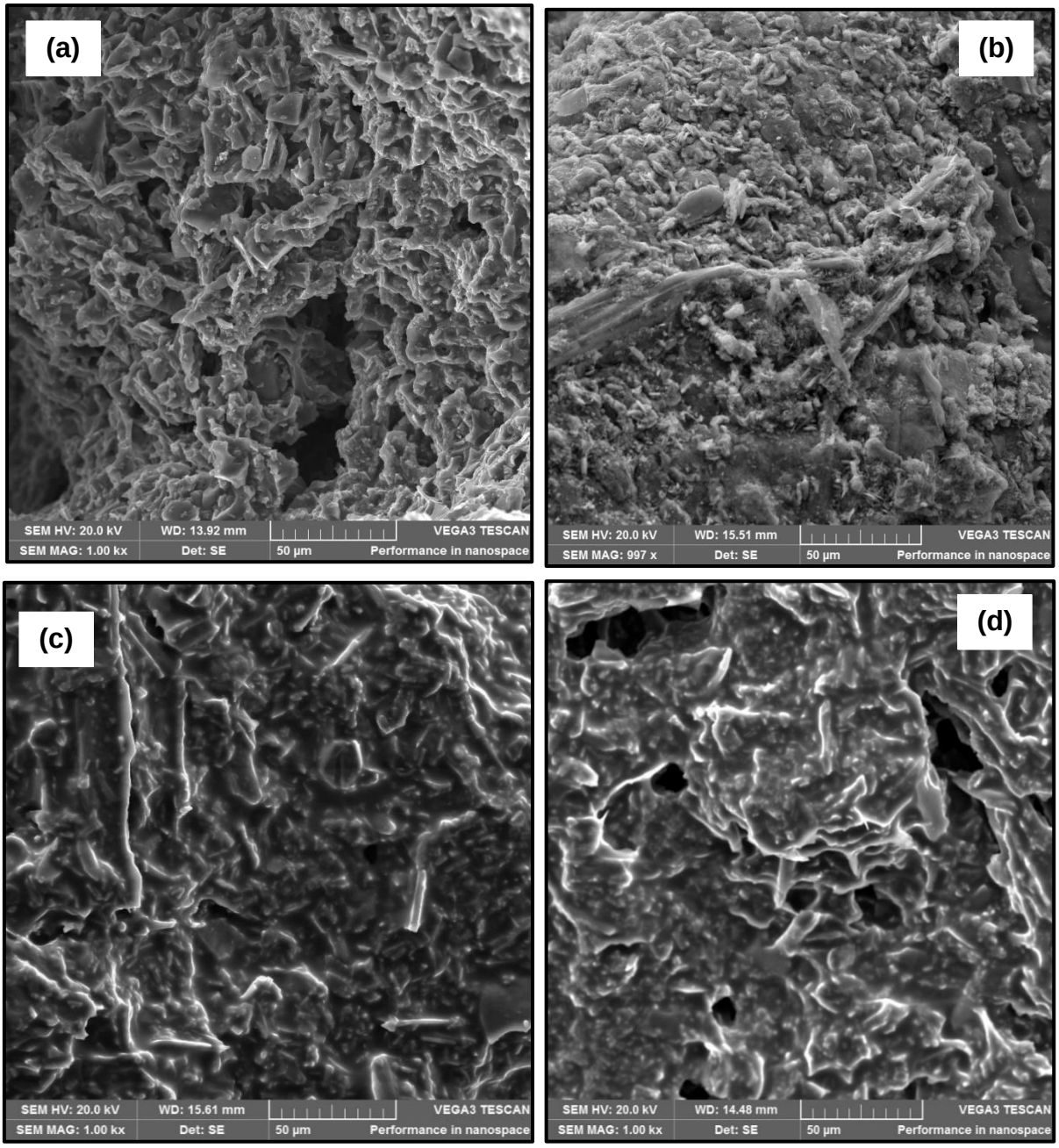

Figure 60: SEM images after the biosorption of As(III) ions (a) and Hg(II) ions (b) from the single-metal synthetic wastewater, after biosorption of As(III) and Hg(II) from the binary-metal synthetic wastewater (c), and after biosorption of As, Hg, Pb, Cd, and Cr ions (d) from industrial wastewater

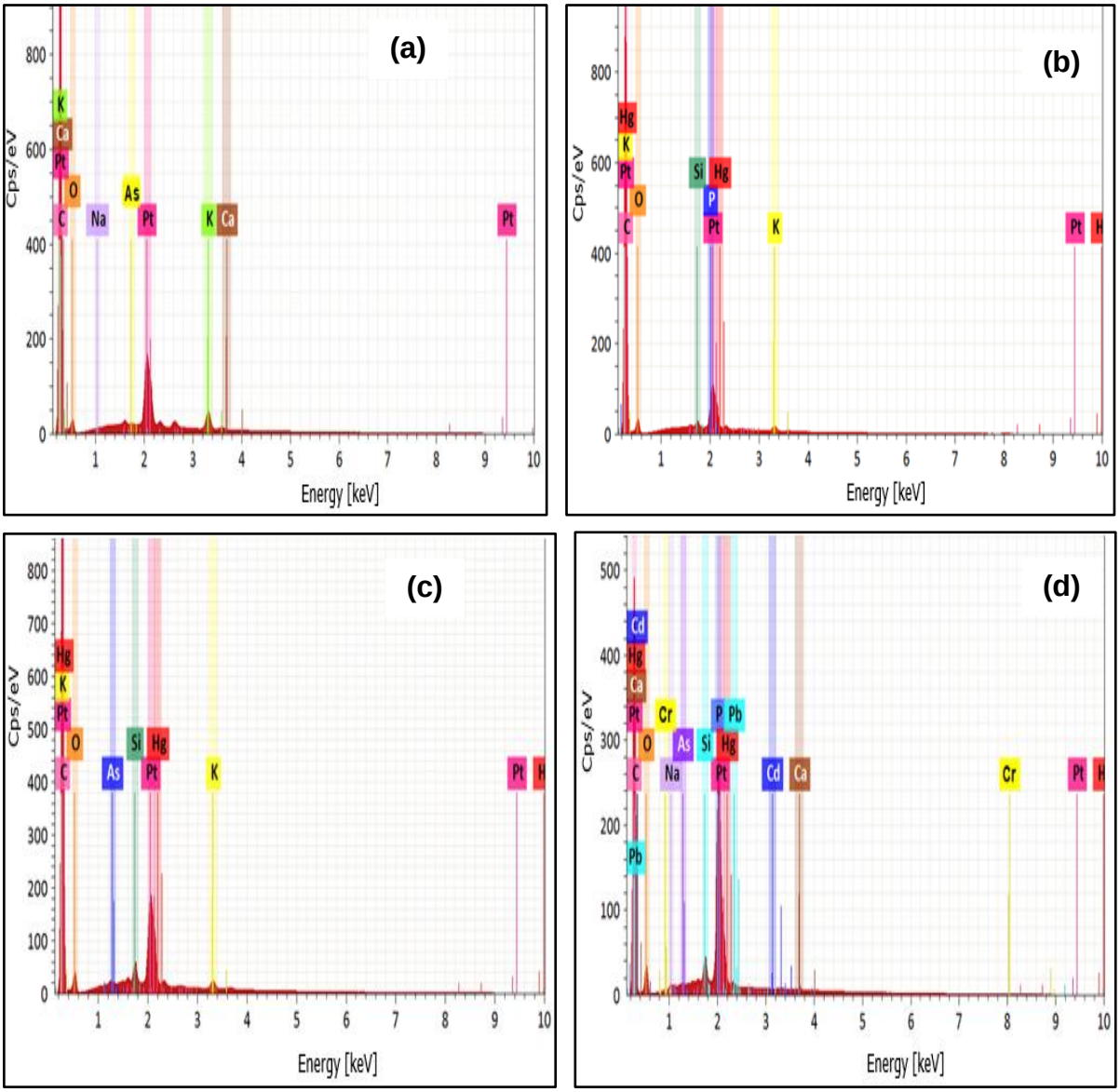

Figure 61: **EDS spectra after the biosorption of As(III) ions (a) and Hg(II) ions (b) from the single-metal synthetic wastewater, after biosorption of As(III) and Hg(II) from the binary-metal synthetic wastewater (c), and after biosorption of As, Hg, Pb, Cd, and Cr ions (d) from industrial wastewater**

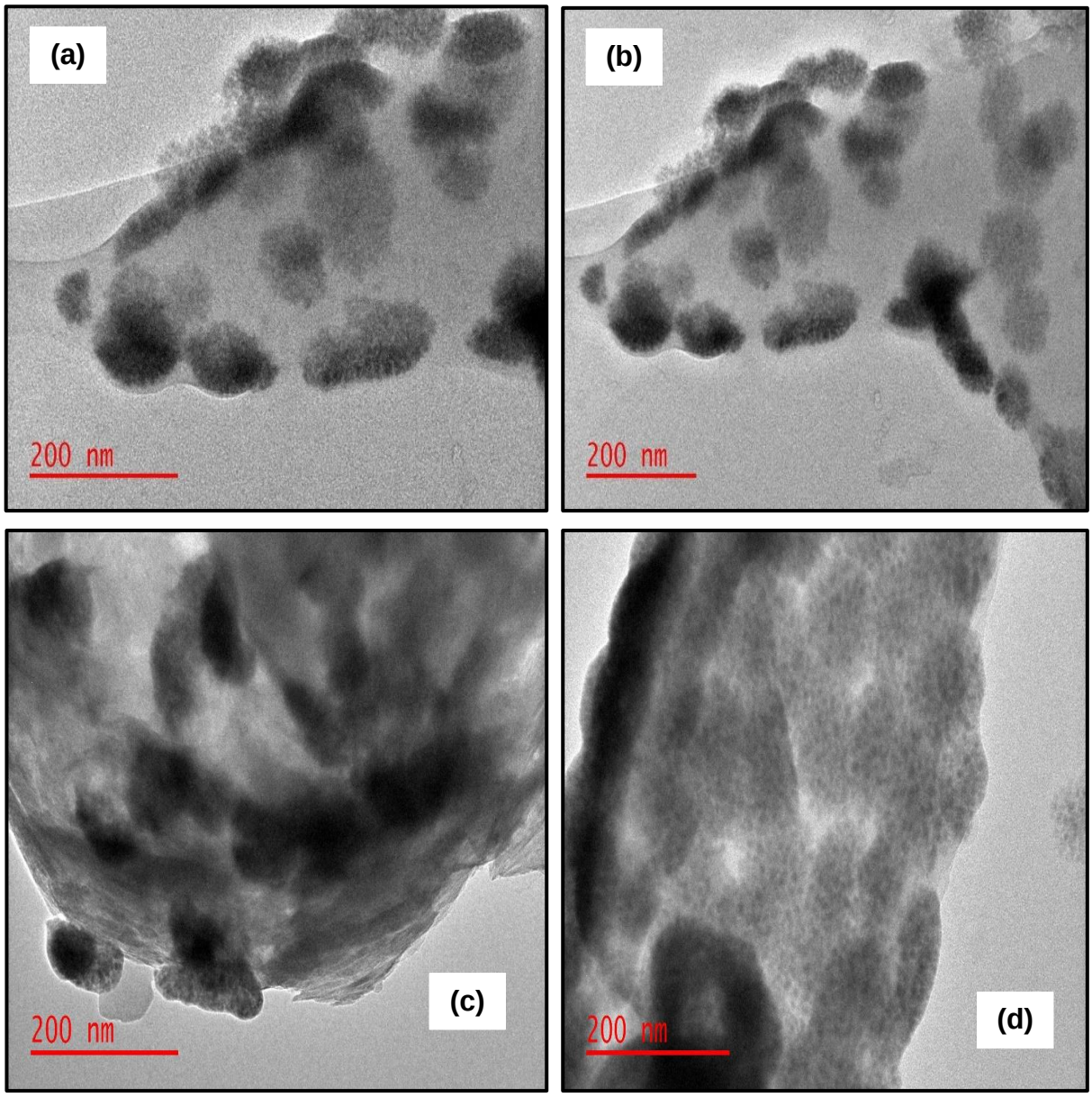

Figure 62: **TEM images after the biosorption of As(III) ions (a) and Hg(II) ions (b) from the single-metal synthetic wastewater, after biosorption of As(III) and Hg(II) from the binary-metal synthetic wastewater (c), and after biosorption of As, Hg, Pb, Cd, and Cr ions (d) from industrial wastewater**

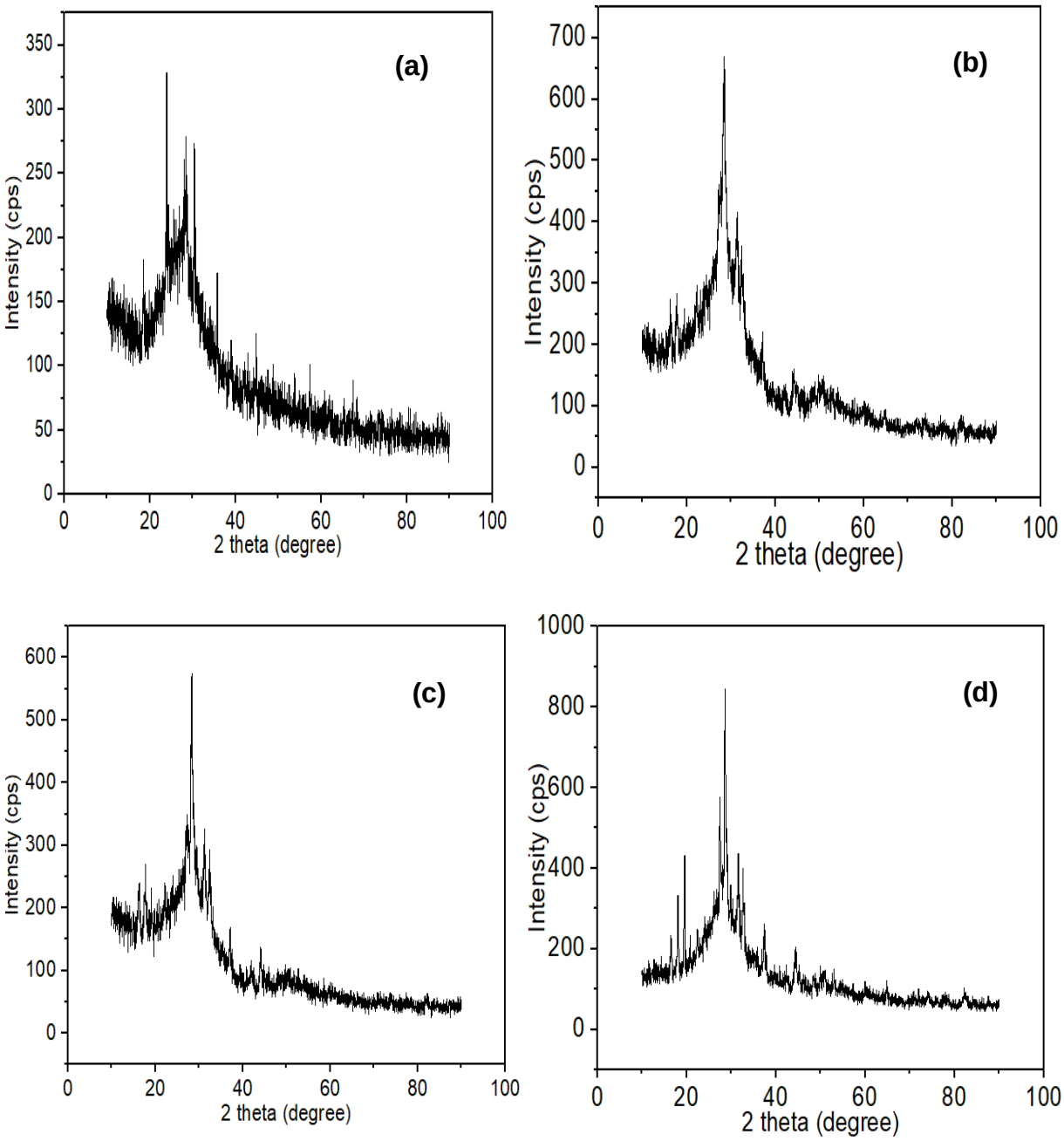

Figure 63: **XRD spectra after the biosorption of As(III) ions (a) and Hg(II) ions (b) from the single-metal synthetic wastewater, after biosorption of As(III) and Hg(II) from the binary-metal synthetic wastewater (c), and after biosorption of As, Hg, Pb, Cd, and Cr ions (d) from industrial wastewater**

Besides, after the biosorption process of As, Hg, Pb, Cd, and Cr ions, the absorption bands that were observed in the biosorbent FTIR spectrum (Fig. 14) before the sorption process shifted and there is also the disappearance and emergence of new absorption peaks as presented in Figs. 64 (a, b, c, and d), respectively. The shifting of these spectral bands suggests that several functional groups aid the biosorption process of As, Hg, Pb, Cd, and Cr ions from the non-

competitive and competitive sorption systems (Elkhatib *et al.*, 2019; Ezeonuegbu *et al.*, 2021). Hence, a complex formation between the major surface functional groups including O–H, C=O, C–O, and C–H, and that of the metal ions occurred during the biosorption process (Wu *et al.*, 2018).

The possible mechanism of reactions between some of the surface functional groups of the biosorbent and heavy metal ions are given in Eqs. (24-26). Where M^{+n} represents to the heavy metal ions (As, Hg, Pb, Cd, and Cr) and their respective charges.

$$R - NH_2 + M^{+n} \rightarrow R - NH_2 - M^{+n} \quad (24)$$

$$R - OH + M^{+n} \rightarrow R - OH - M^{+n} \quad (25)$$

$$R - C = O + M^{+n} \rightarrow R - C = O - M^{+n} \quad (26)$$

$$R - COOH + M^{+n} \rightarrow R - COOH - M^{+n} \quad (27)$$

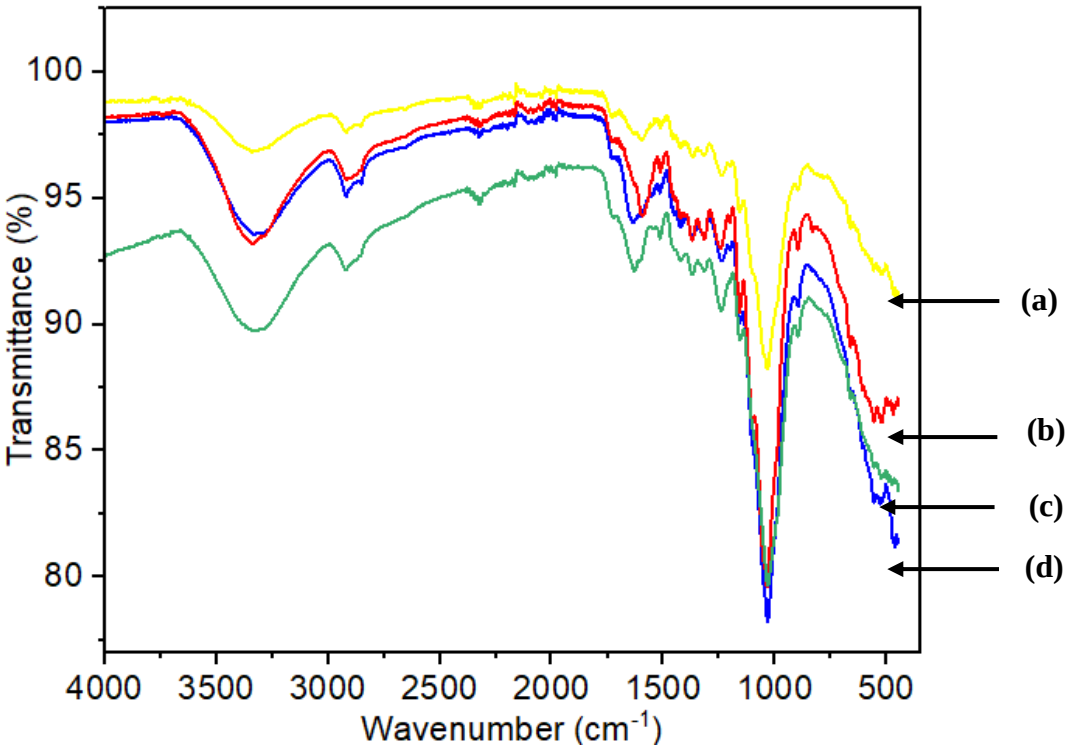

Figure 64: FT-IR spectra after the biosorption of As(III) ions (a) and Hg(II) ions (b) from the single-metal synthetic wastewater, after biosorption of As(III) and Hg(II) from the binary-metal synthetic wastewater (c), and after biosorption of As, Hg, Pb, Cd, and Cr ions (d) from industrial wastewater

Table 46: Textural properties of the activated carbon (AC) after the biosorption of the heavy metal ions from non-competitive and competitive sorption systems

Textural parameter	AC-with As(III)	AC- with Hg(II)	AC-with As(III)+Hg(II)	AC-with As, Hg, Pb, Cd, and Cr ions
BET surface area (m^2/g)	690.2	582.9	657.4	485.7
Micropore surface area (m^2/g)	251.8	290.3	253.8	196.3
Total pore volume (cm^3/g)	0.0641	0.0727	0.0677	0.0495
Micropore volume (cm^3/g)	0.0109	0.0128	0.0200	0.0016

From the SEM-EDS, TEM, XRD, BET, and FT-IR analysis of the spent HGAC, the proposed mechanisms of heavy metal ions removal from the non-competitive and competitive sorption systems could be due to pore filling, surface complexation, electrostatic attraction, ion exchange, physisorption, chemisorption, hydrogen bonding, and the $\pi - \pi$ interaction with the aromatic compounds on the surface of the biosorbent as illustrated in Fig. 65.

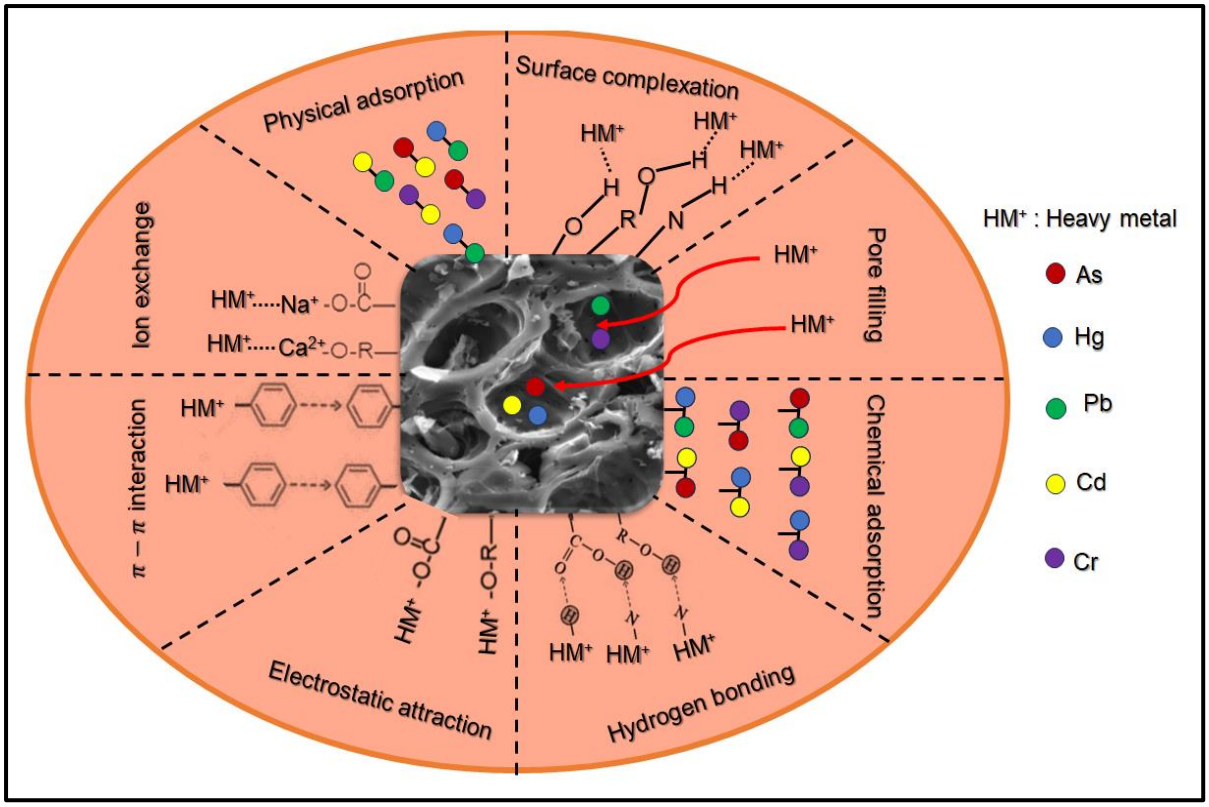

Figure 65: A schematic diagram illustrating the possible biosorption mechanisms of the heavy metal ions (As, Hg, Pb, Cd, and Cr) in industrial wastewater onto the activated carbon

4.11 Comparison to Literature

The related studies for As(III) and Hg(II) ions removal from monocomponent biosorption systems were compiled to compare the uptake capacity of the hybrid granular activated carbon prepared from three different parts of maize plants including cobs, stalks, and tassels. Table 47 shows the Langmuir uptake capacity (q_m) of various adsorbents applied for the decontamination of As(III) and Hg(II) ions from aquatic systems. It was found that among the complied results, the hybrid granular activated carbon prepared from the maize plant residues shows higher sorption capacity than almost all the other adsorbents utilized in the previous studies. Therefore, the prepared biosorbent employed in this current study is more proficient for As(III) and Hg(II) ions removal and could be utilized as a cheap biosorbent for the decontamination of other heavy metal ions from aquatic environments.

Table 47: Comparison between the present study and reported adsorbents materials for As(III) and Hg(II) removal from the aqueous systems

Adsorbent	Heavy metal	Uptake capacity (mg/g)	Reference
Hybrid granular activated carbon	As(III)	155.42	Present study
Ferrihydrite-modified biochar	As(III)	18.38	Tian *et al.* (2022)
Amaltash seed	As(III)	1.42	Giri *et al.* (2021)
Java plum seed	As(III)	1.45	Giri *et al.* (2021)
Activated hematite (Fe_2O_3) iron ore	As(III)	14.96	Memon *et al.* (2021)
Nano-porous carbon magnetic composite	As(III)	6.69	Joshi *et al.* (2019)
Fly ash/zeolite-graphene oxide	As(III)	0.05	Soni & Shukla (2019)
Chitosan	As(III)	8.00	Kwok *et al.* (2018)
Nano-chitosan	As(III)	13.00	Kwok *et al.* (2018)
Potato peel and rice husk ash	As(III)	0.03	Bibi *et al.* (2017)
Mulberry wood	As(III)	5.00	Zama *et al.* (2017)
Hybrid granular activated carbon	Hg(II)	112.46	Present study
$KMnO_4$-modified corn cob carbon	Hg(II)	184.76	Liu *et al.* (2021)
KOH-modified corn cob carbon	Hg(II)	222.20	Liu *et al.* (2021)
Activated carbon from corn cob by KOH	Hg(II)	2.39	Liu *et al.* (2020)
Pistachio wood wastes activated carbon	Hg(II)	201.09	Sajjadi *et al.* (2018)
Raw coal-activated carbon	Hg(II)	59.50	Guo *et al.* (2017)
Raw coconut husk-activated carbon	Hg(II)	48.90	Guo *et al.* (2017)
Raw peach stone-activated carbon	Hg(II)	44.90	Guo *et al.* (2017)
Corn straw	Hg(II)	5.10	Tan *et al.* (2016)
Bagasse biochar	Hg(II)	13.0	Xu *et al.* (2016)
Phragmites karka	Hg(II)	2.30	Raza *et al.* (2015)
Coconut activated carbon	Hg(II)	5.20	Lu *et al.* (2014)
Brazilian pepper	Hg(II)	15.10	Dong *et al.* (2013)
Soybean stalk	Hg(II)	0.67	Kong *et al.* (2011)

CHAPTER FIVE

CONCLUSION AND RECOMMENDATIONS

5.1 Conclusion

The biosorption and desorption characteristics of heavy metal ions from non-competitive and competitive aqueous solutions onto hybrid granular activated carbon produced from maize residues were investigated. The study showed that the prepared hybrid granular activated carbon could be effectively used as an excellent alternative for As(III) and Hg(II) ions decontamination from monocomponent and bicomponent synthetic wastewater using batch technique. The efficient sequestration of As(III) and Hg(II) ions from both monocomponent and bicomponent synthetic wastewater were found to show dependence on the physicochemical properties of the biosorbent as well as all the studied independent biosorption process factors including contact time, pH of the solution, biosorbent particle size, biosorbent dosage, initial heavy metal ion concentration, and reaction temperature. The study also found that the spent biosorbent impregnated with the heavy metal ions from the monocomponent and bicomponent synthetic wastewater could be regenerated by 0.10 M HCl and 0.10M EDTA, respectively. The regenerated biosorbent could be reused up to the eighth cycle for the sequestration of As(III) and Hg(II) ions from the synthetic wastewater without significantly losing its adsorptive properties. This indicates that the biosorbent offers an economical potential to be used repeatedly in As(III) and Hg(II) remediation from aqueous environments.

The equilibrium biosorption data attained by the biosorbent from both monocomponent and bicomponent synthetic wastewater were well explained by the Langmuir isotherm and pseudo-second-order kinetic models indicating the mechanism of As(III) and Hg(II) biosorption was mainly chemisorption. The Langmuir monolayer uptake capacity (q_m) obtained for the removal of As(III) and Hg(II) ions from the synthetic wastewater were found to be 155.42 and 112.46 mg/g, respectively suggesting the high uptake capacity of the as-prepared biosorbent. Whilst the evaluated thermodynamic parameters suggested that the biosorptive removal of As(III) and Hg(II) ions from both sorption systems was feasible, spontaneous, and endothermic with increasing randomness on the liquid-solid interface.

The response surface quadratic models developed using the CCD-RSM, provided accurate prediction for the tested independent and response variables in the biosorption of As(III) and Hg(II) ions from the synthetic wastewater. Under the selected optimum experimental

conditions of 90.00 min contact time, 0.50 g/L biosorbent dosage, and 10.00 mg/L initial As(III) concentration, maximum As(III) removal and biosorption capacity were found to be 93.14% and 7.04 mg/g, respectively with the desirability of 0.844. For the optimal decontamination of Hg(II) ions from the synthetic wastewater, the best operating conditions of 30.00 min contact time, 0.50 g/L biosorbent dosage, and 15.00 mg/L initial Hg(II) concentration were found at 0.903 desirability with maximum removal rate and uptake capacity of Hg(II) of 96.68% and 10.83 mg/g, respectively.

The applicability of the biosorbent synthesized from the maize residues for the simultaneous decontamination of As, Hg, Pb, Cd, and Cr species found in real industrial wastewater as a function of agitation speed, contact time, pH of the solution, biosorbent particle size, biosorbent dosage, initial heavy metal ion concentration, and temperature was investigated. The results showed that the biosorbent could competitively decontaminate over 96.00% of As, Hg, Pb, Cd, and Cr species in the textile industrial wastewater indicating its efficiency and suitability in wastewater treatment. The regeneration of the spent biosorbent using 0.10 M HCl as the best-selected desorption eluent suggested that the biosorbent is capable of being used effectively, recycled, and reused severally for the sequestration of As, Hg, Pb, Cd, and Cr species from the textile wastewater and even up to the ten cycles implying the economic potential and the sustainability of the biosorbent in environmental pollutants remediation, especially heavy metals.

To determine the interactive effects and optimize the independent factors for As and Hg ions removal from the industrial wastewater in the coexistence of other three heavy metals (Pb, Cd, and Cr), batch experiments with varying combinations of the biosorption factors were conducted according to the CCD-RSM. For the optimal decontamination of As and Hg ions from the real industrial wastewater, the best experimental conditions were found at contact time $= 119.00\ min$, solution pH $= 7.00$, biosorbent dosage $= 2.00$ g/L, agitation speed $= 194.00$ rpm, and tenperature$= 30.00$ ℃, which gave maximum removal efficiencies of 97.72 and 99.99% for As and Hg species, respectively.

For the four biosorption isotherm models analyzed, the Langmuir isotherm model best correlated with the equilibrium sorption data of As, Hg, Pb, Cd, and Cr attained by the biosorbent with the highest correlation coefficients of 0.9998, 0.9993, 0.9995, 0.9993, and 0.9991, respectively. Therefore, it could be explained that the biosorption of As, Hg, Pb, Cd, and Cr ions was mainly chemical biosorption forming a monolayer on the surface of the hybrid

granular activated carbon. The Langmuir maximum monolayer sorption capacity attained by the biosorbent was 30.26, 90.71, 50.81, 80.14, and 120.44 mg/g for the adsorptive removal of As, Hg, Pb, Cd, and Cr ions from the industrial wastewater, respectively. The pseudo-second-order kinetic model was also found to have the highest correlation coefficients of 0.9991, 0.9991, 0.9927, 0.9965, and 0.9988, which are close to unity for As, Hg, Pb, Cd, and Cr, respectively. Therefore, the kinetic data attained from the competitive sorption systems were best described by the pseudo-second-order model indicating that the biosorptive removal of As and Hg in the presence of Pb, Cd, and Cr ions by the biosorbent was mainly chemisorption.

The study also found that for the temperature range studied, the ΔG^0 values were negative suggesting the feasibility and spontaneous sorption of the heavy metal ions from the real industrial wastewater. Also, the ΔH^0 and ΔS^0 values were positive implying that the biosorption process is endothermic and at the solid-solute interface, randomness increases during the sorption process. The characterization of the hybrid granular activated carbon using TGA, SEM-EDS, TEM, XRD, BET, and FTIR showed that the biosorbent surface characteristics could facilitate the heavy metal ions removal from the non- and competitive biosorption media. The main biosorption mechanisms of the heavy metal ions on the biosorbent involved surface complexation, electrostatic attraction, and replacement of hydroxyl groups.

In comparison to the literature, the hybrid granular activated carbon prepared from the maize plant residues was found to have a higher sorption capacity than almost all the other sorbent materials utilized in the previous studies. Therefore, this novel biosorbent is found to be promising and could effectively be employed for heavy metals remediation in aquatic environments.

5.2 Recommendations

The present study provided important fundamental knowledge regarding the physiochemical properties of the hybrid granular activated carbon produced from the maize residues as well as the biosorption and desorption characteristics of heavy metals on the biosorbent. Based on the findings of this study, the following recommendations have been made for further studies to improve the application of this novel biosorbent to small-scale industrial wastewater treatment.

More pretreatment studies should be conducted to improve the physicochemical characteristics such as specific surface area, pore volume, and active sites to increase the adsorption capabilities of inexpensive adsorbents. The effectiveness of the adsorbents is significantly

impacted by these characteristics. To prepare activated carbon from maize plant biomass, for example, more carbonization, activation, and characterization studies are needed to determine the ideal conditions for preparation that would enhance the surface chemistry of the activated carbon using the design of experiments.

Due to the lack of confidence in the engineering of sorbent materials and practicality, they are not utilized on an industrial scale level. Therefore, it is critical to reconsider multidimensional and multidisciplinary research approaches in sorbent production for commercial and industrial applications in the near future to minimize metal burdens in aquatic systems.

Continuous flow adsorption experiments in column systems ought to be performed since sorbent materials can be a good choice for biofilters in the treatment of industrial effluent. Analyzing the synergistic impacts of cationic and anionic pollutants removal in aqueous systems could be accomplished through column adsorption experiments.

Before being disposed of, it is important to thoroughly examine efficient analytical techniques for recovering the desorbed heavy metal ions in aqueous solution following desorption, either by electro-recovery or bio-hydrometallurgy. Therefore, to ensure economic feasibility and sustainability, cost evaluations and the complexity of recovering and regenerating exhausted sorbent materials for reusability should be investigated.

Desorption parameters and adsorbent production processes should be optimized utilizing efficient optimization strategies, such as the design of experiments, to improve the recovery yield and recycling of the spent adsorbent to ensure economic and environmental sustainability.

The dynamic batch adsorption reactor developed should be employed in the simultaneous sequestration of various inorganic and organic contaminants from real industrial wastewater using natural and engineered sorbent materials derived from different biomass feedstocks.

REFERENCES

Abd El-Ghany, N. A., Elella, M. H. A., Abdallah, H. M., Mostafa, M. S., & Samy, M. (2023). Recent advances in various starch formulation for wastewater purification via adsorption technique: A Review. *Journal of Polymers and the Environment*, *31*(7), 2792–2825. https://doi.org/10.1007/s10924-023-02798-x

Abdi, O., & Kazemi, M. (2015). A review study of biosorption of heavy metals and comparison between different biosorbents. *Journal of Materials and Environmental Science*, *6*(5), 1386–1399.

Abdulrahman, O. A., Abd Latiff, A. A., Daud, Z., Saphira Radin Mohamed, R. M., Ismail, N., Ab Aziz, A., Rafatullah, M., Hossain, K., Ahmad, A., & Kamoldeen Abiodun, A. (2019). Adsorption of cadmium and lead from palm oil mill effluent using bone-composite: optimisation and isotherm studies. *International Journal of Environmental Analytical Chemistry*, *99*(8), 707–725. https://doi.org/10.1080/03067319.2019.1607318

Abedpour, M., Kamyab Moghadas, B., & Tamjidi, S. (2020). Equilibrium and kinetic study of simultaneous removal of Cd(II) and Ni(II) by acrylamide-based polymer as effective adsorbent: optimisation by response surface methodology (RSM). *International Journal of Environmental Analytical Chemistry*, *00*(00), 1–18. https://doi.org/10.1080/03067319.-2020.1772768

Abegunde, S. M., Idowu, K. S., Adejuwon, O. M., & Adeyemi-Adejolu, T. (2020). A review on the influence of chemical modification on the performance of adsorbents. *Resources, Environment and Sustainability*, *1*(100001). https://doi.org/10.1016/j.resenv.2020.-100001

Abidli, A., Huang, Y., Ben Rejeb, Z., Zaoui, A., & Park, C. B. (2021). Sustainable and efficient technologies for removal and recovery of toxic and valuable metals from wastewater: Recent progress, challenges, and future perspectives. *Chemosphere*, *292*, 133102. https://doi.org/10.-1016/j.chemosphere.2021.133102

Abou Taleb, M. F., Albalwi, H., & Abou El Fadl, F. I. (2021). Removal of mercury(II) from aqueous solution using silver nanocomposite: Synthesis and Adsorption Mechanism. *Journal of Inorganic and Organometallic Polymers and Materials*, *31*(4), 1825–1835.

https://doi.org/10.1007/s10904-020-01839-5

Abu Al-Rub, F. A., Kandah, M., & Al-Dabaybeh, N. (2003). Competitive adsorption of nickel and cadmium on sheep manure wastes: Experimental and prediction studies. *Separation Science and Technology*, *38*(2), 483–497. https://doi.org/10.1081/SS-120016586

Acevedo-Páez, J. C., Durán, J. M., Posso, F., & Arenas, E. (2020). Hydrogen production from palm kernel shell: Kinetic modeling and simulation. *International Journal of Hydrogen Energy*, *45*(47), 25689–25697. https://doi.org/10.1016/j.ijhydene.2019.10.146

Adane, T., Haile, D., Dessie, A., Abebe, Y., & Dagne, H. (2020). Response surface methodology as a statistical tool for optimization of removal of chromium (VI) from aqueous solution by Teff (Eragrostis teff) husk activated carbon. *Applied Water Science*, *10*(1), 1–13. https://doi.org/10.1007/s13201-019-1120-8

Adelaja, O. A., Bankole, A. C., Oladipo, M. E., & Lene, D. B. (2019). Biosorption of Hg(II) ions, Congo red and their binary mixture using raw and chemically activated mango leaves. *International Journal of Energy and Water Resources*, *3*(1), 1–12. https://doi.org/10.-1007/s42108-019-00012-0

Adetokun, A. A., Uba, S., & Garba, Z. N. (2019). Optimization of adsorption of metal ions from a ternary aqueous solution with activated carbon from Acacia senegal (L.) Willd pods using Central Composite Design. *Journal of King Saud University - Science*, *31*(4), 1452–1462. https://doi.org/10.1016/j.jksus.2018.12.007

Adio, S. O., Basheer, C., Hussein, M. O., Siddiqui, M. N., & Tawabini, B. (2019). Comparative evaluation of biosynthesized nanoscale zerovalent iron and iron-oxide nanoparticles in mercury adsorption. *Journal of Environmental Engineering*, *145*(7), 04019037. https://doi.-org/10.1061/(asce)ee.1943-7870.0001515

Aeisyah, A., Ismail, M. H. S. H. S., Lias, K., Izhar, S., Abas, S. N. A., Ismail, M. H. S. H. S., Kamal, M. L., & Izhar, S. (2014). Adsorption process of heavy metals by low-cost adsorbent: A review. *Research Journal of Chemistry and Environment*, *18*(4), 91–102. https://doi.org/10.5829/idosi.wasj.2013.28.11.1874

Afolabi, F. O., Musonge, P., & Bakare, B. F. (2021). Bio-sorption of a bi-solute system of copper and lead ions onto banana peels: Characterization and optimization. *Journal of*

Environmental Health Science and Engineering, *19*(1), 613–624. https://doi.org/10.-1007/s40201-021-00632-x

Afroze, S., & Sen, T. K. (2018). A Review on heavy metal ions and dye adsorption from water by agricultural solid waste adsorbents. *Water, Air, and Soil Pollution*, *229*(7), 1–50. https://doi.org/10.1007/s11270-018-3869-z

Agarwal, S., Tyagi, I., Gupta, V. K., Bagheri, A. R., Ghaedi, M., Asfaram, A., Hajati, S., & Bazrafshan, A. A. (2016). Rapid adsorption of ternary dye pollutants onto copper (I) oxide nanoparticle loaded on activated carbon: Experimental optimization via response surface methodology. *Journal of Environmental Chemical Engineering*, *4*(2), 1769–1779. https://doi.org/10.1016/j.jece.2016.03.002

Agarwal, Shilpi, Tyagi, I., Gupta, V. K., Dehghani, M. H., Jaafari, J., Balarak, D., & Asif, M. (2016). Rapid removal of noxious nickel(II) using novel γ-alumina nanoparticles and multiwalled carbon nanotubes: Kinetic and isotherm studies. *Journal of Molecular Liquids*, *224*, 618–623. https://doi.org/10.1016/j.molliq.2016.10.032

Agbajelola, D. O. , Okafor, J. O., & Peter, S. (2015). Studies on the adsorption of heavy metals in a paint industry effluent using activated maize cob. *Journal of Multidisciplinary Engineering Science and Technology*, *2*(2), 3159–3199. www.jmest.org

Ahamad, K. U., Singh, R., Baruah, I., Choudhury, H., & Sharma, M. R. (2018). Equilibrium and kinetics modeling of fluoride adsorption onto activated alumina, alum and brick powder. *Groundwater for Sustainable Development*, *7*, 452–458. https://doi.org/10.-1016/j.gsd.2018.06.005

Ahmad, R., & Haseeb, S. (2015). Competitive adsorption of Cu(II) and Ni(II) on Luffa acutangula modified Tetraethoxysilane (LAP-TS) from the aqueous solution: Thermodynamic and isotherm studies. *Groundwater for Sustainable Development*, *1*(1–2), 146–154. https://doi.-org/10.1016/j.gsd.2016.03.001

Ahmaruzzaman, M. (2011). Industrial wastes as low-cost potential adsorbents for the treatment of wastewater laden with heavy metals. *Advances in Colloid and Interface Science*, *166*(1–2), 36–59. https://doi.org/10.1016/j.cis.2011.04.005

Ahmed, S., Unar, I. N., Khan, H. A., Maitlo, G., Mahar, R. B., Jatoi, A. S., Memon, A. Q., &

Shah, A. K. (2020). Experimental study and dynamic simulation of melanoidin adsorption from distillery effluent. *Environmental Science and Pollution Research*, *27*(9), 9619–9636. https://doi.org/10.1007/s11356-019-07441-8

Aigbe, U. O., Ukhurebor, K. E., Onyancha, R. B., Osibote, O. A., Darmokoesoemo, H., & Kusuma, H. S. (2021). Fly ash-based adsorbent for adsorption of heavy metals and dyes from aqueous solution: A review. *Journal of Materials Research and Technology*, *14*, 2751–2774. https://doi.org/10.1016/j.jmrt.2021.07.140

Ajiboye, T. O., Oyewo, O. A., & Onwudiwe, D. C. (2021). Simultaneous removal of organics and heavy metals from industrial wastewater: A review. *Chemosphere*, *262*, 1–20. https://doi.org/10.1016/j.chemosphere.2020.128379

Akhter, F., Zoppas, F. M., Soomro, M., Jatoi, A. S., Noureen, F., Akhtar, M. N., & Mehreen, F. (2021). Carbon-based sorbets for heavy metal removal from aqueous solution, discrepancies, and future prospects: A state-of-the-art review. *Biomass Conversion and Biorefinery*, *0123456789*, 1–17. https://doi.org/10.1007/s13399-021-01866-3

Akpen, G. D., Aho, M. I., & Baba, N. (2016). Preparation and characterization of activated carbons from Albizia Saman pod. *Journal of Science and Technology*, *36*(3), 44–53. https://doi.org/10.1021/ef00041a016

Al-Qodah, Z., Yahya, M. A., & Al-Shannag, M. (2017). On the performance of bioadsorption processes for heavy metal ions removal by low-cost agricultural and natural by-products bioadsorbent: A review. *Desalination and Water Treatment*, *85*(August), 339–357. https://doi.org/10.5004/dwt.2017.21256

Alalwan, H. A., Kadhom, M. A., & Alminshid, A. H. (2020). Removal of heavy metals from wastewater using agricultural byproducts. *Journal of Water Supply: Research and Technology - AQUA*, *69*(2), 99–112. https://doi.org/10.2166/aqua.2020.133

Alam, M. A., Shaikh, W. A., Alam, M. O., Bhattacharya, T., Chakraborty, S., Show, B., & Saha, I. (2018). Adsorption of As(III) and As(V) from aqueous solution by modified Cassia fistula (golden shower) biochar. *Applied Water Science*, *8*(7), 1–14. https://doi.org/10.1007/s13201-018-0839-y

Alghamdi, A. A., Al-Odayni, A. B., Saeed, W. S., Al-Kahtani, A., Alharthi, F. A., & Aouak,

T. (2019). Efficient adsorption of lead(II) from aqueous phase solutions using polypyrrole-based activated carbon. *Materials*, *12*(12), 1–16. https://doi.org/10.3390/ma12122020

Ali, H., Khan, E., & Ilahi, I. (2019). Environmental chemistry and ecotoxicology of hazardous heavy metals: Environmental persistence, toxicity, and bioaccumulation. *Journal of Chemistry*, *2019*, 1–14. https://doi.org/10.1155/2019/6730305

Alimohammadi, M., Saeedi, Z., Akbarpour, B., Rasoulzadeh, H., Yetilmezsoy, K., Al-Ghouti, M. A., Khraisheh, M., & McKay, G. (2017). Adsorptive removal of arsenic and mercury from aqueous solutions by eucalyptus leaves. *Water, Air, and Soil Pollution*, *228*(11), 1–27. https://doi.org/10.1007/s11270-017-3607-y

Alimohammady, M., Jahangiri, M., Kiani, F., & Tahermansouri, H. (2017). Highly efficient simultaneous adsorption of Cd(II), Hg(II) and As(III) ions from aqueous solutions by modification of graphene oxide with 3-aminopyrazole: Central composite design optimization. *New Journal of Chemistry*, *41*(17), 8905–8919. https://doi.org/10.1039/-c7nj01450c

Amar, M. Ben, Walha, K., & Salvadó, V. (2020). Evaluation of Olive Stones for Cd(II), Cu(II), Pb(II) and Cr(VI) Biosorption from Aqueous Solution: Equilibrium and Kinetics. *International Journal of Environmental Research*, *14*(2), 193–204. https://doi.org/10.-1007/s41742-020-00246-5

Ameri, A., Tamjidi, S., Dehghankhalili, F., Farhadi, A., & Saati, M. A. (2020). Application of algae as low cost and effective bio-adsorbent for removal of heavy metals from wastewater: A review study. *Environmental Technology Reviews*, *9*(1), 85–110. https://doi.org/10.-1080/21622515.2020.1831619

Anupam, K., Dutta, S., Bhattacharjee, C., & Datta, S. (2011). Adsorptive removal of chromium(VI) from aqueous solution over powdered activated carbon: Optimisation through response surface methodology. *Chemical Engineering Journal*, *173*(1), 135–143. https://doi.org/10.-1016/j.cej.2011.07.049

Anyika, C., Asri, N. A. M., Majid, Z. A., Jaafar, J., & Yahya, A. (2017). Batch sorption–desorption of As(III) from waste water by magnetic palm kernel shell activated carbon

using optimized Box–Behnken design. *Applied Water Science*, *7*(8), 4573–4591. https://doi.-org/10.-1007/s13201-017-0610-9

APHA. (1989). *APHA- Standard method for the examination of water and waste water*. American Water Works Association and Water Pollution; Control Federation.

Archin, S., Sharifi, S. H., & Asadpour, G. (2019). Optimization and modeling of simultaneous ultrasound-assisted adsorption of binary dyes using activated carbon from tobacco residues: Response surface methodology. *Journal of Cleaner Production*, *239*, 264–80. https://doi.org/10.1016/j.jclepro.2019.118136

Aslani, H., Kosari, T. E., Naseri, S., Nabizadeh, R., & Khazaei, M. (2018). Hexavalent chromium removal from aqueous solution using functionalized chitosan as a novel nano-adsorbent: Modeling and optimization, kinetic, isotherm, and thermodynamic studies, and toxicity testing Time X 4 Initial concentration of chromium X i Variabl. *Environmental Science and Pollution Research*, 1–15

Azadegan, F., Bidhendi, M. E., & Badiei, A. (2019). Removal of Hg(II) Ions from Aqueous Environment with the Use of Modified LUS-1 as New Nanostructured Adsorbent. *International Journal of Environmental Research*, *13*(3), 557–569. https://doi.org/10.1007/-s41742-019-00195-8

Babapoor, A., Rafiei, O., Mousavi, Y., Azizi, M. M., Paar, M., & Nuri, A. (2022). Comparison and Optimization of operational parameters in removal of heavy metal ions from aqueous solutions by low-cost adsorbents. *International Journal of Chemical Engineering*, *2022*, 1–21. https://doi.org/10.1155/2022/3282448

Baby, R., Saifullah, B., & Hussein, M. Z. (2019). Palm Kernel Shell as an effective adsorbent for the treatment of heavy metal contaminated water. *Scientific Reports*, *9*(1), 1–11. https://doi.org/10.1038/s41598-019-55099-6

Baby, S. R., Saifullah, B., & Rehman, F. U. (2018). Greener method for the removal of toxic metal ions from the wastewater by application of agricultural waste as an adsorbent. *Water*, *10*(10), 1316. https://doi.org/10.3390/w10101316

Bakshe, P., & Jugade, R. (2023). Phytostabilization and rhizofiltration of toxic heavy metals by heavy metal accumulator plants for sustainable management of contaminated industrial

sites: A comprehensive review. *Journal of Hazardous Materials Advances*, *10*, 1–16. https://doi.org/10.1016/j.hazadv.2023.100293

Banchhor, A., Pandey, M., & Pandey, P. K. (2021). Optimization of Adsorption parameters for effective removal of hexavalent chromium using simarouba glauca from aqueous solution. *Water Conservation Science and Engineering*, *6*(3), 127–144. https://doi.org/10.-1007/s41101-021-00106-z

Bandara, Y. W., Gamage, P., & Gunarathne, D. S. (2020). Hot water washing of rice husk for ash removal: The effect of washing temperature, washing time and particle size. *Renewable Energy*, *153*, 646–652. https://doi.org/10.1016/j.renene.2020.02.038

Bangaraiah, P., & Sarathbabu, B. (2019). Optimization of process parameters in removal of lead from aqueous solution through response surface methodology. *Chemical Engineering Communications*, *206*(8), 986–993. https://doi.org/10.1080/00986445.2018.1541800

Barakat, M. A. (2011). New trends in removing heavy metals from industrial wastewater. *Arabian Journal of Chemistry*, *4*(4), 361–377. https://doi.org/10.1016/j.arabjc.2010.-07.019

Bashir, A., Malik, L. A., Ahad, S., Manzoor, T., Bhat, M. A., Dar, G. N., & Pandith, A. H. (2019). Removal of heavy metal ions from aqueous system by ion-exchange and biosorption methods. *Environmental Chemistry Letters*, *17*(2), 729–754. https://doi.org/10.1007/s10311-018-00828-y

Bastami, S., Ghassa, S., Seyedhakimi, A., & Chelgani, S. C. (2020). Adsorption of mercury from a cyanide leaching solution using various activation rates of granular activated carbon: A laboratory-and industrial-scale study. *Sustainability (Switzerland)*, *12*(8), 1–10. https://doi.org/10.3390/SU12083287

Batool, S., Idrees, M., Al-Wabel, M. I., Ahmad, M., Hina, K., Ullah, H., Cui, L., & Hussain, Q. (2019). Sorption of Cr(III) from aqueous media via naturally functionalized microporous biochar: Mechanistic study. *Microchemical Journal*, *144*(June 2018), 242–253. https://doi-.org/10.1016/j.microc.2018.09.012

Baysal, A., Ozbek, N., & Akm, S. (2013). Determination of Trace Metals in Waste Water and Their Removal Processes. *Waste Water - Treatment Technologies and Recent Analytical*

Developments. https://doi.org/10.5772/52025

Bayuo, J, Abukari, M. A., & Pelig-Ba, K. B. (2020). Desorption of chromium(VI) and lead(II) ions and regeneration of the exhausted adsorbent. *Applied Water Science*, *10*(7), 1–6. https://doi.org/10.1007/s13201-020-01250-y

Bayuo, J, Kenneth, B. P., & Abukari, M. A. (2019). Optimization of adsorption parameters for effective removal of lead(II) from aqueous solution. *Physical Chemistry: An Indian Journal Research Article* |, *14*(1), 123. www.tsijournals.com

Bayuo, J, Pelig-Ba, K. B., & Abukari, M. A. (2019). Adsorptive removal of chromium(VI) from aqueous solution unto groundnut shell. *Applied Water Science*, *9*(4), 1–11. https://doi.org/10.1007/s13201-019-0987-8

Bayuo, J, Rwiza, M. J., & Mtei, K. M. (2023). Non-competitive and competitive detoxification of As(III) ions from single and binary biosorption systems and biosorbent regeneration. *Biomass Conversion and Biorefinery*, 1–28. https://doi.org/10.1007/s13399-022-03734-0

Bayuo, J. (2021). Decontamination of cadmium(II) from synthetic wastewater onto shea fruit shell biomass. *Applied Water Science*, *11*(5), 1–8. https://doi.org/10.1007/s13201-021-01416-2

Bayuo, J., Abukari, M. A., & Pelig-Ba, K. B. (2020). Optimization using central composite design (CCD) of response surface methodology (RSM) for biosorption of hexavalent chromium from aqueous media. *Applied Water Science*, *10*(6). https://doi.org/10.1007/-s13201-020-01213-3

Bayuo, J., Pelig-ba, K. B., Abdullaiabukari, M., & Abukari, M. A. (2018). Isotherm modeling of lead(II) adsorption from aqueous solution using groundnut shell as a low-cost adsorbent. *IOSR Journal of Applied Chemistry*, *11*(11), 18–23. https://doi.-org/10.9790/5736-1111011823

Bayuo, J., Pelig-Ba, K. B., & Abukari, M. A. (2019). Adsorptive removal of chromium(VI) from aqueous solution unto groundnut shell. *Applied Water Science*, *9*(4), 1–11. https://doi.org/10.-1007/s13201-019-0987-8

Bayuo, J., Rwiza, M., Abukari, M. A., Pelig-Ba, K. B., & Mtei, K. (2022). Modeling and

optimization of independent factors influencing lead(II) biosorption from aqueous systems: A statistical approach. *Scientific African*, *16*, 1–16. https://doi.org/10.-1016/j.sciaf.2022.-e01270

Bazrchi, S., Bahram, M., & Nouri, S. (2018). Equilibrium and Kinetic studies on the removal of acid red-14 from aqueous solutions using PSMA. *Iranian Journal of Science and Technology, Transaction A: Science*, *42*(1), 203–208. https://doi.org/10.1007/s40995-018-0489-9

Bedia, J., Peñas-Garzón, M., Gómez-Avilés, A., Rodriguez, J. J., & Belver, C. (2020). Review on Activated Carbons by Chemical Activation with FeCl3. *C — Journal of Carbon Research*, *6*(2), 21. https://doi.org/10.3390/c6020021

Belachew, N., & Hinsene, H. (2020). Preparation of cationic surfactant-modified kaolin for enhanced adsorption of hexavalent chromium from aqueous solution. *Applied Water Science*, *10*(1), 1–8. https://doi.org/10.1007/s13201-019-1121-7

Ben Khalifa, E., Rzig, B., Chakroun, R., Nouagui, H., & Hamrouni, B. (2019). Application of response surface methodology for chromium removal by adsorption on low-cost biosorbent. *Chemometrics and Intelligent Laboratory Systems*, *189*, 18–26. https://doi.org/10.1016/j.-chemolab.2019.03.014

Bergna, D., Hu, T., Prokkola, H., Romar, H., & Lassi, U. (2020). Effect of Some Process Parameters on the Main Properties of Activated Carbon Produced from Peat in a Lab-Scale Process. *Waste and Biomass Valorization*, *11*(6), 2837–2848. https://doi.org/10.-1007/-s12649-019-00584-2

Bessaha, F., Mahrez, N., Marouf-Khelifa, K., Çoruh, A., & Khelifa, A. (2019). Removal of Congo red by thermally and chemically modified halloysite: equilibrium, FTIR spectroscopy, and mechanism studies. *International Journal of Environmental Science and Technology*, *16*(8), 4253–4260. https://doi.org/10.1007/s13762-018-2041-z

Bhatti, Z. A. (2021). Arsenic(III) Removal from aqueous water by indigenous iron ore adsorbent from balochistan province of Pakistan. *Mehran University Research Journal of Engineering and Technology*, *40*(1), 16–30. https://doi.org/10.22581/muet1982.2101.02

Bibi, S., Farooqi, A., Yasmin, A., Kamran, M. A., & Niazi, N. K. (2017). Arsenic and fluoride

removal by potato peel and rice husk (PPRH) ash in aqueous environments. *International Journal of Phytoremediation*, *19*(11), 1029–1036. https://doi.org/10.1080/15226514.-2017.1319329

Binaeian, E., Maleki, S., Motaghedi, N., & Arjmandi, M. (2020). Study on the performance of Cd(II) sorption using dimethylethylenediamine-modified zinc-based MOF (ZIF-8-mmen): Optimization of the process by RSM technique. *Separation Science and Technology (Philadelphia)*, *55*(15), 2713–2728. https://doi.org/10.1080/01496395.2019.1655056

Biswas, R., & Sarkar, A. (2019). Characterization of arsenite-oxidizing bacteria to decipher their role in arsenic bioremediation. *Preparative Biochemistry and Biotechnology*, *49*(1), 30–37. https://doi.org/10.1080/10826068.2018.1476883

Biswas, S., Meikap, B. C., & Sen, T. K. (2019). Adsorptive removal of aqueous phase copper (Cu^{2+}) and Nickel (Ni^{2+}) Metal ions by synthesized biochar–biopolymeric hybrid adsorbents and process optimization by response surface methodology (RSM). *Water, Air, and Soil Pollution*, *230*(8). https://doi.org/10.1007/s11270-019-4258-y

Bordoloi, S., Chetia, R., Borah, G., & Konwer, S. (2022). Removal of As(III) and As(V) from water using reduced GO-Fe0 filled PANI composite. *Journal of Applied Water Engineering and Research*, *10*(2), 117–128. https://doi.org/10.1080/23249676.2021.-1948361

Boulaiche, W., Belhamdi, B., Hamdi, B., & Trari, M. (2019). Kinetic and equilibrium studies of biosorption of M(II) (M = Cu, Pb, Ni, Zn and Cd) onto seaweed Posidonia oceanica fibers. *Applied Water Science*, *9*(8), 1–11. https://doi.org/10.1007/s13201-019-1062-1

Bratby, J. (2006). Coagulation and flocculation in water and wastewater treatment. In *Water 21* (Issue AUG.). IWA Publishing. https://doi.org/10.2166/9781780407500

Calderón, R. O. A., Abdeldayem, O. M., Pugazhendhi, A., & Rene, E. R. (2020). Current updates and perspectives of biosorption technology: An alternative for the removal of heavy metals from wastewater. *Current Pollution Reports*, *6*(1), 8–27. https://doi.org/10.-1007/s40726-020-00135-7

Chaduka, M., Guyo, U., Zinyama, N. P., Tshuma, P., & Matsinha, L. C. (2020). Modeling and Optimization of lead(II) adsorption by a novel peanut hull-g-methyl methacrylate

biopolymer using response surface methodology (RSM). *Analytical Letters*, *53*(8), 1294–1311. https://doi.org/10.1080/00032719.2019.1702993

Chai, W. S., Cheun, J. Y., Kumar, P. S., Mubashir, M., Majeed, Z., Banat, F., Ho, S. H., & Show, P. L. (2021). A review on conventional and novel materials towards heavy metal adsorption in wastewater treatment application. *Journal of Cleaner Production*, *296*, 126589. https://doi.org/10.1016/j.jclepro.2021.126589

Chen, O. P., Lin, Y. J., Cao, W. Z., & Chang, C. T. (2017). Arsenic removal with phosphorene and adsorption in solution. *Materials Letters*, *190*, 280–282. https://doi.org/10.1016/j.-matlet.2017.01.030

Chen, X., Yu, L., Zou, S., Xiao, L., & Fan, J. (2020). Zeolite Cotton in Tube: A simple robust household water treatment filter for heavy metal removal. *Scientific Reports*, *10*(1), 1–9. https://doi.org/10.1038/s41598-020-61776-8

Chen, Y., Chen, Q., Zhao, H., Dang, J., Jin, R., Zhao, W., & Li, Y. (2020). Wheat straws and corn straws as adsorbents for the removal of Cr(VI) and Cr(III) from aqueous solution: Kinetics, Isotherm, and Mechanism. *ACS Omega*, *5*(11), 6003–6009. https://doi.org/10.-1021/acsomega.9b04356

Cheng, J., Gao, J., Zhang, J., Yuan, W., Yan, S., Zhou, J., Zhao, J., & Feng, S. (2021). Optimization of Hexavalent Chromium Biosorption by Shewanella putrefaciens Using the Box-Behnken Design. *Water, Air, and Soil Pollution*, *232*(3), 1–14. https://doi.org/10.-1007/-s11270-020-04947-7

Chidozie, C. N., Chinwe, J. E., & Emmanuel, I. U. (2017). Physicochemical Conditions for Adsorption of Lead from Water by Rice Husk Ash. *Bioresources*, *12*(Demirbas 2008), 799–818

Chigondo, F., & Nyamunda, B. (2013). Removal of lead(II) and copper(II) ions from aqueous solution by baobab (Adononsia digitata) fruit shells biomass. *IOSR Journal of Applied Chemistry*, *5*(1), 43–50. http://www.iosrjournals.org/iosr-jac/papers/vol5-issue1/G0514-350.pdf

Chmielewská, E. (2019). Chapter 4-Natural zeolite: Alternative adsorbent in purification or post-treatment of waters. In Modified Clay and Zeolite Nanocomposite Materials:

Environmental and Pharmaceutical Applications. Elsevier.

Choi, S. H. (2016). On the brine re-utilization of a multi-stage flashing (MSF) desalination plant. *Desalination*, *398*, 64–76. https://doi.org/10.1016/j.desal.2016.07.020

Choudhary, M., & Bhattacharyya, K. G. (2020). As(III) and As(V) remediation in an aqueous medium using a cellulosic biosorbent: kinetics, equilibrium, and thermodynamics study. *SN Applied Sciences*, *2*(10), 1–17. https://doi.org/10.1007/s42452-020-03426-2

Çiçek, E., Cojocaru, C., Zakrzewska-Trznadel, G., Harasimowicz, M., & Miskiewicz, A. (2012). Response surface methodology for the modelling of 85Sr adsorption on zeolite 3A and pumice. *Environmental Technology*, *33*(1), 51–59. https://doi.org/10.1080/-09593330.2010.549514

Crini, G., Lichtfouse, E., Wilson, L. D., & Morin-Crini, N. (2019). Conventional and non-conventional adsorbents for wastewater treatment. *Environmental Chemistry Letters*, *17*(1), 195–213. https://doi.org/10.1007/s10311-018-0786-8

Dada, A. O., Adekola, F. A., Odebunmi, E. O., Ogunlaja, A. S., & Bello, O. S. (2021). Two–three parameters isotherm modeling, kinetics with statistical validity, desorption and thermodynamic studies of adsorption of Cu(II) ions onto zerovalent iron nanoparticles. *Scientific Reports*, *11*(1), 1–15. https://doi.org/10.1038/s41598-021-95090-8

Dahake, R., Tiwari, P., & Bansiwal, A. (2021). Multicycle adsorption and desorption for recovery of U(VI) from aqueous solution using oxime modified zeolite-A. *Journal of Radioanalytical and Nuclear Chemistry*, *327*(1), 133–142. https://doi.org/10.1007/-s10967-020-07482-1

Dakhil, I. H., Naser, G. F., & Ali, A. H. (2021). Response Surface Modeling of Arsenic Adsorption by Modified Spent Tea Leaves. *IOP Conference Series: Materials Science and Engineering*, *1090*(1), 1–11. https://doi.org/10.1088/1757-899x/1090/1/012129

Daneshvar, E., Zarrinmehr, M. J., Kousha, M., Hashtjin, A. M., Saratale, G. D., Maiti, A., Vithanage, M., & Bhatnagar, A. (2019). Hexavalent chromium removal from water by microalgal-based materials: Adsorption, desorption and recovery studies. *Bioresource Technology*, *293*(12), 56–64. https://doi.org/10.1016/j.biortech.2019.122064

Das, B. (2017). Response surface modeling of copper (II) adsorption from aqueous solution onto neem (Azadirachta indica) bark powder: Central composite design approach. *Journal of Materials and Environmental Science*, *8*(7), 2442–2454

Dawodu, F. A., Akpan, B. M., & Akpomie, K. G. (2020). Sequestered capture and desorption of hexavalent chromium from solution and textile wastewater onto low cost Heinsia crinita seed coat biomass. *Applied Water Science*, *10*(1), 1–15. https://doi.org/10.1007/-s13201-019-1114-6

Dehghani, M. H., Zarei, A., Mesdaghinia, A., Nabizadeh, R., Alimohammadi, M., & Afsharnia, M. (2017). Response surface modeling, isotherm, thermodynamic and optimization study of arsenic(V) removal from aqueous solutions using modified bentonite-chitosan (MBC). *Korean Journal of Chemical Engineering*, *34*(3), 757–767. https://doi.org/10.-1007/s11814-016-0330-0

Deravanesiyan, M., Beheshti, M., & Malekpour, A. (2015). Alumina nanoparticles immobilization onto the NaX zeolite and the removal of Cr(III) and Co(II) ions from aqueous solutions. *Journal of Industrial and Engineering Chemistry*, *21*, 580–586. https://doi.org/10.-1016/j.jiec.2014.03.023

Dewi, A. K., Sharma, R. K., Das, K., Sukul, U., Lin, P. Y., Huang, Y. H., Lu, C. M., Lu, C. K., Chen, T. H., & Chen, C. Y. (2023). Biologically-induced synthetic manganese carbonate precipitate (BISMCP) for potential applications in heavy metal removal. *Heliyon*, *9*(5), 1–12. https://doi.org/10.1016/j.heliyon.2023.e15919

Dhabab, J., Hussien, K., & Nasser, T. (2012). Removal of cadmium ions from industrial wastewater Using Iraqi Ceratophyllum demersum. *Al-Mustansiriyah Journal of Science*, *23*(8), 71–84

Dhiman, N. (2021). Binary adsorption of [Pb(II) + Co(II)] from aqueous solution using thiolated saw dust. *Water Science and Technology*, *84*(9), 2591–2600. https://doi.org/10.-2166/wst.-2021.454

Dhoble, R. M., Maddigapu, P. R., Bhole, A. G., & Rayalu, S. (2018). Development of bark-based magnetic iron oxide particle (BMIOP), a bio-adsorbent for removal of arsenic (III) from water. *Environmental Science and Pollution Research*, *25*(20), 19657–19674.

https://doi.-org/10.1007/s11356-018-1792-x

Díaz, A., Marrero, J., Cabrera, G., Coto, O., & Gómez, J. M. (2022). Biosorption of nickel, cobalt, zinc and copper ions by Serratia marcescens strain 16 in mono and multimetallic systems. *Biodegradation*, *33*(1), 33–43. https://doi.org/10.1007/s10532-021-09964-9

Djaghout, I., Affoune, A. M., Chelaghmia, M. L., & Bendjaballah, M. (2015). Experimental investigation of nickel electrodeposits brightness in the presence of surfactants: Modeling, optimization and polarization studies. *Portugaliae Electrochimica Acta*, *33*(4), 209–222. https://doi.org/10.4152/pea.201504209

Dong, X., Ma, L. Q., Zhu, Y., Li, Y., & Gu, B. (2013). Mechanistic investigation of mercury sorption by Brazilian pepper biochars of different pyrolytic temperatures based on x-ray photoelectron spectroscopy and flow calorimetry. *Environmental Science and Technology*, *47*(21), 12156–12164. https://doi.org/10.1021/es4017816

Dong, Y., & Lin, H. (2017). Competitive adsorption of Pb(II) and Zn(II) from aqueous solution by modified beer lees in a fixed bed column. *Process Safety and Environmental Protection*, *111*(Ii), 263–269. https://doi.org/10.1016/j.psep.2017.06.016

Drweesh, S. A., Fathy, N. A., Wahba, M. A., Hanna, A. A., Akarish, A. I. M., Elzahany, E. A. M., El-Sherif, I. Y., & Abou-El-Sherbini, K. S. (2016). Equilibrium, kinetic and thermodynamic studies of Pb(II) adsorption from aqueous solutions on HCl-treated Egyptian kaolin. *Journal of Environmental Chemical Engineering*, *4*(2), 1674–1684. https://doi.org/10.1016/j.-jece.2016.02.005

Dula, T., & Duke, T. N. (2019). Removal Methods of Heavy Metals from Laboratory Wastewater. *Journal of Natural Sciences Research*, *9*(2), 36–42. https://doi.org/10.-7176/jnsr/9-2-04

Dzigbor, A., & Chimphango, A. (2019). Production and optimization of NaCl-activated carbon from mango seed using response surface methodology. *Biomass Conversion and Biorefinery*, *9*(2), 421–431. https://doi.org/10.1007/s13399-018-0361-3

Ecer, Ü., Yılmaz, Ş., & Şahan, T. (2020). Investigation of Mercury(II) and Arsenic(V) adsorption onto sulphur functionalised pumice: A response surface approach for optimisation and modelling. *International Journal of Environmental Analytical Chemistry*,

00(00), 1–21. https://doi.org/10.1080/03067319.2020.1838495

Egirani, D., Latif, M. T., Wessey, N., Poyi, N. R., & Shehata, N. (2021). Preparation and characterization of powdered and granular activated carbon from Palmae biomass for mercury removal. *Applied Water Science*, *11*(1), 1–11. https://doi.org/10.1007/s13201-020-01343-8

El-Bouhy, Z. M., Reda, R. M., Mahboub, H. H., & Gomaa, F. N. (2021). Bioremediation effect of pomegranate peel on subchronic mercury immunotoxicity on African catfish (Clarias gariepinus). *Environmental Science and Pollution Research*, *28*(2), 2219–2235. https://doi.org/10.1007/s11356-020-10599-1

El-Hendawy, A. N. A., Samra, S. E., & Girgis, B. S. (2001). Adsorption characteristics of activated carbons obtained from corncobs. *Colloids and Surfaces A: Physicochemical and Engineering Aspects*, *180*(3), 209–221. https://doi.org/10.1016/S0927-7757(00)00682-8

El-Moselhy, M. M., Ates, A., & Çelebi, A. (2017). Synthesis and characterization of hybrid iron oxide silicates for selective removal of arsenic oxyanions from contaminated water. *Journal of Colloid and Interface Science*, *488*, 335–347. https://doi.org/10.1016/j.-jcis.2016.11.003

Elbah, M., Aouici, H., Meddour, I., Yallese, M. A., & Boulanouar, L. (2016). Application of response surface methodology in describing the performance of mixed ceramic tool when turning AISI 4140 steel. *Mechanics and Industry*, *17*(3), 46–58. https://doi.org/10.1051/-meca/2015076

Elkhatib, E., Moharem, M., & Hamadeen, H. (2019). Low-cost and efficient removal of mercury from contaminated water by novnanoparticles from water industry waste. *Desalination and Water Treatment*, *144*(March), 79–88. https://doi.org/10.5004/dwt.-2019.23686

Emenike, P. C., Omole, D. O., Ngene, B. U., & Tenebe, I. T. (2016). Potentiality of agricultural adsorbent for the sequestering of metal ions from wastewater. *Global Journal of Environmental Science Management*, *2*(4), 411–442. https://doi.org/10.22034/gjesm.-2016.02.04.010

Essomba, J. S., Nsami, J. N. D. I., Desire, P., Belibi, B., Tagne, G. M., & Mbadcam, J. K.

(2014). Adsorption of Cadmium (II) Ions from Aqueous Solution onto Kaolinite and Metakaolinite. *2*(1), 11–30.

Ezeonuegbu, B. A., Machido, D. A., Whong, C. M. Z., Japhet, W. S., Alexiou, A., Elazab, S. T., Qusty, N., Yaro, C. A., & Batiha, G. E. S. (2021). Agricultural waste of sugarcane bagasse as efficient adsorbent for lead and nickel removal from untreated wastewater: Biosorption, equilibrium isotherms, kinetics and desorption studies. *Biotechnology Reports*, *30*, 1–10. https://doi.org/10.1016/j.btre.2021.e00614

Fabre, E., Lopes, C. B., Vale, C., Pereira, E., & Silva, C. M. (2020). Valuation of banana peels as an effective biosorbent for mercury removal under low environmental concentrations. *Science of the Total Environment*, *709*, 135883. https://doi.org/10.1016/j.scitotenv.-2019.135883

Fan, H. J., & Anderson, P. R. (2005). Copper and cadmium removal by Mn oxide-coated granular activated carbon. *Separation and Purification Technology*, *45*(1), 61–67. https://doi.org/10.-1016/j.seppur.2005.02.009

Fanta, F. T., Dubale, A. A., Bebizuh, D. F., & Atlabachew, M. (2019). Copper doped zeolite composite for antimicrobial activity and heavy metal removal from waste water. *BMC Chemistry*, *13*(3), 1–12. https://doi.org/10.1186/s13065-019-0563-1

Farnane, M., Machrouhi, A., Elhalil, A., Abdennouri, M., Qourzal, S., Tounsadi, H., & Barka, N. (2018). New Sustainable Biosorbent Based on Recycled Deoiled Carob Seeds: Optimization of Heavy Metals Remediation. *Journal of Chemistry*, *2018*, 1–17. https://doi.-org/10.1155/2018/5748493

Filote, C., Volf, I., Santos, S. C. R., & Botelho, C. M. S. (2019). Bioadsorptive removal of Pb(II) from aqueous solution by the biorefinery waste of Fucus spiralis. *Science of the Total Environment*, *648*, 1201–1209. https://doi.org/10.1016/j.scitotenv.2018.08.210

Fiyadh, S. S., Alardhi, S. M., Al Omar, M., Aljumaily, M. M., Al Saadi, M. A., Fayaed, S. S., Ahmed, S. N., Salman, A. D., Abdalsalm, A. H., Jabbar, N. M., & El-Shafi, A. (2023). A comprehensive review on modelling the adsorption process for heavy metal removal from waste water using artificial neural network technique. *Heliyon*, *9*(4), 1–11. https://doi.-org/10.1016/j.heliyon.2023.e15455

Flores-Trujillo, A. K. I., Mussali-Galante, P., de Hoces, M. C., Blázquez-García, G., Saldarriaga-Noreña, H. A., Rodríguez-Solís, A., Tovar-Sánchez, E., Sánchez-Salinas, E., & Ortiz-Hernández, L. (2021). Biosorption of heavy metals on Opuntia fuliginosa and Agave angustifolia fibers for their elimination from water. *International Journal of Environmental Science and Technology*, *18*(2), 441–454. https://doi.org/10.1007/s13762-020-02832-8

Flores, C. G., Schneider, H., Marcilio, N. R., Ferret, L., & Oliveira, J. C. P. (2017). Potassic zeolites from Brazilian coal ash for use as a fertilizer in agriculture. *Waste Management*, *70*, 263–271. https://doi.org/10.1016/j.wasman.2017.08.039

Fooladgar, S., Teimouri, A., & Ghanavati Nasab, S. (2019). Highly efficient removal of lead ions from aqueous solutions using chitosan/rice husk ash/nano alumina with a focus on optimization by response surface methodology: Isotherm, Kinetic, and Thermodynamic Studies. *Journal of Polymers and the Environment*, *27*(5), 1025–1042. https://doi.org/10.-1007/s10924-019-01385-3

Foroutan, R., Mohammadi, R., Adeleye, A. S., Farjadfard, S., Esvandi, Z., Arfaeinia, H., Sorial, G. A., Ramavandi, B., & Sahebi, S. (2019). Efficient arsenic(V) removal from contaminated water using natural clay and clay composite adsorbents. *Environmental Science and Pollution Research*, *26*(29), 29748–29762. https://doi.org/10.1007/s11356-019-06070-5

Gaur, N., Kukreja, A., Yadav, M., & Tiwari, A. (2018). Adsorptive removal of lead and arsenic from aqueous solution using soya bean as a novel biosorbent: Equilibrium isotherm and thermal stability studies. *Applied Water Science*, *8*(4), 1–12. https://doi.org/10.1007/-s13201-018-0743-5

Gautam, P. K., Gautam, R. K., Banerjee, S., Chattopadhyaya, M. C., & Pandey, J. D. (2016). Heavy metals in the environment: Fate, transport, toxicity and remediation technologies. In *Heavy Metals: Sources, Toxicity and Remediation Techniques* (pp. 101–130).

Gerard, N., Santhana Krishnan, R., Ponnusamy, S. K., Cabana, H., & Vaidyanathan, V. K. (2016). Adsorptive potential of dispersible chitosan coated iron-oxide nanocomposites toward the elimination of arsenic from aqueous solution. *Process Safety and Environmental Protection*, *104*, 185–195. https://doi.org/10.1016/j.psep.2016.09.006

Ghaee, M., Shariaty-Niassar, M., Barzin, J., & Zarghan, A. (2012). Adsorption of macroporous membrane: Equilibrium study. *Applied Surface Science*, *258*, 7732–7743

Ghanavati Nasab, S., Teimouri, A., Hemmasi, M., Jafari Harandi, Z., & Javaheran Yazd, M. (2021). Removal of Cd(II) ions from aqueous solutions by nanodiopside as a novel and green adsorbent: Optimisation by response surface methodology. *International Journal of Environmental Analytical Chemistry*, *101*(14), 2128–2149. https://doi.org/10.1080/-03067319.2019.1699917

Ghosh, R. K., Ray, D. P., Chakraborty, S., Saha, B., Manna, K., Tewari, A., & Sarkar, S. (2021). Cadmium removal from aqueous medium by jute stick activated carbon using response surface methodology: factor optimisation, equilibrium, and regeneration. *International Journal of Environmental Analytical Chemistry*, *101*(14), 2171–2188. https://doi.org/10.-1080/03067319.2019.1700964

Gilcreas, F. W. (1967). Future of standard methods for the examination of water and wastewater. In *Health laboratory science* (23rd ed., Vol. 4, Issue 3). American Public Health Association, American Water Works Association, and Water Environment Federation. http://www.-ajph.org/cgi/doi/10.2105/AJPH.51.6.940-a

Giraldo, S., Robles, I., Ramirez, A., Flórez, E., & Acelas, N. (2020). Mercury removal from wastewater using agroindustrial waste adsorbents. *SN Applied Sciences*, *2*(6), 1–17. https://doi.org/10.1007/s42452-020-2736-x

Giri, D. D., Jha, J. M., Tiwari, A. K., Srivastava, N., Hashem, A., Alqarawi, A. A., Abd_Allah, E. F., & Pal, D. B. (2021). Java plum and amaltash seed biomass based bio-adsorbents for synthetic wastewater treatment. *Environmental Pollution*, *280*, 116890. https://doi.-org/10.1016/j.envpol.2021.116890

Gottipati, R., & Mishra, S. (2010). Process optimization of adsorption of Cr(VI) on activated carbons prepared from plant precursors by a two-level full factorial design. *Chemical Engineering Journal*, *160*(1), 99–107. https://doi.org/10.1016/j.cej.2010.03.015

Guo, Y., Wang, Z., Zhou, X., & Bai, R. (2017). Removal of mercury (II) from aqueous solution with three commercial raw activated carbons. *Research on Chemical Intermediates*, *43*(4), 2273–2297. https://doi.org/10.1007/s11164-016-2761-y

Gupta, A. D., Singh, H., Jaiswal, V. K., Goswami, M., & Bhadauria, V. (2021). Improved arsenite adsorption using iron-impregnated marble dust with surface functionalized by quaternary ammonium ions. *International Journal of Environmental Science and Technology*, *18*(10), 2955–2974. https://doi.org/10.1007/s13762-020-03013-3

Gupta, S., Garg, D., & Kumar, A. (2022). Cadmium biosorption using Aloe. barbadensis Miller leaves waste powder treated with sodium bicarbonate. *Cleaner Waste Systems*, *3*(September), 100032. https://doi.org/10.1016/j.clwas.2022.100032

Gupta, V. K., Rastogi, A., Dwivedi, M. K., & Mohan, D. (1997). Process development for the removal of zinc and cadmium from wastewater using slag: A blast furnace waste material. *Separation Science and Technology*, *32*(17), 2883–2912. https://doi.org/Doi 10.1080/-496399708002227

Hadiani, M. R., Khosravi-Darani, K., & Rahimifard, N. (2019). Optimization of As(III) and As(V) removal by Saccharomyces cerevisiae biomass for biosorption of critical levels in the food and water resources. *Journal of Environmental Chemical Engineering*, *7*(2), 1–9. https://doi.org/10.1016/j.jece.2019.102949

He, H., Gan, Q., & Feng, C. (2017). Preparation and application of Ni(II) ion-imprinted silica gel polymer for selective separation of Ni(II) from aqueous solution. *RSC Advances*, *7*(25), 15102–15111. https://doi.org/10.1039/c7ra00101k

He, S., Li, Y., Weng, L., Wang, J., He, J., Liu, Y., Zhang, K., Wu, Q., Zhang, Y., & Zhang, Z. (2018). Competitive adsorption of Cd2+, Pb2+ and Ni2+ onto Fe3+-modified argillaceous limestone: Influence of pH, ionic strength and natural organic matters. *Science of the Total Environment*, *637–638*, 69–78. https://doi.org/10.1016/j.scitotenv.2018.04.300

Heidarinejad, Z., Dehghani, M. H., Heidari, M., Javedan, G., Ali, I., & Sillanpää, M. (2020). Methods for preparation and activation of activated carbon: A review. *Environmental Chemistry Letters*, *18*(2), 393–415. https://doi.org/10.1007/s10311-019-00955-0

Hernández, A. M., Labady, M., & Laine, J. (2014). Granular Activated Carbon from Wood Originated from Tropical Virgin Forest. *Open Journal of Forestry*, *04*(03), 208–211. https://doi.org/10.4236/ojf.2014.43027

Herrera-Barros, A., Tejada-Tovar, C., Villabona-Ortiz, A. D., Gonzalez-Delgado, A. D., &

Alvarez-Calderon, J. (2018). Adsorption of nickel and cadmium by corn cob biomass chemically modified with alumina nanoparticles. *Indian Journal of Science and Technology*, *11*(22), 1–11. https://doi.org/10.17485/ijst/2018/v11i22/126125

Hiew, B. Y. Z., Lee, L. Y., Lee, X. J., Thangalazhy-Gopakumar, S., & Gan, S. (2021). Utilisation of environmentally friendly okara-based biosorbent for cadmium(II) removal. *Environmental Science and Pollution Research*, *28*(30), 40608–40622. https://doi.-org/10.1007/s11356-020-09594-3

Hinkelmann, K. (2012). Design & Analysis of Experiments. In *Design and Analysis of Experiments* (4th ed., Vol. 3). Wiley. https://doi.org/10.1002/9781118147634

Hosseini-Bandegharaei, A., Hosseini, M. S., Jalalabadi, Y., Sarwghadi, M., Nedaie, M., Taherian, A., Ghaznavi, A., & Eftekhari, A. (2011). Removal of Hg(II) from aqueous solutions using a novel impregnated resin containing 1-(2-thiazolylazo)-2-naphthol (TAN). *Chemical Engineering Journal*, *168*(3), 1163–1173. https://doi.org/10.1016/j.-cej.2011.02.004

Hu, C., Hu, H., Tang, Y., Dai, Y., Wang, Z., & Yan, R. (2020). Comparative study on adsorption and immobilization of Cd(II) by rape component biomass. *Environmental Science and Pollution Research*, *27*(8), 8028–8033. https://doi.org/10.1007/s11356-019-07535-3

Hu, Q., Shao, J., Yang, H., Yao, D., Wang, X., & Chen, H. (2015). Effects of binders on the properties of bio-char pellets. *Applied Energy*, *157*, 508–516. https://doi.org/10.1016/j.-apenergy.2015.05.019

Hu, Q., Yang, H., Yao, D., Zhu, D., Wang, X., Shao, J., & Chen, H. (2016). The densification of bio-char: Effect of pyrolysis temperature on the qualities of pellets. *Bioresource Technology*, *200*, 521–527. https://doi.org/10.1016/j.biortech.2015.10.077

Hu, Y., Liu, X., Bai, J., Shih, K., Zeng, E. Y., & Cheng, H. (2013). Assessing heavy metal pollution in the surface soils of a region that had undergone three decades of intense industrialization and urbanization. *Environmental Science and Pollution Research*, *20*(9), 6150–6159. https://doi.org/10.1007/s11356-013-1668-z

Ideta, K., Kim, D. W., Kim, T., Nakabayashi, K., Miyawaki, J., Park, J. Il, & Yoon, S. H.

(2020). 19F ex situ solid-state nmr study on structural differences in pores of activated carbon series derived from chemical and physical activation processes for EDLCs. *Journal of Physical Chemistry C*, *124*(23), 12457–12465. https://doi.org/10.1021/acs.-jpcc.0c02106

Iftekhar, S., Ramasamy, D. L., Srivastava, V., Asif, M. B., & Sillanpää, M. (2018). Understanding the factors affecting the adsorption of Lanthanum using different adsorbents: A critical review. *Chemosphere*, *204*, 413–430. https://doi.org/10.1016/j.-chemosphere.-2018.04.053

Igberase, E., & Osifo, P. (2015). Equilibrium, kinetic, thermodynamic and desorption studies of cadmium and lead by polyaniline grafted cross-linked chitosan beads from aqueous solution. *Journal of Industrial and Engineering Chemistry*, *26*, 340–347. https://doi.-org/10.1016/j.jiec.2014.12.007

Igberase, E., Osifo, P., & Ofomaja, A. (2017). The Adsorption of Pb, Zn, Cu, Ni, and Cd by Modified ligand in a single component aqueous solution: Equilibrium, Kinetic, Thermodynamic, and Desorption Studies. *International Journal of Analytical Chemistry*, *2017*, 1–15. https://doi.org/10.1155/2017/6150209

Imla Syafiqah, M. S., & Yussof, H. W. (2018). Adsorption of mercury from aqueous solutions using palm oil fuel ash as an adsorbent - Batch studies. *IOP Conference Series: Materials Science and Engineering*, *334*(1), 1–8. https://doi.org/10.1088/1757-899X/334/1/012039

Iqbal, M., Iqbal, N., Bhatti, I. A., Ahmad, N., & Zahid, M. (2016). Response surface methodology application in optimization of cadmium adsorption by shoe waste: A good option of waste mitigation by waste. *Ecological Engineering*, *88*(265), 265–275. https://doi.org/10.1016/j.-ecoleng.2015.12.041

Jagirani, M. S., Balouch, A., Mahesar, S. A., Kumar, A., Abdullah, Mustafai, F. A., & Bhanger, M. I. (2020). Preparation of novel arsenic-imprinted polymer for the selective extraction and enhanced adsorption of toxic As(III) ions from the aqueous environment. *Polymer Bulletin*, *77*(10), 5261–5279. https://doi.org/10.1007/s00289-019-03008-2

Jahangiri, K., Yousefi, N., Ghadiri, S. K., Fekri, R., Bagheri, A., & Talebi, S. S. (2019). Enhancement adsorption of hexavalent chromium onto modified fly ash from aqueous

solution; optimization; isotherm, kinetic and thermodynamic study. *Journal of Dispersion Science and Technology*, *40*(8), 1147–1158. https://doi.org/10.1080/01932691.2018.-1496841

Jain, M., Garg, V. K., Paliwal, R., Kadirvelu, K., & Chaudhry, S. (2021). Optimization of cadmium(II) removal from water using sunflower waste carbon: A statistical approach. *Toxin Reviews*, *40*(4), 1373–1382. https://doi.org/10.1080/15569543.2020.1718163

Jalees, M. I., Farooq, M. U., Basheer, S., & Asghar, S. (2019). Removal of Heavy Metals from Drinking Water Using Chikni Mitti (Kaolinite): Isotherm and Kinetics. *Arabian Journal for Science and Engineering*, *44*(7), 6351–6359. https://doi.org/10.1007/s13369-019-03722-z

Jamileh, K., Ghorbani, M. H., Aghaie, H., & Fazaeli, R. (2020). Investigation of Zn(II) Adsorption from aqueous solution onto copper oxide with different morphologies: Optimization Using Response Surface Methodology. *Russian Journal of Physical Chemistry A*, *94*(9), 1921–1929. https://doi.org/10.1134/S0036024420090149

Janković, B., Manić, N., Dodevski, V., Radović, I., Pijović, M., Katnić, Đ., & Tasić, G. (2019). Physico-chemical characterization of carbonized apricot kernel shell as precursor for activated carbon preparation in clean technology utilization. *Journal of Cleaner Production*, *236*, 117614. https://doi.org/10.1016/j.jclepro.2019.117614

Javid, A., Roudbari, A., Yousefi, N., Fard, M. A., Barkdoll, B., Talebi, S. S., Nazemi, S., Ghanbarian, M., & Ghadiri, S. K. (2020). Modeling of chromium(VI) removal from aqueous solution using modified green-Graphene: RSM-CCD approach, optimization, isotherm, and kinetic studies. *Journal of Environmental Health Science and Engineering*, *18*(2), 515–529. https://doi.org/10.1007/s40201-020-00479-8

Javidi Alsadi, K., & Esfandiari, N. (2019). Synthesis of activated carbon from sugarcane bagasse and application for mercury adsorption. *Pollution*, *5*(3), 585–596. https://doi.org/10.22059/-poll.2019.269364.540

Jayakumar, V., Govindaradjane, S., & Rajasimman, M. (2019). Isotherm and kinetic modeling of sorption of cadmium onto a novel red algal sorbent, Hypnea musciformis. *Modeling Earth Systems and Environment*, *5*(3), 793–803. https://doi.org/10.1007/s40808-018-

0566-2

Jjagwe, J., Olupot, P. W., Menya, E., and Kalibbala, H. M. (2021). Synthesis and application of granular activated carbon from biomass waste materials for water treatment: A Review. *Journal of Bioresources and Bioproducts*, *6*(4), 292–322. https://doi.org/10.1016/j.jobab.-2021.03.003

Joseph, L., Jun, B. M., Flora, J. R. V., Park, C. M., & Yoon, Y. (2019). Removal of heavy metals from water sources in the developing world using low-cost materials: A review. *Chemosphere*, *229*, 142–159. https://doi.org/10.1016/j.chemosphere.2019.04.198

Joshi, S., Sharma, M., Kumari, A., Shrestha, S., & Shrestha, B. (2019). Arsenic removal fromwater by adsorption onto iron oxide/nano-porous carbon magnetic composite. *Applied Sciences (Switzerland)*, *9*(18), 1–12. https://doi.org/10.3390/app9183732

Kaakani, M. . (2012). *Heavy metal removal from wastewater using novel adsorbent*. American University of Sharjah, College of Engineering.

Kanaujia, S., Singh, B., & Singh, S. K. (2015). Removal of Fluoride from groundwater by carbonised punica granatum carbon bio-adsorbent. *Journal of Geoscience and Environment Protection*, *03*(04), 1–9. https://doi.org/10.4236/gep.2015.34001

Kango, S., and Kumar, R. (2016). Low-cost magnetic adsorbent for As(III) removal from water: adsorption kinetics and isotherms. *Environmental Monitoring and Assessment*, *188*(1), 1–14. https://doi.org/10.1007/s10661-015-5077-2

Karami, A., Karimyan, K., Davoodi, R., Karimaei, M., Sharafie, K., Rahimi, S., Khosravi, T., Miri, M., Sharafi, H., & Azari, A. (2017). Application of response surface methodology for statistical analysis, modeling, and optimization of malachite green removal from aqueous solutions by manganese-modified pumice adsorbent. *Desalination and Water Treatment*, *89*, 150–161. https://doi.org/10.5004/dwt.2017.21366

Karmaker, S. C., Eljamal, O., & Saha, B. B. (2021). Response surface methodology for strontium removal process optimization from contaminated water using zeolite nanocomposites. *Environmental Science and Pollution Research*, 1–17. https://doi.org/10.1007/s11356-021-14503-3

Khan, F. S. A., Mubarak, N. M., Khalid, M., Walvekar, R., Abdullah, E., Mazari, S. A., Nizamuddin, S., & Karri, R. R. (2020). Magnetic nanoadsorbents' potential route for heavy metals removal: A review. *Environmental Science and Pollution Research*, *27*(19), 24342–24356. https://doi.org/10.1007/s11356-020-08711-6

Khan, N., Kumar, D., & Kumar, P. (2019). Microwave Assisted synthesis of polyvinylbutyral-silica composites for mercury removal application. *ChemistrySelect*, *4*(6), 1979–1984. https://doi.org/10.1002/slct.201803426

Khan, S. A., & Imteaz, M. A. (2021). Experimental Studies on arsenic removal efficiencies through adsorption using different natural adsorbents. *Water, Air, and Soil Pollution*, *232*(1), 1–10. https://doi.org/10.1007/s11270-020-04977-1

Khan, S. U., Zaidi, R., Shaik, F., Farooqi, I. H., Azam, A., Abuhimd, H., & Ahmed, F. (2021). Evaluation of fe-mg binary oxide for As (III) adsorption - synthesis, characterization and kinetic modelling. *Nanomaterials*, *11*(3), 1–16. https://doi.org/10.3390/nano11030805

Khelifi, O., Affoune, A. M., Nacef, M., Chelaghmia, M. L., & Laksaci, H. (2022). Response Surface modeling and optimization of Ni(II) and Cu(II) ions competitive adsorption capacity by sewage sludge activated carbon. *Arabian Journal for Science and Engineering*, *47*(5), 5797–5809. https://doi.org/10.1007/s13369-021-05534-6

Khorshidi, P., Shirazi, R. H. S. M., Miralinaghi, M., Moniri, E., & Saadi, S. (2020). Adsorptive removal of mercury(II), copper(II), and lead(II) ions from aqueous solutions using glutathione-functionalized $NiFe_2O_4$/graphene oxide composite. *Research on Chemical Intermediates*, *46*(7), 3607–3627. https://doi.org/10.1007/s11164-020-04164-1

Kim, K. J., Kim, D. H., Yoo, J. C., & Baek, K. (2011). Electrokinetic extraction of heavy metals from dredged marine sediment. *Separation and Purification Technology*, *79*(2), 164–169. https://doi.org/10.1016/j.seppur.2011.02.010

Kobayashi, Y., Ogata, F., Nakamura, T., & Kawasaki, N. (2020). Synthesis of novel zeolites produced from fly ash by hydrothermal treatment in alkaline solution and its evaluation as an adsorbent for heavy metal removal. *Journal of Environmental Chemical Engineering*, *8*(2), 103687. https://doi.org/10.1016/j.jece.2020.103687

Kong, H., He, J., Gao, Y., Wu, H., & Zhu, X. (2011). Cosorption of phenanthrene and

mercury(II) from aqueous solution by soybean stalk-based biochar. *Journal of Agricultural and Food Chemistry*, *59*(22), 12116–12123. https://doi.org/10.1021/-jf202924a

Kragović, M., Pašalić, S., Marković, M., Petrović, M., Nedeljković, B., Momčilović, M., & Stojmenović, M. (2018). Natural and modified zeolite—alginate composites. Application for removal of heavy metal cations from contaminated water solutions. *Minerals*, *8*(1), 1–16. https://doi.org/10.3390/min8010011

Krika, F., Azzouz, N., & Ncibi, M. C. (2016). Adsorptive removal of cadmium from aqueous solution by cork biomass: Equilibrium, dynamic and thermodynamic studies. *Arabian Journal of Chemistry*, *9*, S1077–S1083. https://doi.org/10.1016/j.arabjc.2011.12.013

Krishna, R. H., & Swamy, A. V. V. S. (2012). Physico-chemical key parameters , Langmuir and Freundlich isotherm and Lagergren rate constant studies on the removal of divalent nickel from the aqueous solutions onto powder of calcined brick. *International Journal of Engineering Research and Development*, *4*(1), 29–38.

Kumar, A., Sidharth, S., & Kandasubramanian, B. (2023). A review on algal biosorbents for heavy metal remediation with different adsorption isotherm models. *Environmental Science and Pollution Research*, 39474–39493. https://doi.org/10.1007/s11356-023-25710-5

Kumar, D., Pandey, L. K., & Gaur, J. P. (2016). Metal sorption by algal biomass: From batch to continuous system. *Algal Res*, *18*, 95–109. https://doi.org/10.1016/j.algal.2016.05.026

Kumar, H., Maurya, K. L., Gehlaut, A. K., Singh, D., Maken, S., Gaur, A., & Kamsonlian, S. (2020). Adsorptive removal of chromium(VI) from aqueous solution using binary bio-polymeric beads made from bagasse. *Applied Water Science*, *10*(1), 1–10. https://doi.org/10.1007/s13201-019-1101-y

Kumar, S., Prasad, S., Yadav, K. K., Shrivastava, M., Gupta, N., Nagar, S., Bach, Q. V., Kamyab, H., Khan, S. A., Yadav, S., & Malav, L. C. (2019). Hazardous heavy metals contamination of vegetables and food chain: Role of sustainable remediation approaches: A review. *Environmental Research*, *179*, 108792. https://doi.org/10.1016/j.envres.2019.-108792

Kumari, B., Tiwary, R. K., Yadav, M., & Singh, K. M. P. (2021). Nonlinear regression analysis and response surface modeling of Cr (VI) removal from synthetic wastewater by an agro-waste Cocos Nucifera: Box-Behnken Design (BBD). *International Journal of Phytoremediation*, *23*(8), 791–808. https://doi.org/10.1080/15226514.2020.1858399

Kunde, G. B., Sehgal, B., & Ganguli, A. K. (2019). Synthesis of mesoporous rebar MWCNT/alumina composite (RMAC) nodules for the effective removal of methylene blue and Cr (VI) from an aqueous medium. *Journal of Hazardous Materials*, *374*(October 2018), 140–151. https://doi.org/10.1016/j.jhazmat.2019.03.099

Kwok, K. C. M., Koong, L. F., Al Ansari, T., & McKay, G. (2018). Adsorption/desorption of arsenite and arsenate on chitosan and nanochitosan. *Environmental Science and Pollution Research*, *25*(15), 14734–14742. https://doi.org/10.1007/s11356-018-1501-9

Labied, R., Benturki, O., Eddine Hamitouche, A. Y., & Donnot, A. (2018). Adsorption of hexavalent chromium by activated carbon obtained from a waste lignocellulosic material (Ziziphus jujuba cores): Kinetic, equilibrium, and thermodynamic study. *Adsorption Science and Technology*, *36*(3–4), 1066–1099. https://doi.org/10.1177/026361741-7750739

Lamzougui, G., Es-Said, A., Nafai, H., Chafik, D., Bouhaouss, A., & Bchitou, R. (2021). Optimization and modeling of Pb(II) adsorption from aqueous solution onto phosphogypsum by application of response surface methodology. *Phosphorus, Sulfur and Silicon and the Related Elements*, *196*(6), 521–529. https://doi.org/10.1080/10426507.-2020.1860985

Lashkenari, M. S., Davodi, B., & Eisazadeh, H. (2011). Removal of arsenic from aqueous solution using polyaniline/rice husk nanocomposite. *Korean Journal of Chemical Engineering*, *28*(7), 1532–1538. https://doi.org/10.1007/s11814-011-0014-8

Lenka, S. P., Shaikh, W. A., Owens, G., Padhye, L. P., Chakraborty, S., & Bhattacharya, T. (2021). Removal of Copper from Water and Wastewater Using Dolochar. *Water, Air, and Soil Pollution*, *232*(5), 1–15. https://doi.org/10.1007/s11270-021-05135-x

Li, C., Zhou, K., Qin, W., Tian, C., Qi, M., Yan, X., & Han, W. (2019). A Review on Heavy metals contamination in soil: Effects, Sources, and Remediation Techniques. *Soil and*

Sediment Contamination, *28*(4), 380–394. https://doi.org/10.1080/15320383.2019.-1592108

Li, Yongkui, Zhu, X., Qi, X., Shu, B., Zhang, X., Li, K., Wei, Y., & Wang, H. (2020). Removal and immobilization of arsenic from copper smelting wastewater using copper slag by in situ encapsulation with silica gel. *Chemical Engineering Journal*, *394*, 124833. https://doi.org/10.1016/j.cej.2020.124833

Li, Yuanling, Yu, H., Liu, L., & Yu, H. (2021). Application of co-pyrolysis biochar for the adsorption and immobilization of heavy metals in contaminated environmental substrates. *Journal of Hazardous Materials*, *420*, 1–12. https://doi.org/10.1016/j.jhazmat.2021.-126655

Li, Yulian, He, J., Zhang, K., Liu, T., Hu, Y., Chen, X., Wang, C., Huang, X., Kong, L., & Liu, J. (2019). Super rapid removal of copper, cadmium and lead ions from water by NTA-silica gel. *RSC Advances*, *9*(1), 397–407. https://doi.org/10.1039/C8RA08638A

Lingamdinne, L. P., Koduru, J. R., Chang, Y. Y., & Karri, R. R. (2018). Process optimization and adsorption modeling of Pb(II) on nickel ferrite-reduced graphene oxide nano-composite. *Journal of Molecular Liquids*, *250*(Ii), 202–211. https://doi.org/10.1016/j.-molliq.2017.11.174

Liu, G., Li, Z., Xu, L., Xu, X., Huang, Q., Zeng, Y., & Wen, M. (2018). The dynamics and adsorption of Cd(II) onto hydroxyapatite attapulgite composites from aqueous solution. *Journal of Sol-Gel Science and Technology*, *87*(2), 269–284. https://doi.org/10.-1007/s10971-018-4717-8

Liu, X., Xu, X., Dong, X., & Park, J. (2020). Competitive adsorption of heavy metal ions from aqueous solutions onto activated carbon and agricultural waste materials. *Polish Journal of Environmental Studies*, *29*(1), 749–761. https://doi.org/10.15244/pjoes/104455

Liu, Y, Xu, X., Qu, B., Liu, X., Yi, W., & Zhang, H. (2021). Study on adsorption properties of modified corn cob activated carbon for mercury ion. *Energies*, *14*(15), 1–22. https://doi.org/10.3390/en14154483

Liu, Yuanli, Xu, J., Cao, Z., Fu, R., Zhou, C., Wang, Z., & Xu, X. (2020). Adsorption behavior and mechanism of Pb(II) and complex Cu(II) species by biowaste-derived char with

amino functionalization. *Journal of Colloid and Interface Science*, *559*(Ii), 215–225. https://doi.org/10.1016/j.jcis.2019.10.035

Liu, Z., Sun, Y., Xu, X., Meng, X., Qu, J., Wang, Z., Liu, C., & Qu, B. (2020). Preparation, characterization and application of activated carbon from corn cob by KOH activation for removal of Hg(II) from aqueous solution. *Bioresource Technology*, *306*(600), 123154. https://doi.org/10.1016/j.biortech.2020.123154

Lu, X., Jiang, J., Sun, K., Wang, J., & Zhang, Y. (2014). Influence of the pore structure and surface chemical properties of activated carbon on the adsorption of mercury from aqueous solutions. *Marine Pollution Bulletin*, *78*(1–2), 69–76. https://doi.org/10.1016/j.-marpolbul.2013.11.007

Ma, H., Yang, J., Gao, X., Liu, Z., Liu, X., & Xu, Z. (2019). Removal of chromium(VI) from water by porous carbon derived from corn straw: Influencing factors, regeneration and mechanism. *Journal of Hazardous Materials*, *369*, 550–560. https://doi.org/10.-1016/j.jhazmat.-2019.02.063

Machrouhi, A., Farnane, M., Tounsadi, H., Kadmi, Y., Favier, L., Qourzal, S., Abdennouri, M., & Barka, N. (2019). Activated carbon from thapsia transtagana stems: Central composite design (CCD) optimization of the preparation conditions and efficient dyes removal. *Desalination and Water Treatment*, *166*, 259–278. https://doi.org/10.5004/dwt.-2019.24471

Maiti, S., Prasad, B., & Minocha, A. K. (2020). Optimization of copper removal from wastewater by fly ash using central composite design of Response surface methodology. *SN Applied Sciences*, *2*(12), 1–14. https://doi.org/10.1007/s42452-020-03892-8

Maity, S., Nanda, S., & Sarkar, A. (2021). Colocasia esculenta stem as novel biosorbent for potentially toxic metals removal from aqueous system. *Environmental Science and Pollution Research*, *28*(42), 58885–58901. https://doi.org/10.1007/s11356-021-13026-1

Makki, H. F. (2014). Removal of Cadmium(II) and lead(II) ions from aqueous solution by zeolite a4 supported on natural carbon. *International Journal of Science and Technology*, *3*(7), 391–399.

Malik, A. H., Nasreen, S., Mahmood, Q., Khan, Z. M., Sarwar, R., Jilani, G., & Khan, A.

(2010). Strategies for low-cost water defluoridation of drinking water: A review of progress. *Journal of the Chemical Society of Pakistan*, *32*(4), 550–558.

Mandal, S., Sahu, M. K., & Patel, R. K. (2013). Adsorption studies of arsenic(III) removal from water by zirconium polyacrylamide hybrid material (ZrPACM-43). *Water Resources and Industry*, *4*, 51–67. https://doi.org/10.1016/j.wri.2013.09.003

Manjuladevi, M., Anitha, R., & Manonmani, S. (2018). Kinetic study on adsorption of Cr(VI), Ni(II), Cd(II) and Pb(II) ions from aqueous solutions using activated carbon prepared from Cucumis melo peel. *Applied Water Science*, *8*(1), 1–8. https://doi.org/10.1007/s13201-018-0674-1

Mbugua, M., Mbuvi, H., & Muthengia, J. (2014). Rice Husk Ash Derived Zeolite Blended with Water Hyacinth Ash for Enhanced Adsorption of Cadmium Ions. *Current World Environment*, *9*(2), 280–286. https://doi.org/10.12944/cwe.9.2.08

Memon, A. Q., Ahmed, S., Bhatti, Z. A., Maitlo, G., Shah, A. K., Mazari, S. A., Muhammad, A., Jatoi, A. S., & Kandhro, G. A. (2021). Experimental investigations of arsenic adsorption from contaminated water using chemically activated hematite (Fe_2O_3) iron ore. *Environmental Science and Pollution Research*, *28*(10), 12898–12908. https://doi.-org/10.1007/s11356-020-11208-x

Meng, Q., Chen, H., Lin, J., Lin, Z., & Sun, J. (2017). Zeolite A synthesized from alkaline assisted pre-activated halloysite for efficient heavy metal removal in polluted river water and industrial wastewater. *Journal of Environmental Sciences (China)*, *56*, 254–262. https://doi.-org/10.1016/j.jes.2016.10.010

Menya, E., Olupot, P. W., Storz, H., Lubwama, M., & Kiros, Y. (2018). Production and performance of activated carbon from rice husks for removal of natural organic matter from water: A review. *Chemical Engineering Research and Design*, *129*, 271–296. https://doi.-org/10.1016/j.cherd.2017.11.008

Meshram, S., Dharmadhikari, S., Singh, R., & Soni, A. B. (2023). Fixed-bed adsorption of lead from battery recycling unit wastewater- Optimization using Box-Behnken method Journal of Hazardous Materials Advances Fixed-bed adsorption of lead from battery recycling unit wastewater-optimization using Box-Behnken method. *Journal of Hazardous*

Materials Advances, *10*(May), 1–8. https://doi.org/10.1016/j.hazadv.2023.100297

Meshram, S., Thakur, R. S., Jyoti, G., Thakur, C., & Soni, A. B. (2022). Optimization of lead adsorption from lead-acid battery recycling unit wastewater using H2SO4 modified activated carbon. *Journal of the Indian Chemical Society*, *99*(6), 100469. https://doi.-org/10.1016/j.jics.2022.100469

Milani, P. A., Consonni, J. L., Labuto, G., & Carrilho, E. N. V. M. (2018). Agricultural solid waste for sorption of metal ions, part II: Competitive assessment in multielemental solution and lake water. *Environmental Science and Pollution Research*, *25*(36), 35906–35914. https://doi.org/10.1007/s11356-018-1726-7

Missagia, B., Guerrero, C., Narra, S., Sun, Y., Ay, P., & Krautz, H. J. (2011). Physicomechanical properties of rice husk pellets for energy generation. *Energy and Fuels*, *25*(12), 5786–5790. https://doi.org/10.1021/ef201271b

Mitra, T., & Das, S. K. (2019). Cr(VI) removal from aqueous solution using Psidium guajava leaves as green adsorbent: column studies. *Applied Water Science*, *9*(7), 1–8. https://doi.org/10.1007/s13201-019-1029-2

Mohamed, M. S. M., El-Arabi, N. I., El-Hussein, A., El-Maaty, S. A., & Abdelhadi, A. A. (2020). Reduction of chromium(VI) by chromium-resistant Escherichia coli FACU: A prospective bacterium for bioremediation. *Folia Microbiologica*, *65*(4), 687–696. https://doi.org/10.-1007/s12223-020-00771-y

Mohd, I., Ahamed, I., & Lichtfouse, E. (2021). Water Pollution and Remediation: Heavy Metals. In *Environmental Chemistry for a Sustainable World* (Vol. 53). http://link.springer.com/10.-1007/978-3-030-54723-3%0Ahttp://link.springer.com/10.-1007/978-3-030-52421-0

Mohdee, V., Maneeintr, K., Wannachod, T., Phatanasri, S., & Pancharoen, U. (2018). Optimization of process parameters using response surface methodology for Pd(II) extraction with quaternary ammonium salt from chloride medium: Kinetic and thermodynamics study. *Chemical Papers*, *72*(12), 3129–3139. https://doi.org/10.-1007/s11696-018-0542-3

Mohubedu, R. P., Diagboya, P. N., Abasi, C. Y., Dikio, E. D., & Mtunzi, F. (2019). Magnetic

valorization of biomass and biochar of a typical plant nuisance for toxic metals contaminated water treatment. *Journal of Cleaner Production*, *209*, 1016–1024. https://doi.org/10.1016/j.-jclepro.2018.-10.215

Mondal, A., Banerjee, B., Bhaumik, A., & Mukhopadhyay, C. (2016). Activated Alumina Balls under Neat Conditions: A Green Catalyst for the Synthesis of Spiro-Heterocyclic Scaffolds by Ring-Opening versus Annulation of the Isatin Moiety. *ChemCatChem*, *8*(6), 1185–1198. https://doi.org/10.1002/cctc.201500885

Mondal, N. K, Basu, S., Sen, K., & Debnath, P. (2019). Potentiality of mosambi (Citrus limetta) peel dust toward removal of Cr(VI) from aqueous solution: An optimization study. *Applied Water Science*, *9*(4), 1–13. https://doi.org/10.1007/s13201-019-0997-6

Mondal, Naba Kumar, Samanta, A., Roy, P., & Das, B. (2019). Optimization study of adsorption parameters for removal of Cr(VI) using Magnolia leaf biomass by response surface methodology. *Sustainable Water Resources Management*, *5*(4), 1627–1639. https://doi.-org/10.1007/s40899-019-00322-5

Mondal, S., Aikat, K., & Halder, G. (2017). Biosorptive uptake of arsenic(V) by steam activated carbon from mung bean husk: Equilibrium, kinetics, thermodynamics and modeling. *Applied Water Science*, *7*(8), 4479–4495. https://doi.org/10.1007/s13201-017-0596-3

Moradi, M., Fazlzadehdavil, M., Pirsaheb, M., Mansouri, Y., Khosravi, T., & Sharafi, K. (2016). Response surface methodology (RSM) and its application for optimization of ammonium ions removal from aqueous solutions by pumice as a natural and low cost adsorbent. *Archives of Environmental Protection*, *42*(2), 33–43. https://doi.org/10.-1515/aep-2016-0018

Motaghi, M., & Ziarati, P. (2016). Adsorptive removal of cadmium and lead from Oryza sativa rice by banana peel as bio-sorbent. *Biomedical and Pharmacology Journal*, *9*(2), 739–749. https://doi.org/10.13005/bpj/998

Mourabet, M., El Rhilassi, A., El Boujaady, H., Bennani-Ziatni, M., & Taitai, A. (2017). Use of response surface methodology for optimization of fluoride adsorption in an aqueous solution by Brushite. *Arabian Journal of Chemistry*, *10*, S3292–S3302.

https://doi.org/10.1016/j.-arabjc.2013.12.028

Mukherjee, S., Thakur, A. K., Goswami, R., Mazumder, P., Taki, K., Vithanage, M., & Kumar, M. (2021). Efficacy of agricultural waste derived biochar for arsenic removal: Tackling water quality in the Indo-Gangetic plain. *Journal of Environmental Management*, *281*, 1–12. https://doi.org/10.1016/j.jenvman.2020.111814

Mukoko, T., Mupa, M., Guyo, U., & Dziike, F. (2015). Preparation of Rice Hull Activated Carbon for the Removal of Selected Pharmaceutical Waste Compounds in Hospital Effluent. *Journal of Environmental & Analytical Toxicology*, *7*(8), 1–12. https://doi.org/10.4172/2161-0525.s7-008

Mulopo, J. (2015). Continuous pilot scale assessment of the alkaline barium calcium desalination process for acid mine drainage treatment. *Journal of Environmental Chemical Engineering*, *3*(2), 1295–1302. https://doi.org/10.1016/j.jece.2014.12.001

Mustapha, S., Shuaib, D. T., Ndamitso, M. M., Etsuyankpa, M. B., Sumaila, A., Mohammed, U. M., & Nasirudeen, M. B. (2019). Adsorption isotherm, kinetic and thermodynamic studies for the removal of Pb(II), Cd(II), Zn(II) and Cu(II) ions from aqueous solutions using Albizia lebbeck pods. *Applied Water Science*, *9*(6), 1–11. https://doi.org/10.1007/-s13201-019-1021-x

Naga, B. A., Raja, S. T., Srinivasa, R. D., Suresh, K. G., & Krishna, M. G. V. (2021). Experimental and statistical analysis of As(III) adsorption from contaminated water using activated red mud doped calcium-alginate beads. *Environmental Technology (United Kingdom)*, *42*(12), 1810–1825. https://doi.org/10.1080/09593330.2019.1681520

Nagy, H., Fawzy, M., Hafez, E., & Mahmoud, A. E. D. (2023). Potentials of mono- and multi-metal ion removal from water with cotton stalks and date palm stone residuals. *Environmental Science and Pollution Research*, *0123456789*. https://doi.org/10.1007/-s11356-023-27137-4

Najafpour, A., Rajabi Khorrami, A., Aberoomand Azar, P., & Saber Tehrani, M. (2020). Study of heavy metals biosorption by tea fungus in Kombucha drink using Central Composite Design. *Journal of Food Composition and Analysis*, *86*, 103359. https://doi.-org/10.1016/j.jfca.2019.103359

Narayanasamy, S., Sundaram, V., Sundaram, T., & Vo, D. V. N. (2022). Biosorptive ascendency of plant based biosorbents in removing hexavalent chromium from aqueous solutions: Insights into isotherm and kinetic studies. *Environmental Research*, *210*(February), 112902. https://doi.org/10.1016/j.envres.2022.112902

Nazerdeylami, S., & Zare-Dorabei, R. (2019). Simultaneous adsorption of Hg2+, Cd2+ and Cu2+ ions from aqueous solution with mesoporous silica/DZ and conditions optimise with experimental design: Kinetic and isothermal studies. *Micro and Nano Letters*, *14*(8), 823–827. https://doi.org/10.1049/mnl.2018.5775

Nemeş, L., & Bulgariu, L. (2016). Optimization of process parameters for heavy metals biosorption onto mustard waste biomass. *Open Chemistry*, *14*(1), 175–187. https://doi.-org/10.1515/chem-2016-0019

Nezami, S., Ghaemi, A., & Yousefi, T. (2023). Application of titanium carbide/nitride (MXene)-based NPs in adsorption of radionuclides and heavy metal ions for wastewater remediation: A review. *Case Studies in Chemical and Environmental Engineering*, *7*, 1–22. https://doi.org/10.1016/j.cscee.2023.100326

Nguyen, K. M., Nguyen, B. Q., Nguyen, H. T., & Nguyen, H. T. H. (2019). Adsorption of arsenic and heavy metals from solutions by unmodified iron-ore sludge. *Applied Sciences (Switzerland)*, *9*(4). https://doi.org/10.3390/app9040619

Nieto-Delgado, C., Terrones, M., & Rangel-Mendez, J. R. (2011). Development of highly microporous activated carbon from the alcoholic beverage industry organic by-products. *Biomass and Bioenergy*, *35*(1), 103–112. https://doi.org/10.1016/j.biombioe.2010.08.025

Nur-E-Alam, M., Abu Sayid Mia, M., Ahmad, F., & Mafizur Rahman, M. (2018). Adsorption of chromium(Cr) from tannery wastewater using low-cost spent tea leaves adsorbent. *Applied Water Science*, *8*(5), 1–7. https://doi.org/10.1007/s13201-018-0774-y

Nyangi, M. J. (2021). Remediation of Arsenic from water using iron and aluminum electrodes in electrocoagulation technology: Adsorption Isotherm and Kinetic Studies. *Chemistry Africa*, *4*(4), 943–954. https://doi.org/10.1007/s42250-021-00268-2

Obaid, S. S., Gaikwad, D. K., Sayyed, M. I., Al-Rashdi, K., & Pawar, P. P. (2018). Heavy metal ions removal from waste water bythe natural zeolites. *Materials Today:*

Proceedings, *5*(9), 17930–17934. https://doi.org/10.1016/j.matpr.2018.06.122

Ogata, F., Tominaga, H., Yabutani, H., Taga, A., & Kawasaki, N. (2012). Granulation of gibbsite with inorganic binder and its ability to adsorb Mo(VI) from aqueous solution. *Toxicological and Environmental Chemistry*, *94*(4), 650–659. https://doi.org/10.1080/-02772248.2012.-671325

Oguz, E. (2022). Comparative study of natural and modified Abies bornmulleriana cones in the removal of copper (II) ions. *International Journal of Environmental Science and Technology*, *19*(6), 5343–5358. https://doi.org/10.1007/s13762-021-03496-8

Olegario-Sanchez, E., & Pelicano, C. M. (2017). Characterization of philippine natural zeolite and its application for heavy metal removal from acid mine drainage (AMD). *Key Engineering Materials*, *737 KEM*, 407–411. https://doi.org/10.4028/www.scientific.-net/KEM.737.407

Olu-Owolabi, B. I., Diagboya, P. N., & Adebowale, K. O. (2014). Evaluation of pyrene sorption-desorption on tropical soils. *Journal of Environmental Management*, *137*, 1–9. https://doi.org/10.1016/j.jenvman.2014.01.048

Olupot, P. W., Candia, A., Menya, E., & Walozi, R. (2016). Characterization of rice husk varieties in Uganda for biofuels and their techno-economic feasibility in gasification. *Chemical Engineering Research and Design*, *107*, 63–72. https://doi.org/10.1016/j.-cherd.2015.11.010

Omri, A., & Benzina, M. (2012). Characterization of Activated Carbon Prepared From a New Raw Lignocellulosic Material: Ziziphus Spina-Christi Seeds. *Journal de La Société Chimique de Tunisie*, *14*, 175–183

Otaru, A. J., Ameh, C. U., Abdulkareem, A. S., Odigure, J. O., & Okafor, J. O. (2013). Development and Characterization of adsorbent from rice husk ash to bleach vegetable oils. *IOSR Journal of Applied Chemistry*, *4*(2), 42–49. https://doi.org/10.9790/5736-0424249

Pachaiyappan, S., Seshadri, S., Sugumaran, P., Priya Susan, V., Ravichandran, P., & Seshadri, S. (2012). Production and characterization of activated carbon from banana empty fruit bunch and delonix regia fruit pod. *Journal of Sustainable Energy & Environment*,

3(January), 125–132. https://www.researchgate.net/publication/236694681

Pakzadeh, B., & Batista, J. R. (2011). Chromium removal from ion-exchange waste brines with calcium polysulfide. *Water Research*, *45*(10), 3055–3064. https://doi.org/10.1016/j.-watres.2011.03.006

Pan, J., Gao, B., Wang, S., Guo, K., Xu, X., & Yue, Q. (2020). Waste-to-resources: Green preparation of magnetic biogas residues-based biochar for effective heavy metal removals. *Science of the Total Environment*, *737*, 1–10. https://doi.org/10.1016/j.scitotenv.-2020.140283

Park, D., Yun, Y., & Park, J. . (2014). The past, present, and future trends of biosorption. *Biotechnol. Bioprocess Eng*, *15*, 86–102.

Parlayici, Ş., & Pehlivan, E. (2019). Comparative study of Cr(VI) removal by bio-waste adsorbents: Equilibrium, kinetics, and thermodynamic. *Journal of Analytical Science and Technology*, *10*(1), 1–8. https://doi.org/10.1186/s40543-019-0175-3

Pasgar, A., Nasiri, A., & Javid, N. (2022). Single and competitive adsorption of Cu2+ and Pb2+ by tea pulp from aqueous solutions. *Environmental Health Engineering and Management*, *9*(1), 65–74. https://doi.org/10.34172/EHEM.2022.08

Pasricha, S., Mathur, V., Garg, A., Lenka, S., Verma, K., & Agarwal, S. (2021). Molecular mechanisms underlying heavy metal uptake, translocation and tolerance in hyperaccumulators-an analysis: Heavy metal tolerance in hyperaccumulators. *Environmental Challenges*, *4*, 1–15. https://doi.org/10.1016/j.envc.2021.100197

Peng, S. H., Wang, R., Yang, L. Z., He, L., He, X., & Liu, X. (2018). Biosorption of copper, zinc, cadmium and chromium ions from aqueous solution by natural foxtail millet shell. *Ecotoxicology and Environmental Safety*, *165*, 61–69. https://doi.org/10.1016/j.ecoenv.-2018.08.084

Poonam, Bharti, S. K., & Kumar, N. (2018). Kinetic study of lead (Pb^{2+}) removal from battery manufacturing wastewater using bagasse biochar as biosorbent. *Applied Water Science*, *8*(4), 1–13. https://doi.org/10.1007/s13201-018-0765-z

Prabhakar, R., & Samadder, S. R. (2020). Use of adsorption-influencing parameters for

designing the batch adsorber and neural network–based prediction modelling for the aqueous arsenate removal using combustion synthesised nano-alumina. *Environmental Science and Pollution Research*, *27*(21), 26367–26384. https://doi.org/10.1007/s11356-020-08975-y

Priyadarshanee, M., & Das, S. (2021). Biosorption and removal of toxic heavy metals by metal tolerating bacteria for bioremediation of metal contamination: A comprehensive review. *Journal of Environmental Chemical Engineering*, *9*(1), 104686. https://doi.org/10.-1016/j.jece.2020.104686

Pyrzynska, K. (2019). Removal of cadmium from wastewaters with low-cost adsorbents. *Journal of Environmental Chemical Engineering*, *7*(1), 102795. https://doi.org/10.-1016/j.jece.2018.11.040

Qiu, G., & Guo, M. (2010). Quality of poultry litter-derived granular activated carbon. *Bioresource Technology*, *101*(1), 379–386. https://doi.org/10.1016/j.biortech.2009.-07.050

Rafique, M., Hajra, S., Tahir, M. B., Gillani, S. S. A., & Irshad, M. (2022). A review on sources of heavy metals, their toxicity and removal technique using physico-chemical processes from wastewater. *Environmental Science and Pollution Research*, *29*(11), 16772–16781. https://doi.org/10.1007/s11356-022-18638-9

Rahaman, M. H., Islam, M. A., Islam, M. M., Rahman, M. A., & Alam, S. M. N. (2021). Biodegradable composite adsorbent of modified cellulose and chitosan to remove heavy metal ions from aqueous solution. *Current Research in Green and Sustainable Chemistry*, *4*(May), 100119. https://doi.org/10.1016/j.crgsc.2021.100119

Rahdar, S., Taghavi, M., Khaksefidi, R., & Ahmadi, S. (2019). Adsorption of arsenic(V) from aqueous solution using modified saxaul ash: Isotherm and thermodynamic study. *Applied Water Science*, *9*(4), 1–9. https://doi.org/10.1007/s13201-019-0974-0

Rahimi, S., Moattari, R. M., Rajabi, L., Derakhshan, A. A., & Keyhani, M. (2015). Iron oxide/hydroxide (α,γ-FeOOH) nanoparticles as high potential adsorbents for lead removal from polluted aquatic media. *Journal of Industrial and Engineering Chemistry*, *23*, 33–43. https://doi.org/10.1016/j.jiec.2014.07.039

Rahman, D. Z., Vijayaraghavan, J., & Thivya, J. (2023). A comprehensive review on zinc(II) sequestration from wastewater using various natural/modified low-cost agro-waste sorbents. *Biomass Conversion and Biorefinery*, *13*(7), 5469–5499. https://doi.org/10.-1007/s13399-021-01822-1

Rahman, M. M., Karmaker, S. C., Pal, A., Eljamal, O., & Saha, B. B. (2021). Statistical techniques for the optimization of cesium removal from aqueous solutions onto iron-based nanoparticle-zeolite composites. *Environmental Science and Pollution Research*, *28*(10), 12918–12931. https://doi.org/10.1007/s11356-020-11258-1

Rai, R., Aryal, R. L., Paudyal, H., Gautam, S. K., Ghimire, K. N., Pokhrel, M. R., & Poudel, B. R. (2023). Acid-treated pomegranate peel: An efficient biosorbent for the excision of hexavalent chromium from wastewater. *Heliyon*, *9*(5), 1–17. https://doi.org/10.1016/j.-heliyon.2023.-e15698

Raj, D., and Maiti, S. K. (2019). Sources, toxicity, and remediation of mercury: An essence review. *Environmental Monitoring and Assessment*, *191*(9), 1–22. https://doi.org/10.-1007/s10661-019-7743-2

Rani, B., Trivedi, A., Pathak, R. K., & Maheshwari, R. K. (2014). Fluoride ion: An inexplicable hydro toxicant. *Journal of Industrial Pollution Control*, *30*(1), 23–32.

Ranjan, S., Yadav, B. K., & Joshi, H. (2022). Removal of arsenic (III and V) from aqueous solution using stable maghemite (γ -Fe_2O_3) loaded pumice composite. *International Journal of Environmental Science and Technology*, *19*(6), 4737–4748. https://doi.org/10.-1007/s13762-021-03326-x

Raza, M. H., Sadiq, A., Farooq, U., Athar, M., Hussain, T., Mujahid, A., & Salman, M. (2015). Phragmites karka as a biosorbent for the removal of mercury metal ions from aqueous solution: Effect of modification. *Journal of Chemistry*, *2015*, 1–12. https://doi.org/10.-1155/2015/293054

Razzak, A., Shafiquzzaman, M., Haider, H., & Alresheedi, M. (2021). Arsenic removal by iron-oxidizing bacteria in a fixed-bed coconut husk column: Experimental study and numerical modeling. *Environmental Pollution*, *272*(xxxx), 1–10. https://doi.org/10.-1016/j.envpol.2020.115977

Reza, R., & Singh, G. (2010). Heavy metal contamination and its indexing approach for river water. *International Journal of Environmental Science and Technology*, *7*(4), 785–792. https://doi.org/10.1007/BF03326187

Rizhikovs, J., Zandersons, J., Spince, B., Dobele, G., & Jakab, E. (2012). Preparation of granular activated carbon from hydrothermally treated and pelletized deciduous wood. *Journal of Analytical and Applied Pyrolysis*, *93*(1), 68–76. https://doi.org/10.1016/j.jaap.-2011.09.009

Rodríguez-Romero, J. A., Mendoza-Castillo, D. I., Reynel-Ávila, H. E., De Haro-Del Rio, D. A., González-Rodríguez, L. M., Bonilla-Petriciolet, A., Duran-Valle, C. J., & Camacho-Aguilar, K. I. (2020). Preparation of a new adsorbent for the removal of arsenic and its simulation with artificial neural network-based adsorption models. *Journal of Environmental Chemical Engineering*, *8*(4), 103928. https://doi.org/10.1016/j.jece.-2020.103928

Rwiza, M. J., Oh, S. Y., Kim, K. W., & Kim, S. D. (2018). Comparative sorption isotherms and removal studies for Pb(II) by physical and thermochemical modification of low-cost agro-wastes from Tanzania. *Chemosphere*, *195*(2), 135–145. https://doi.org/10.1016/j.-chemosphere.2017.12.043

Saadi, R., Saadi, Z., Fazaeli, R., & Fard, N. E. (2015). Monolayer and multilayer adsorption isotherm models for sorption from aqueous media. *Korean Journal of Chemical Engineering*, *32*(5), 787–799. https://doi.org/10.1007/s11814-015-0053-7

Sabah, H., Thouraya, T., Melek, H., & Nadia, M. (2018). Application of response surface methodology for optimization of cadmium ion removal from an aqueous solution by eggshell powder. *Chemical Research in Chinese Universities*, *34*(2), 302–310. https://doi.org/10.-1007/s40242-018-7163-9

Saeed, B., Anwer, H., Naqvi, S., Siddiqui, A., & Hashim, S. (2020). Biosorption of hexavalent chromium metal ions from an aqueous solution of leaves and bark of Cinnamomum verum via green route. *SN Applied Sciences*, *2*(4), 1–14. https://doi.org/10.1007/s42452-020-2334-y

Sagharloo, N. G., Rabani, M., Salimi, L., Ghafourian, H., & Sadatipour, S. M. T. (2021).

Immobilized ZnO/TiO_2 activated carbon (I ZnO/TiO_2 AC) to removal of arsenic from aqueous environments: optimization using response surface methodology and kinetic studies. *Biomass Conversion and Biorefinery*, 1.12. https://doi.org/10.1007/s13399-021-01741-1

Şahan, T., Erol, F., & Yılmaz, Ş. (2018). Mercury(II) adsorption by a novel adsorbent mercapto-modified bentonite using ICP-OES and use of response surface methodology for optimization. *Microchemical Journal*, *138*, 360–368. https://doi.org/10.1016/j.-microc.2018.01.028

Sahmoune, M. N., Louhab, K., & Boukhiar, A. (2011). Advanced biosorbents materials for removal of chromium from water and wastewaters. *Environmental Progress and Sustainable Energy*, *30*(3), 284–293. https://doi.org/10.1002/ep.10473

Sajjadi, S. A., Mohammadzadeh, A., Tran, H. N., Anastopoulos, I., Dotto, G. L., Lopičić, Z. R., Sivamani, S., Rahmani-Sani, A., Ivanets, A., & Hosseini-Bandegharaei, A. (2018). Efficient mercury removal from wastewater by pistachio wood wastes-derived activated carbon prepared by chemical activation using a novel activating agent. *Journal of Environmental Management*, *223*, 1001–1009. https://doi.org/10.1016/j.jenvman.2018.-06.077

Salah, A. S. (2015). Assessing the Potential of Laterite in Adsorbing Cadmium from Mine Leachate and Surrogate Cadmium Solutions: A Case Study at Anglogold Ashanti Iduaperiem Gold Mine Ltd, Tarkwa. http://hdl.handle.net/123456789/6810

Salih, S. S., Mahdi, A., Kadhom, M., & Ghosh, T. K. (2019). Competitive adsorption of As(III) and As(V) onto chitosan/diatomaceous earth adsorbent. *Journal of Environmental Chemical Engineering*, *7*(5), 103407. https://doi.org/10.1016/j.jece.2019.103407

Samaniego, J. O., & Tanchuling, M. A. N. (2019). Removal of heavy metals from an actual small scale gold mining wastewater by sorption onto cocopeat. *ASEAN Journal on Science and Technology for Development*, *36*(1), 1–7. https://doi.org/10.29037/ajstd.558

Samuel, M. S., Shang, M., Klimchuk, S., & Niu, J. (2021). Novel Regenerative hybrid composite adsorbent with improved removal capacity for lead ions in water. *Industrial and Engineering Chemistry Research*, *60*(14), 5124–5132. https://doi.org/10.1021/acs.-

iecr.0c06277

Sanjeev, K., Sapna, J., Kumar, S., & Jain, S. (2013). History, introduction, and kinetics of ion exchange materials. *Journal of Chemistry*, 1–13. https://doi.org/10.1155/2013/957647

Sarma, G. K., Sen Gupta, S., & Bhattacharyya, K. G. (2019). Nanomaterials as versatile adsorbents for heavy metal ions in water: A review. *Environmental Science and Pollution Research*, *26*(7), 6245–6278. https://doi.org/10.1007/s11356-018-04093-y

Sellaoui, L., Edi Soetaredjo, F., Ismadji, S., Cláudio Lima, É., Dotto, G. L., Ben Lamine, A., & Erto, A. (2017). New insights into single-compound and binary adsorption of copper and lead ions on a treated sea mango shell: Experimental and theoretical studies. *Physical Chemistry Chemical Physics*, *19*(38), 25927–25937. https://doi.org/10.1039/c7cp03770h

Sha, H., Wu, Y., & Fan, Y. (2018). Utilization of industrial waste as a novel adsorbent: Mono/competitive adsorption of chromium(VI) and nickel(II) using diatomite waste modified by EDTA. *Applied Organometallic Chemistry*, *32*(1), 1–15. https://doi.org/10.-1002/aoc.3977

Shafaghat, J., & Ghaemi, A. (2021). Comparison of Pb(II) Adsorption by Ground Granulated Blast-Furnace and Phosphorus Slags: Exploitation of RSM. *Iranian Journal of Science and Technology, Transaction A: Science*, *45*(3), 899–911. https://doi.org/10.-1007/s40995-021-01075-7

Shahedi, A., Darban, A. K., Taghipour, F., & Jamshidi-Zanjani, A. (2020). A review on industrial wastewater treatment via electrocoagulation processes. *Current Opinion in Electrochemistry*, *22*, 154–169. https://doi.org/10.1016/j.coelec.2020.05.009

Shahrin, S., Lau, W. J., Goh, P. S., Jaafar, J., & Ismail, A. F. (2018). Adsorptive removal of As(V) ions from water using graphene oxide-manganese ferrite and titania nanotube-manganese ferrite hybrid nanomaterials. *Chemical Engineering and Technology*, *41*(11), 2250–2258. https://doi.org/10.1002/ceat.201800322

Sharifi, S., Nabizadeh, R., Akbarpour, B., Azari, A., Ghaffari, H. ., Nazmara, S., Mahmoudi, B., Shiri, L., & Yousefi, M. (2019). Modeling and optimizing parameters affecting hexavalent chromium adsorption from aqueous solutions using Ti-XAD7 nanocomposite: RSM-CCD approach, kinetic, and isotherm studies. *Journal of Environmental Health*

Science and Engineering, *17*(2), 873–888. https://doi.org/10.1007/s40201-019-00405-7

Sharma, Amita, Anjana, Rana, H., & Goswami, S. (2022). A Comprehensive review on the heavy metal removal for water remediation by the application of lignocellulosic biomass-derived nanocellulose. *Journal of Polymers and the Environment*, *30*(1), 1–18. https://doi.org/10.-1007/s10924-021-02185-4

Sharma, Anjali, Tomer, A., Singh, J., & Chhikara, B. S. (2019). Biosorption of metal toxicants and other water pollutants by Corn (Maize) plant: A comprehensive review. *Journal of Integrated Science and Technology*, *7*(2), 19–29. http://pubs.iscience.in/journal/index.-php/jist/-article/view/918

Sheikh, Z., Amin, M., Khan, N., Khan, M. N., Sami, S. K., Khan, S. B., Hafeez, I., Khan, S. A., Bakhsh, E. M., & Cheng, C. K. (2021). Potential application of Allium Cepa seeds as a novel biosorbent for efficient biosorption of heavy metals ions from aqueous solution. *Chemosphere*, *279*, 130545. https://doi.org/10.1016/j.chemosphere.2021.130545

Siddiqui, S. I., Singh, P. N., Tara, N., Pal, S., Chaudhry, S. A., & Sinha, I. (2020). Arsenic removal from water by starch functionalized maghemite nano-adsorbents: Thermodynamics and kinetics investigations. *Colloids and Interface Science Communications*, *36*(May), 100263. https://doi.org/10.1016/j.colcom.2020.100263

Singh, A., Kumar, S., & Panghal, V. (2021). Adsorption of chromium (Cr^{6+}) on dead biomass of Salvinia molesta (Kariba weed) and Typha latifolia (broadleaf cattail): Isotherm, kinetic, and thermodynamic study. *Applied Water Science*, *11*(9), 1–16. https://doi.org/10.1007/-s13201-021-01481-7

Singh, U., & Kumar Kaushal, R. (2013). Review article treatment of waste water with low cost adsorbent: A review. *VSRD International Journal of Technical & Non-Technical Research*, *4*(3), 33–42.

Siriwardena, D. P., James, R., Dasu, K., Thorn, J., Iery, R. D., Pala, F., Schumitz, D., Eastwood, S., & Burkitt, N. (2021). Regeneration of per- and polyfluoroalkyl substance-laden granular activated carbon using a solvent based technology. *Journal of Environmental Management*, *289*, 112439. https://doi.org/10.1016/j.jenvman.2021.112439

Smith, K. M., Fowler, G. D., Pullket, S., & Graham, N. J. D. (2012). The production of attrition

resistant, sewage-sludge derived, granular activated carbon. *Separation and Purification Technology*, *98*, 240–248. https://doi.org/10.1016/j.seppur.2012.07.026

Soliman, N. K., & Moustafa, A. F. (2020). Industrial solid waste for heavy metals adsorption features and challenges: A review. *Journal of Materials Research and Technology*, *9*(5), 10235–10253. https://doi.org/10.1016/j.jmrt.2020.07.045

Soni, R., & Shukla, D. P. (2019). Synthesis of fly ash based zeolite-reduced graphene oxide composite and its evaluation as an adsorbent for arsenic removal. *Chemosphere*, *219*, 504–509. https://doi.org/10.1016/j.chemosphere.2018.11.203

Sonone, S. S., Jadhav, S. V, Sankhla, M. S., & Kumar, R. (2020). Water Contamination by Heavy Metals and their Toxic Effect on Aquaculture and Human Health through Food Chain. *Letters in Applied NanoBioScience*, *10*(2), 2148–2166. https://doi.org/10.-33263/lianbs102.21482166

Steingräber, L. F., Ludolphy, C., Metz, J., Kierdorf, H., & Kierdorf, U. (2022). Uptake of lead and zinc from soil by blackberry plants (Rubus fruticosus L. agg.) and translocation from roots to leaves. *Environmental Advances*, *9*, 1–10. https://doi.org/10.1016/j.envadv.2022.-100313

Sujatha, S., Venkatesan, G., & Sivarethinamohan, R. (2020). Optimization of lead removal in exhausting Manilkara zapota based activated carbon: application of response surface methodology. *Environmental Technology (United Kingdom)*, *41*(19), 2478–2493. https://doi.org/10.1080/09593330.2019.1570347

Sun, C., Li, C., Wang, C., Qu, R., Niu, Y., & Geng, H. (2012). Comparison studies of adsorption properties for Hg(II) and Au(III) on polystyrene-supported bis-8-oxyquinoline-terminated open-chain crown ether. *Chemical Engineering Journal*, *200–202*, 291–299. https://doi.-org/10.1016/j.cej.2012.06.007

Sun, X., Huang, H., Zhu, Y., Du, Y., Yao, L., Jiang, X., & Gao, P. (2019). Adsorption of Pb(II) and Cd(II) onto Spirulina platensis harvested by polyacrylamide in single and binary solution systems. *Colloids and Surfaces A: Physicochemical and Engineering Aspects*, *583*(June), 123926. https://doi.org/10.1016/j.colsurfa.2019.123926

Sun, Y., Yang, Y., Yang, M., Yu, F., & Ma, J. (2019). Response surface methodological

evaluation and optimization for adsorption removal of ciprofloxacin onto graphene hydrogel. *Journal of Molecular Liquids*, *284*, 124–130. https://doi.org/10.1016/j.molliq.-2019.03.118

Supong, A., Bhomick, P. C., Baruah, M., Pongener, C., Sinha, U. B., & Sinha, D. (2019). Adsorptive removal of Bisphenol A by biomass activated carbon and insights into the adsorption mechanism through density functional theory calculations. *Sustainable Chemistry and Pharmacy*, *13*, 100159. https://doi.org/10.1016/j.scp.2019.100159

Taha, G. M., Arifien, a. E., & El-Nahas, S. (2011). Removal efficiency of potato peels as a new biosorbent material for uptake of Pb(II) Cd(II) and Zn(II) From Their Aqueous Solutions. *The Journal of Solid Waste Technology and Management*, *37*(2), 128–140. https://doi.org/10.5276/JSWTM.2011.128

Tan, G., Sun, W., Xu, Y., Wang, H., & Xu, N. (2016). Sorption of mercury(II) and atrazine by biochar, modified biochars and biochar based activated carbon in aqueous solution. *Bioresource Technology*, *211*, 727–735. https://doi.org/10.1016/j.biortech.2016.03.147

Tang, C., Shu, Y., Zhang, R., Li, X., Song, J., Li, B., Zhang, Y., & Ou, D. (2017). Comparison of the removal and adsorption mechanisms of cadmium and lead from aqueous solution by activated carbons prepared from Typha angustifolia and Salix matsudana. *RSC Advances*, *7*(26), 16092–16103. https://doi.org/10.1039/c6ra28035h

Tang, J., Ptacek, C. J., Blowes, D. W., Liu, Y. Y., Feng, Y., Finfrock, Y. Z., & Liu, P. (2022). Mercury adsorption kinetics on sulfurized biochar and solid-phase digestion using aqua regia: A synchrotron-based study. *Chemical Engineering Journal*, *428*, 1–9. https://doi.org/10.1016/j.cej.2021.131362

Tang, N., Niu, C. G., Li, X. T., Liang, C., Guo, H., Lin, L. S., Zheng, C. W., & Zeng, G. M. (2018). Efficient removal of Cd(II) and Pb(II) from aqueous solution with amino- and thiol-functionalized activated carbon: Isotherm and kinetics modeling. *Science of the Total Environment*, *635*, 1331–1344. https://doi.org/10.1016/j.scitotenv.2018.04.236

Tekin, B., & Açikel, U. (2022). Adsorption isotherms for removal of heavy metal ions (copper and nickel) from aqueous solutions in single and binary adsorption processes. *Gazi University Journal of Science*, *36*(2), 495–509. https://doi.org/10.35378/gujs.1066137

Tian, X., Xie, Q., Chai, G., & Li, G. (2022). Simultaneous adsorption of As(III) and Cd(II) by ferrihydrite-modified biochar in aqueous solution and their mutual effects. *Scientific Reports*, *12*(1), 1–11. https://doi.org/10.1038/s41598-022-09648-1

Tokay, B., & Akpınar, I. (2021). A comparative study of heavy metals removal using agricultural waste biosorbents. *Bioresource Technology Reports*, *15*, 1–9. https://doi.org/10.1016/j.biteb.2021.100719

Türkmen, D., Özkaya Türkmen, M., Akgönüllü, S., & Denizli, A. (2022). Development of ion imprinted based magnetic nanoparticles for selective removal of arsenic (III) and arsenic (V) from wastewater. *Separation Science and Technology (Philadelphia)*, *57*(6), 990–999. https://doi.org/10.1080/01496395.2021.1956972

Uddin, M. K., & Baig, U. (2019). Synthesis of Co_3O_4 nanoparticles and their performance towards methyl orange dye removal: Characterisation, adsorption and response surface methodology. *Journal of Cleaner Production*, *211*, 1141–1153. https://doi.org/10.1016/j.-jclepro.2018.11.232

Vakili, M., Deng, S., Cagnetta, G., Wang, W., Meng, P., Liu, D., & Yu, G. (2019). Regeneration of chitosan-based adsorbents used in heavy metal adsorption: A review. *Separation and Purification Technology*, *224*, 373–387. https://doi.org/10.1016/j.-seppur.2019.05.040

Vega-Páez, J. D., Rivas, R. E., & Dussán-Garzón, J. (2019). High efficiency mercury sorption by dead biomass of Lysinibacillus sphaericus-new insights into the treatment of contaminated water. *Materials*, *12*(8), 1–13. https://doi.org/10.3390/ma12081296

Velusamy, S., Roy, A., Sundaram, S., & Kumar Mallick, T. (2021). A review on heavy metal ions and containing dyes removal through graphene oxide-based adsorption strategies for textile wastewater treatment. *Chemical Record*, *21*(7), 1570–1610. https://doi.org/10.-1002/tcr.202000153

Vijayalakshmi, K., Devi, B. M., Latha, S., Gomathi, T., Sudha, P. N., Venkatesan, J., & Anil, S. (2017). Batch adsorption and desorption studies on the removal of lead(II) from aqueous solution using nanochitosan/sodium alginate/microcrystalline cellulose beads. *International Journal of Biological Macromolecules*, *104*(II), 1483–1494. https://doi.-

org/10.1016/j.ijbiomac.2017.04.120

Waghmare. (2015). Fluoride removal from water by various techniques - review. *International Journal of Innovative Science, Engineering & Technology*, *2*(9), 560–571.

Wahid, S. N., Maharaj, R., Boodlal, D., & Smith, J. V. (2022). The adsorption of phenol on granular activated carbon prepared from waste coconut shell in Trinidad. *Environmental Progress and Sustainable Energy*, *41*(1), 1–30. https://doi.org/10.1002/ep.13729

Wang, B., Lan, J., Bo, C., Gong, B., & Ou, J. (2023). Adsorption of heavy metal onto biomass-derived activated carbon: Review. *RSC Advances*, *13*(7), 4275–4302. https://doi.-org/10.1039/-d2ra07911a

Wang, L., Li, Z., Wang, Y., Brookes, P. C., Wang, F., Zhang, Q., Xu, J., & Liu, X. (2021). Performance and mechanisms for remediation of Cd(II) and As(III) co-contamination by magnetic biochar-microbe biochemical composite: Competition and synergy effects. *Science of the Total Environment*, *750*, 141672. https://doi.org/10.1016/j.scitotenv.-2020.141672

Wang, M., Bera, G., Mitra, K., Wade, T. L., Knap, A. H., & Phillips, T. D. (2021). Tight sorption of arsenic, cadmium, mercury, and lead by edible activated carbon and acid-processed montmorillonite clay. *Environmental Science and Pollution Research*, *28*(6), 6758–6770. https://doi.org/10.1007/s11356-020-10973-z

Wang, X., Zheng, G., Chen, T., Nie, E., Wang, Y., Shi, X., & Liu, J. (2019). Application of ceramsite and activated alumina balls as recyclable bulking agents for sludge composting. *Chemosphere*, *218*, 42–51. https://doi.org/10.1016/j.chemosphere.2018.11.103

Wimalawansa, S. J. (2013). Purification of Contaminated water with reverse osmosis: effective solution of providing clean water for human needs in developing countries. *International Journal of Emerging Technology and Advanced Engineering*, *3*(12), 15.

Wu, J., Huang, D., Liu, X., Meng, J., Tang, C., & Xu, J. (2018). Remediation of As(III) and Cd(II) co-contamination and its mechanism in aqueous systems by a novel calcium-based magnetic biochar. *Journal of Hazardous Materials*, *348*(Iii), 10–19. https://doi.-org/10.1016/j.jhazmat.2018.01.011

Wu, L. K., Wu, H., Zhang, H. Bin, Cao, H. Z., Hou, G. Y., Tang, Y. P., & Zheng, G. Q. (2018). Graphene oxide/CuFe2O4 foam as an efficient absorbent for arsenic removal from water. *Chemical Engineering Journal*, *334*(November 2017), 1808–1819. https://doi.org/10.-1016/j.cej.2017.11.096

Xavier, A. L. P., Adarme, O. F. H., Furtado, L. M., Ferreira, G. M. D., da Silva, L. H. M., Gil, L. F., & Gurgel, L. V. A. (2018). Modeling adsorption of copper(II), cobalt(II) and nickel(II) metal ions from aqueous solution onto a new carboxylated sugarcane bagasse. Part II: Optimization of monocomponent fixed-bed column adsorption. *Journal of Colloid and Interface Science*, *516*, 431–445. https://doi.org/10.1016/j.jcis.2018.01.068

Xia, S., Song, Z., Jeyakumar, P., Bolan, N., & Wang, H. (2020). Characteristics and applications of biochar for remediating Cr(VI)-contaminated soils and wastewater. *Environmental Geochemistry and Health*, *42*(6), 1543–1567. https://doi.org/10.1007/-s10653-019-00445-w

Xiao, B., Jia, J., Wang, W., Zhang, B., Ming, H., Ma, S., Kang, Y., & Zhao, M. (2023). A review on magnetic biochar for the removal of heavy metals from contaminated soils: Preparation, application, and microbial response. *Journal of Hazardous Materials Advances*, *10*, 1–13. https://doi.org/10.1016/j.hazadv.2023.100254

Xu, X., Schierz, A., Xu, N., & Cao, X. (2016). Comparison of the characteristics and mechanisms of Hg(II) sorption by biochars and activated carbon. *Journal of Colloid and Interface Science*, *463*, 55–60. https://doi.org/10.1016/j.jcis.2015.10.003

Xu, Z., & Dong, J. (2008). Synthesis, characterization, and application of magnetic nanocomposites for the removal of heavy metals from industrial effluents. *Emerging Environmental Technologies*, 105–148. https://doi.org/10.1007/978-1-4020-8786-8_6

Yan, B., Liang, T., Yang, X., & Gadgil, A. J. (2021). Superior removal of As(III) and As(V) from water with Mn-doped β-FeOOH nanospindles on carbon foam. *Journal of Hazardous Materials*, *418*(June), 1–27. https://doi.org/10.1016/j.jhazmat.2021.126347

Yang, D., Wang, L., Li, Z., Tang, X., He, M., Yang, S., Liu, X., and Xu, J. (2020). Simultaneous adsorption of Cd(II) and As(III) by a novel biochar-supported nanoscale zero-valent iron in aqueous systems. *Science of the Total Environment*, *708*, 134823. https://doi.org/10.-

1016/j.scitotenv.2019.134823

Yang, W., Tang, Q., Wei, J., Ran, Y., Chai, L., & Wang, H. (2016). Enhanced removal of Cd(II) and Pb(II) by composites of mesoporous carbon stabilized alumina. *Applied Surface Science*, *369*(Ii), 215–223. https://doi.org/10.1016/j.apsusc.2016.01.151

Yeo, K. F. H., Li, C., Zhang, H., Chen, J., Wang, W., & Dong, Y. (2021). Arsenic removal from contaminated water using natural adsorbents: A Review. *Coatings*, *11*(11), 1407. https://doi.org/10.3390/coatings11111407

Yılmaz, Ş., Zengin, A., Akbulut, Y., & Şahan, T. (2019). Magnetic nanoparticles coated with aminated polymer brush as a novel material for effective removal of Pb(II) ions from aqueous environments. *Environmental Science and Pollution Research*, *26*(20), 20454–20468. https://doi.org/10.1007/s11356-019-05360-2

Yusuff, A. S, Owolabi, J. O., & Igbomezie, C. O. (2021). Optimization of process parameters for adsorption of heavy metals from aqueous solutions by alumina-onion skin composite. *Chemical Engineering Communications*, *208*(1), 14–28. https://doi.org/10.1080/0098-6445.2019.1680371

Yusuff, A. S. (2018). Optimization of adsorption of Cr(VI) from aqueous solution by Leucaena leucocephala seed shell activated carbon using design of experiment. *Applied Water Science*, *8*(8), 1–11. https://doi.org/10.1007/s13201-018-0850-3

Zaimee, M. Z. A., Sarjadi, M. S., & Rahman, M. L. (2021). Heavy metals removal from water by efficient adsorbents. *Water (Switzerland)*, *13*(19), 1–22. https://doi.org/10.3390/-w13192659

Zama, E. F., Zhu, Y. G., Reid, B. J., & Sun, G. X. (2017). The role of biochar properties in influencing the sorption and desorption of Pb(II), Cd(II) and As(III) in aqueous solution. *Journal of Cleaner Production*, *148*, 127–136. https://doi.org/10.1016/j.jclepro.2017.-01.125

Zeng, H., Yu, Y., Wang, F., Zhang, J., & Li, D. (2020). Arsenic(V) removal by granular adsorbents made from water treatment residuals materials and chitosan. *Colloids and Surfaces A: Physicochemical and Engineering Aspects*, *585*, 1–10. https://doi.org/10.-1016/j.colsurfa.2019.124036

Zhang, C., Wang, X., Jiang, S., Zhou, M., Li, F., Bi, X., Xie, S., & Liu, J. (2021). Heavy metal pollution caused by cyanide gold leaching: A case study of gold tailings in central China. *Environmental Science and Pollution Research*, *28*(23), 29231–29240. https://doi.-org/10.1007/s11356-021-12728-w

Zhang, H., Wu, X., & Li, X. (2012). Oxidation and coagulation removal of COD from landfill leachate by Fered-Fenton process. *Chemical Engineering Journal*, *210*, 188–194. https://doi.org/10.1016/j.cej.2012.08.094

Zhang, L., Tang, S., He, F., Liu, Y., Mao, W., & Guan, Y. (2019). Highly efficient and selective capture of heavy metals by poly(acrylic acid) grafted chitosan and biochar composite for wastewater treatment. *Chemical Engineering Journal*, *378*, 122215. https://doi.org/10.-1016/j.cej.2019.122215

Zhang, X., Li, M., Yang, H., Li, X., & Cui, Z. (2018). Physiological responses of Suaeda glauca and Arabidopsis thaliana in phytoremediation of heavy metals. *Journal of Environmental Management*, *223*(June), 132–139. https://doi.org/10.1016/j.jenvman.2018.06.025

Zhang, Y., Song, X., Zhang, P., Gao, H., Ou, C., & Kong, X. (2020). Production of activated carbons from four wastes via one-step activation and their applications in Pb2+ adsorption: Insight of ash content. *Chemosphere*, *245*, 1–9. https://doi.org/10.1016/j.chemosphere.-2019.125587

Zhao, Jiaming, Yu, L., Ma, H., Zhou, F., Yang, K., & Wu, G. (2020). Corn stalk-based activated carbon synthesized by a novel activation method for high-performance adsorption of hexavalent chromium in aqueous solutions. *Journal of Colloid and Interface Science*, *578*, 650–659. https://doi.org/10.1016/j.jcis.2020.06.031

Zhao, Jianhai, Liu, T., Shi, H., Zhang, J., Li, H., Ge, W., & Chi, Y. (2019). Preparation and characterization of MnO2-impregnated granular activated carbon for Reactive Black 5 removal. *Desalination and Water Treatment*, *171*, 428–435. https://doi.org/10.5004/dwt.-2019.24782

Zhou, R., Zhang, M., Li, J., & Zhao, W. (2020). Optimization of preparation conditions for biochar derived from water hyacinth by using response surface methodology (RSM) and its application in Pb(II) removal. *Journal of Environmental Chemical Engineering*, *8*(5),

104198. https://doi.org/10.1016/j.jece.2020.104198

Zhu, S., Qu, T., Irshad, M. K., & Shang, J. (2020). Simultaneous removal of Cd(II) and As(III) from co-contaminated aqueous solution by α-FeOOH modified biochar. *Biochar*, *2*(1), 81–92. https://doi.org/10.1007/s42773-020-00040-8

Zhu, W., Wang, J., Wu, D., Li, X., Luo, Y., Han, C., Ma, W., & He, S. (2017). Investigating the heavy metal adsorption of mesoporous silica materials prepared by microwave synthesis. *Nanoscale Research Letters*, *12*(1), 1–19. https://doi.org/10.1186/s11671-017-2070-4

APPENDICES

Appendix 1. Effect of contact time on As(III) ions removal from monocomponent and bicomponent synthetic wastewater

Contact time (min)	As(III)			As(III)[As(III)+Hg(II)]		
	Residual concentration (mg/L)	Removal efficiency (%)	Biosorption capacity (mg/g)	Residual concentration (mg/L)	Removal efficiency (%)	Biosorption capacity (mg/g)
10	14.93±0.07	40.30	6.72	19.37±0.10	22.52	3.75
20	12.90±0.05	48.41	8.07	15.24±0.03	39.05	6.51
30	9.42±0.05	62.31	10.39	13.40±0.05	46.41	7.74
40	4.46±0.13	82.15	13.69	7.60±0.02	69.60	11.60
60	1.94±0.02	92.26	15.38	5.82±0.04	76.73	12.79
90	2.24±0.03	91.03	15.17	4.87±0.02	80.53	13.42
120	2.62±0.01	89.52	14.92	3.77±0.04	84.93	14.16
150	3.56±0.02	85.77	14.30	5.95±0.02	76.19	12.70
180	3.70±0.05	85.19	14.20	6.09±0.06	75.65	12.61

Appendix 2. Effect of contact time on Hg(II) ions removal from monocomponent and bicomponent synthetic wastewater

Contact time (min)	Hg(II)			Hg(II)[Hg(II)+ As(III)]		
	Residual concentration (mg/L)	Removal efficiency (%)	Biosorption capacity (mg/g)	Residual concentration (mg/L)	Removal efficiency (%)	Biosorption capacity (mg/g)
10	19.73±0.02	21.09	3.52	18.16±0.01	27.36	4.56
20	13.30±0.06	46.81	7.80	12.76±0.03	48.97	8.16
30	8.91±0.05	64.35	10.73	10.47±0.02	58.11	9.68
40	4.13±0.04	83.47	13.91	7.37±0.05	70.52	11.75
60	1.76±0.09	92.95	15.49	3.56±.04	85.77	14.30
90	0.98±0.10	96.09	16.02	2.24±0.06	91.05	15.18
120	3.97±0.03	84.12	14.02	1.04±0.09	95.84	15.97
150	4.15±0.02	83.39	13.90	2.96±0.03	88.17	14.70
180	4.54±0.03	81.83	13.64	3.09±0.04	87.64	14.61

Appendix 3. Effect of solution pH on As(III) ions removal from monocomponent and bicomponent synthetic wastewater

Solution pH	As(III)			As(III)[As(III)+Hg(II)]		
	Residual concentration (mg/L)	Removal efficiency (%)	Biosorption capacity (mg/g)	Residual concentration (mg/L)	Removal efficiency (%)	Biosorption capacity (mg/g)
2	16.33±0.51	34.67	5.78	6.15±0.03	75.41	12.57
4	12.49±0.42	50.05	8.34	4.80±0.05	80.81	13.47
6	3.54±0.08	85.83	14.30	7.94±0.07	68.24	11.37
8	8.56±0.45	65.77	10.96	11.58±0.04	53.68	8.95
10	14.27±0.32	42.93	7.16	16.18±0.06	35.29	5.88
12	14.46±0.39	42.17	7.03	17.38±0.03	30.48	5.08
14	14.70±0.23	41.19	6.86	17.96±0.05	28.15	4.69

Appendix 4. Effect of solution pH on Hg(II) ions removal from monocomponent and bicomponent synthetic wastewater

Solution pH	Hg(II)			Hg(II)[Hg(II)+ As(III)]		
	Residual concentration (mg/L)	Removal efficiency (%)	Biosorption capacity (mg/g)	Residual concentration (mg/L)	Removal efficiency (%)	Biosorption capacity (mg/g)
2	9.61±0.14	61.57	10.26	18.06±0.10	27.77	4.63
4	2.33±0.03	90.67	15.11	10.31±0.01	58.75	9.79
6	4.37±0.06	82.51	13.75	8.31±0.02	66.76	11.13
8	5.90±0.15	76.41	12.74	3.58±0.03	85.68	14.28
10	10.52±0.03	57.93	9.66	6.92±0.02	72.32	12.05
12	12.89±0.02	48.45	8.08	11.94±0.10	52.24	8.71
14	13.02±0.09	47.91	7.98	12.25±0.04	51.00	8.50

Appendix 5. **Effect of biosorbent particle size on As(III) ions removal from monocomponent and bicomponent synthetic wastewater**

Biosorbent particle size (µm)	As(III)			As(III)[As(III)+Hg(II)]		
	Residual concentration (mg/L)	Removal efficiency (%)	Biosorption capacity (mg/g)	Residual concentration (mg/L)	Removal efficiency (%)	Biosorption capacity (mg/g)
90	2.14±0.12	91.43	15.24	4.48±0.07	82.09	13.68
125	4.16±0.19	83.37	13.90	8.90±0.10	64.40	10.73
180	8.08±0.08	67.68	11.28	11.31±0.05	54.76	9.13
355	11.46±0.11	54.17	9.03	14.78±0.03	40.87	6.81
450	14.44±0.15	42.25	7.04	17.23±0.02	31.08	5.18

Appendix 6. **Effect of biosorbent particle size on Hg(II) ions removal from monocomponent and bicomponent synthetic wastewater**

Biosorbent particle size (μm)	Hg(II)			Hg(II)[Hg(II)+ As(III)]		
	Residual concentration (mg/L)	Removal efficiency (%)	Biosorption capacity (mg/g)	Residual concentration (mg/L)	Removal efficiency (%)	Biosorption capacity (mg/g)
90	1.64±0.06	93.45	15.58	2.94±0.04	88.25	14.71
125	5.88±0.07	76.47	12.74	7.31±0.02	70.77	11.80
180	9.33±0.09	62.69	10.45	10.47±0.05	58.12	9.69
355	13.11±0.10	47.56	7.93	15.04±0.13	39.85	6.64
450	16.13±0.17	35.47	5.91	18.44±0.03	26.25	4.38

Appendix 7. Effect of biosorbent dosage on As(III) ions removal from monocomponent and bicomponent synthetic wastewater

Biosorbent dossage (g/L)	As(III)			As(III)[As(III)+Hg(II)]		
	Residual concentration (mg/L)	Removal efficiency (%)	Biosorption capacity (mg/g)	Residual concentration (mg/L)	Removal efficiency (%)	Biosorption capacity (mg/g)
0.5	8.26±0.07	66.95	33.47	7.38±0.03	70.47	35.23
1.0	5.55±0.02	77.79	19.45	6.40±0.05	74.41	18.60
1.5	3.54±0.10	85.84	14.31	5.41±0.03	78.35	13.06
2.0	2.62±0.03	89.51	11.19	3.46±0.11	86.17	10.77
2.5	2.43±0.03	90.27	9.03	1.56±0.08	93.75	9.37
3.0	0.34±0.04	98.63	8.22	2.34±0.03	90.63	7.55
3.5	6.17±0.06	75.32	5.38	8.12±0.04	67.52	4.82
4.0	7.18±0.07	71.28	4.46	9.33±0.02	62.68	3.92
4.5	8.20±0.02	67.20	3.73	11.05±0.04	55.79	3.10
5.0	9.32±0.33	62.73	3.14	11.25±0.01	54.99	2.75

Appendix 8. Effect of biosorbent dossage on Hg(II) ions removal from monocomponent and bicomponent synthetic wastewater

Biosorbent dosage (g/L)	Hg(II)			Hg(II)[Hg(II)+ As(III)]		
	Residual concentration (mg/L)	Removal efficiency (%)	Biosorption capacity (mg/g)	Residual concentration (mg/L)	Removal efficiency (%)	Biosorption capacity (mg/g)
0.5	11.67±0.06	53.33	26.67	13.74±0.01	45.05	22.53
1.0	9.61±0.03	61.57	15.39	7.10±0.01	71.60	17.90
1.5	7.13±0.12	71.48	11.91	3.19±0.03	87.25	14.54
2.0	5.49±0.04	78.03	9.75	1.34±0.14	94.63	11.83
2.5	3.87±0.08	84.52	8.45	4.90±0.02	80.40	8.04
3.0	2.13±0.10	91.48	7.62	5.08±0.05	79.67	6.64
3.5	0.47±0.02	98.13	7.01	5.71±0.04	77.17	5.51
4.0	4.24±0.10	83.05	5.19	5.90±0.02	76.41	4.78
4.5	4.11±0.07	83.55	4.64	6.10±0.03	75.61	4.20
5.0	4.25±0.01	83.00	4.15	6.10±0.03	75.59	3.78

Appendix 9. **Effect of initial heavy metal ion concentration on As(III) ions removal from monocomponent and bicomponent synthetic wastewater**

Initial heavy metal ion concentration (mg/L)	As(III)			As(III)[As(III)+Hg(II)]		
	Residual concentration (mg/L)	Removal efficiency (%)	Biosorption capacity (mg/g)	Residual concentration (mg/L)	Removal efficiency (%)	Biosorption capacity (mg/g)
5	2.39±0.14	52.27	0.87	1.63±0.09	67.47	1.35
10	2.84±0.06	71.57	2.39	1.33±0.10	86.70	3.47
15	2.95±0.02	80.31	4.02	1.67±0.04	88.89	5.33
25	2.90±0.12	88.40	7.37	2.34±0.08	90.65	9.07
30	2.02±0.68	93.26	9.33	4.25±0.42	85.84	10.30
45	7.65±0.07	83.00	12.45	12.29±0.01	72.69	13.08
60	16.54±0.09	72.44	14.49	20.51±0.03	65.82	15.80
75	24.55±0.10	67.27	16.82	28.26±0.05	62.32	18.70
100	32.85±0.06	67.15	22.38	37.28±0.02	62.72	25.09

Appendix 10. **Effect of initial heavy metal ion concentration on Hg(II) ions removal from monocomponent and bicomponent synthetic wastewater**

Initial heavy metal ion concentration (mg/L)	Hg(II)			Hg(II)[Hg(II)+ As(III)]		
	Residual concentration (mg/L)	Removal efficiency (%)	Biosorption capacity (mg/g)	Residual concentration (mg/L)	Removal efficiency (%)	Biosorption capacity (mg/g)
5	2.90±0.03	42.00	0.60	2.67±0.02	46.53	1.16
10	4.15±0.06	58.53	1.67	2.09±0.02	79.13	3.96
15	3.87±0.02	74.18	3.18	0.73±0.10	95.13	7.14
25	3.46±0.04	86.17	6.16	3.45±0.05	86.20	10.78
30	2.93±0.12	90.24	7.74	5.74±0.04	80.88	12.13
45	1.45±0.09	96.78	12.44	8.33±0.07	81.48	18.33
60	14.73±0.03	75.46	12.94	11.93±0.02	80.11	24.03
75	18.40±0.02	75.46	16.17	14.59±0.03	80.55	30.21
100	24.10±0.08	75.90	21.69	19.75±0.01	80.25	40.13

Appendix 11. Effect of reaction temperature on As(III) ions removal from monocomponent and bicomponent synthetic wastewater

Initial heavy metal ion concentration (mg/L)	As(III)			As(III)[As(III)+Hg(II)]		
	Residual concentration (mg/L)	Removal efficiency (%)	Biosorption capacity (mg/g)	Residual concentration (mg/L)	Removal efficiency (%)	Biosorption capacity (mg/g)
10	16.34±0.06	45.54	4.55	7.31±0.03	51.24	3.07
15	12.36±0.08	58.81	5.88	5.24±0.06	65.04	3.90
25	7.42±0.12	75.27	7.53	4.25±0.09	71.67	4.30
35	1.81±0.06	93.98	9.40	3.20±0.11	78.69	4.72
45	4.35±0.10	85.50	8.55	2.95±0.02	80.31	4.82
55	8.66±0.09	71.12	7.11	2.68±0.10	82.13	4.93
65	13.50±0.03	55.00	5.50	8.37±0.04	44.22	2.65
75	15.69±0.01	47.70	4.77	10.31±0.07	31.29	1.88
85	17.70±0.02	41.00	4.10	11.44±0.01	23.76	1.43

Appendix 12. Effect of reaction temperature on Hg(II) ions removal from monocomponent and bicomponent synthetic wastewater

Initial heavy metal ion concentration (mg/L)	Hg(II)			Hg(II)[Hg(II)+ As(III)]		
	Residual concentration (mg/L)	Removal efficiency (%)	Biosorption capacity (mg/g)	Residual concentration (mg/L)	Removal efficiency (%)	Biosorption capacity (mg/g)
10	16.42±0.02	63.51	8.17	6.63±0.03	55.80	4.19
15	11.42±0.04	74.62	9.59	5.53±0.07	63.13	4.74
25	6.77±0.10	84.95	10.92	4.31±0.05	71.27	5.35
35	5.20±0.03	88.44	11.37	3.11±0.10	79.27	5.95
45	1.84±0.09	95.91	12.33	2.20±0.04	85.33	6.40
55	9.40±0.03	79.12	10.17	1.47±0.09	90.20	6.77
65	11.72±0.01	73.95	9.51	6.90±0.03	54.00	4.05
75	13.14±0.08	70.81	9.10	8.25±0.02	44.98	3.37
85	17.42±0.10	61.30	7.88	11.18±0.01	25.49	1.91

Appendix 13. **Desorption eluents for adsorbed As(III) ions recovery on spent biosorbent surface from monocomponent and bicomponent sorption systems**

Desorption eluent	As(III)			As(III)[As(III)+Hg(II)]		
	Concentration of heavy metal ions adsorbed (mg/L)	Residual concentration after desorption (mg/L)	Desorption efficiency (%)	Concentration of heavy metal ions adsorbed (mg/L)	Residual concentration after desorption (mg/L)	Desorption efficiency (%)
Distilled water	24.85±0.01	0.61±0.03	2.45	20.33±0.01	0.33±0.10	1.64
H_2SO_4	24.89±0.02	15.55±0.05	62.48	20.05±0.04	13.43±0.09	66.97
HNO_3	24.92±0.02	19.94±0.02	80.03	19.94±0.05	13.96±0.03	70.01
HCl	25.01±0.03	23.43±0.06	93.71	20.17±0.03	12.14±0.02	60.21
EDTA	25.01±0.03	17.25±0.04	68.97	20.06±0.06	16.85±0.04	84.00

Appendix 14. **Desorption eluents for adsorbed Hg(II) ions recovery on spent biosorbent surface from monocomponent and bicomponent sorption systems**

Desorption eluent	Hg(II)			Hg(II)[Hg(II)+ As(III)]		
	Concentration of heavy metal ions adsorbed (mg/L)	Residual concentration after desorption (mg/L)	Desorption efficiency (%)	Concentration of heavy metal ions adsorbed (mg/L)	Residual concentration after desorption (mg/L)	Desorption efficiency (%)
Distilled water	40.05±0.02	1.06±0.13	2.65	11.14±0.03	0.46±0.12	4.13
H_2SO_4	40.10±0.01	28.27±0.06	70.49	11.11±0.01	7.14±0.04	64.22
HNO_3	40.95±0.03	37.46±0.01	91.47	11.03±0.06	7.94±0.03	72.01
HCl	40.02±0.05	30.93±0.03	77.28	10.96±0.04	8.86±0.02	80.85
EDTA	40.82±0.02	24.66±0.04	60.41	9.95±0.02	7.47±0.02	75.07

Appendix 15. **Regeneration and reusability of the spent biosorbent in the removal of As(III) ions from monocomponent and bicomponent sorption systems**

Number of cycles	As(III)			As(III)[As(III)+Hg(II)]		
	Concentration of heavy metal ions adsorbed (mg/L)	Residual concentration after desorption (mg/L)	Removal efficiency (%)	Concentration of heavy metal ions adsorbed (mg/L)	Residual concentration after desorption (mg/L)	Removal efficiency (%)
1	25.88±0.12	23.41±0.01	90.45	23.36±0.02	20.73±0.05	88.74
2	25.58±0.07	22.17±0.02	86.67	22.84±0.02	20.02±0.09	87.64
3	25.00±0.02	20.95±0.09	83.81	22.08±0.04	18.95±0.02	85.82
4	25.15±0.07	20.22±0.02	80.39	21.73±0.06	18.17±0.03	83.59
5	25.66±0.12	19.42±0.09	75.66	21.02±0.01	17.35±0.04	82.56
6	24.93±0.02	18.26±0.04	73.25	20.68±0.02	15.04±0.02	72.72
7	25.17±0.18	16.04±0.09	63.74	17.31±0.03	12.07±0.06	69.71
8	26.04±0.04	12.49±0.06	47.98	15.94±0.05	9.79±0.01	61.42
9	24.96±0.12	11.06±0.10	44.32	14.08±0.04	6.03±0.02	42.82
10	25.17±0.08	9.87±0.04	39.23	13.76±0.03	1.76±0.07	12.77

Appendix 16. **Regeneration and reusability of the spent biosorbent in the removal of Hg(II) ions from monocomponent and bicomponent sorption systems**

Number of cycles	Hg(II)			Hg(II)[Hg(II)+ As(III)]		
	Concentration of heavy metal ions adsorbed (mg/L)	Residual concentration after desorption (mg/L)	Desorption efficiency (%)	Concentration of heavy metal ions adsorbed (mg/L)	Residual concentration after desorption (mg/L)	Desorption efficiency (%)
1	39.81±0.03	36.75±0.07	92.31	13.16±0.03	11.43±0.03	86.88
2	40.05±0.05	33.91±0.05	84.67	12.78±0.06	10.34±0.04	80.95
3	39.93±0.08	31.18±0.04	78.07	11.97±0.02	9.36±0.02	78.20
4	41.00±0.03	30.25±0.08	73.78	11.13±0.01	8.47±0.07	76.13
5	40.01±0.02	29.05±0.11	72.61	9.25±0.09	5.66±0.05	61.15
6	40.11±0.04	27.47±0.12	68.48	7.54±0.10	4.06±0.02	53.85
7	40.24±0.06	26.70±0.03	66.34	6.62±0.06	3.18±0.05	48.06
8	40.45±0.08	20.16±0.09	49.84	6.05±0.02	2.22±0.04	36.77
9	39.94±0.03	16.39±0.05	41.04	5.85±0.08	1.83±0.08	31.34
10	39.91±0.04	15.07±0.04	37.75	5.53±0.04	1.45±0.02	26.21

Appendix 17. Effect of agitation speed on As, Hg, Pb, Cd, and Cr ions removal from textile wastewater

Agitation Speed (rpm)	As		Hg		Pb		Cd		Cr	
	Ce (mg/L)	% Removal	Ce (mg/L)	% Removal	Ce (mg/L)	% Removal	Ce (mg/L)	% Removal	Ce (mg/L)	% Removal
25	0.6362	33.83	0.1376	45.57	1.3820	24.37	1.0032	26.10	1.2925	49.16
50	0.5218	45.73	0.1242	49.76	1.2634	30.86	0.7650	43.65	1.1020	56.65
100	0.3853	59.93	0.1191	51.78	1.0862	40.55	0.5384	60.34	1.0058	60.44
150	0.2192	77.20	0.0857	64.99	0.1945	89.36	0.4927	63.71	0.4653	81.70
200	0.1004	89.56	0.0645	73.38	0.1547	91.53	0.1928	85.80	0.2539	90.01
250	0.0026	99.73	0.0001	98.85	0.0305	98.33	0.0254	98.13	0.0520	97.95
300	0.0733	92.38	0.0264	88.45	0.1026	94.38	0.2436	82.06	0.3746	85.27
350	0.0781	91.88	0.0269	88.25	0.1023	94.40	0.2398	82.34	0.3795	85.07
400	0.0790	91.78	0.0270	88.21	0.1029	94.37	0.2377	82.49	0.3811	85.01

Appendix 18. Effect of contact time on As, Hg, Pb, Cd, and Cr ions removal from textile wastewater

Contact time (min)	As		Hg		Pb		Cd		Cr	
	Ce (mg/L)	% Removal	Ce (mg/L)	% Removal	Ce (mg/L)	% Removal	Ce (mg/L)	% Removal	Ce (mg/L)	% Removal
10	0.5381	44.04	0.1726	31.72	1.1168	38.88	0.7523	44.59	1.2014	52.74
20	0.4153	56.81	0.1522	39.79	1.0052	44.99	0.5160	61.99	1.0075	60.37
30	0.2674	72.19	0.1405	44.42	0.7175	60.73	0.2842	79.07	0.6572	74.15
40	0.1985	79.36	0.0908	64.08	0.5246	71.29	0.2001	85.26	0.3886	84.71
60	0.0198	97.94	0.0274	89.16	0.1563	91.45	0.0250	98.16	0.2448	90.37
90	0.0376	96.09	0.0001	99.96	0.0198	98.92	0.1024	92.46	0.1143	95.50
120	0.1043	89.15	0.0410	83.78	0.1363	92.54	0.1836	86.48	0.0641	97.48
150	0.1052	89.06	0.0418	83.47	0.1395	92.37	0.1857	86.32	0.1039	95.91
180	0.1057	89.01	0.0424	83.23	0.1400	92.34	0.1885	86.12	0.1084	95.74
240	0.1064	88.93	0.0445	82.40	0.1430	92.17	0.1890	86.08	0.1085	95.73

Appendix 19. Effect of solution pH on As, Hg, Pb, Cd, and Cr ions removal from textile wastewater

Solution pH	As		Hg		Pb		Cd		Cr	
	Ce (mg/L)	% Removal	Ce (mg/L)	% Removal	Ce (mg/L)	% Removal	Ce (mg/L)	% Removal	Ce (mg/L)	% Removal
2	0.6985	27.35	0.1765	30.18	1.0362	43.29	0.6766	50.16	1.0145	60.10
3	0.3874	59.71	0.1054	58.31	0.5284	71.08	0.3172	76.64	0.3526	86.13
4	0.0311	96.77	0.0520	79.43	0.2653	85.48	0.1208	91.10	0.0411	98.38
5	0.0795	91.73	0.0136	94.62	0.1145	93.73	0.0073	99.46	0.1458	94.27
6	0.1153	88.01	0.0005	99.80	0.0251	98.63	0.0614	95.48	0.1956	92.31
7	0.1390	85.54	0.0187	92.60	0.3240	82.27	0.1580	88.36	0.2347	90.77
8	0.1827	81.00	0.0248	90.19	0.4096	77.58	0.1922	85.84	0.4273	83.19
10	0.1946	79.76	0.0422	83.31	0.5124	71.96	0.3563	73.76	0.5904	76.78
12	0.1949	79.73	0.0424	83.23	0.5249	71.27	0.3600	73.48	0.6065	76.14
14	0.1950	79.72	0.0428	83.07	0.5250	71.27	0.3641	73.18	0.6200	75.61

Appendix 20. Effect of biosorbent particle size on As, Hg, Pb, Cd, and Cr ions removal from textile wastewater

Biosorbent particle size (µm)	As		Hg		Pb		Cd		Cr	
	Ce (mg/L)	% Removal	Ce (mg/L)	% Removal	Ce (mg/L)	% Removal	Ce (mg/L)	% Removal	Ce (mg/L)	% Removal
63	0.0015	99.84	0.0042	98.34	0.0382	97.91	0.0066	99.51	0.0625	97.54
90	0.0939	90.23	0.0175	91.97	0.1475	91.93	0.1348	90.07	0.2148	91.55
125	0.1895	80.29	0.0586	75.71	0.4064	77.76	0.2635	80.59	0.5754	77.37
180	0.2654	72.40	0.0914	62.74	0.5938	67.50	0.3936	71.01	0.9463	62.78
355	0.5848	39.18	0.1573	36.67	1.0546	42.28	0.7421	45.34	1.6823	33.83
450	0.7746	19.44	0.1806	27.45	1.5629	14.46	0.9004	33.68	1.9011	25.22

Appendix 21. Effect of biosorbent dosage on As, Hg, Pb, Cd, and Cr ions removal from textile wastewater

Biosorbent dosage	As		Hg		Pb		Cd		Cr	
	Ce	%	Ce	%	Ce	%	Ce	%	Ce	%
(g/L)	(mg/L)	Removal	(mg/L)	Removal	(mg/L)	Removal	(mg/L)	Removal	(mg/L)	Removal
0.5	0.1258	86.92	0.0854	66.22	0.7952	56.48	0.2476	81.76	0.5621	77.89
1.0	0.0675	92.98	0.0314	87.58	0.4724	74.15	0.1232	90.93	0.2788	89.03
1.5	0.0186	98.07	0.0008	99.68	0.0538	97.06	0.0743	94.53	0.1554	93.89
2.0	0.0862	91.03	0.0125	95.06	0.0935	94.88	0.0156	98.85	0.0065	99.74
2.5	0.1684	82.49	0.0265	89.52	0.1749	90.43	0.0824	93.93	0.1987	92.18
3.0	0.1964	79.57	0.0551	78.20	0.3022	83.46	0.1571	88.43	0.4898	80.73
3.5	0.2507	73.93	0.0833	67.05	0.3986	78.19	0.2945	78.31	0.7543	70.33
4.0	0.4044	57.94	0.1026	59.41	0.5471	70.06	0.3928	71.07	0.9566	62.37
4.5	0.5241	45.49	0.1429	43.47	0.8430	53.86	0.5630	58.53	1.1429	55.04
5.0	0.5823	39.44	0.1650	34.7310	1.0447	42.83	0.6229	54.12	1.2765	49.79

Appendix 22. Effect of temperature on As, Hg, Pb, Cd, and Cr ions removal from textile wastewater

Temp (℃)	As		Hg		Pb		Cd		Cr	
	Ce (mg/L)	% Removal	Ce (mg/L)	% Removal	Ce (mg/L)	% Removal	Ce (mg/L)	% Removal	Ce (mg/L)	% Removal
20	0.4762	50.47	0.1345	46.80	1.0792	40.94	0.5680	58.16	1.0000	60.67
25	0.3233	66.38	0.1144	54.75	0.8567	53.11	0.3824	71.83	0.8285	67.41
30	0.1466	84.75	0.0732	71.04	0.5835	68.07	0.1946	85.67	0.6124	75.91
35	0.0485	94.96	0.0128	94.94	0.3286	82.02	0.1575	88.40	0.4356	82.87
40	0.0098	98.98	0.0045	98.22	0.1450	92.06	0.0283	97.92	0.2128	91.63
45	0.1987	79.33	0.0240	90.51	0.0054	99.70	0.1891	86.07	0.0109	99.57
50	0.2546	73.52	0.0385	84.77	0.2981	83.69	0.2964	78.17	0.7253	71.47
55	0.2619	72.76	0.0386	84.73	0.3115	82.95	0.3002	77.89	0.7724	69.62
60	0.2700	71.92	0.0400	84.18	0.3162	82.69	0.3072	77.37	0.7988	68.58
65	0.2724	71.67	0.0402	84.10	0.3179	82.60	0.3124	76.99	0.8000	68.53

Appendix 23. **Desorption eluents for adsorbed As, Hg, Pb, Cd, and Cr ions recovery on spent biosorbent surface from monocomponent and bicomponent sorption systems**

	As	Hg	Pb	Cd	Cr
Desorption eluent	**Desorption efficiency (%)**	**Desorption efficiency (%)**	**Desorption efficiency (%)**	**Desorption efficiency (%)**	**Desorption efficiency (%)**
H_2O	0.54	0.76	0.95	0.63	0.78
H_3PO_4	78.96	82.07	69.43	85.26	71.71
H_2SO_4	68.37	90.26	74.88	92.95	81.72
HNO_3	92.81	77.61	93.54	74.53	80.22
HCl	98.17	99.56	98.71	97.14	99.54
EDTA	84.92	85.95	72.41	71.77	89.75
NaOH	45.72	60.77	83.38	57.09	72.83
NaCl	60.88	66.81	55.39	62.75	61.69
KOH	71.00	75.04	53.97	41.06	41.37
$CaCl_2$	76.36	59.06	37.74	28.20	17.86

Appendix 24. **Regeneration and reusability of the biosorbent spent in the removal of As, Hg, Pb, Cd, and Cr ions from the textile wastewater**

Number of cycles	As	Hg	Pb	Cd	Cr
	Removal efficiency (%)	Removal efficiency (%)	Removal efficiency (%)	Removal efficiency (%)	Removal efficiency (%)
1	98.22	99.84	97.35	96.73	98.07
2	92.02	90.70	94.67	94.13	89.82
3	84.68	85.75	87.40	83.73	80.63
4	78.64	83.49	83.48	74.37	79.63
5	76.31	80.21	74.08	71.24	77.57
6	70.90	77.76	71.40	70.03	72.91
7	67.85	75.43	69.08	64.72	70.38
8	60.08	66.84	65.98	63.11	61.53
9	56.81	56.56	57.22	59.29	57.07
10	53.98	51.30	54.34	57.83	53.27

RESEARCH OUTPUTS

The under-listed are the peer-reviewed journal and book chapter publications made from this research work.

(i) Journal Publications

1. **Bayuo, J.,** Rwiza, M. J., Choi, J. W., Sillanpää, M., and Mtei, M. (2024). Optimization of desorption parameters using response surface methodology for enhanced recovery of arsenic from spent reclaimable activated carbon : Eco-friendly and sorbent sustainability approach. *Ecotoxicology and Environmental Safety,* 280, 1–11. https://doi.org/10.1016/j.ecoenv.2024.116550

2. **Bayuo, J.,** Rwiza, M. J., Choi, W. J., Mtei, K. M., Hosseini-Bandegharaei, A., and Sillanpää, M. (2024). Adsorption and desorption processes of toxic heavy metals, regeneration and reusability of spent adsorbents : an economic and environmental sustainability approach. *Advances in Colloid and Interface Science,* 329, 1–19. https://doi.org/10.1016/j.cis.2024.103196

3. **Bayuo, J.,** Rwiza, M. J., and Mtei, K. M. (2023). Optimization of divalent mercury removal from synthetic wastewater using desirability function in central composite design of response surface methodology. *Journal of Environmental Health Science and Engineering,* 888, 1-19. https://doi.org/10.1007/s40201-023-00888-5

4. **Bayuo, J.,** Rwiza, M. J., and Mtei, K. M. (2023). Adsorption and desorption ability of divalent mercury from an interactive bicomponent sorption system using hybrid granular activated carbon. *Environmental Monitoring and Assessment,* 195(935), 1–17. https://doi.org/10.1007/s10661-023-11540-y

5. **Bayuo, J.,** Rwiza, M. J., and Mtei, K. M. (2023a). Applicability of bio-adsorbents synthesized from maize/corn plant residues for heavy metals removal from aquatic environments: an insight review. *EQA-International Journal of Environmental Quality*, 56, 15–35. https://doi.org/10.6092/issn.2281-4485/16951

6. **Bayuo, J.,** Rwiza, M. J., and Mtei, K. M. (2023b). Modeling and optimization of trivalent arsenic removal from wastewater using activated carbon produced from maize plant biomass: a multivariate experimental design approach. *Biomass Conversion and*

Biorefinery, 0123456789, 1–24. https://doi.org/10.1007/s13399-023-04494-1

7. **Bayuo, J.,** Rwiza, M. J., Sillanpaa, M., and Mtei, K. M. (2023). Removal of heavy metals from binary and multicomponent adsorption systems using various adsorbents – a systematic review. *RSC Advances*, 13, 13052–13093. https://doi.org/10.1039/-D3RA01660A

8. **Bayuo, J.,** Rwiza, M. J., and Mtei, K. M. (2023). Non-competitive and competitive detoxification of As(III) ions from single and binary biosorption systems and biosorbent regeneration. *Biomass Conversion and Biorefinery*, 1–28. https://doi.org/10.1007/s13399-022-03734-0

9. **Bayuo, J.,** Rwiza, M., and Mtei, K. (2022). Response surface optimization and modeling in heavy metal removal from wastewater—a critical review. *Environmental Monitoring and Assessment*, 194(5). https://doi.org/10.1007/s10661-022-09994-7

10. **Bayuo, J.,** Rwiza, M., Abukari, M. A., Pelig-Ba, K. B., and Mtei, K. (2022). Modeling and optimization of independent factors influencing lead(II) biosorption from aqueous systems: A statistical approach. *Scientific African*, 16, 1–16. https://doi.org/10.1016/j.sciaf.-2022.e01270

11. **Bayuo, J.,** Rwiza, M., and Mtei, K. (2022). A comprehensive review on the decontamination of lead(II) from water and wastewater by low-cost biosorbents. *RSC Advances*, 12, 11233–11254. https://doi.org/10.1039/D2RA00796G

(ii) Book Chapters Publications

1. **Bayuo, J.,** Rwiza, M.J., Mtei, K.M., Choi, J.W. (2024). Adsorptive Removal of Heavy Metals from Wastewater Using Low-Cost Adsorbents Derived from Agro-based Materials. In: Kumar, N. (eds) Heavy Metal Remediation. Earth and Environmental Sciences Library. Springer, Cham. https://doi.org/10.1007/978-3-031-53688-5_11

2. **Bayuo, J.,** Alayande, A.B., Mtei, K. M., and Rwiza, M. J. (2024). Biochar-Based Technology in Water and Wastewater Treatment. In: Pandey, A., and Bui, X. T. (eds) Low-Cost Water and Wastewater Treatment Systems. Elsevier. 1-43. https://doi.org/10.1016/B978-0-443-23662-4.00012-3

(iii) Patent

A Dynamic Batch Adsorption Reactor and the Method thereof for the Enhanced Remediation of Heavy Metals from Wastewater (Under Review).

(iv) Scientific Conferences Attended

1. 2024 NM-AIST International Scientific Conference organized by the Nelson Mandela African Institution of Science and Technology (NM-AIST) at Mount Meru Hotel, Arusha, Tanzania on 17-19th July, 2024.

2. 6th PASET Forum and Rsif Annual Conference organized by Partnership for Skills in Applied Sciences, Engineering, and Technology (PASET)-Regional Scholarship and Innovation Fund (Rsif) at Nairobi, Kenya on 23rd -24th April, 2024.

3. The 2024 Korean Wood Engineering Society Spring Conference organized by the Korean Society of Wood Engineers at Seoul National University, Siheung Campus, South Korea on 18-19th April 2024.

4. The 2024 Forest Science Joint Academic Conference organized by the Korean Society of Forest Science at the Korean Science and Technology Centre, Gangnam-gu, Seoul, South Korea on 13-14th February 2024.

5. 2023 Zanzibar Water Conference organized by the Revolutionary Government of Zanzibar Ministry of Water, Energy and Minerals at Hotel Verde, Zanzibar, Tanzania on 16–17th August 2023.

6. 2nd International Maji Scientific Conference organized by Water Institute at Ubungo Plaza Centre in Dar es Salaam, Tanzania on 8-10th March 2023.

7. 15th Annual Interdisciplinary Conference (AIC) organized by the University for Development Studies (UDS) in Tamale, Ghana on September 7-8th, 2022.

8. 4th Mwenge Catholic University International Conference at Bishop Amedeus Msarikie Learning Resource Centre, Moshi-Kilimanjaro-Tanzania on 25-29th July 2022.

9. Maji Scientific Conference organized by the Water Institute at Julius Nyerere International Convention Centre in Dar es Salaam, Tanzania on 4-5th April 2022.

10. 2nd Science, Technology and Innovation Conference organized by the East African Science and Technology Commission at Hotel Club du Lac Tanganyika, Burundi on 27-29th October 2021.

11. RSIF Virtual Pre-Conference on African-led Science, Technology, and Innovation for contributing to the SDGs and stimulating global development on 16-17th November 2021.

(v) **Poster Presentation**

Optimization of Arsenic(III) and Mercury(II) Removal from Non-Competitive and Competitive Sorption Systems onto Activated Carbon

Jonas Bayuo[*1, 2], Mwemezi J. Rwiza[2], Joon Weon Choi[1], Kelvin Mark Mtei[2]

[1] School of Materials, Energy, Water, and Environmental Sciences (MEWES), The Nelson Mandela African Institution of Science and Technology (NM-AIST), P.O. Box 447, Tanzania

[2] Institutes of Green Bio Science and Technology, Seoul National University, Pyeongchang-daero1447, Gangwon-do, South Korea

[*]Contact: bayuoj@nm-aist.ac.tz/+233543290589

Introduction

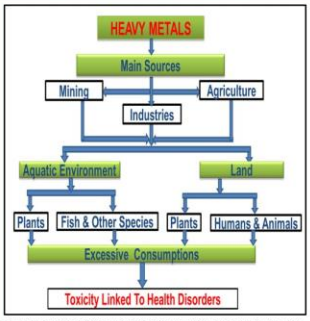

Figure 1: Sources of heavy metals and their impact on living organisms

❖Water contamination due to heavy metals is a serious global challenge because these pollutants are non-biodegradable and are harmful to humans and other life forms (Bayuo et al., 2020).

❖For instance As(III), Hg(II), Pb(II), Cd(II), and Cr(VI) are hazardous heavy metals found in industrial wastewater (Kumar et al., 2020).

❖The exposure to higher levels of heavy metals cause acute and chronic health problems in humans (Badr et al., 2020).

❖Due to their toxicity, various purification technologies have been employed to remove heavy metals from wastewater.

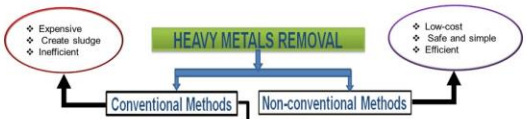

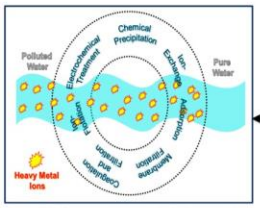

Figure 2: Various treatment methods for heavy metals

❖In biosorption, natural occurring agro-waste or biomass are use to remove heavy metals from wastewater.

❖The biosorption of heavy metals using agro-waste materials as become an innovative treatment technology (Nazari et al., 2021).

❖In this present study, the adsorptive removal of As(III) and Hg(II) from non-competitive and competitive sorption systems onto activated carbon prepared from maize biomass was investigated.

Materials & Methods

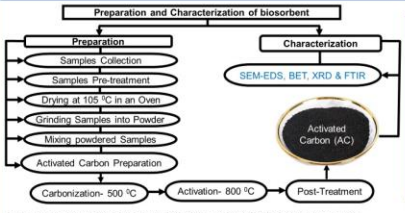

Figure 3: Methodological framework for adsorbent preparation and characterization

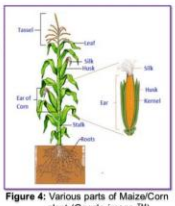

Figure 4: Various parts of Maize/Corn plant (Google image ™)

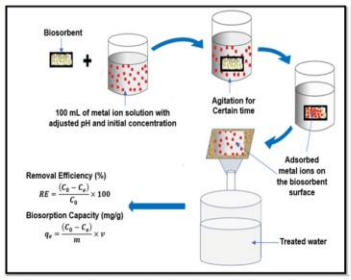

Figure 5: Biosorption technology for heavy metals removal in wastewater

❖Batch tests were carried out to determine the effect of the following biosorption factors:

1. Contact time (10-180 min)
2. pH of solution (2-14)
3. Biosorbent particle size (90-450 µm)
4. Biosorbent dose (0.5-5.0 g/L)
5. Concentration (5-100 mg/L)
6. Temperature (10-85 ℃)

Measurement equipment

TGA (Mettler-Toledo, Switzerland) | BET (Belsorp-max, MicrotracBEL, Japan) | Elemental Analyzer (Flash 2000, Thermo Scientific™, USA)

Results & Discussion

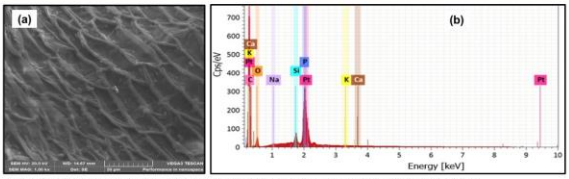

Figure 6: SEM image **(a)** and EDS spectrum **(b)** of the pristine activated carbon before the biosorption process

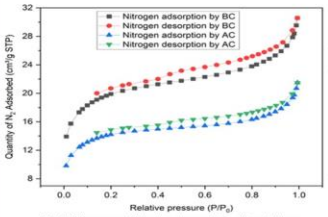

Fig. 7. Nitrogen gas (N_2) adsorption and desorption isotherm

Table 1: Textural properties of the biochar and activated carbon derived from maize residues

Textural parameter	Biochar	Activated carbon
BET surface area (m^2/g)	473.6	1365.8
Micropore surface area (m^2/g)	124.3	312.7
Total pore volume (cm^3/g)	0.0286	0.0413
Micropore volume (cm^3/g)	0.0119	0.0450

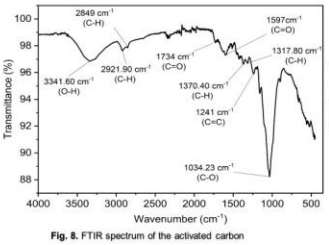

Fig. 8. FTIR spectrum of the activated carbon

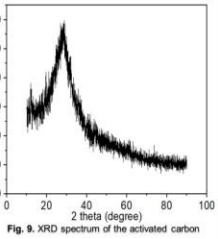

Fig. 9. XRD spectrum of the activated carbon

❖ To determine the overall removal efficiency of As(III), batch experiments were conducted at the following best operating conditions attained for both single and binary sorption systems, respectively.

❖ Single sorption System:

1. Initial concentration=30.0 mg/L
2. Solution pH=6.0
3. Biosorbent dosage=3.0 g/L
4. Biosorbent particle size=90.0 µm
5. Reaction temperature=35.0 ℃
6. Reaction time=60.0 min

❑ As(III) removal efficiency = 95.33%

❖ Binary sorption System:

1. Initial concentration=25.0 mg/L
2. Solution pH=4.0
3. Biosorbent dosage=2.5 g/L
4. Biosorbent particle size=90.0 µm
5. Reaction temperature=55.0 ℃
6. Reaction time=90.0 min

❑ As(III) removal efficiency = 91.74%

❖ To determine the overall removal efficiency of Hg(II), batch experiments were conducted at the following best operating conditions attained for both single and binary sorption systems, respectively.

❖ Single sorption System:

1. Initial concentration=45.0 mg/L
2. Solution pH=4.0
3. Biosorbent dosage=3.5 g/L
4. Biosorbent particle size=90.0 µm
5. Reaction temperature=45.0 ℃
6. Reaction time=90.0 min

❑ Hg(II) removal efficiency = 97.06%

❖ Binary sorption System:

1. Initial concentration=15.0 mg/L
2. Solution pH=8.0
3. Biosorbent dosage=2.0 g/L
4. Biosorbent particle size=90.0 µm
5. Reaction temperature=55.0 ℃
6. Reaction time=120.0 min

❑ Hg(II) removal efficiency = 93.58%

Conclusion

❖The removal of As(III) and Hg(II) from non-competitive and competitive sorption systems onto activated carbon was found to be depended on the independent influencing biosorption factors.

❖At the optimum operating conditions attained, the activated carbon could remove about 95 and 92% of As(III) from the single and binary sorption systems, respectively.

❖While about 97 and 94% of Hg(II) could be decontaminated from the single and binary sorption systems, respectively at the optimum operating conditions attained.

❖In comparison to the literature, the activated carbon prepared from the maize biomass was found to have higher uptake capacity than almost all the other adsorbents employed in As(III) and Hg(II) remediation.

❖Therefore, this novel activated carbon is found to be promising and could effectively be employed for heavy metals remediation in aquatic environments.

Acknowledgement: This work was supported by the Partnership for Applied Sciences, Engineering, and Technology-Regional Scholarship and Innovation Fund (PASET- Rsif) and the Carnegie Corporation of New York (CCNY).